Multistage Expansion Planning of Active Distribution Systems: Towards Network Integration of Distributed Energy Resources

A Thesis

Submitted to the College of Graduate and Postdoctoral Studies

in Partial Fulfillment of the Requirements

for the Degree of Doctor of Philosophy

in the Department of Electrical and Computer Engineering

University of Saskatchewan

Saskatoon, Saskatchewan, Canada

by

Alireza Zare

Permission to Use

In presenting this thesis in partial fulfillment of the requirements for a Postgraduate degree from the University of Saskatchewan, I agree that the Libraries of this University may make it freely available for inspection. I further agree that permission for copying of this thesis in any manner, in whole or in part, for scholarly purposes may be granted by the professor or professors who supervised my thesis work or, in their absence, by the Head of the Department or the Dean of the College in which my thesis work was done. It is understood that any copying or publication or use of this thesis or parts thereof for financial gain shall not be allowed without my written permission. It is also understood that due recognition shall be given to me and to the University of Saskatchewan in any scholarly use which may be made of any material in my thesis.

Requests for permission to copy or to make other uses of materials in this thesis in whole or part should be addressed to:

Head of the Department of Electrical and Computer Engineering
University of Saskatchewan
57 Campus Drive
Saskatoon, Saskatchewan, S7N 5A9
Canada

OR

Dean of the College of Graduate and Postdoctoral Studies
University of Saskatchewan
116 Thorvaldson Building, 110 Science Place
Saskatoon, Saskatchewan S7N 5C9
Canada

Abstract

Over the last few years, driven by several technical and environmental factors, there has been a growing interest in the concept of active distribution networks (ADNs). Based on this new concept, traditional passive distribution networks will evolve into modern active ones by employing distributed energy resources (DERs) such as distributed generators (DGs), energy storage systems (ESSs), and demand responsive loads (DRLs). Such a transition from passive to active networks poses serious challenges to distribution system planners. On the one hand, the ability of DGs to directly inject active and reactive powers into the system nodes leads to bidirectional power flows through the distribution feeders. This issue, if not adequately addressed at the design stage, can adversely affect various operational aspects of ADNs, specifically the reactive power balance and voltage regulation. Therefore, the new context where DGs come into play necessitates the development of a planning methodology which incorporates an accurate network model reflecting realistic operational characteristics of the system. On the other hand, large-scale integration of renewable DGs results in the intermittent and highly volatile nodal power injections and the implementation of demand response programs further complicates the long-term predictability of the load growth. These factors introduce a tremendous amount of uncertainty to the planning process of ADNs. As a result, effective approaches must also be devised to properly model the major sources of uncertainty.

Based on the above discussion, successful transition from traditional passive distribution networks to modern active ones requires a planning methodology that firstly includes an accurate network model, and secondly accounts for the major sources of uncertainty. However, incorporating these two features into the planning process of ADNs is a very complex task and requires sophisticated mathematical programming techniques that are not currently available in the literature. Therefore, this research project aim to develop a comprehensive planning methodology for ADNs, which is capable of dealing with different types of DERs (i.e., DGs, ESSs, and DRLs), while giving full consideration to the above-mentioned two key features. To achieve this objective, five major steps are defined for the project.

Step 1 develops a deterministic mixed-integer linear programming (MILP) model for integrated expansion planning of distribution network and renewable/conventional DGs, which includes a highly accurate network model based on a linear format of AC power flow equations. This MILP model can be solved using standard off-the-shelf mathematical programming solvers that not only guarantee convergence to the global optimal solution, but also provide a measure of the distance to the global optimum during the solution process. Step 2 proposes a distributionally robust chance-constrained programming approach to characterize the inherent uncertainties of renewable DGs and loads. The key advantage of this approach is that it requires limited information about the uncertain parameters, rather than perfect knowledge of their probability distribution functions. Step 3 devises a fast Benders decomposition-based solution procedure that paves the way for effective incorporation of ESSs and DRLs into the developed planning methodology. To this end, two effective acceleration strategies are proposed to significantly enhance the computational performance of the classical Benders decomposition algorithm. Eventually, Steps 4 and 5 propose appropriate models for ESSs and DRLs and integrate them into the developed planning methodology. In this regard, a sequential-time power flow simulation method is also proposed to incorporate the short-term operation analysis of ADNs into their long-term planning studies.

By completing the above-defined steps, the planning model developed in Step 1 will be gradually evolved, so that Step 5 will yield the final comprehensive planning methodology for ADNs.

Acknowledgments

First and foremost, I am deeply grateful to God Almighty for giving me the knowledge, ability, and opportunity to undertake this research study and to complete it satisfactorily. Without his blessings, this achievement would not have been possible.

I would like to express my sincere gratitude to my supervisor, Prof. C. Y. Chung, for his valuable guidance, constant encouragement, and useful critiques during my studies at the University of Saskatchewan. His continuous support was crucial toward the completion of my Ph.D. degree. It was truly an honor for me to work under his supervision.

I would like to express my appreciation to my advisory committee members for their insightful comments and valuable suggestions which helped me to improve the quality of my thesis. I am also thankful to the past and current members of the Smart Grid and Renewable Energy Technology Lab for sharing their knowledge and providing their invaluable assistance.

Last but not least, I would like to pay special thanks to my family for supporting me spiritually throughout my Ph.D. studies and my life in general.

Table of Contents

List of Tables

List of Figures

List of Symbols and Abbreviations

Abbreviations

AA-CAES	Advanced Adiabatic Compressed Air Energy Storage
ABC	Artificial Bee Colony
AC	After-Cooler
ADN	Active Distribution Network
AFM	Automatic Fault Management
AST	Air Storage Tank
AVVC	Automatic Voltage and VAR Control
BD	Benders Decomposition
BESS	Battery Energy Storage System
CAES	Compressed Air Energy Storage
CC	Chance Constraint
CCG	Column-and-Constraint Generation
CCP	Chance-Constrained Programming
COT	Cold Oil Tank
CPP	Critical Peak Pricing
DEP	Distribution Expansion Planning
DER	Distributed Energy Resources
DG	Distributed Generator
DR	Distributionally Robust
DRCC	Distributionally Robust Chance-Constrained
DRCCP	Distributionally Robust Chance-Constrained Programming
DRL	Demand Responsive Load
EPRI	Electric Power Research Institute
ESS	Energy Storage System
EV	Electric Vehicle
FWES	Flywheel Energy Storage

GA	Genetic Algorithm
GCC	Gaussian Chance-Constrained
HOT	Hot Oil Tank
HPC	High Pressure Compressor
HPT	High Pressure Turbine
IC	Inter-Cooler
IH	Inter-Heater
IGA	Immune Genetic Algorithm
IPM-DGA	Interior-Point-Method-embedded Discrete Genetic Algorithm
LCOE	Levelized Cost of Electricity
LHS	Latin Hypercube Sampling
LP	Linear Programming
LPC	Low Pressure Compressor
LPT	Low Pressure Turbine
MDEP	Multistage Distribution Expansion Planning
MILP	Mixed-Integer Linear Programming
MINLP	Mixed-Integer Nonlinear Programming
MISOCP	Mixed-Integer Second-Order Conic Programming
NLP	Nonlinear Programming
NSGA	Non-dominated Sorting Genetic Algorithm
OO	Ordinal Optimization
PDF	Probability Distribution Function
PEM	Point Estimate Method
PH	Pre-Heater
PHS	Pumped Hydroelectric Storage
2-PEM	Two-Point Estimate Method
PSO	Particle Swarm Optimization
RC	Recuperator
RO	Robust Optimization
RTP	Real-Time Pricing
SA	Simulated Annealing

SBSP	Scenario-Based Stochastic Programming
SCES	Supercapacitor Energy Storage
SDEP	Single-Stage Distribution Expansion Planning
SFL	Shuffled Frog-Leaping
SMES	Superconducting Magnetic Energy Storage
SOC	State-of-Charge
SPFS	Static Power Flow Simulation
STPFS	Sequential-Time Power Flow Simulation
STS	Sequential-Time Simulation
TES	Thermal Energy Storage
TOU	Time-of-Use
TS	Tabu Search
UT	Unscented Transformation
V2G	Vehicle-to-Grid

Sets/Indices

Ω^a/a , ω	Set/indices of conductor types
$\Omega^b/\ b$	Set/index of alternatives for substations
Ω^{es}/s	Set/index of alternatives for ESSs
$\Omega^F/\ ij$, ki	Set/indices of feeder sections ($\Omega^{FC} \cup \Omega^{FI} \cup \Omega^{FR}$)
Ω^{FC}	Set of candidate feeder sections for construction
Ω^{FI}	Set of existing irreplaceable feeder sections
Ω^{FR}	Set of existing replaceable feeder sections
$\Omega^{gc}/\ g$	Set/index of alternatives for conventional DGs
$\Omega^{gr}/\ g$	Set/index of alternatives for renewable DGs
$\Omega^H/h, \gamma$	Set/index of hours in a day
$\Omega^N/\ i$, j	Set/indices of nodes ($\Omega^{NG} \cup \Omega_t^{NL} \cup \Omega^{NS} \cup \Omega_t^{NT}$)
Ω^{NES}	Set of candidate nodes for ESS installation
Ω^{NG}	Set of candidate nodes for DG installation
Ω_t^{NL}	Sets of load nodes
Ω^{NS}	Sets of substation nodes

Ω^{NSM}	Set of candidate nodes for smart meter installation
Ω_t^{NT}	Set of transfer nodes
Ω^{sm}/p	Set/index of smart meter penetration levels
Ω^{S}	Set of substations ($\Omega^{SC} \cup \Omega^{SR}$)
Ω^{SC}	Set of candidate substations for construction
Ω^{SR}	Set of existing reinforceable substations
$\Omega^{T}/\ t, \upsilon$	Set/indices of planning stages

Constants

a_{ij}^{FI}	Initial conductor type of existing irreplaceable feeder sections
a_{ij}^{FR}	Initial conductor type of existing replaceable feeder sections
c^{Air}	Specific heat of air at constant pressure (MJ/kg.K)
c^{E}	Energy cost ($/MWh)
c_h^E	Real-time electricity price ($/MWh)
$\overline{\overline{c^E}}$	Fixed electricity price ($/MWh)
c_g^{EGC}	Generation cost of conventional DGs ($/MWh)
c_s^{ES}	Investment cost required to install ESSs ($)
c_a^{FC}	Investment cost required to construct new feeder sections ($/km)
c_a^{FR}	Investment costs required to replace existing feeder sections ($/km)
c_g^{GC}	Investment cost required to install conventional DGs ($)
c_g^{GR}	Investment cost required to install renewable DGs ($)
c^{Oil}	Specific heat of heat transfer oil (MJ/kg.K)
c_b^{SC}	Investment cost required to construct new substations ($)
c_b^{SR}	Investment costs required to reinforce existing substations ($)
c^{SM}	Investment cost required to install smart meters ($)
D	Number of years in each planning stage
$\overline{I_a}$	Maximum current flow of conductors (kA)
$\overline{I_b}$	Current flow capacity of alternatives for substations (kA)
$\overline{I_s^{Ch}}$	Upper limit for charging current of ESSs (kA)
$\overline{I_s^{Dch}}$	Upper limits for discharging current of ESSs (kA)

$\overline{\overline{I_{i,t}^{D}}}$, $\overline{\overline{I_{i,h,t}^{D}}}$	Expected current flow demand of load nodes (kA)
$\overline{I_{g}^{GC}}$	Upper limit for current flow of conventional DGs (kA)
$\overline{\overline{I_{g}^{GR}}}$, $\overline{\overline{I_{g,h}^{GR}}}$	Expected current flow of renewable DGs (kA)
$\overline{I_{i}^{S0}}$	Initial current flow capacity of existing substations (kA)
l_{ij}	Length of feeder sections (km)
$N_{i,t}^{C}$	Number of consumers connected to load nodes
$\overline{N^{ES}}$	Maximum number of installed ESSs
$\overline{N^{SM}}$	Maximum number of nodes equipped with smart meters
$\overline{N^{GC}}$	Maximum number of installed conventional DGs
$\overline{N^{GR}}$	Maximum number of installed renewable DGs
$\underline{p^{AST}}$	Lower limit of air pressure in air storage tank (bar)
$\overline{p^{AST}}$	Upper limit of air pressure in air storage tank (bar)
$\overline{P_{s}^{Ch}}$	Upper limit for charging power of ESSs (MW)
$\overline{P_{s}^{Dch}}$	Upper limit for discharging power of ESSs (MW)
$\overline{\overline{P_{i,t}^{D}}}$, $\overline{\overline{P_{i,h,t}^{D}}}$	Expected active power demand of load nodes (MW)
$\overline{P_{g}^{GC}}$	Upper limit for active power of conventional DGs (MW)
$\overline{\overline{P_{g}^{GR}}}$	Expected active power of renewable DGs (MW)
$\overline{P_{g}^{GR}}$	Rated active power of renewable DGs (MW)
$\overline{\overline{Q_{i,t}^{D}}}$	Expected reactive power demand of load nodes (MVAR)
$\overline{Q_{g}^{GC}}$	Upper limit for reactive power of conventional DGs (MVAR)
r	Annual interest rate
R_{a}	Resistance of conductors (Ω/km)
R^{Air}	Specific gas constant for air (bar.m^3/kg.K)
$\overline{S_{b}}$	Apparent power capacity of alternatives for substations (MVA)
$\overline{S_{i}^{0}}$	Initial apparent power capacity of existing substations (MVA)
T^{AST}	Air temperature in air storage tank (K)

$\overline{T_s^{Ch}}$	Maximum charging time of ESSs at rated power (h)
$\overline{T_s^{Dch}}$	Maximum discharging time of ESSs at rated power (h)
T^{HOT}	Oil temperature in hot oil tank (K)
T^{COT}	Oil temperature in cold oil tank (K)
$T^{HPC,in}$	Inlet air temperature of high pressure compressor (K)
$T^{HPC,out}$	Outlet air temperature of high pressure compressor (K)
$T^{HPT,in}$	Inlet air temperature of high pressure turbine (K)
$T^{HPT,out}$	Outlet air temperature of high pressure turbine (K)
$T^{LPC,in}$	Inlet air temperature of low pressure compressor (K)
$T^{LPC,out}$	Outlet air temperature of low pressure compressor (K)
$T^{LPT,in}$	Inlet air temperature of low pressure turbine (K)
$T^{LPT,out}$	Outlet air temperature of low pressure turbine (K)
$T^{RC,out}$	Outlet air temperature of recuperator (K)
V^{nom}	Nominal voltage of the system (kV)
$\underline{V}$, $\overline{V}$	Lower and upper voltage magnitude limits (kV)
V^{AST}	Volume of air storage tank (m^3)
V^{HOT}	Volume of hot oil tank (m^3)
X_a	Reactance of conductors (Ω/km)
Z_a	Impedance of conductors (Ω/km)
γ^{Air}	Ratio of specific heats of air
$\overline{\Delta V}$	Upper bound of the variable $\Delta V_{ij,t}$
ε^{RC}	Effectiveness of recuperator
ε^{Self}	Self-price elasticity of demand
ε^{Cross}	Cross-price elasticity of demand
η^{G}	Efficiency of generator
η^{M}	Efficiency of motor
η^{LPC}	Isentropic efficiency of low pressure compressor
η^{HPC}	Isentropic efficiency of high pressure compressor
η^{HPT}	Isentropic efficiency of high pressure turbine

η^{LPT} Isentropic efficiency of low pressure turbine

$\tilde{\theta}_{i,t}^{D}$ Fictitious current flow demand of load nodes

κ_{p}^{SM} Penetration level of smart meters

π^{LPC} Pressure ratio of low pressure compressor

π^{HPC} Pressure ratio of high pressure compressor

π^{HPT} Pressure ratio of high pressure turbine

π^{LPT} Pressure ratio of low pressure turbine

ρ^{D} Load power factor

ρ^{GR} Power factor of renewable DGs

ρ^{Oil} Density of heat transfer oil (kg/m^3)

τ^{DinY} Number of days in one year

τ^{HinY} Number of hours in one year

τ^{SinH} Number of seconds in one hour

ϕ^{S} Loss factor of substations

Decision Variables

$f_{ij,a,t}^{F}$, $f_{ij,a,h,t}^{F}$ Square of current flow of feeder sections

$f_{i,t}^{S}$, $f_{i,h,t}^{S}$ Square of current flow provided by substations

$I_{i,s,h,t}^{Ch}$ Charging current of ESSs (kA)

$I_{i,s,h,t}^{Dch}$ Discharging current of ESSs (kA)

$I_{i,h,t}^{D}$ Current flow demand of load nodes (kA)

$I_{i,h,t}^{D,Resp}$ Responsive current flow demand of load nodes (kA)

$I_{i,h,t}^{D,Unresp}$ Unresponsive current flow demand of load nodes (kA)

$I_{i,h,t}^{D,SM}$ Smart meter-equipped portion of current flow demand of load nodes (kA)

$I_{ij,a,t}^{F}$, $I_{ij,a,h,t}^{F}$ Current flow of feeder sections (kA)

$I_{i,g,t}^{GC}$, $I_{i,g,h,t}^{GC}$ Current flow provided by conventional DGs (kA)

$I_{i,g,t}^{GR}$, $I_{i,g,h,t}^{GR}$ Current flow provided by renewable DGs (kA)

$I_{i,t}^{S}$, $I_{i,h,t}^{S}$ Current flow provided by substations (kA)

$m_{i,s,h,t}^{Air,AST}$ Mass of air in air storage tank (kg)

$\dot{m}_{i,s,h,t}^{Air,AST}$	Net air mass flow entering air storage tank (kg/s)
$\dot{m}_{i,s,h,t}^{Air,CT}$	Air mass flow rate in compression train (kg/s)
$\dot{m}_{i,s,h,t}^{Air,ET}$	Air mass flow rate in expansion train (kg/s)
$m_{i,s,h,t}^{Oil,HOT}$	Mass of oil in hot oil tank (kg)
$\dot{m}_{i,s,h,t}^{Oil,HOT}$	Net oil mass flow entering hot oil tank (kg/s)
$\dot{m}_{i,s,h,t}^{Oil,IC}$	Oil mass flow rate in inter-cooler (kg/s)
$\dot{m}_{i,s,h,t}^{Oil,AC}$	Oil mass flow rate in after-cooler (kg/s)
$\dot{m}_{i,s,h,t}^{Oil,PH}$	Oil mass flow rate in pre-heater (kg/s)
$\dot{m}_{i,s,h,t}^{Oil,IH}$	Oil mass flow rate in inter-heater (kg/s)
$p_{i,s,h,t}^{AST}$	Air pressure in the air storage tank (bar)
$P_{i,s,h,t}^{Ch}$	Charging power of ESSs (MW)
$P_{i,s,h,t}^{Dch}$	Discharging power of ESSs (MW)
$P_{i,h,t}^{D}$	Active power demand of load nodes (MW)
$Q_{i,h,t}^{D}$	Reactive power demand of load nodes (MVAR)
$P_{i,h,t}^{D,Resp}$	Responsive active power demand of load nodes (MW)
$P_{i,h,t}^{D,Unresp}$	Unresponsive active power demand of load nodes (MW)
$P_{i,h,t}^{D,SM}$	Smart meter-equipped portion of active power demand of load nodes (MW)
$P_{ij,a,t}^{F}$, $P_{ij,a,h,t}^{F}$	Active power flow of feeder sections (MW)
$Q_{ij,a,t}^{F}$,$Q_{ij,a,h,t}^{F}$	Reactive power flow of feeder sections (MVAR)
$P_{i,g,t}^{GC}$, $P_{i,g,h,t}^{GC}$	Active power generated by conventional DGs (MW)
$Q_{i,g,t}^{GC}$, $Q_{i,g,h,t}^{GC}$	Reactive power generated by conventional DGs (MVAR)
$P_{i,g,t}^{GR}$, $P_{i,g,h,t}^{GR}$	Active power generated by renewable DGs (MW)
$Q_{i,g,t}^{GR}$, $Q_{i,g,h,t}^{GR}$	Reactive power generated by renewable DGs (MVAR)
$P_{i,t}^{S}$, $P_{i,h,t}^{S}$	Active power provided by substations (MW)
$Q_{i,t}^{S}$, $Q_{i,h,t}^{S}$	Reactive power provided by substations (MVAR)
$S_{ij,a,t}^{F}$, $S_{ij,a,h,t}^{F}$	Apparent power flow of feeder sections (MVA)

$S_{i,t}^{S}$, $S_{i,h,t}^{S}$	Apparent power provided by substations (MVA)
$u_{i,t}$, $u_{i,h,t}$	Square of voltage magnitude of nodes
$V_{i,t}$, $V_{i,h,t}$	Voltage magnitude of nodes (kV)
$W_{i,s,h,t}^{LPC}$	Mechanical power consumed by low pressure compressor (MW)
$W_{i,s,h,t}^{HPC}$	Mechanical power consumed by high pressure compressor (MW)
$W_{i,s,h,t}^{HPT}$	Mechanical power generated by high pressure turbine (MW)
$W_{i,s,h,t}^{LPT}$	Mechanical power generated by low pressure turbine (MW)
$x_{i,s,t}^{ES}$	Binary investment variable for installation of ESSs
$x_{ij,a,t}^{FC}$	Binary investment variable for construction of new feeder sections
$x_{ij,a,t}^{FR}$	Binary investment variables for replacement of existing feeder sections
$x_{i,g,t}^{GC}$	Binary investment variable for installation of conventional DGs
$x_{i,g,t}^{GR}$	Binary investment variable for installation of renewable DGs
$x_{i,b,t}^{SC}$	Binary investment variable for construction of new substations
$x_{i,b,t}^{SR}$	Binary investment variable for reinforcement of existing substations
$x_{i,p,t}^{SM}$	Binary investment variable for installation of smart meters
$y_{ij,a,t}$	Binary utilization variable of feeder sections
$z_{i,t}$	Binary utilization variable of transfer nodes
$\Delta V_{ij,t}$, $\Delta V_{ij,h,t}$	Auxiliary variable used for applying Kirchhoff's voltage law to feeder sections
$\tilde{\theta}_{ij,t}^{F}$	Fictitious current flow of feeder sections
$\tilde{\theta}_{i,t}^{S}$	Fictitious current supplied by substations
$\alpha_{i,s,h,t}^{Ch}$	Binary variable indicating charging process of ESSs
$\alpha_{i,s,h,t}^{Dch}$	Binary variable indicating discharging process of ESSs

1. Introduction

1.1 Motivation

Power distribution networks need to be expanded to meet the growing demand in an economic, reliable, and safe manner [1], [2]. In general, the distribution expansion planning (DEP) problem consists of finding the optimal location, size, and time for construction, replacement, or reinforcement of the system equipment such as substations and feeders [3]. These expansion decisions are usually made with the objective of minimizing a specific cost function while taking a set of technical and financial constraints into account [4], [5]. From the viewpoint of planning horizon, the DEP problem can be either single-stage (also called static) or multistage (also known as dynamic). In the single-stage DEP (SDEP) problem, the expansion plans are determined at one single time step in order to meet the demand forecasted for the end of the planning horizon [6]. Whereas, in the multistage DEP (MDEP) problem, the planning period is divided into several stages and, accordingly, the expansion plans are distributed among the specified stages to gradually satisfy the increasing demand [7], [8]. The MDEP problem is more challenging to model and solve due to the correlations and interdependencies among the stages, but its ability to provide better solutions makes it more attractive compared with the SDEP problem. As a result, the focus of this research project is mainly on the MDEP problem.

In recent years, driven by several technical and environmental factors, there has been a growing interest in the concept of active distribution networks (ADNs) [9]. Based on this new concept, traditional passive distribution networks will evolve into modern active ones by employing distributed energy resources (DERs) such as distributed generators (DGs), energy storage systems (ESSs), and demand responsive loads (DRLs), as shown in Figure 1.1. Such a transition from passive to active networks poses serious challenges to distribution system planners. On the one hand, the ability of DGs to directly inject active and reactive powers into the system nodes leads

to bidirectional power flows through the distribution feeders [10]. This issue, if not adequately addressed at the design stage, can adversely affect various operational aspects of ADNs, specifically the reactive power balance and voltage regulation. Therefore, the new context where DGs come into play necessitates the development of a planning methodology which incorporates an accurate network model reflecting realistic operational characteristics of the system. On the other hand, large-scale integration of renewable DGs results in the intermittent and highly volatile nodal power injections [11], [12], and the implementation of demand response programs further complicates the long-term predictability of the load growth [10]. Furthermore, the coordinated operation of DGs, ESSs, and DRLs reduces the peak load and damps the effect of the load growth, which can postpone the need for network reinforcement. These factors introduce a tremendous amount of uncertainty to the planning process of ADNs. As a result, effective approaches must also be devised to properly model the major sources of uncertainty.

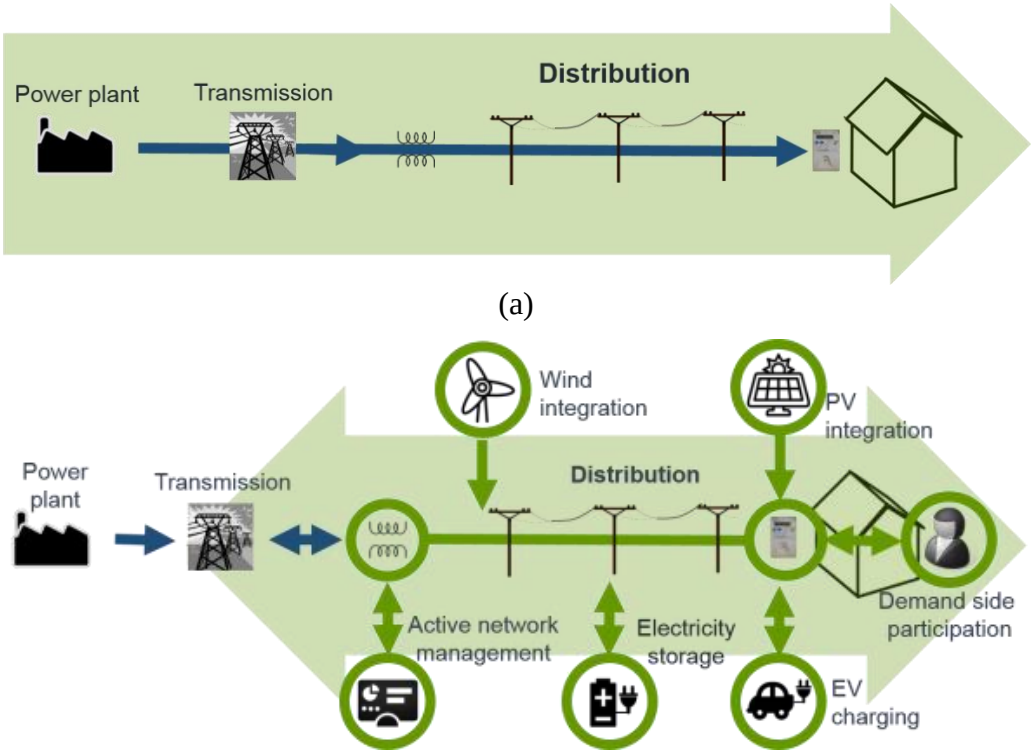

Figure 1.1 Illustration of the passive and active distribution networks [13]: (a) Traditional passive distribution networks; (b) Modern active distribution networks.

Based on the above discussion, it is obvious that obtaining dependable expansion plans for ADNs requires a planning methodology which has two key features:

- **Feature 1:** It should consider an accurate network model representing AC power flow equations and energy losses.
- **Feature 2:** It should adequately account for the uncertainties associated with DERs and loads.

In other words, successful transition from traditional passive distribution networks to modern active ones requires a planning methodology which firstly includes an accurate network model, and secondly accounts for the major sources of uncertainty. However, incorporating these two features into the planning process of ADNs is a very complex task and requires sophisticated mathematical programming techniques that are not currently available in the literature. As a result, this research project aims to develop a planning methodology that is able to jointly expand both the distribution network assets (feeders and substations) and DERs, while giving full consideration to the above-mentioned key features. The final outcome of this research project will be a comprehensive planning tool for ADNs, which is capable of dealing with different DER technologies.

1.2 Literature Review

Over the last few years, many researchers have devoted their attention to modelling the MDEP problem in the context of ADNs [5]. The following presents a careful and thorough review of the current literature from the perspectives of the above-described features, i.e., distribution network modelling, and uncertainty modelling.

1.2.1 Distribution Network Modelling Perspective

From the perspective of distribution network modelling, the existing MDEP models can be categorized into two main groups: 1) nonlinear MDEP models, and 2) linear MDEP models.

1.2.1.1 Nonlinear MDEP Models

The first group of MDEP models precisely reflect the nonlinear characteristics of the network (i.e., AC power flow equations and energy losses), but they are formulated as mixed-integer nonlinear programming (MINLP) problems which are very difficult to solve [1-3], [9], [14-34]. For instance, the authors of [1] propose a profit-based multistage expansion planning model for a

distribution system equipped with automatic voltage and VAR control (AVVC) and automatic fault management (AFM). This model is formulated as an MINLP problem and the genetic algorithm (GA) is employed to solve it. In [3], a nonlinear model is developed to investigate the impacts of large-scale electric vehicle (EV) penetration on the expansion planning of distribution networks, while taking both controlled and uncontrolled EV charging modes into account. The optimal solution of this planning model is also found using the GA. A long-term planning model to determine the optimal location, capacity, and power rating of battery storage units in a distribution network integrated with wind-based DGs is presented in [9]. This nonlinear model, which incorporates AC power flow equations, is solved using a hybrid algorithm based on tabu search (TS) and particle swarm optimization (PSO). The authors of [15] propose an optimization model for the MDEP problem in the presence of DGs, which aims at enhancing the reliability and security levels of distribution networks. This model has a nonlinear formulation involving many local optimums and is solved using a modified version of the PSO algorithm. A nonlinear DG planning framework that considers voltage regulation and energy losses as the key determinant factors of the optimization problem is presented in [16], where the PSO algorithm is utilized to find the optimal solution. In [17], a Pareto-based multi-objective problem formulation subject to AC power flow constraints is proposed to determine the optimal size and location of the utility-operated DG units, where a hybrid evolutionary approach based on the combination of the PSO and shuffled frog-leaping (SFL) algorithms is employed to solve the problem. A multi-objective framework which aims to incorporate the specific reliability requirements of different customers into the expansion planning process of distribution systems is proposed in [23]. This multi-objective optimization problem is solved using the non-dominated sorting genetic algorithm (NSGA) along with a fuzzy decision making approach. The authors of [26] develop an MINLP model for the expansion planning of active distribution systems, while taking the reactive power generation capability of different renewable DG technologies into consideration. The optimal solution of this MINLP model is found by employing a hybrid solution algorithm based on the PSO and ordinal optimization (OO).

As can be seen, the MINLP models are often solved using heuristic methods which not only cannot guarantee obtaining the global optimal solution, but also do not provide a measure of the quality of the obtained solution as they cannot estimate the distance to the global optimum.

1.2.1.2 Linear MDEP Models

To overcome the above-mentioned drawbacks, the second group of MDEP models are presented in the form of mixed-integer linear programming (MILP) problems achieved by eliminating the nonlinearities of the network model [6-8], [11], [12], [35-45] . However, these models also have their own shortcomings. For instance, an MILP model, based on an extension of the linear disjunctive model normally used in the expansion planning of transmission networks, is proposed for the MDEP problem in [7], [8]. This linear model is obtained by making some simplifications such as employing DC power flow equations and ignoring energy losses. Similarly, the authors of [11], [12] propose an MILP model incorporating an adapted version of DC power flow equations, where energy loss and reactive power balance (i.e., the essential factors in any study on ADNs) are entirely neglected. Using these simplified network models may cause the solutions found for the MDEP problem to be optimistic or even deficient. The MILP models presented in [36-38] have a relative advantage over the ones proposed in [7], [8], [11], [12] due to taking the energy losses into account. Nevertheless, they also utilize a variant of DC power flow equations. It is an unquestionable fact that a linear MDEP model will provide dependable expansion plans for ADNs only if it incorporates a complete study of the network operation based on AC power flow equations. This issue has recently attracted the attention of some researchers [6], [35], [40-42]. As an example, the MILP model proposed in [40], [41] employs a linearized version of AC power flow equations to better capture the inherent characteristics of the network. However, the presented linearized network model is obtained by making several error-prone assumptions which adversely affect its correctness. In [6], a more accurate MILP model reflecting AC power flow equations is developed for the MDEP problem, which makes use of a piecewise-based linearization technique to overcome the nonlinearities. Nevertheless, the accuracy of the adopted linearization technique needs to be improved.

To sum up, it can be stated that the MILP models proposed in the literature for the MDEP problem have sacrificed the accuracy of the network model. As a result, these MILP models may lead to optimistic or even deficient expansion plans for ADNs because they fail to conduct a complete and accurate study of the network operation at the planning stage. Based on this fact, it is indispensable to develop new MILP models which not only can overcome the drawbacks of the

MINLP models, but also are able to reflect the operational characteristics of the distribution network in a highly accurate manner.

1.2.2 Uncertainty Modelling Perspective

From the perspective of uncertainty modelling, several different approaches have been utilized in the available literature. These approaches can be categorized into four main groups: 1) deterministic approaches, 2) scenario-based stochastic programming approaches, 3) probabilistic approaches, and 4) robust optimization approaches.

1.2.2.1 Deterministic Approaches

Many of the reported works utilize a deterministic approach in which one or a few certain values are considered for each uncertain parameter [1], [2], [6-8], [14-18], [36], [42], [43], [45], [46]. In [1], [2], [6], for example, the expansion planning studies are conducted by considering one single load level (i.e., the forecasted peak power demand) for each planning stage, without taking the related uncertainties into account. In [7], [8], each planning stage is assumed to have three load levels representing the on-peak, mid-peak, and off-peak parts of a typical load duration curve. In [14-18], all DG units are presumed to be conventional (i.e., no renewable DG units are considered) and the uncertainties associated with loads are completely neglected. In [36], the system demand is characterized by three load levels and the wind power generation is determined based on three given wind speed values that are assumed to remain unchanged during the whole planning horizon. The authors of [42], [45], [46] also consider three deterministic load levels (obtained by multiplying the predicted peak power demand by three certain factors) to model the heavy, medium, and light loading conditions.

The above-mentioned research works have entirely ignored the uncertainties. Such a simplistic approach will obviously result in inaccurate and unreliable solutions for the MDEP problem, especially in the context of ADNs where the network integration of DERs gives rise to a tremendous amount of uncertainty.

1.2.2.2 Scenario-Based Stochastic Programming Approaches

Another group of works adopt a scenario-based stochastic programming (SBSP) approach [10-12], [22], [31], [35], [38-41], [44], [47], [48] which models the uncertainties by defining a finite

number of scenarios for the random variables and finds the optimal solution of the MDEP problem by weighting the objective function of each scenario in proportion to its probability of occurrence. In [11], [12], for example, the historical data of load demand, wind speed, and solar radiation are first split into several blocks based on quarters, working/non-working days, and day/night hours. Each block of historical data is then approximated by a relatively large number of operating conditions obtained by combining different levels of load demand, wind speed, and solar radiation. These operating conditions are finally assigned appropriate probability values and used for implementation of the SBSP approach. In [31], a number of typical daily profiles are considered for the load demand and power outputs of wind-based/solar-based DGs, and then the Latin hypercube sampling (LHS) method is employed to create large series of samples for the load demand and wind/solar generation. A scenario reduction algorithm based on the idea of minimum probabilistic distance is also utilized to reduce the number of generated samples and improve the computational performance of the SBSP approach. In [40], [41], first a simple method is used to create a long series of samples for each of the uncertain parameters (i.e., load demand, wind speed, and solar radiation). After that, in order to better model the uncertainties, two additional series are also generated for each of the uncertain parameters by assuming ±5% deviations from the initially generated series. Then, a standard scenario reduction algorithm based on the k-means clustering method is adopted to shorten the length of the generated series. Finally, different combinations of these series are considered to define the scenarios required by the SBSP approach. The authors of [47] assume that load demand, wind speed, and solar radiation follow certain probability distributions and, based on this assumption, they generate a set of scenarios and make use of the SBSP approach to incorporate the uncertainties into the expansion planning process of ADNs.

Several studies available in the current literature have demonstrated that the SBSP approach is very computationally demanding as it requires a large number of scenarios to precisely describe the uncertainties [49]. For example, in [11], [12] a total number of 1296 operating conditions are defined for each planning stage to model the uncertainties associated with renewable DGs and loads. As another example, the authors of [40], [41] generate a total number of 5400 scenarios to account for different uncertainties. It is obvious that such a large number of scenarios can easily cause the MDEP problem to become intractable, especially when dealing with large-scale distribution systems.

1.2.2.3 Probabilistic Approaches

Probabilistic approaches such as point estimate method (PEM) [9], [50-53], cumulant method [54], and unscented transformation (UT) method [55], [56] have also attracted the attention of many researchers due to their computational tractability. However, the main drawback of these approaches is that they assume the existence of perfect knowledge about the probability distribution functions (PDFs) of random variables, which are very difficult to obtain in practice. In [9], for example, a Gaussian PDF is considered for load demand and a two-point estimate method (2-PEM) is utilized to approximate this PDF by two concentration points located around its mean value. In [26], different PDF types are utilized to characterize the uncertainties associated with wind speed, solar radiation, and load demand. In this regard, a Weibull distribution is employed to describe the wind speed characteristics, the uncertainty in solar radiation is modelled by a Beta distribution, and the random behavior of load demand is described by a truncated Gaussian distribution. The authors of [54] propose a cumulant-based method to model the uncertainties presuming that load demand follows a Gaussian distribution and wind speed has a Weibull distribution. In [56], a UT-based probabilistic approach is employed to model the correlated uncertainties, where load demand and wind speed are both assumed to be Gaussian distributed.

1.2.2.4 Robust Optimization Approaches

Another approach gaining widespread use is the robust optimization (RO) in which a suitable uncertainty space is defined for each uncertain parameter and the optimal solution of the problem is found for the worst-case scenario [57-67]. For instance, the authors of [57] define some polyhedral uncertainty sets for wind and solar power generations as well as load demand, and propose a min-max-min optimization problem whose solution works well for all possible scenarios belonging to the defined uncertainty sets. This complex min-max-min optimization problem is solved using the column-and-constraint generation (CCG) algorithm. In [60], the uncertainties of load demand and renewable generations are included in the planning problem by introducing appropriate uncertainty intervals and developing a max-min optimization problem that finds the optimal solution under worst-case operational conditions. The developed max-min optimization problem is solved using the Benders decomposition algorithm. In [64], a two-stage RO approach is proposed, which assumes that the power outputs of renewable DGs lie within some predefined

uncertainty intervals covering a wide range of scenarios. The duality theory of linear programs is employed to reformulate the proposed two-stage optimization problem as a one-stage problem, and the CCG algorithm is adopted to find the optimal solution under the worst-case scenario of renewable generation.

The RO approach has a low computational demand as opposed to the SBSP approach, and also does not need detailed knowledge about the PDFs of uncertain parameters in contrast to the probabilistic approaches. However, it often leads to over-conservative solutions as it cannot effectively control the degree of conservatism.

1.3 Research Objectives

In light of the above literature review, despite the efforts of previous researchers, it is indispensable to develop a new planning methodology that firstly incorporates an accurate network model reflecting the realistic operational characteristics of distribution system, and secondly accounts for the uncertainties in an efficient manner. Based on this fact, the final objective of this research project is to develop a comprehensive planning methodology for ADNs, which is capable of dealing with different types of DERs (i.e., DGs, ESSs, and DRLs) while giving full consideration to the above-mentioned essential features (i.e., accurate distribution network modelling, and efficient uncertainty modelling). To achieve this objective, five major steps are defined for the project, as described in the following:

- **Step 1:** To develop a deterministic MILP model for integrated expansion planning of distribution network and renewable/conventional DGs. This model will include a highly accurate network model based on a linear format of AC power flow equations, but it will not take the uncertainties into account.
- **Step 2:** To propose a sophisticated uncertainty modelling approach which not only is able to adequately characterize the inherent uncertainties of renewable DGs and loads, but also results in a reasonable computational cost. The already developed deterministic MILP model will be modified to incorporate this uncertainty modelling approach.
- **Step 3:** To devise a fast Benders decomposition-based solution procedure for improving the computational performance. This fast solution procedure will pave the way for effective incorporation of ESSs and DRLs into the developed planning methodology.

- **Step 4:** To model an ESS technology which is appropriate for integration into ADNs. The ESS model will be incorporated into the developed planning methodology considering its short-term operational impacts on the long-term planning studies.
- **Step 5:** To model DRLs and incorporate them into the developed planning methodology. The short-term impacts of DRLs on the long-term expansion planning problem of ADNs will be thoroughly investigated.

As can be seen, the MILP model developed in Step 1 will be gradually evolved, so that Step 5 will yield the final comprehensive planning methodology. To shed light on this point, the logic behind the steps defined for the project is illustrated in Figure 1.2.

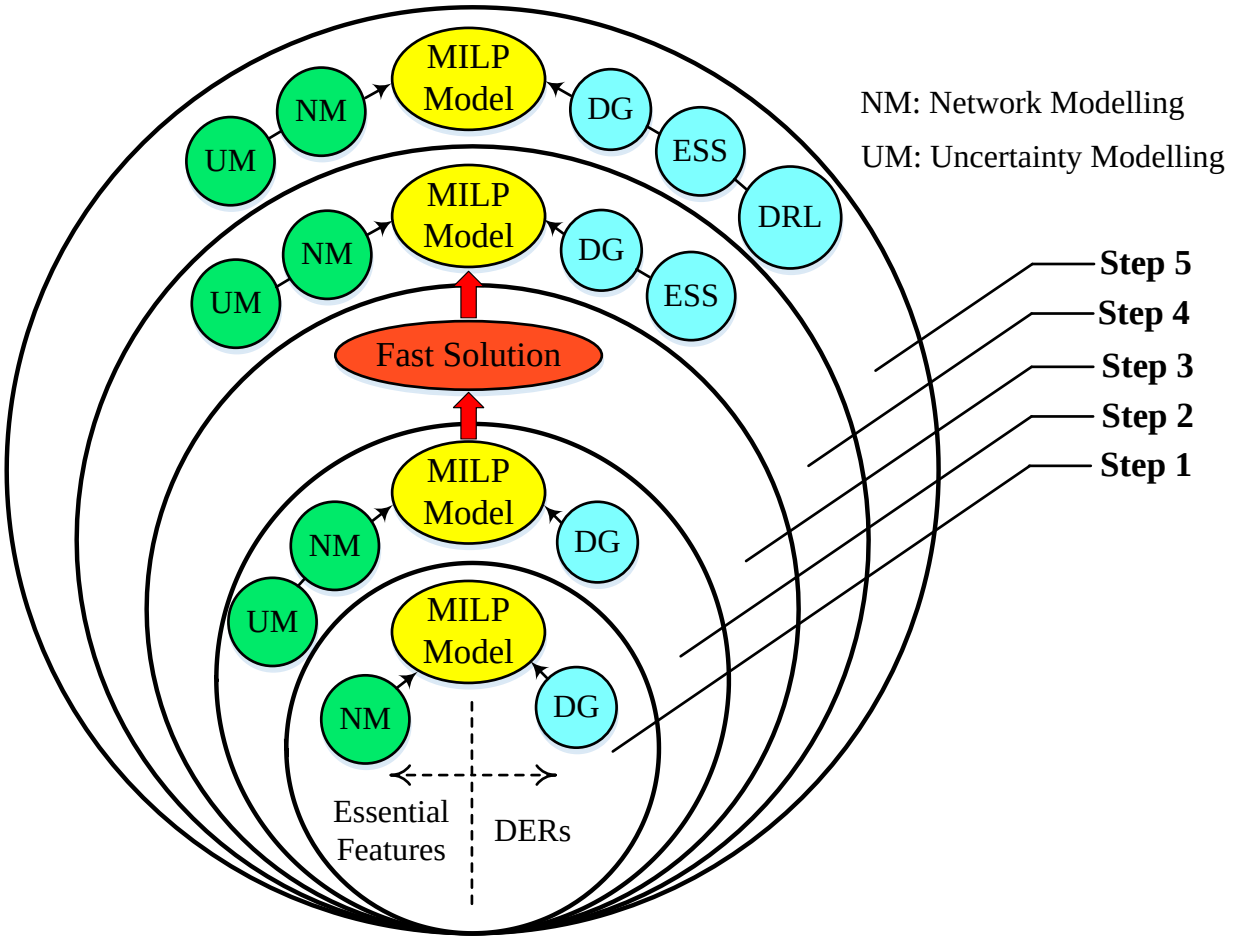

Figure 1.2 Illustration of the logic behind the steps defined for the project.

In order to demonstrate the step-by-step evolution of the project, the above-defined steps are also compared with each other in Table 1.1.

Table 1.1 Comparison of the steps defined for the project

Project Steps	MILP Model for MDEP Problem	Essential Features		Fast Solution Procedure	Incorporated DERs		
		Network Modelling	Uncertainty Modelling		DGs	ESSs	DRLs
Step 1	✓	✓	×	×	✓	×	×
Step 2	✓	✓	✓	×	✓	×	×
Step 3	✓	✓	✓	✓	✓	×	×
Step 4	✓	✓	✓	✓	✓	✓	×
Step 5	✓	✓	✓	✓	✓	✓	✓

1.4 Contributions of the Thesis

All the steps defined in the previous section have been successfully completed. In the following, a summary of the main contributions of different steps of the project is presented.

With regard to Step 1 of the project, first a deterministic non-convex MINLP model is developed for the MDEP problem, which incorporates an accurate network model reflecting the realistic operational characteristics of distribution system. This model provides several expansion alternatives including construction of new feeder sections, replacement of existing feeder sections, construction of new substations, reinforcement of existing substations, and installation of renewable/conventional DGs. After that, with the aim of obtaining a more tractable problem formulation, the developed non-convex MINLP model is converted to a convex mixed-integer second-order conic programming (MISOCP) model by proposing a conic quadratic format for AC power flow equations. Finally, a highly accurate polyhedral-based linearization method [68] is utilized to approximate the conic quadratic constraints with a number of linear constraints. This linearization results in an accurate MILP model for the MDEP problem that is computationally tractable and ensures the optimality of the solution found, while fully incorporating the first essential feature (i.e., accurate distribution network modelling).

With regard to Step 2 of the project, we have employed a chance-constrained programming (CCP) approach which is a powerful technique to control the risk in decision making under uncertainty [69]. In this approach, the uncertainties are handled by defining a number of chance constraints (CCs) which ensure that the constraints subject to uncertainty will be satisfied with a

certain probability level specified by the decision maker. That is, the CCP approach enables the decision maker to effectively adjust the degree of conservatism of the solution by changing a controllable risk parameter incorporated into the CCs. The only difficulty of using the CCP approach is that the CCs, due to their implicit form, are not straightforward to deal with and, hence, need to be reformulated as explicit constraints. In most of the existing research works (such as [70-72]), this reformulation is carried out assuming that the random variables affecting CCs are Gaussian distributed. In practice, however, it is quite unrealistic to make such an assumption. Some other works (such as [73], [74]) do not consider any specific PDFs for random variables, but they propose approximate reformulations (not exact ones) for CCs, which can adversely affect the correctness and dependability of the CCP approach. To address these issues, we have proposed a distributionally robust (DR) reformulation for CCs, which not only is exact, but also does not make any assumption about the uncertainty distributions [75]. To this end, first a moment-based ambiguity set, covering all PDFs whose first two moments lie within its confidence intervals, is constructed. This ambiguity set is then used to derive the DR variants of CCs. After that, using the duality theory of conic linear programming problems [76] and the S-Lemma [77], the DR variants of CCs are equivalently reformulated as a number of explicit nonlinear constraints. Finally, the nonlinear DR reformulations of CCs are expressed in the form of some conic and bilinear constraints which can be linearized using suitable linearization methods. By doing so, a distributionally robust chance-constrained mixed-integer linear programming (DRCC-MILP) model is obtained, which offers four significant advantages: first, it has a low computational demand and provides the opportunity to deal with large-scale distribution systems; second, it requires limited information about the random variables, rather than perfect knowledge of their PDFs; third, it immunizes the expansion plans against the uncertain renewable generations and loads; fourth, it enables the decision maker to effectively control the degree of conservatism of the solution.

With regard to Step 3 of the project, a fast solution procedure based on an accelerated version of the Benders decomposition (BD) algorithm is proposed to solve the MDEP problem. By making use of the BD algorithm, the MDEP problem is partitioned into a master problem and two subproblems, and the optimal solution is found through an iterative process in which multiple feasibility and optimality cuts are generated. Note that the straightforward implementation of the BD algorithm converges very slowly, requiring a huge number of iterations. Therefore, two novel

strategies are also proposed to accelerate the BD algorithm: 1) modification of the master problem, and 2) generation of auxiliary optimality cuts. These acceleration strategies, when used together, not only significantly decrease the number of iterations required to achieve the convergence, but also considerably shorten the time consumed by each iteration. In this way, the performance of the BD algorithm is greatly enhanced and a very fast solution procedure is obtained for the MDEP problem.

With regard to Steps 4 and 5 of the project, a decomposed model based on the accelerated BD algorithm is developed for the MDEP problem, which takes ESSs and DRLs along with renewable/conventional DGs into consideration. The incorporation of ESSs and DRLs into the MDEP problem requires integrating the short-term operation analysis of distribution system into its long-term planning studies. Based on this fact, the developed planning model carries out sequential-time power flow simulation (STPFS) [78], [79] over a series of time slots (e.g., 24 hours) to analyze the short-term operational impacts of ESSs and DRLs when deciding about the long-term expansion plans. A major challenge is that the STPFS calls for simultaneous analysis of a relatively large number of operating states, which causes the MDEP problem to become very computationally demanding or even intractable, especially when dealing with large-scale distribution systems. To achieve the computational speed required for performing STPFS, the fast solution procedure proposed in Step 3 of the project is employed. In this regard, the MDEP problem is decomposed into a master problem which determines the long-term expansion plans and two subproblems which conduct the short-term operation analysis. Regarding ESS modeling, after exploring different technologies that are appropriate for employment in distribution systems, advanced adiabatic compressed air energy storage (AA-CAES) is chosen as the energy storage option due to its lower costs and significantly longer lifetime compared to other technologies [80], and a detailed model is proposed for it. Regarding DRL modelling, an hourly real-time pricing (RTP) scheme is considered and a demand function based on self-price and cross-price elasticities is employed to model the reaction of DRLs to electricity price changes. Furthermore, a new robust optimization-based approach is proposed to model the uncertainties of renewable generations, loads, and electricity prices, which does not have the drawbacks of other RO approaches existing in the literature.

It should be mentioned that in each of the above-described steps, two different test systems (i.e., 24-node and 138-node) are employed to demonstrate the effectiveness of the proposed planning methodology.

1.5 Organization of the Thesis

The remainder of the thesis is organized as follows:

Chapter 2 provides a detailed description of the works done in Step 1 of the project. In this chapter, the uncertainties are ignored and a deterministic MILP model is developed for integrated planning of distribution network and renewable/conventional DGs. This chapter is part of a paper titled "A distributionally robust chance-constrained MILP model for multistage distribution system planning with uncertain renewables and loads", which is published in *IEEE Transactions on Power Systems* (Volume: 33, Issue: 5, Pages: 5248-5262, 2018). As the lead author of this paper, I developed and implemented the MILP model, carried out the simulations, analyzed the results, and wrote the paper. Dr. Junpeng Zhan and Dr. Sherif Omar Faried, as the co-authors of this paper, provided me with valuable comments and suggestions during the development of the MILP model.

Chapter 3 provides a detailed description of the works done in Step 2 of the project. In this chapter, a novel distributionally robust chance-constrained programming (DRCCP) approach is proposed to model the uncertainties of renewable DGs and loads. This chapter is part of a paper titled "A distributionally robust chance-constrained MILP model for multistage distribution system planning with uncertain renewables and loads", which is published in *IEEE Transactions on Power Systems* (Volume: 33, Issue: 5, Pages: 5248-5262, 2018). As the lead author of this paper, I developed and implemented the DRCCP approach, carried out the simulations, analyzed the results, and wrote the paper. Dr. Junpeng Zhan and Dr. Sherif Omar Faried, as the co-authors of this paper, provided me with valuable comments and suggestions during the development of the DRCCP approach.

Chapter 4 provides a detailed description of the works done in Step 3 of the project. In this chapter, a fast solution procedure based on an accelerated version of the BD algorithm is proposed to enhance the computational efficiency of the developed planning methodology. This chapter is part of a paper titled "A robust sequential-time simulation-based decomposed model for

distribution network and DER planning—part I: deterministic formulation", which is going to be submitted to *IEEE Transactions on Power Systems*. As the lead author of this paper, I developed and implemented the accelerated BD algorithm, carried out the simulations, analyzed the results, and wrote the paper. Mr. Benyamin Khorramdel, as the co-author of this paper, assisted me in programming the proposed fast solution procedure in MATLAB software. Moreover, Dr. Sherif Omar Faried, as another co-author of this paper, provided me with valuable comments and suggestions during the preparation of the paper.

Chapter 5 provides a detailed description of the works done in Steps 4 and 5 of the project. In this chapter, a robust decomposed model is developed for integrated expansion planning of distribution network assets (i.e., feeders and substations) and different types of DERs (i.e., DGs, ESSs, and DRLs), which is capable of performing sequential-time simulation (STS). This chapter is part of two papers titled "A robust sequential-time simulation-based decomposed model for distribution network and DER planning—part I: deterministic formulation" and "A robust sequential-time simulation-based decomposed model for distribution network and DER planning—part II: uncertainty modelling and numerical analysis", which are going to be submitted to *IEEE Transactions on Power Systems*. As the lead author of these papers, I developed and implemented the robust STS-based planning model, carried out the simulations, analyzed the results, and wrote the papers. Mr. Benyamin Khorramdel and Dr. Sherif Omar Faried, as the co-authors of these papers, provided me with helpful comments and suggestions during the preparation of the papers.

Chapter 6 presents the concluding remarks of the thesis.

2. A Deterministic MILP Model for Integrated Planning of Distribution Network and Distributed Generation

2.1 Introduction

In this chapter, the uncertainties are ignored and a deterministic mathematical formulation is proposed for the MDEP problem. To this end, first a non-convex MINLP model is developed. This model is then changed to a convex MISOCP model by employing an exact relaxation technique. Finally, using a highly accurate linearization method, the convex MISOCP model is converted to an MILP model. The key advantage of the proposed MILP model is that it can be solved using standard off-the-shelf mathematical programming solvers (e.g., branch-and-cut algorithm) which not only guarantee convergence to the global optimal solution, but also provide a measure of the distance to the global optimum during the solution process.

2.2 Non-Convex MINLP Model Developed for the MDEP Problem

This model, which is partly based on the models described in [6] and [36], provides several expansion alternatives (construction/replacement of feeder sections, construction/reinforcement of substations, and installation of renewable/conventional DGs), while minimizing the total investment and operation costs and taking all the necessary constraints into account.

2.2.1 Objective Function

The optimization aims at minimizing the present value of the costs distributed through time, as given in (2.1), (2.2), and (2.3).

Minimize $c = c^{Inv.} + c^{Oper.}$ (2.1)

$$c^{Inv.} = \sum_{t\in\Omega^T} \frac{1}{(1+r)^{(t-1)D}} \Big[\sum_{(ij)\in\Omega^{FR}} \sum_{a\in\left(\Omega^a - a_{ij}^{FR}\right)} c_a^{FR} l_{ij} x_{ij,a,t}^{FR} + \sum_{(ij)\in\Omega^{FC}} \sum_{a\in\Omega^a} c_a^{FC} l_{ij} x_{ij,a,t}^{FC}$$

$$+ \sum_{i\in\Omega^{SR}} \sum_{b\in\Omega^b} c_b^{SR} x_{i,b,t}^{SR} + \sum_{i\in\Omega^{SC}} \sum_{b\in\Omega^b} c_b^{SC} x_{i,b,t}^{SC} + \sum_{i\in\left(\Omega^{NG}\cap\Omega_t^{NL}\right)} \sum_{g\in\Omega^{gr}} c_g^{GR} x_{i,g,t}^{GR}$$

$$+ \sum_{i\in\left(\Omega^{NG}\cap\Omega_t^{NL}\right)} \sum_{g\in\Omega^{gc}} c_g^{GC} x_{i,g,t}^{GC} \Big] \tag{2.2}$$

$$c^{Oper.} = \sum_{t\in\Omega^T} \frac{1}{(1+r)^{(t-1)D}} \frac{(1+r)^D - 1}{r(1+r)^D} \Big[\sum_{i\in\Omega^S} \tau^{HinY} c^E P_{i,t}^S + \sum_{i\in\Omega^s} \tau^{HinY} c^E \phi^S f_{i,t}^S$$

$$+ \sum_{i\in\left(\Omega^{NG}\cap\Omega_t^{NL}\right)} \sum_{g\in\Omega^{gc}} \tau^{HinY} c_g^{EGC} P_{i,g,t}^{GC} \Big] \tag{2.3}$$

The objective function is comprised of two parts. In (2.2), $c^{Inv.}$ represents the present value of the investment costs required for replacement of existing feeder sections, construction of new feeder sections, reinforcement of existing substations, construction of new substations, and installation of renewable/conventional DGs. In (2.3), $c^{Oper.}$ represents the present value of the system operation costs including cost of electrical energy received from the upstream power grid, operation costs of substations, and generation costs of conventional DGs. In (2.3), $c^{Oper.}$ also includes the costs of energy losses in feeder sections; this is because the active power received from the upstream grid (i.e., $P_{i,t}^S$) includes the power losses in feeder sections as well.

In the above objective function, the decision variables are $x_{ij,a,t}^{FR}$, $x_{ij,a,t}^{FC}$, $x_{i,b,t}^{SR}$, $x_{i,b,t}^{SC}$, $x_{i,g,t}^{GR}$, $x_{i,g,t}^{GC}$, $P_{i,t}^S$, $f_{i,t}^S$, and $P_{i,g,t}^{GC}$. In this regard, $x_{ij,a,t}^{FR}$ is the binary investment variable for replacement of existing feeder sections; $x_{ij,a,t}^{FC}$ is the binary investment variable for construction of new feeder sections; $x_{i,b,t}^{SR}$ is the binary investment variable for reinforcement of existing substations; $x_{i,b,t}^{SC}$ is the binary investment variable for construction of new substations; $x_{i,g,t}^{GR}$ is the binary investment variable for installation of renewable DGs; $x_{i,g,t}^{GC}$ is the binary investment variable for installation of conventional DGs; $P_{i,t}^S$ is the active power provided by substations; $f_{i,t}^S$ is square of the current flow provided by substations; and $P_{i,g,t}^{GC}$ is the active power generated by conventional DGs. Note that the planning horizon is divided into a number of planning stages with known duration (e.g., one year), and the index "t" is used to indicate the decision variables associated with each planning stage. For example, $x_{ij,a,t}^{FC} = 1$ means that feeder section ij with conductor type a is constructed at planning stage t. By contrast, $x_{ij,a,t}^{FC} = 0$ means that feeder section ij with conductor type a is

not constructed at planning stage t. That is, the index "t" is used to determine the optimal time for addition of new equipment to the system. Moreover, it is worthwhile to mention that in (2.2), $\frac{1}{(1+r)^{(t-1)D}}$ is employed to calculate the present value of the investment costs associated with planning stage t. Similarly, in (2.3), $\frac{1}{(1+r)^{(t-1)D}}\frac{(1+r)^{D}-1}{r(1+r)^{D}}$ is used to calculate the present value of the operation costs related to planning stage t.

2.2.2 Technical and Operational Constraints

The constraints of the MDEP problem can be categorized into four main groups: 1) power flow equations, 2) voltage, current, and capacity limits, 3) constraints on binary investment and utilization variables, and 4) radiality constraints.

2.2.2.1 Power Flow Equations

Constraints (2.4)-(2.14) represent the AC power flow model in a radial distribution network based on a set of recursive equations called *DistFlow branch equations* [6], [81]. More specifically, constraints (2.4) and (2.5) ensure the active and reactive power balances in system nodes. Constraints (2.6)-(2.8) relate the active, reactive, and apparent power flows and the current flow of a feeder section to the voltages of its sending and receiving ends. These three constraints are somehow applying the Kirchhoff's voltage law (KVL) to each feeder section. Note that $\Delta V_{ij,t}$ is an auxiliary variable which gets a zero value if feeder section ij is utilized to connect nodes i and j, otherwise it will have a positive/negative value corresponding to the difference between variables $u_{i,t}$ and $u_{j,t}$. In other words, when feeder section ij is operated, the voltage magnitude difference between nodes i and j will be represented by the first part of the right-hand side of (2.6), and hence $\Delta V_{ij,t}$ should have a value of zero. However, when feeder section ij is not operated, the first part of the right-hand side of (2.6) is equal to zero and consequently $\Delta V_{ij,t}$ should have a nonzero value to represent the voltage magnitude difference between nodes i and j. Constraints (2.9)-(2.12), which actually complement constraints (2.7) and (2.8), are employed based on the fact that each feeder section uses only one of the candidate conductor types at each planning stage. Constraints (2.13) and (2.14) relate the active, reactive, and apparent power flows provided by a substation to its current flow and voltage magnitude.

It should be noted that *DistFlow branch equations* are an exact representation of AC power flow equations. A proof of this exactness is given in Appendix A.

$$\sum_{(ki)\in\Omega^F}\sum_{a\in\Omega^a}\left[P^F_{ki,a,t}-R_a l_{ki} f^F_{ki,a,t}\right]-\sum_{(ij)\in\Omega^F}\sum_{a\in\Omega^a}P^F_{ij,a,t}+P^S_{i,t}+\sum_{g\in\Omega^{gc}}P^{GC}_{i,g,t}$$

$$+\sum_{g\in\Omega^{gr}}P^{GR}_{i,g,t}=\overline{\overline{P^D_{i,t}}} \qquad \forall i\in\Omega^N,\forall t\in\Omega^T \tag{2.4}$$

$$\sum_{(ki)\in\Omega^F}\sum_{a\in\Omega^a}\left[Q^F_{ki,a,t}-X_a l_{ki} f^F_{ki,a,t}\right]-\sum_{(ij)\in\Omega^F}\sum_{a\in\Omega^a}Q^F_{ij,a,t}+Q^S_{i,t}+\sum_{g\in\Omega^{gc}}Q^{GC}_{i,g,t}$$

$$+\sum_{g\in\Omega^{gr}}Q^{GR}_{i,g,t}=\overline{\overline{Q^D_{i,t}}} \qquad \forall i\in\Omega^N,\forall t\in\Omega^T \tag{2.5}$$

$$u_{i,t}-u_{j,t}=\sum_{a\in\Omega^a}\left[2\left(R_a l_{ij}P^F_{ij,a,t}+X_a l_{ij}Q^F_{ij,a,t}\right)-\left(Z_a l_{ij}\right)^2 f^F_{ij,a,t}\right]+\Delta V_{ij,t}$$

$$\forall(ij)\in\Omega^F,\forall t\in\Omega^T \tag{2.6}$$

$$u_{i,t}\hat{f}^F_{ij,t}=\left(\hat{S}^F_{ij,t}\right)^2 \qquad \forall(ij)\in\Omega^F,\forall t\in\Omega^T \tag{2.7}$$

$$\left(\hat{S}^F_{ij,t}\right)^2=\left(\hat{P}^F_{ij,t}\right)^2+\left(\hat{Q}^F_{ij,t}\right)^2 \qquad \forall(ij)\in\Omega^F,\forall t\in\Omega^T \tag{2.8}$$

$$\hat{f}^F_{ij,t}=\sum_{a\in\Omega^a}f^F_{ij,a,t} \qquad \forall(ij)\in\Omega^F,\forall t\in\Omega^T \tag{2.9}$$

$$\hat{P}^F_{ij,t}=\sum_{a\in\Omega^a}P^F_{ij,a,t} \qquad \forall(ij)\in\Omega^F,\forall t\in\Omega^T \tag{2.10}$$

$$\hat{Q}^F_{ij,t}=\sum_{a\in\Omega^a}Q^F_{ij,a,t} \qquad \forall(ij)\in\Omega^F,\forall t\in\Omega^T \tag{2.11}$$

$$\hat{S}^F_{ij,t}=\sum_{a\in\Omega^a}S^F_{ij,a,t} \qquad \forall(ij)\in\Omega^F,\forall t\in\Omega^T \tag{2.12}$$

$$u_{i,t}f^S_{i,t}=\left(S^S_{i,t}\right)^2 \qquad \forall i\in\Omega^S,\forall t\in\Omega^T \tag{2.13}$$

$$\left(S^S_{i,t}\right)^2=\left(P^S_{i,t}\right)^2+\left(Q^S_{i,t}\right)^2 \qquad \forall i\in\Omega^S,\forall t\in\Omega^T \tag{2.14}$$

2.2.2.2 Voltage, Current, and Capacity Limits

Constraint (2.15) determines the acceptable range of the nodal voltage magnitudes. Constraint (2.16) represents the limits on the current flows of feeder sections based on the conductor types used for constructing them. This constraint also makes sure that the current flows assigned to the feeder sections which are not operated (i.e., feeder sections with $y_{ij,a,t}=0$) are equal to zero. Constraint (2.17) sets appropriate bounds on the variable $\Delta V_{ij,t}$ and also causes it to have a zero

value for operated feeder sections (i.e., feeder sections with $y_{ij,a,t} = 1$). Constraints (2.18) and (2.19) cause the apparent power provided by each substation to be less than its installed capacity. Constraints (2.20) and (2.21) limit the active and reactive powers generated by conventional DGs. Constraints (2.22) and (2.23) set the active and reactive power generations of renewable DGs equal to their expected values. Note that renewable DGs are assumed to be operated at a constant power factor (ρ^{GR}) as they often lack the ability to provide controlled reactive power.

$$\left(\underline{V}\right)^2 \leq u_{i,t} \leq \left(\overline{V}\right)^2 \qquad \forall i \in \Omega^N, \forall t \in \Omega^T \qquad (2.15)$$

$$f_{ij,a,t}^F \leq \left(\overline{I_a}\right)^2 y_{ij,a,t} \qquad \forall (ij) \in \Omega^F, a \in \Omega^a, \forall t \in \Omega^T \qquad (2.16)$$

$$\left|\Delta V_{ij,t}\right| \leq \overline{\Delta V}\left(1 - \sum_{a \in \Omega^a} y_{ij,a,t}\right) \qquad \forall (ij) \in \Omega^F, \forall t \in \Omega^T \qquad (2.17)$$

$$S_{i,t}^S \leq \overline{S_i^0} + \sum_{v=1}^{t} \sum_{b \in \Omega^b} \overline{S_b}\, x_{i,b,v}^{SR} \qquad \forall i \in \Omega^{SR}, \forall t \in \Omega^T \qquad (2.18)$$

$$S_{i,t}^S \leq \sum_{v=1}^{t} \sum_{b \in \Omega^b} \overline{S_b}\, x_{i,b,v}^{SC} \qquad \forall i \in \Omega^{SC}, \forall t \in \Omega^T \qquad (2.19)$$

$$P_{i,g,t}^{GC} \leq \sum_{v=1}^{t} \overline{P_g^{GC}} x_{i,g,v}^{GC} \qquad \forall i \in (\Omega^{NG} \cap \Omega_t^{NL}), g \in \Omega^{gc}, \forall t \in \Omega^T \qquad (2.20)$$

$$\left|Q_{i,g,t}^{GC}\right| \leq \sum_{v=1}^{t} \overline{Q_g^{GC}}\, x_{i,g,v}^{GC} \qquad \forall i \in (\Omega^{NG} \cap \Omega_t^{NL}), g \in \Omega^{gc}, \forall t \in \Omega^T \qquad (2.21)$$

$$P_{i,g,t}^{GR} = \sum_{v=1}^{t} \overline{\overline{P_g^{GR}}} x_{i,g,v}^{GR} \qquad \forall i \in (\Omega^{NG} \cap \Omega_t^{NL}), g \in \Omega^{gr}, \forall t \in \Omega^T \qquad (2.22)$$

$$Q_{i,g,t}^{GR} = \sum_{v=1}^{t} \tan\left(\cos^{-1}(\rho^{GR})\right) \overline{\overline{P_g^{GR}}} x_{i,g,v}^{GR} \qquad \forall i \in (\Omega^{NG} \cap \Omega_t^{NL}), g \in \Omega^{gr}, \forall t \in \Omega^T \qquad (2.23)$$

2.2.2.3 Constraints on Binary Investment and Utilization Variables

Constraints (2.24)-(2.27) ensure that a maximum of one construction or reinforcement is performed for each feeder section or substation during the planning horizon. Constraint (2.28) limits the number DG installations at each candidate node to one. Constraints (2.29) and (2.30) specify the maximum number of renewable and conventional DGs that can be installed in the system during the planning horizon. Constraints (2.31)-(2.35) address the operating conditions of different feeder section categories including existing irreplaceable feeder sections, existing replaceable feeder sections, and candidate feeder sections for construction. In this regard, $y_{ij,a,t}$ is equal to one if its corresponding feeder section is operated, otherwise it will be equal to zero. In

fact, imposing these constraints on the utilization variables denoted by "y" guarantees that a feeder section with a specific conductor type can be used only if its corresponding investment has already been made.

$$\sum_{t\in\Omega^T}\sum_{a\in\Omega^a} x_{ij,a,t}^{FC} \le 1 \qquad \forall (ij)\in\Omega^{FC} \tag{2.24}$$

$$\sum_{t\in\Omega^T}\sum_{a\in\left(\Omega^a - a_{ij}^{FR}\right)} x_{ij,a,t}^{FR} \le 1 \qquad \forall (ij)\in\Omega^{FR} \tag{2.25}$$

$$\sum_{t\in\Omega^T}\sum_{b\in\Omega^b} x_{i,b,t}^{SC} \le 1 \qquad \forall i\in\Omega^{SC} \tag{2.26}$$

$$\sum_{t\in\Omega^T}\sum_{b\in\Omega^b} x_{i,b,t}^{SR} \le 1 \qquad \forall i\in\Omega^{SR} \tag{2.27}$$

$$\sum_{t\in\Omega^T}\sum_{g\in\Omega^{gc}} x_{i,g,t}^{GC} + \sum_{t\in\Omega^T}\sum_{g\in\Omega^{gr}} x_{i,g,t}^{GR} \le 1 \qquad \forall i\in\Omega^{NG} \tag{2.28}$$

$$\sum_{t\in\Omega^T}\sum_{i\in\left(\Omega^{NG}\cap\Omega_t^{NL}\right)}\sum_{g\in\Omega^{gr}} x_{i,g,t}^{GR} \le \overline{N^{GR}} \tag{2.29}$$

$$\sum_{t\in\Omega^T}\sum_{i\in\left(\Omega^{NG}\cap\Omega_t^{NL}\right)}\sum_{g\in\Omega^{gc}} x_{i,g,t}^{GC} \le \overline{N^{GC}} \tag{2.30}$$

$$y_{ij,a,t} \le \sum_{v=1}^{t} x_{ij,a,v}^{FR} \qquad \forall (ij)\in\Omega^{FR}, \forall a\in\left(\Omega^a - a_{ij}^{FR}\right), \forall t\in\Omega^T \tag{2.31}$$

$$y_{ij,a,t} \le 1 - \sum_{v=1}^{t}\sum_{\omega\in\left(\Omega^a - a_{ij}^{FR}\right)} x_{ij,\omega,v}^{FR} \qquad \forall (ij)\in\Omega^{FR}, \forall a = a_{ij}^{FR}, \forall t\in\Omega^T \tag{2.32}$$

$$y_{ij,a,t} = 0 \qquad \forall (ij)\in\Omega^{FI}, \forall a\in\left(\Omega^a - a_{ij}^{FI}\right), \forall t\in\Omega^T \tag{2.33}$$

$$y_{ij,a,t} \le 1 \qquad \forall (ij)\in\Omega^{FI}, \forall a = a_{ij}^{FI}, \forall t\in\Omega^T \tag{2.34}$$

$$y_{ij,a,t} \le \sum_{v=1}^{t} x_{ij,a,v}^{FC} \qquad \forall (ij)\in\Omega^{FC}, \forall a\in\Omega^a, \forall t\in\Omega^T \tag{2.35}$$

2.2.2.4 Radiality Constraints

Constraints (2.36)-(2.44) guarantee the radiality of the distribution network [36], [82]. When DGs are not considered as expansion alternatives, constraints (2.36)-(2.39) are enough to ensure the radiality. However, when DGs are brought into play, constraints (2.40)-(2.44) should also be considered in order to prevent the existence of areas exclusively supplied by DGs. These constraints assign fictitious current flow demands to the candidate nodes for DG installation and, in this way, keep them connected to the substations to preclude formation of isolated areas (see [36]). Another important point is that the distribution system is here assumed to include a number

of so-called "transfer nodes" at some of the planning stages [82]. These nodes are not connected to the loads or substations, but they can be used to connect different load nodes to each other and, in this way, may help to find better planning solutions. The binary variables denoted by "z" indicate the operating conditions of the transfer nodes. In this regard, $z_{i,t}$ will be equal to one if its corresponding transfer node is utilized, otherwise it will be equal to zero.

$$\sum_{(ij)\in\Omega^F}\sum_{a\in\Omega^a} y_{ij,a,t} = |\Omega^N| - |\Omega^{NS}| - \sum_{i\in\Omega_t^{NT}}\left(1 - z_{i,t}\right) \quad \forall t \in \Omega^T \tag{2.36}$$

$$\sum_{(ki)\in\Omega^F}\sum_{a\in\Omega^a} y_{ki,a,t} + \sum_{(ij)\in\Omega^F}\sum_{a\in\Omega^a} y_{ij,a,t} \geq 2z_{i,t} \qquad \forall i \in \Omega_t^{NT}, \forall t \in \Omega^T \tag{2.37}$$

$$\sum_{a\in\Omega^a} y_{ki,a,t} \leq z_{i,t} \qquad \forall (ki) \in \Omega^F, \forall i \in \Omega_t^{NT}, \forall t \in \Omega^T \tag{2.38}$$

$$\sum_{a\in\Omega^a} y_{ij,a,t} \leq z_{i,t} \qquad \forall (ij) \in \Omega^F, \forall i \in \Omega_t^{NT}, \forall t \in \Omega^T \tag{2.39}$$

$$\sum_{(ki)\in\Omega^F} \tilde{\theta}_{ki,t}^F - \sum_{(ij)\in\Omega^F} \tilde{\theta}_{ij,t}^F + \tilde{\theta}_{i,t}^S = \tilde{\theta}_{i,t}^D \quad \forall i \in \Omega^N, \forall t \in \Omega^T \tag{2.40}$$

$$0 \leq \tilde{\theta}_{ij,t}^F \leq |\Omega^{NG}| \sum_{a\in\Omega^a} y_{ij,a,t} \qquad \forall (ij) \in \Omega^F, \forall t \in \Omega^T \tag{2.41}$$

$$0 \leq \tilde{\theta}_{i,t}^S \leq |\Omega^{NG}| \qquad \forall i \in \Omega^{SR}, \forall t \in \Omega^T \tag{2.42}$$

$$0 \leq \tilde{\theta}_{i,t}^S \leq |\Omega^{NG}|\left(\sum_{v=1}^{t}\sum_{b\in\Omega^b} x_{i,b,v}^{SC}\right) \qquad \forall i \in \Omega^{SC}, \forall t \in \Omega^T \tag{2.43}$$

$$\tilde{\theta}_{i,t}^D = \begin{cases} 1 & \forall i \in (\Omega^{NG} \cap \Omega_t^{NL}), \forall t \in \Omega^T \\ 0 & \forall i \notin (\Omega^{NG} \cap \Omega_t^{NL}), \forall t \in \Omega^T \end{cases} \tag{2.44}$$

2.3 Convex MISOCP Model Proposed for the MDEP Problem

Although the above-described model well reflects the essential characteristics of the MDEP problem, it is a non-convex MINLP model which not only is very difficult to solve, but also cannot guarantee obtaining the global optimal solution. To overcome these drawbacks, it should be changed to a convex model.

The non-convexity of the model arises from (2.7), (2.8), (2.13), and (2.14). In order to convexify the model, first the objective function should be modified in the following manner:

$$c = c^{Inv.} + c^{Oper.} + c^{Conv.} \tag{2.45}$$

$$c^{Conv.} = \partial\left[\sum_{t\in\Omega^T}\sum_{(ij)\in\Omega^F} \hat{S}_{ij,t}^F + \sum_{t\in\Omega^T}\sum_{i\in\Omega^S} S_{i,t}^S\right] \tag{2.46}$$

The main purpose of this modification is to add positive multiples of the variables $\hat{S}^F_{ij,t}$ and $S^S_{i,t}$ to the objective function. Accordingly, ∂ is a positive coefficient that can be set to a small value. Considering the modified objective function, convexity can now be obtained by relaxing the equality constraints (2.7), (2.8), (2.13), and (2.14) as follows:

$$\left(\hat{S}^F_{ij,t}\right)^2 \geq \left(\hat{P}^F_{ij,t}\right)^2 + \left(\hat{Q}^F_{ij,t}\right)^2 \qquad \forall (ij) \in \Omega^F, \forall t \in \Omega^T \tag{2.47}$$

$$\left(S^S_{i,t}\right)^2 \geq \left(P^S_{i,t}\right)^2 + \left(Q^S_{i,t}\right)^2 \qquad \forall i \in \Omega^S, \forall t \in \Omega^T \tag{2.48}$$

$$u_{i,t}\hat{f}^F_{ij,t} \geq \left(\hat{S}^F_{ij,t}\right)^2 \qquad \forall (ij) \in \Omega^F, \forall t \in \Omega^T \tag{2.49}$$

$$u_{i,t}f^S_{i,t} \geq \left(S^S_{i,t}\right)^2 \qquad \forall i \in \Omega^S, \forall t \in \Omega^T \tag{2.50}$$

It should be noted that the above relaxation technique is exact and hence the inequality constraints (2.47)-(2.50) act exactly as equality constraints. The detailed proof of the exactness of this relaxation technique can be found in [83]. Based on [83], the proposed relaxation technique will be exact if: 1) the network is radial; and 2) the objective function is strictly increasing with respect to $\hat{S}^F_{ij,t}$, $S^S_{i,t}$, $\hat{f}^F_{ij,t}$, and $f^S_{i,t}$, which appear on the left-hand sides of (2.47)-(2.50), respectively. It is obvious that the first condition is fully satisfied because the radiality constraints force the network to be always radial. However, in order to satisfy the second condition, the objective function should contain positive multiples of $\hat{S}^F_{ij,t}$, $S^S_{i,t}$, $\hat{f}^F_{ij,t}$, and $f^S_{i,t}$. A carful look at the objective function reveals that it already includes positive multiples of $\hat{f}^F_{ij,t}$ and $f^S_{i,t}$, but it does not contain $\hat{S}^F_{ij,t}$ and $S^S_{i,t}$. Therefore, the new component (2.46) is included in the objective function to make it strictly increasing with respect to $\hat{S}^F_{ij,t}$ and $S^S_{i,t}$, as required by the second condition. In this way, both of the above conditions are satisfied and the exactness of the proposed relaxation technique is ensured.

Using the above relaxation technique, the resultant MDEP problem is now a convex MISOCP model which, in contrast to the initial non-convex MINLP model, is tractable and ensures obtaining the global optimal solution. However, it is still computationally demanding due to the nonlinearities of (2.47)-(2.50). Therefore, these four constraints should also be linearized.

2.4 Polyhedral-Based MILP Model Proposed for the MDEP Problem

As the first step to overcome the nonlinearities, (2.47) and (2.48) are rewritten in the following manner:

$$\hat{S}_{ij,t}^{F} \geq \sqrt{\left(\hat{P}_{ij,t}^{F}\right)^{2} + \left(\hat{Q}_{ij,t}^{F}\right)^{2}} \qquad \forall (ij) \in \Omega^{F}, \forall t \in \Omega^{T} \tag{2.51}$$

$$S_{i,t}^{S} \geq \sqrt{\left(P_{i,t}^{S}\right)^{2} + \left(Q_{i,t}^{S}\right)^{2}} \qquad \forall i \in \Omega^{S}, \forall t \in \Omega^{T} \tag{2.52}$$

On the other hand, the left-hand sides of (2.49) and (2.50) can be expressed as follows:

$$u_{i,t}\hat{f}_{ij,t}^{F} = \left[\left(u_{i,t} + \hat{f}_{ij,t}^{F}\right)/2\right]^{2} - \left[\left(u_{i,t} - \hat{f}_{ij,t}^{F}\right)/2\right]^{2} \tag{2.53}$$

$$u_{i,t}f_{i,t}^{S} = \left[\left(u_{i,t} + f_{i,t}^{S}\right)/2\right]^{2} - \left[\left(u_{i,t} - f_{i,t}^{S}\right)/2\right]^{2} \tag{2.54}$$

As a result, (2.49) and (2.50) can also be written as:

$$\left[\left(u_{i,t} + \hat{f}_{ij,t}^{F}\right)/2\right] \geq \sqrt{\left[\left(u_{i,t} - \hat{f}_{ij,t}^{F}\right)/2\right]^{2} + \left(\hat{S}_{ij,t}^{F}\right)^{2}} \quad \forall (ij) \epsilon \Omega^{F}, \forall t \epsilon \Omega^{T} \tag{2.55}$$

$$\left[\left(u_{i,t} + f_{i,t}^{S}\right)/2\right] \geq \sqrt{\left[\left(u_{i,t} - f_{i,t}^{S}\right)/2\right]^{2} + \left(S_{i,t}^{S}\right)^{2}} \qquad \forall i \epsilon \Omega^{S}, \forall t \epsilon \Omega^{T} \tag{2.56}$$

In this way, (2.47)-(2.50) are respectively represented as the second-order conic constraints (2.51), (2.52), (2.55), and (2.56) which all have the following form:

$$x_3 \geq \sqrt{(x_1)^2 + (x_2)^2} \tag{2.57}$$

Using a highly accurate method based on polyhedral approximation, the second-order conic constraint (2.57) can be approximated by a system of linear equalities and inequalities which are expressed in terms of x_1, x_2, x_3, and a number of auxiliary variables (i.e., ξ_ℓ and η_ℓ) [68]:

$$\begin{cases} \xi_\ell \geq |x_1| \\ \eta_\ell \geq |x_2| \end{cases} \qquad \forall \ell = 0 \tag{2.58}$$

$$\begin{cases} \xi_\ell = \xi_{\ell-1}\cos\left(\frac{\pi}{2^{\ell+1}}\right) + \eta_{\ell-1}\sin\left(\frac{\pi}{2^{\ell+1}}\right) \\ \eta_\ell \geq \left|-\xi_{\ell-1}\sin\left(\frac{\pi}{2^{\ell+1}}\right) + \eta_{\ell-1}\cos\left(\frac{\pi}{2^{\ell+1}}\right)\right| \end{cases} \quad \forall \ell = 1, \dots, \mathcal{L} \tag{2.59}$$

$$\begin{cases}\xi_\ell \le x_3 \\ \eta_\ell \le \xi_\ell \tan\left(\frac{\pi}{2^{\ell+1}}\right)\end{cases} \qquad \forall \ell = \mathcal{L} \tag{2.60}$$

Note that $\mathcal{L}$ is a parameter that determines the number of additional constraints and variables required to linearize (2.57), and the linearization error will decrease as this parameter increases. In [68], it is proved that the set of linear constraints (2.58)-(2.60) approximate (2.57) in such a way that:

$$x_3(1+\varrho) \ge \sqrt{(x_1)^2 + (x_2)^2} \tag{2.61}$$

where ϱ is dependent on $\mathcal{L}$ and can be calculated as follows:

$$\varrho = \left[1/\cos\left(\frac{\pi}{2^{\mathcal{L}+1}}\right)\right] - 1 \tag{2.62}$$

It is obvious that choosing an appropriate value for $\mathcal{L}$ will result in a highly accurate approximation. Table 2.1 shows the approximation errors associated with different values of $\mathcal{L}$. As an example, choosing $\mathcal{L} = 8$ leads to $\varrho = 1.88 \times 10^{-5}$, which demonstrates the high accuracy of the polyhedral approximation.

Table 2.1 Approximation errors associated with different values of $\mathcal{L}$.

$\mathcal{L}$	2	3	4	5	6	7	8
ϱ	0.0824	0.0196	0.0048	0.0012	3.01×10^{-4}	7.53×10^{-5}	1.88×10^{-5}

In a similar manner, each of the conic quadratic constraints (2.51), (2.52), (2.55), and (2.56) can also be replaced by the polyhedral approximation represented by (2.58)-(2.60). This causes the MISOCP model to be converted to an MILP one.

2.5 Simulation Results and Discussion

In this section, the most important results obtained from the implementation of the proposed MILP model are presented and discussed. This model has been implemented on a PC with a 3.40 GHz Intel Core i7-4770 processor and 16 GB of RAM using MATLAB R2015a [84] and CPLEX 12.6.1 [85].

2.5.1 Test System Description

A 24-node distribution system, based on [36], is utilized to carry out the simulations. Figure 2.1 shows the one-line diagram of this test system. As can be seen, the system consists of 4 substations (2 existing ones with reinforcement possibility and 2 candidate ones), 20 load nodes, and 33 feeder sections (2 existing replaceable ones, 2 existing irreplaceable ones, and 29 candidate ones).

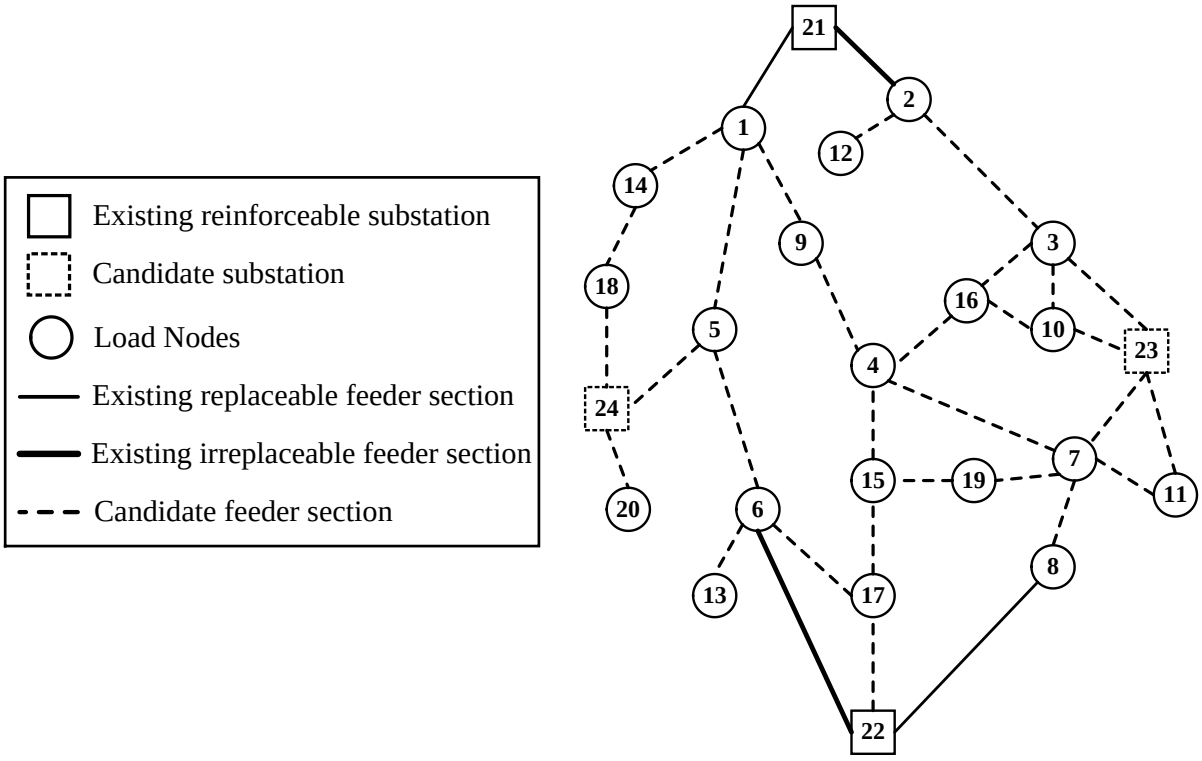

Figure 2.1 One-line diagram of the 24-node distribution system.

Table 2.2 shows the data related to candidate conductor types considered for replacement and construction of feeder sections. The existing reinforceable substations located at nodes 21 and 22 are both assumed to have the initial apparent power capacities of 7.5 MVA. Moreover, two alternatives are proposed for reinforcement and construction of substations, as shown in Table 2.3.

Table 2.2 Data related to candidate conductor types.

Ω^a	R_a (Ω/km)	X_a (Ω/km)	$\overline{I_a}$ (A)	c_a^{FR} (US$/km)	c_a^{FC} (US$/km)
1	0.342	0.387	260	19000	25000
2	0.202	0.204	410	30000	36000

Table 2.3 Data related to alternatives for substation reinforcement/construction.

Ω^b	$\overline{S_b}$ (MVA)	c_b^{SR} (US$)	c_b^{SC} (US$)
1	12	750000	790000
2	15	950000	1000000

The data related to the alternatives for installation of renewable and conventional DGs are given in Tables 2.4 and 2.5, respectively. Furthermore, the set of candidate nodes for DG installation is defined as $\Omega^{NG} = \{ 1, 2, 3, 4, 5, 7, 9, 13, 14, 15, 16, 17, 18, 19 \}$.

Table 2.4 Data related to alternatives for installation of renewable DGs.

Ω^{gr}	$\overline{P_g^{GR}}$ (MW)	c_g^{GR} (US$)
1	1	450000
2	2	850000

Table 2.5 Data related to alternatives for installation of conventional DGs.

Ω^{gc}	$\overline{P_g^{GC}}$ (MW)	c_g^{GC} (US$)	c_g^{EGC} (US$/MWh)
1	1	350000	45
2	2	650000	45

Table 2.6 presents the nodal power demands at different stages of the planning horizon. The data related to the lengths of feeder sections are given in Table 2.7.

Table 2.6 Nodal power demands at different planning stages (MVA).

Nodes	Stages		Nodes	Stages	
	1	2		1	2
1	4.05	5.42	11	0	2.8
2	0.78	1.21	12	0	1.29
3	2.58	3.98	13	0	1.87
4	0.32	2.43	14	0	3.16
5	0.28	0.47	15	0	1.62

6	1.17	1.81	16	0	1.22
7	4.04	4.36	17	0	2.4
8	0.72	0.94	18	0	2.1
9	1.14	1.77	19	0	1.81
10	1.56	2.4	20	0	3.79

Table 2.7 Lengths of feeder sections (km).

Sections		l_{ij}	Sections		l_{ij}	Sections		l_{ij}
i	j		i	j		i	j	
1	5	2.22	4	9	1.2	7	23	0.9
1	9	1.2	4	15	1.6	8	22	1.9
1	14	1.2	4	16	1.3	10	16	1.6
1	21	2.2	5	6	2.4	10	23	1.3
2	3	2	5	24	0.7	11	23	1.6
2	12	1.1	6	13	1.2	14	18	1
2	21	1.7	6	17	2.2	15	17	1.2
3	10	1.1	6	22	2.7	15	19	0.8
3	16	1.2	7	8	2	17	22	1.5
3	23	1.2	7	11	1.1	18	24	1.5
4	7	2.6	7	19	1.2	20	24	0.9

For all load nodes, the power factor is set to 0.9. Other required data are given in Table 2.8.

Table 2.8 Other required data.

Parameters	Values	Parameters	Values
V^{nom}	20 (kV)	r	0.1
$\underline{V}$	0.95× V^{nom} = 19 (kV)	D	1 (year)
$\overline{V}$	1.05×V^{nom}=21 (kV)	a_{ij}^{FR}	1
$\overline{\Delta V}$	$\left(\overline{V}\right)^2 - \left(\underline{V}\right)^2$= 80	a_{ij}^{FI}	2
c^E	85 (US$/MWh)	ϕ^S	0.15
$\overline{N^{GC}}$	4	ρ^{GR}	0.9
$\overline{N^{GR}}$	4	$\overline{\overline{P_g^{GR}}}$	0.45× $\overline{P_g^{GR}}$

2.5.2 A Discussion on the Accuracy and Computation Time of the Proposed MILP Model

A comparative analysis is here conducted to assess the performance of the proposed MILP model from the aspects of accuracy and computational efficiency. The logic behind this comparative analysis is illustrated in Figure 2.2.

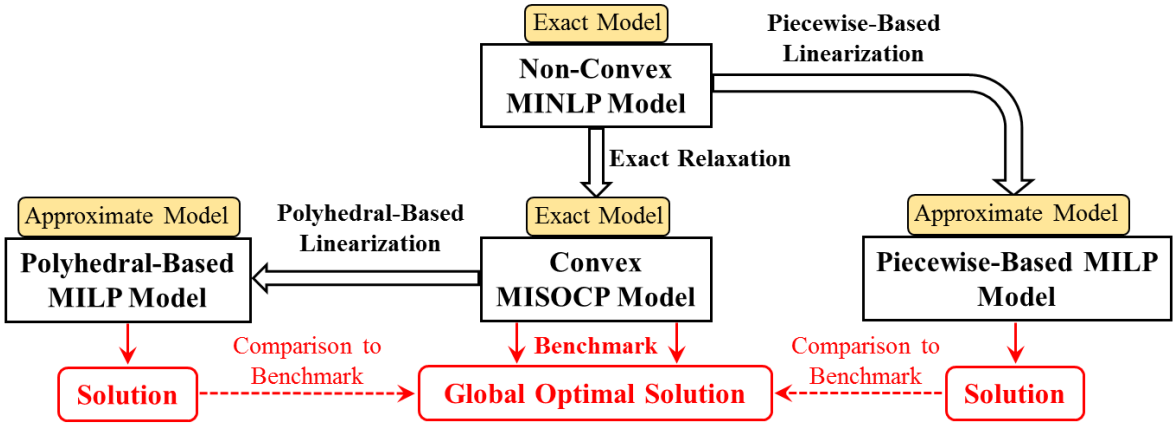

Figure 2.2 Illustration of the logic behind the conducted comparative analysis.

As previously discussed in Section 2.3, the developed MISOCP model is exact and does not involve any approximations. Based on this fact, we have used the MISOCP model as a benchmark against which the approximate MILP models can be compared. In this regard, first the MISOCP model is solved and the global optimal solution of the problem is found. This solution is then used as a benchmark for assessing the solution quality of two different approximate MILP models: 1) our proposed polyhedral-based MILP model; and 2) a piecewise-based MILP model presented in [6]. Note that the main reason for choosing the model presented in [6] is that it is the most accurate MILP model existing in the literature.

The optimal expansion plans obtained by solving the MISOCP model are depicted in Figure 2.3. The investment, operation, and total costs associated with these expansion plans are US$6,699,691, US$31,892,808, and US$38,592,499, respectively. The MISOCP model, in spite of its ability to find the global optimal solution of the MDEP problem, is time-consuming and requires 182 min to be solved. This fact demonstrates the necessity of introducing an MILP model which is able to significantly improve the computational efficiency.

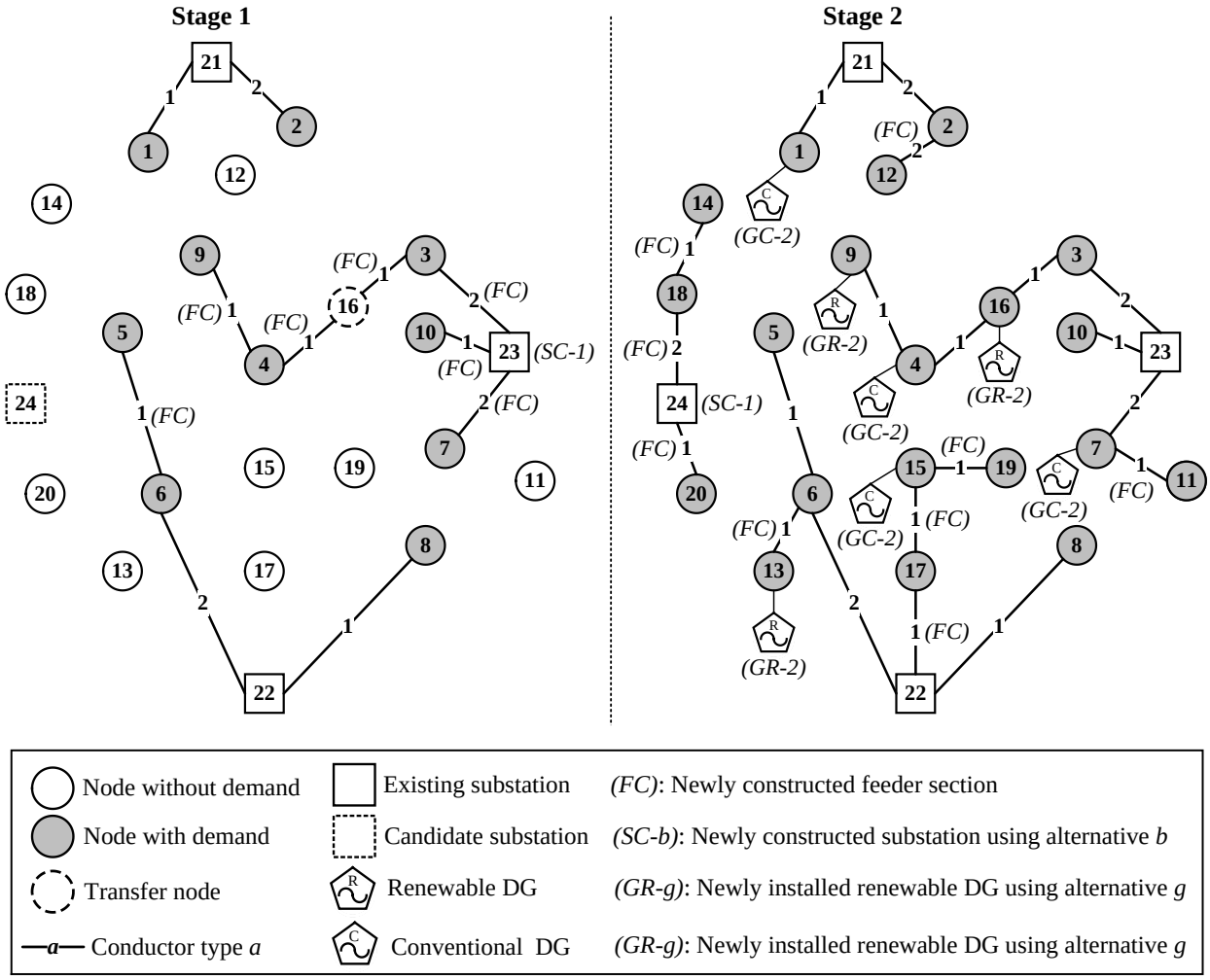

Figure 2.3 Expansion plans obtained for the 24-node distribution system by solving the MISOCP model.

Table 2.9 compares our proposed polyhedral-based MILP model with the piecewise-based MILP model presented in [6] from the accuracy and computation time perspectives. Note that the errors presented in this table, in fact, indicate the amount by which the solutions of the MILP models deviate from the global optimal solution found by the MISOCP model. These errors are calculated as follows:

$$Error = \frac{c^{MILP} - c^{MISOCP}}{c^{MISOCP}} \times 100\% \tag{2.63}$$

where c^{MILP} denotes the costs associated with the MILP models; c^{MISOCP} denotes the costs associated with the MISOCP model; and $Error$ is the percent error.

Table 2.9 Comparison of the performances of the polyhedral-based and piecewise-based MILP models for the 24-node distribution system.

MILP models	Linearization parameter ($\mathcal{L}$)	Errors in different costs (%)			Computation Time (min)
		Investment	Operation	Total	
Polyhedral-based	3	2.91	1.47	0.71	4.5
	4	1.83	0.98	0.49	5
	5	0.35	0.62	0.45	8
	6	0.00	0.34	0.28	9.5
	7	0.00	0.05	0.04	12
	8	**0.00**	**0.01**	**0.01**	**15**
Piecewise-based	10	3.62	2.34	2.56	3
	20	2.54	1.24	1.47	4
	30	1.97	0.93	1.11	6.5
	40	1.97	1.08	1.23	10
	50	1.97	1.26	1.38	13
	60	1.97	0.99	1.16	14.5
	70	**1.97**	**1.15**	**1.29**	**17**

As can be seen, the accuracy of the piecewise-based model cannot be improved beyond a certain level, even if the linearization parameter is set to large values such as 60 and 70. Whereas, the polyhedral-based model is capable of reaching extremely high degrees of accuracy, so that setting the linearization parameter to 8 results in the accuracies of 100%, 99.99%, and 99.99% for the investment, operation, and total costs, respectively. On the other hand, by investigating the results shown in Table 2.9, it can be realized that after spending almost the same amount of computation time on both models, the polyhedral-based model provides better solutions. For instance, as shown in the bold rows of the table, when a computation time of 15 min is spent on the polyhedral-based model, the errors in the investment, operation, and total costs are notably lower than the case in which 17 min is spent on the piecewise-based model. These facts prove the superiority of the polyhedral-based model over the piecewise-based one. Moreover, it is obvious that our proposed MILP model is able to provide the same solution as the MISOCP model, while its required computation time is around 12 times shorter than that of the MISOCP model. Given the presented results, it can concluded that the proposed MILP model has a great performance in deterministic expansion planning studies of ADNs.

2.5.3 Demonstration of the Scalability of the Proposed MILP Model

A 138-node distribution system, based on [36], is here employed to demonstrate the scalability of the proposed MILP model. This test system, as shown in Figure 2.4, consists of 3 substations (2 existing ones with reinforcement possibility and 1 candidate one), 135 load nodes, and 151 feeder sections (12 existing replaceable ones, 88 existing irreplaceable ones, and 51 candidate ones). The candidate conductor types for replacement and construction of feeder sections, and the alternatives for reinforcement and construction of substations are the same as those presented in Tables 2.2 and 2.3. The existing reinforceable substations located at nodes 136 and 137 are both assumed to have the initial apparent power capacities of 12 MVA. The set of candidate nodes for DG installation is defined as $\Omega^{NG} = \{$ 4, 10, 19, 25, 28, 31, 42, 52, 56, 64, 68, 72, 78, 85, 94, 97, 100, 103, 106, 108, 111, 116, 120, 122, 126, 133 $\}$. The data related to the alternatives for installation of renewable and conventional DGs are the same as those presented in Tables 2.4 and 2.5. The nodal power demands at different stages of the planning horizon and the lengths of feeder sections can be found in Appendix B. For all load nodes, the power factor is assumed to be equal to 0.9. Other required data are the same as those given in Table 2.8, except that the nominal voltage of the system is 13.8 kV (i.e., V^{nom}=13.8 kV, $\underline{V}$=0.95×V^{nom}=13.11 kV, $\overline{V}$=1.05×V^{nom}=14.49 kV, and $\overline{\Delta V}$=$\left(\overline{V}\right)^2 - \left(\underline{V}\right)^2$=38.08).

The simulation results show that for the linearization parameter of $\mathcal{L}$=8, the proposed MILP model consumes a computation time of 83 min to find the optimal expansion plans of the 138-node distribution system. It is obvious that the model is solved within a very reasonable computation time. This fact demonstrates another outstanding merit of the proposed MILP model, i.e., its ability to deal with the MDEP problem of large distribution systems in a computationally efficient manner.

The expansion plans obtained by solving the proposed MILP model are tabulated in Table 2.10. The numbers shown in brackets denote the conductor types used for construction/replacement of feeder sections, the alternatives utilized for construction/reinforcement of substations, and the alternatives chosen for installation of renewable/conventional DGs. The investment, operation, and total costs associated with these expansion plans are US$7,785,341, US$39,787,373, US$47,572,714, respectively.

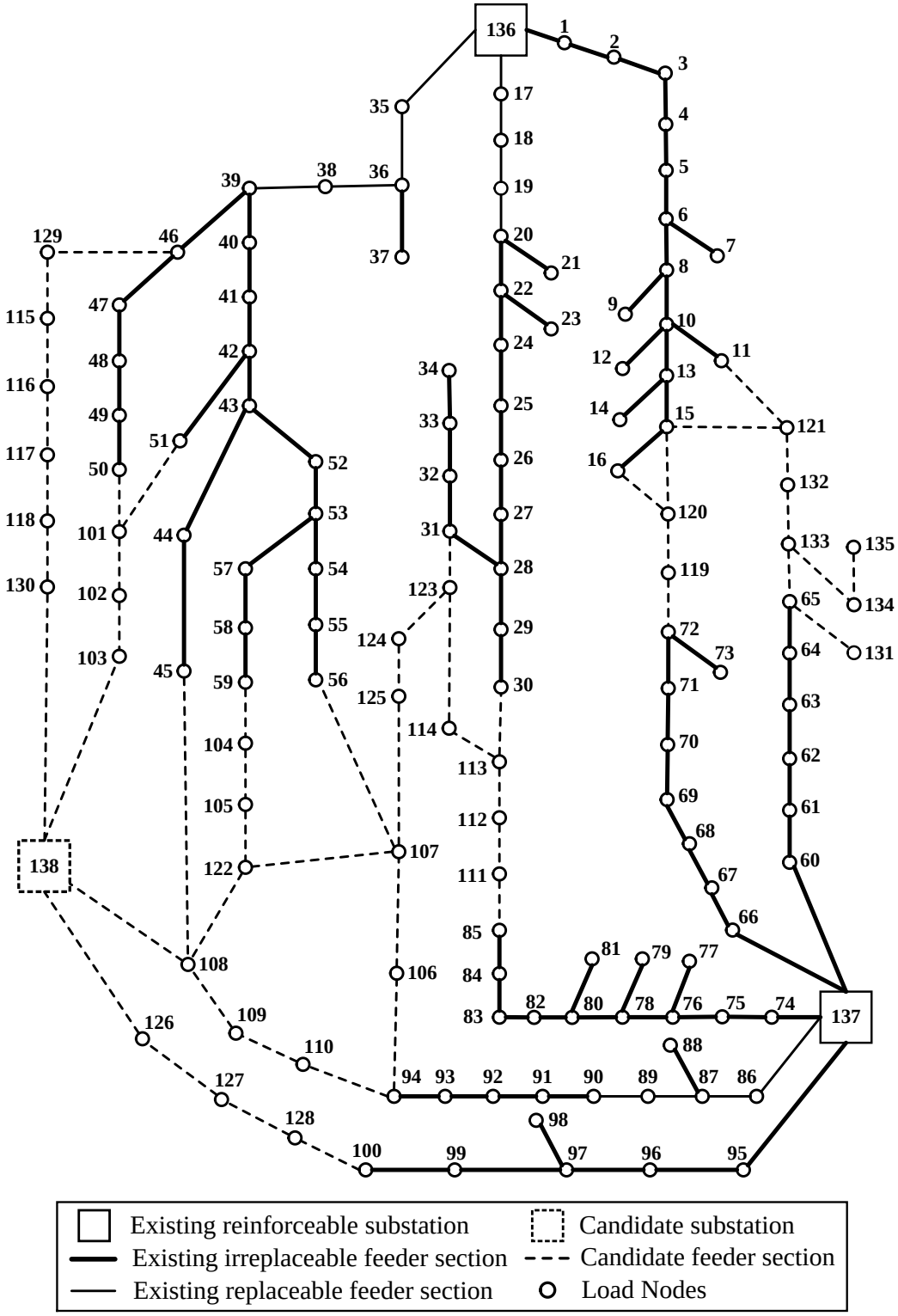

Figure 2.4 One-line diagram of the 138-node distribution system.

Table 2.10 Expansion plans obtained for the 138-node distribution system by solving the proposed MILP model.

Expansion plans	Planning stages							
	1				2			
Feeder section construction	106-107 (1)	103-102 (1)	111-112 (1)	130-118 (1)				
	108-109 (1)	138-103 (1)	112-113 (1)	120-119 (1)				
	108-122 (1)	105-104 (1)	113-114 (2)	138-130 (1)				
	109-110 (1)	122-105 (1)	114-123 (1)	123-31 (1)				
	126-127 (1)	138-108 (2)	123-124 (1)	104-59 (2)				
	127-128 (1)	121-15 (1)	124-125 (1)	119-72 (1)				
	138-126 (2)	108-45 (1)	133-134 (1)	16-120 (1)				
	133-132 (1)	101-50 (2)	134-135 (1)	46-129 (2)				
	128-100 (1)	65-133 (1)	116-115 (1)	65-131 (1)				
	102-101 (2)	94-106 (1)	117-116 (1)	85-111 (1)				
	132-121 (1)		118-117 (1)					
Feeder section replacement	17-18 (2)	86-87 (2)	136-35 (2)					
	18-19 (2)	136-17 (2)						
	19-20 (2)	137-86 (2)						
Substation construction	138 (1)				–			
Substation reinforcement	–				–			
Renewable DG installation	28 (2)				72 (2)	100 (1)	108 (2)	
Conventional DG installation	–				10 (1)	85 (1)	133 (2)	
Transfer node	121	122	126	127	–			
	128	132	133					

The optimal topologies of the 138-node distribution system at different stages of the planning horizon are also depicted in Figure 2.5. As can be observed, the multistage planning approach has yielded a different system topology at each planning stage. This fact shows the greater flexibility of the multistage planning approach in reducing the total costs through the appropriate utilization of resources, when compared to the static planning method.

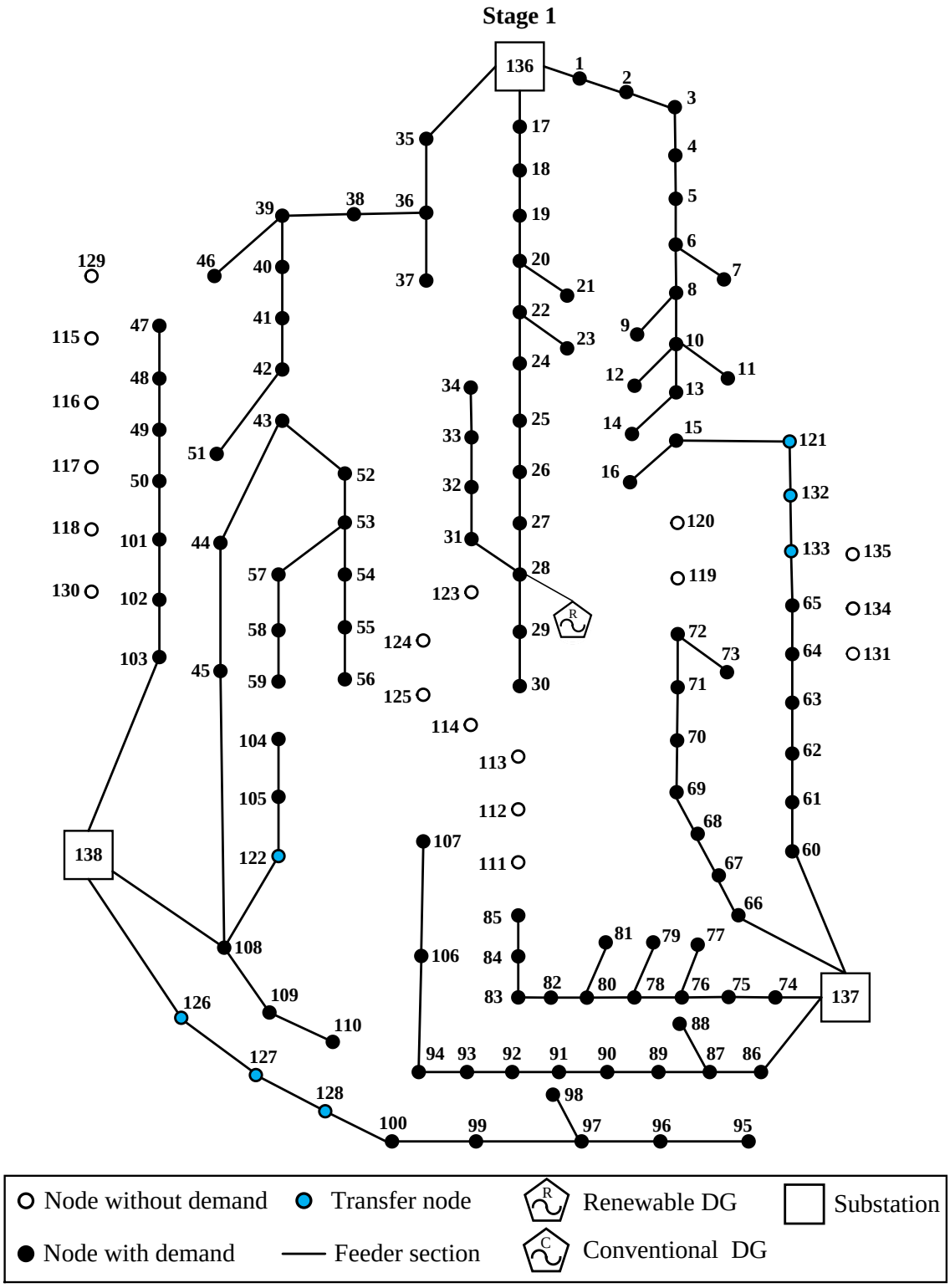
Stage 1
136
137
138
R
C
Node without demand
Transfer node
Renewable DG
Substation
Node with demand
Feeder section
Conventional DG

(a)

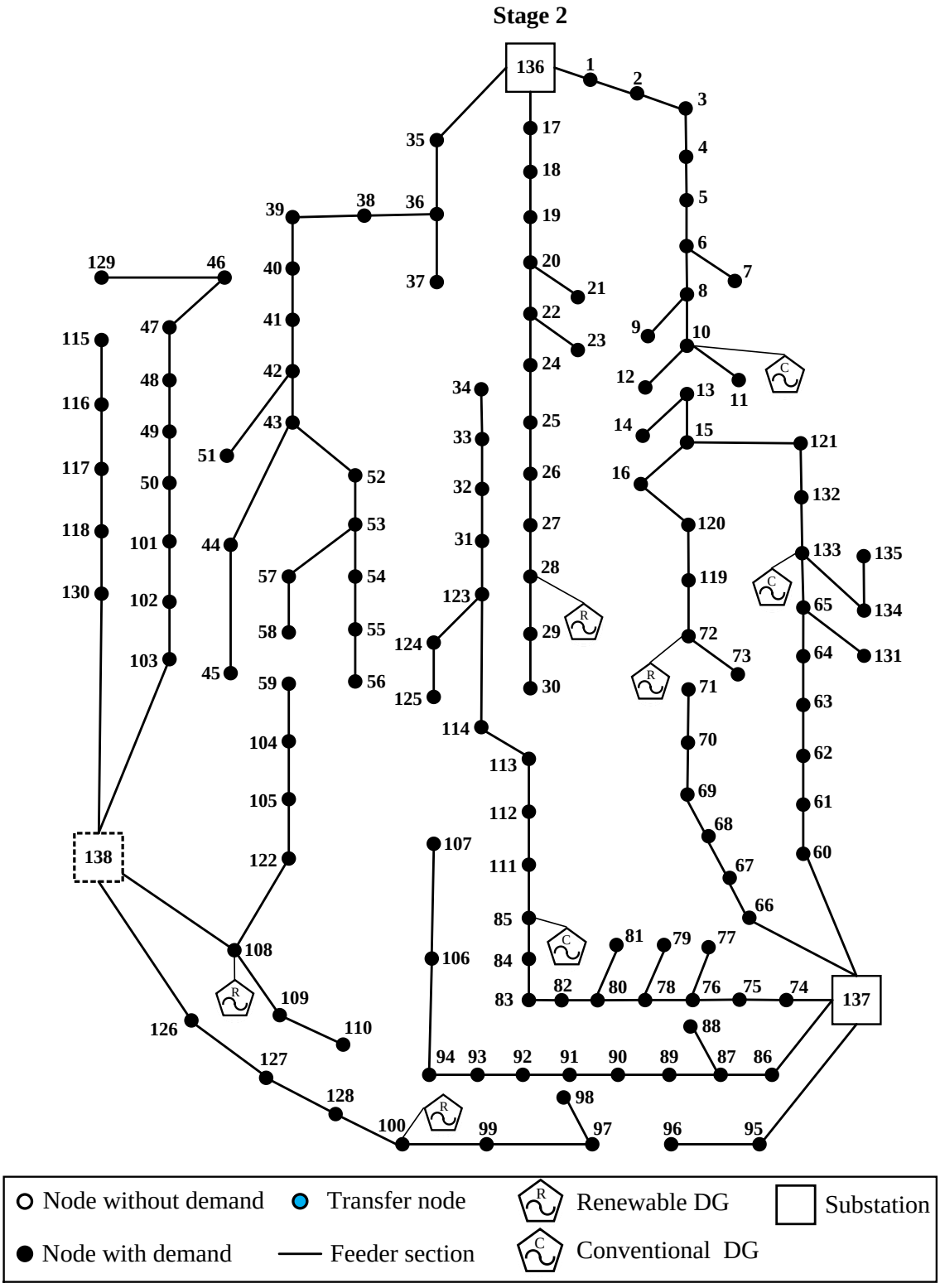

(b)

Figure 2.5 Optimal topologies obtained for the 138-node distribution system by solving the proposed MILP model: (a) Planning stage 1; (b) Planning stage 2.

2.6 Summary

In this chapter, a novel MILP model has been proposed for the MDEP problem, which is able to jointly expand both the network assets (i.e., feeders and substations) and renewable/conventional DGs. This MILP model has two outstanding merits: first, it incorporates a highly accurate linearized network model reflecting AC power flow equations and energy losses; second, its linear formulation ensures the computational tractability and solution optimality. Note that a highly accurate polyhedral-based linearization method has been utilized to eliminate the nonlinearities of the MDEP problem.

The proposed planning methodology has been successfully validated using two different distribution systems (24-node and 138-node). The simulation results show that the MILP model developed in this chapter is able to provide better solutions than the most accurate MILP model available in the literature, while both models consume almost the same amounts of computation time. This superiority is due to the great performance of the polyhedral-based linearization method, so that the accuracy of this method can go up to almost 100% by choosing an appropriate value for the linearization parameter. The simulation results also demonstrate the ability of the developed MILP model to deal with the MDEP problem of large distribution systems in a computationally efficient manner.

As previously discussed, careful consideration of the major sources of uncertainty is of crucial importance in the MDEP problem of ADNs. To address this issue, in the next chapter, an efficient approach is proposed to model the uncertainties associated with renewable DGs and loads.

3. A Distributionally Robust Chance-Constrained Programming Approach to Model the Uncertainties of Renewables and Loads

3.1 Introduction

In this chapter, by employing a chance-constrained programming (CCP) approach, the deterministic MILP model developed in Chapter 2 is modified to incorporate the uncertainties of renewable DGs and loads. In this regard, first a number of chance constraints (CCs) are added to the model to guarantee that the constraints subject to uncertainty will be satisfied with a certain probability level. After that, as the probability distribution functions (PDFs) of uncertain parameters are not perfectly known, a distributionally robust (DR) reformulation is proposed for the CCs, which guarantees the robustness of the expansion plans against all uncertainty distributions defined within a moment-based ambiguity set. Finally, effective linearization techniques are devised to eliminate the nonlinearities of the DR reformulation proposed for the CCs.

By doing the above, a distributionally robust chance-constrained mixed-integer linear programming (DRCC-MILP) model is obtained, which offers four significant advantages: first, it has a low computational demand and provides the opportunity to deal with large-scale distribution systems; second, it requires limited information about the random variables, rather than perfect knowledge of their PDFs; third, it immunizes the expansion plans against the uncertain renewable generations and loads; fourth, it enables the decision maker to effectively control the degree of conservatism of the solution. These properties make the proposed DRCC-MILP model highly applicable for the expansion planning of ADNs, especially when long-term data about the uncertain parameters are difficult to acquire.

3.2 Chance Constraints

Taking a careful look at the model developed in the previous chapter reveals that the uncertainties of renewable DGs and loads mainly affect constraints (2.4) and (2.5) which represent the active and reactive power balances. Based on this fact, with the help of two random variables ($\widetilde{\chi^{GR}}$ and $\widetilde{\chi^{D}}$) defined to characterize the stochasticity of renewable generations and loads, constraints (2.4) and (2.5) are changed to the following CCs:

$$\mathbb{P}\Big\{\sum_{(ki)\in\Omega^F}\sum_{a\in\Omega^a}\big[P^F_{ki,a,t}-R_a l_{ki} f^F_{ki,a,t}\big]-\sum_{(ij)\in\Omega^F}\sum_{a\in\Omega^a}P^F_{ij,a,t}+P^S_{i,t}+\sum_{g\in\Omega^{gc}}P^{GC}_{i,g,t}$$

$$+\Big(\sum_{g\in\Omega^{gr}}P^{GR}_{i,g,t}\Big)\widetilde{\chi^{GR}}\geq\overline{\overline{P^D_{i,t}}}\,\widetilde{\chi^{D}}\Big\}\geq 1-\epsilon \qquad \forall i\in\Omega^N,\forall t\in\Omega^T \tag{3.1}$$

$$\mathbb{P}\Big\{\sum_{(ki)\in\Omega^F}\sum_{a\in\Omega^a}\big[Q^F_{ki,a,t}-X_a l_{ki} f^F_{ki,a,t}\big]-\sum_{(ij)\in\Omega^F}\sum_{a\in\Omega^a}Q^F_{ij,a,t}+Q^S_{i,t}+\sum_{g\in\Omega^{gc}}Q^{GC}_{i,g,t}$$

$$+\Big(\sum_{g\in\Omega^{gr}}Q^{GR}_{i,g,t}\Big)\widetilde{\chi^{GR}}\geq\overline{\overline{Q^D_{i,t}}}\,\widetilde{\chi^{D}}\Big\}\geq 1-\epsilon \qquad \forall i\in\Omega^N,\forall t\in\Omega^T \tag{3.2}$$

In fact, these CCs ensure that the active and reactive power balance constraints are satisfied with a probability of at least $1-\epsilon$, where ϵ is a controllable risk parameter that enables the decision maker to adjust the degree of conservatism of the solution. It is obvious that decreasing the value of ϵ results in more conservative solutions for the MDEP problem. Note that the risk parameter ϵ is normally set to a very small value (less than 0.05) to ensure that CCs will be satisfied with a very high level of probability.

Unfortunately, (3.1) and (3.2) are very challenging to handle due to their implicit form. The implicitness of these CCs arises from the fact that evaluation of the probability statements given on their left-hand sides is not straightforward to carry out as the PDFs of $\widetilde{\chi^{GR}}$ and $\widetilde{\chi^{D}}$ are not perfectly known. Most of the existing research works using the CCP approach (such as [70-72]) assume that the random variables follow a Gaussian distribution and, based on this unrealistic assumption, reformulate the CCs as a number of explicit constraints. In this chapter, however, a novel method is proposed to reformulate the CCs, which does not make any assumption about the PDF types of the random variables [75]. That is, we obtain the explicit counterparts of the CCs in such a way that their satisfaction is guaranteed irrespective of the PDF types of the random variables. In this way, the CCs are in fact immunized against the probability distributions of the random variables. Based on this fact, the proposed method is called "distributionally robust" which

means “robust with respect to probability distributions”. Accordingly, the word “distributionally” means “with respect to probability distributions”. In the following, the DR reformulation proposed for the CCs is described in detail.

3.3 Distributionally Robust Reformulation of Chance Constraints

In order to simplify the notation, each of the constraints (3.1) and (3.2) can be rewritten in the following form:

$$\mathbb{P}\{\boldsymbol{A}^T\widetilde{\boldsymbol{\chi}} \leq B\} \geq 1-\epsilon \tag{3.3}$$

where $\widetilde{\boldsymbol{\chi}} = \langle \widetilde{\chi_1}, \widetilde{\chi_2} \rangle = \langle \widetilde{\chi^{GR}}, \widetilde{\chi^{D}} \rangle$ is the vector of random variables; $\boldsymbol{A} = \langle A_1, A_2 \rangle$ is a vector including the coefficients of random variables; and B is a variable representing the remaining part of the power balance constraints. For constraint (3.1), $\boldsymbol{A}$ and B are as follows:

$$\boldsymbol{A} = \langle -\left(\sum_{g\in\Omega^{gr}} P_{i,g,t}^{GR}\right), \overline{\overline{P_{i,t}^{D}}} \rangle \tag{3.4}$$

$$B = \sum_{(ki)\in\Omega^F}\sum_{a\in\Omega^a}\left[P_{ki,a,t}^{F} - R_a l_{ki} f_{ki,a,t}^{F}\right] - \sum_{(ij)\in\Omega^F}\sum_{a\in\Omega^a} P_{ij,a,t}^{F} + P_{i,t}^{S} + \sum_{g\in\Omega^{gc}} P_{i,g,t}^{GC} \tag{3.5}$$

For constraint (3.2), $\boldsymbol{A}$ and B can be similarly obtained as:

$$\boldsymbol{A} = \langle -\left(\sum_{g\in\Omega^{gr}} Q_{i,g,t}^{GR}\right), \overline{\overline{Q_{i,t}^{D}}} \rangle \tag{3.6}$$

$$B = \sum_{(ki)\in\Omega^F}\sum_{a\in\Omega^a}\left[Q_{ki,a,t}^{F} - X_a l_{ki} f_{ki,a,t}^{F}\right] - \sum_{(ij)\in\Omega^F}\sum_{a\in\Omega^a} Q_{ij,a,t}^{F} + Q_{i,t}^{S} + \sum_{g\in\Omega^{gc}} Q_{i,g,t}^{GC} \tag{3.7}$$

Now, we describe how to derive the DR reformulation of (3.7). As the first step, a moment-based ambiguity set ($\mathcal{D}$) is built to define all PDFs for which the satisfaction of (3.7) must be guaranteed [75]:

$$\mathcal{D} = \left\{ f(\widetilde{\boldsymbol{\chi}}) \middle| \begin{array}{ll} \int_{\widetilde{\boldsymbol{\chi}}\in\mathbb{S}} f(\widetilde{\boldsymbol{\chi}}) d\widetilde{\boldsymbol{\chi}} = 1 & \\ \underline{\mu_n} \leq \mathbb{E}[\tilde{\chi}_n] \leq \overline{\mu_n} & \forall n = 1,2 \\ \underline{\sigma_n} \leq \mathbb{E}[(\tilde{\chi}_n)^2] \leq \overline{\sigma_n} & \forall n = 1,2 \end{array} \right\} \tag{3.8}$$

where $f(\widetilde{\boldsymbol{\chi}})$ is the PDF of $\widetilde{\boldsymbol{\chi}}$; $\mathbb{S} \in \mathbb{R}^2$ is the support of $f(\widetilde{\boldsymbol{\chi}})$; $[\underline{\mu_n}, \overline{\mu_n}]$ is the confidence interval of the first moment of the nth random variable; and $[\underline{\sigma_n}, \overline{\sigma_n}]$ is the confidence interval of the second moment of nth random variable.

The three conditions in $\mathcal{D}$ make sure that: (i) the integral of $f(\tilde{\boldsymbol{\chi}})$ over its support is equal to one; (ii) the first moment of $\tilde{\chi}_n$ lies in the determined interval; and (iii) the second moment of $\tilde{\chi}_n$ falls within the specified range. Note that $\mathcal{D}$ covers all PDFs whose first and second moments agree with its conditions and, hence, it can be used to define a huge family of uncertainty distributions. Considering this ambiguity set, the DR variant of (3.7) can be obtained as follows:

$$\inf_{f(\tilde{\boldsymbol{\chi}})\in\mathcal{D}} \mathbb{P}\left\{\boldsymbol{A}_{i,t}^T\tilde{\boldsymbol{\chi}} \le B_{i,t}\right\} \ge 1-\epsilon \qquad \forall i \in \Omega^N, \forall t \in \Omega^T \tag{3.9}$$

The left-hand side of (3.9) yields the worst-case probability bound of $\mathbb{P}\left\{\boldsymbol{A}_{i,t}^T\tilde{\boldsymbol{\chi}} \le B_{i,t}\right\}$ over $\mathcal{D}$ and is equal to the objective value of the following optimization problem:

$$\Gamma = \min_{f(\tilde{\boldsymbol{\chi}})} \int_{\tilde{\boldsymbol{\chi}}\in\mathbb{S}} \mathbb{I}_{\mathcal{C}}(\tilde{\boldsymbol{\chi}}) f(\tilde{\boldsymbol{\chi}}) d\tilde{\boldsymbol{\chi}} \tag{3.10}$$

$$\text{s.t.} \quad \int_{\tilde{\boldsymbol{\chi}}\in\mathbb{S}} f(\tilde{\boldsymbol{\chi}}) d\tilde{\boldsymbol{\chi}} = 1 \tag{3.11}$$

$$\underline{\mu_n} \le \int_{\tilde{\boldsymbol{\chi}}\in\mathbb{S}} \tilde{\chi}_n f(\tilde{\boldsymbol{\chi}}) d\tilde{\boldsymbol{\chi}} \le \overline{\mu_n} \qquad \forall n = 1,2 \tag{3.12}$$

$$\underline{\sigma_n} \le \int_{\tilde{\boldsymbol{\chi}}\in\mathbb{S}} (\tilde{\chi}_n)^2 f(\tilde{\boldsymbol{\chi}}) d\tilde{\boldsymbol{\chi}} \le \overline{\sigma_n} \qquad \forall n = 1,2 \tag{3.13}$$

where $\mathbb{I}_{\mathcal{C}}(\tilde{\boldsymbol{\chi}})$ is the indicator function over the set $\mathcal{C} = \left\{\tilde{\boldsymbol{\chi}} \middle| \boldsymbol{A}_{i,t}^T\tilde{\boldsymbol{\chi}} \le B_{i,t}\right\}$; that is, $\mathbb{I}_{\mathcal{C}}(\tilde{\boldsymbol{\chi}}) = 1$ if $\tilde{\boldsymbol{\chi}} \in \mathcal{C}$ and $\mathbb{I}_{\mathcal{C}}(\tilde{\boldsymbol{\chi}}) = 0$ otherwise.

Obviously, (3.9) will be satisfied when $\Gamma \ge 1-\epsilon$. In [75], it is demonstrated that by applying the duality theory of conic linear programming problems [76] to the optimization problem (3.10)-(3.13) and using the S-Lemma [77], (3.9) can be equivalently reformulated as follows:

$$q_{i,t} + \sum_{n=1}^{2}\left(\underline{\mu_n}\, p_{i,t,n}^L - \overline{\mu_n}\, p_{i,t,n}^U\right) + \sum_{n=1}^{2}\left(\underline{\sigma_n}\, h_{i,t,n}^L - \overline{\sigma_n}\, h_{i,t,n}^U\right) \ge 1-\epsilon \quad \forall i \in \Omega^N, \forall t \in \Omega^T \tag{3.14}$$

$$q_{i,t} + \sum_{n=1}^{2} \alpha_{i,t,n} \le 1 \qquad \forall i \in \Omega^N, \forall t \in \Omega^T \tag{3.15}$$

$$q_{i,t} + \sum_{n=1}^{2} \beta_{i,t,n} \le \Upsilon_{i,t} B_{i,t} \qquad \forall i \in \Omega^N, \forall t \in \Omega^T \tag{3.16}$$

$$\left\|\begin{bmatrix} p_{i,t,n}^L - p_{i,t,n}^U \\ \alpha_{i,t,n} + h_{i,t,n}^L - h_{i,t,n}^U \end{bmatrix}\right\| \le \alpha_{i,t,n} - h_{i,tn}^L + h_{i,t,n}^U \quad \forall i \in \Omega^N, \forall t \in \Omega^T, \forall n = 1,2 \tag{3.17}$$

$$\left\|\begin{bmatrix} p_{i,t,n}^L - p_{i,t,n}^U + \Upsilon_{i,t} A_{i,t,n} \\ \beta_{i,t,n} + h_{i,t,n}^L - h_{i,t,n}^U \end{bmatrix}\right\| \le \beta_{i,t,n} - h_{i,t,n}^L + h_{i,t,n}^U \; \forall i \in \Omega^N, \forall t \in \Omega^T, \forall n = 1,2 \tag{3.18}$$

where $q_{i,t}$, $p^{L}_{i,t,n}$, $p^{U}_{i,t,n}$, $h^{L}_{i,t,n}$, $h^{U}_{i,t,n}$, $\alpha_{i,t,n}$, $\beta_{i,t,n}$, $\Upsilon_{i,t} \geq 0$ are auxiliary variables.

By deriving (3.14)-(3.18), the DR reformulation of (3.7) over $\mathcal{D}$ is achieved. In other words, utilization of (3.14)-(3.18) guarantees that (3.7) will be satisfied for all PDFs covered by $\mathcal{D}$. It is worthwhile to note that (3.14) explicitly includes the risk parameter ϵ. As a result, the proposed DRCC programming approach is able to directly control the robustness level of the solution based on the value chosen for the risk parameter ϵ. This ability to directly control the robustness level prevents the proposed DRCC programming approach from resulting in over-conservative solutions.

However, (3.16)-(3.18) are highly nonlinear and make the MDEP problem intractable. To address this issue, the nonlinearities of the noted constraints must be eliminated.

3.4 Linearization of the Distributionally Robust Reformulation

In this section, constraints (3.16)-(3.18) are linearized to attain a tractable DRCC-MILP model for the MDEP problem.

- **Linearization of Constraint (3.16)**

The nonlinearity of this constraint is only due to the bilinear term $\Upsilon_{i,t}B_{i,t}$ on the right-hand side of it. This bilinear term can be rewritten as follows:

$$\Upsilon_{i,t}B_{i,t} = \left[\left(B_{i,t} + \Upsilon_{i,t}\right)/2\right]^2 - \left[\left(B_{i,t} - \Upsilon_{i,t}\right)/2\right]^2 \qquad \forall i \in \Omega^N, \forall t \in \Omega^T \tag{3.19}$$

As a result, (3.16) can also be expressed as:

$$q_{i,t} + \sum_{n=1}^{2} \beta_{i,t,n} \leq \left[\left(B_{i,t} + \Upsilon_{i,t}\right)/2\right]^2 - \left[\left(B_{i,t} - \Upsilon_{i,t}\right)/2\right]^2 \forall i \in \Omega^N, \forall t \in \Omega^T \tag{3.20}$$

Now, (3.20) can be linearized using a piecewise-based linearization method:

$$q_{i,t} + \sum_{n=1}^{2} \beta_{i,t,n} \leq \sum_{\lambda=1}^{\Lambda}\left(m^{+}_{\lambda}\delta^{+}_{i,t,\lambda} + n^{+}_{\lambda}\Delta^{+}_{i,t,\lambda}\right) - \sum_{\lambda=1}^{\Lambda}\left(m^{-}_{\lambda}\delta^{-}_{i,t,\lambda} + n^{-}_{\lambda}\Delta^{-}_{i,t,\lambda}\right) \forall i \in \Omega^N, \forall t \in \Omega^T \tag{3.21}$$

$$\left(B_{i,t} + \Upsilon_{i,t}\right)/2 = \sum_{\lambda=1}^{\Lambda} \delta^{+}_{i,t,\lambda} \qquad \forall i \in \Omega^N, \forall t \in \Omega^T \tag{3.22}$$

$$\left(B_{i,t} - \Upsilon_{i,t}\right)/2 = \sum_{\lambda=1}^{\Lambda} \delta^{-}_{i,t,\lambda} \qquad \forall i \in \Omega^N, \forall t \in \Omega^T \tag{3.23}$$

$$\psi^{+}_{\lambda-1}\Delta^{+}_{i,t,\lambda} \leq \delta^{+}_{i,t,\lambda} \leq \psi^{+}_{\lambda}\Delta^{+}_{i,t,\lambda} \qquad \forall i \in \Omega^N, \forall t \in \Omega^T, \forall \lambda = 1, \dots, \Lambda \tag{3.24}$$

$$\psi_{\lambda-1}^{-}\Delta_{i,t,\lambda}^{-} \leq \delta_{i,t,\lambda}^{-} \leq \psi_{\lambda}^{-}\Delta_{i,t,\lambda}^{-} \qquad \forall i \in \Omega^N, \forall t \in \Omega^T, \forall \lambda = 1, \dots, \Lambda \qquad (3.25)$$

$$\sum_{\lambda=1}^{\Lambda} \Delta_{i,t,\lambda}^{+} \leq 1 \qquad \forall i \in \Omega^N, \forall t \in \Omega^T \qquad (3.26)$$

$$\sum_{\lambda=1}^{\Lambda} \Delta_{i,t,\lambda}^{-} \leq 1 \qquad \forall i \in \Omega^N, \forall t \in \Omega^T \qquad (3.27)$$

where the superscripts "+" and "−" respectively indicate the elements associated with the quadratic terms $\left[\left(B_{i,t} + \Upsilon_{i,t}\right)/2\right]^2$ and $\left[\left(B_{i,t} - \Upsilon_{i,t}\right)/2\right]^2$; $\delta_{i,t,\lambda} \geq 0$ and $\Delta_{i,t,\lambda} \in \{0,1\}$ respectively denote the continuous and binary auxiliary variables needed to obtain the piecewise linear expressions of the quadratic terms; and ψ_λ, m_λ, and n_λ are constant parameters that can be obtained as follows:

$$\psi_{\lambda}^{+} = (\lambda)(1/\Lambda)\overline{\left[\left(B_{i,t} + \Upsilon_{i,t}\right)/2\right]} \qquad \forall \lambda = 1, \dots, \Lambda \qquad (3.28)$$

$$\psi_{\lambda}^{-} = (\lambda)(1/\Lambda)\overline{\left[\left(B_{i,t} - \Upsilon_{i,t}\right)/2\right]} \qquad \forall \lambda = 1, \dots, \Lambda \qquad (3.29)$$

$$m_{\lambda}^{+} = [(\psi_{\lambda}^{+})^2 - (\psi_{\lambda-1}^{+})^2]/[\psi_{\lambda}^{+} - \psi_{\lambda-1}^{+}] \qquad \forall \lambda = 1, \dots, \Lambda \qquad (3.30)$$

$$m_{\lambda}^{-} = [(\psi_{\lambda}^{-})^2 - (\psi_{\lambda-1}^{-})^2]/[\psi_{\lambda}^{-} - \psi_{\lambda-1}^{-}] \qquad \forall \lambda = 1, \dots, \Lambda \qquad (3.31)$$

$$n_{\lambda}^{+} = (\psi_{\lambda}^{+})^2 - m_{\lambda}^{+}\psi_{\lambda}^{+} \qquad \forall \lambda = 1, \dots, \Lambda \qquad (3.32)$$

$$n_{\lambda}^{-} = (\psi_{\lambda}^{-})^2 - m_{\lambda}^{-}\psi_{\lambda}^{-} \qquad \forall \lambda = 1, \dots, \Lambda \qquad (3.33)$$

where $\overline{\left[\left(B_{i,t} + \Upsilon_{i,t}\right)/2\right]}$ and $\overline{\left[\left(B_{i,t} - \Upsilon_{i,t}\right)/2\right]}$ denote the upper bounds of the quadratic terms $\left[\left(B_{i,t} + \Upsilon_{i,t}\right)/2\right]^2$ and $\left[\left(B_{i,t} - \Upsilon_{i,t}\right)/2\right]^2$, respectively.

In order to clarify the proposed linearization method, the piecewise linear approximation of the quadratic term $\left[\left(B_{i,t} + \Upsilon_{i,t}\right)/2\right]^2$ is illustrated in Figure 3.1. As can be seen, first the distance between zero and $\overline{\left[\left(B_{i,t} + \Upsilon_{i,t}\right)/2\right]}$ is partitioned into Λ segments. Then, corresponding to each segment λ, a line with the slope of m_{λ}^{+} and the intercept of n_{λ}^{+} is considered. Finally, using the binary variables denoted by $\Delta_{i,t,\lambda}^{+}$, only one of the lines is chosen to represent the quadratic term $\left[\left(B_{i,t} + \Upsilon_{i,t}\right)/2\right]^2$.

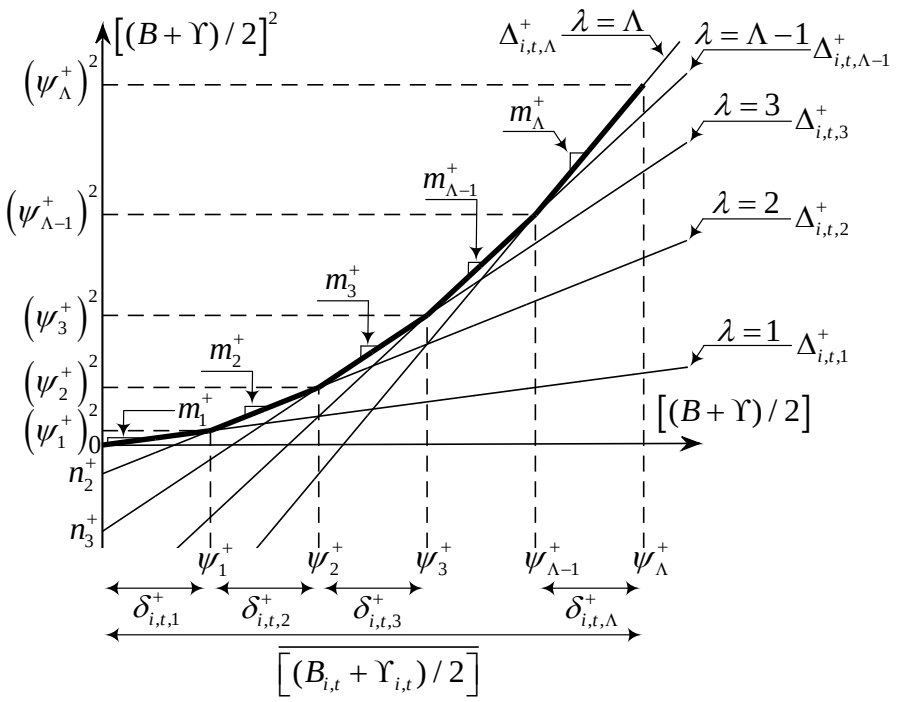

Figure 3.1 Illustration of the proposed piecewise linear approximation.

- **Linearization of Constraints (3.17) and (3.18)**

With the help of some auxiliary variables ($p_{i,t,n}, h_{i,t,n}, d_{i,t,n}$), (3.17) and (3.18) can be simplified and rewritten as:

$$p_{i,t,n} = p^L_{i,t,n} - p^U_{i,t,n} \qquad \forall i \in \Omega^N, \forall t \in \Omega^T, \forall n = 1,2 \tag{3.34}$$

$$h_{i,t,n} = h^L_{i,t,n} - h^U_{i,t,n} \qquad \forall i \in \Omega^N, \forall t \in \Omega^T, \forall n = 1,2 \tag{3.35}$$

$$d_{i,t,n} = p_{i,t,n} + \Upsilon_{i,t} A_{i,t,n} \qquad \forall i \in \Omega^N, \forall t \in \Omega^T, \forall n = 1,2 \tag{3.36}$$

$$\left(p_{i,t,n}\right)^2 \le -4\alpha_{i,t,n} h_{i,t,n} \qquad \forall i \in \Omega^N, \forall t \in \Omega^T, \forall n = 1,2 \tag{3.37}$$

$$\left(d_{i,t,n}\right)^2 \le -4\beta_{i,t,n} h_{i,t,n} \qquad \forall i \in \Omega^N, \forall t \in \Omega^T, \forall n = 1,2 \tag{3.38}$$

Now, (3.36) can be linearized in a similar way as (3.16) by employing the above-described piecewise-based linearization method. On the other hand, the right-hand sides of (3.37) and (3.38) can be expressed as follows:

$$-4\alpha_{i,t,n} h_{i,t,n} = \left(\alpha_{i,t,n} - h_{i,t,n}\right)^2 - \left(\alpha_{i,t,n} + h_{i,t,n}\right)^2 \quad \forall i \in \Omega^N, \forall t \in \Omega^T, \forall n = 1,2 \tag{3.39}$$

$$-4\beta_{i,t,n}h_{i,t,n}=\left(\beta_{i,t,n}-h_{i,t,n}\right)^2-\left(\beta_{i,t,n}+h_{i,t,n}\right)^2 \quad \forall i\in\Omega^N,\forall t\in\Omega^T,\forall n=1,2 \tag{3.40}$$

Therefore, (3.37) and (3.38) can be written as:

$$\alpha_{i,t,n}-h_{i,t,n}\geq\sqrt{\left(p_{i,t,n}\right)^2+\left(\alpha_{i,t,n}+h_{i,t,n}\right)^2} \qquad \forall i\in\Omega^N,\forall t\in\Omega^T,\forall n=1,2 \tag{3.41}$$

$$\beta_{i,t,n}-h_{i,t,n}\geq\sqrt{\left(d_{i,t,n}\right)^2+\left(\beta_{i,t,n}+h_{i,t,n}\right)^2} \qquad \forall i\in\Omega^N,\forall t\in\Omega^T,\forall n=1,2 \tag{3.42}$$

It is obvious that (3.41) and (3.42) are second-order conic constraints which have the same form as (2.57). Therefore, they can be linearized using the polyhedral-based method described in Section 2.4. That is, each of the conic quadratic constraints (3.41) and (3.42) can be replaced by the polyhedral approximation represented by (2.58)-(2.60).

Linearization of constraints (3.16)-(3.18) results in a DRCC-MILP model for the MDEP problem, which is able to efficiently account for the uncertainties associated with renewable DGs and loads.

3.5 Simulation Results and Discussion

In this section, the most important results obtained from the implementation of the proposed DRCC-MILP model are presented and discussed. This model has been implemented on a PC with a 3.40 GHz Intel Core i7-4770 processor and 16 GB of RAM using MATLAB R2015a [84] and CPLEX 12.6.1 [85]. The 24-node and 138-node distribution systems are again utilized to carry out the simulations. The data related to the candidate conductor types, alternatives for construction/reinforcement of substations, alternatives for installation of renewable/conventional DGs, power demands, lengths of feeder sections, and other parameters of the problem are exactly the same as those presented in Chapter 2. Note that as an illustrative example, renewable DGs are here assumed to be wind turbines. However, the proposed planning methodology is fully applicable to other renewables DG technologies such as photovoltaic panels.

3.5.1 Robustness Evaluation of the Proposed DRCC-MILP Model

In this subsection, we demonstrate the robustness of the proposed DRCC-MILP model against the uncertain wind generations and loads having various types of PDFs. This model is also

compared with two other models based on the deterministic and Gaussian chance-constrained (GCC) approaches which are widely used in the existing literature. That is, the following three models are considered:

- **Model 1:** Deterministic MILP model in which, similar to [1], [2], [6-8], [14-18], [36], [42], [43], [45], [46], the uncertainties are totally ignored.
- **Model 2:** GCC-MILP model in which, similar to [70-72], all the uncertainties are assumed to be Gaussian distributed.
- **Model 3:** Proposed DRCC-MILP model in which the uncertainty distributions are assumed to be unknown.

In Model 3, in order to build the ambiguity set ($\mathcal{D}$), the confidence intervals of the first and second moments of the random variables need to be specified. These confidence intervals should be defined based on historical data of random variables. In this regard, given a series of data samples $\{\tilde{\chi}_{n,w}\}_{w=1}^{\mathcal{W}}$ for the random variable $\tilde{\chi}_n$, the estimated values of the first and second moments can be obtained using the following formulas:

$$\widehat{\mu_n} = \frac{1}{\mathcal{W}}\sum_{w=1}^{\mathcal{W}} \tilde{\chi}_{n,w} \qquad \forall n = 1,2 \tag{3.43}$$

$$\widehat{\sigma_n} = \frac{1}{\mathcal{W}}\sum_{w=1}^{\mathcal{W}} \left(\tilde{\chi}_{n,w}\right)^2 \qquad \forall n = 1,2 \tag{3.44}$$

where $\widehat{\mu_n}$ denotes the estimated value of the first moment of the nth random variable; $\widehat{\sigma_n}$ denotes the estimated value of the second moment of the nth random variable; $\tilde{\chi}_{n,w}$ denotes the wth data sample of the nth random variable; and $\mathcal{W}$ is the total number of data samples.

Now, the confidence intervals $[\underline{\mu_n}, \overline{\mu_n}]$ and $[\underline{\sigma_n}, \overline{\sigma_n}]$ can be obtained by defining reasonable ranges around $\widehat{\mu_n}$ and $\widehat{\sigma_n}$, respectively. It is obvious that defining a wider range around $\widehat{\mu_n}$ or $\widehat{\sigma_n}$ will result in robustness against a larger family of PDFs. In this chapter, the historical data of wind generation and load are acquired from [86], [87], respectively. These historical data are converted to per-unit values and utilized to calculate $\widehat{\mu_n}$ and $\widehat{\sigma_n}$. The obtained values are as follows: $\widehat{\mu_1}$ = 0.427, $\widehat{\mu_2}$ = 0.988, $\widehat{\sigma_1}$ = 0.0519, and $\widehat{\sigma_2}$=0.0126. Considering plausible ranges around these values, the confidence intervals are defined as: $[\underline{\mu_1}, \overline{\mu_1}]$ = [0.3, 0.5], $[\underline{\mu_2}, \overline{\mu_2}]$ = [0.95, 1.05], $[\underline{\sigma_1}, \overline{\sigma_1}]$ =

[0.02, 0.08], and [$\underline{\sigma_2}, \overline{\sigma_2}$] = [0.01, 0.02]. Note that these confidence intervals can be flexibly tailored to meet the decision maker's requirements.

After solving Models 1-3, the solution robustness of each of them is assessed taking into account several different PDFs for wind generation and load. To this end, as shown in Figure 3.2, three typical PDFs are considered for each of the random variables $\widetilde{\chi^{GR}}$and $\widetilde{\chi^{D}}$. Then, regarding all combinations of W1-W3 and L1-L3, a total number of nine test cases are defined for PDFs of wind generation and load. Lastly, under each defined PDF case, 10000 samples of wind generation and load are produced and used for robustness evaluations.

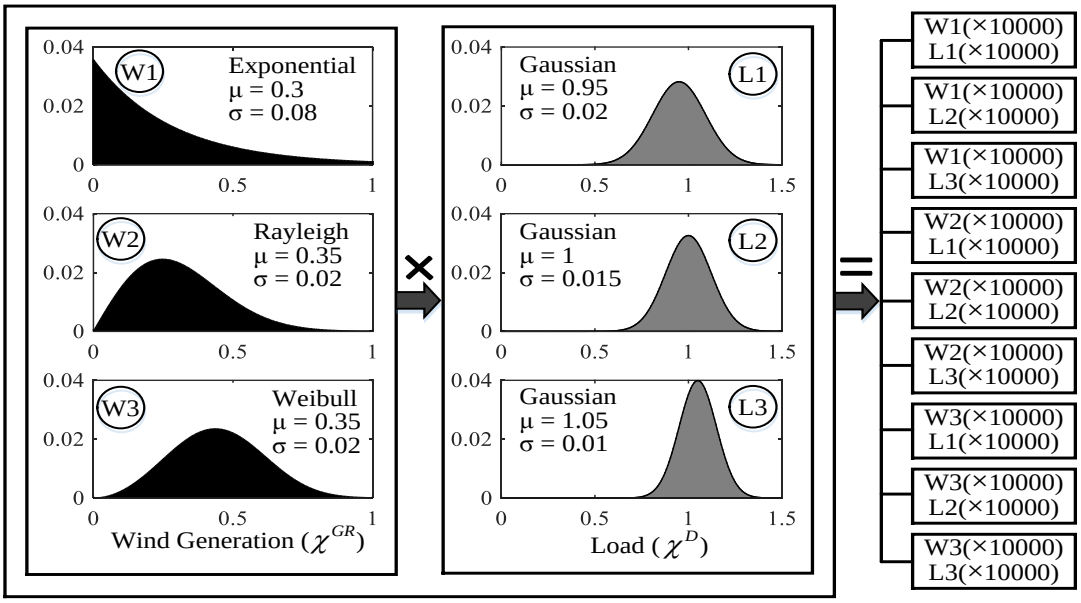

Figure 3.2 Illustration of the nine test cases defined for PDFs of wind generation and load (μ and σ denote the first and second moments, respectively).

Table 3.1 compares the performances of Models 1-3 from the viewpoints of solution robustness, investment cost, and computation time, while considering two different risk parameters (ϵ = 0.1 and ϵ = 0.05). In this table, the abbreviations Avg., Min., and Max. respectively represent the average, minimum, and maximum of the robustness levels found by testing the defined PDF cases. The details of the robustness levels of Models 1-3 for each PDF case are also provided in Figure 3.3. It can be seen that Model 1 has the lowest level of robustness, so that its average robustness level is only 29.86%. This poor performance is obviously due to the fact that Model 1 does not have any information about the uncertainties when deciding about the expansion plans. Model 2

results in higher robustness levels; however, as can be seen in Figure 3.3, its robustness is always below the requirement (i.e., $1-\epsilon$) for different PDF cases. The reason is that Model 2 finds the solution of the MDEP problem assuming Gaussian PDFs for wind generation and load and, hence, it cannot sufficiently account for other types of uncertainty distributions. In contrast, Model 3 is highly robust against the uncertainties and, as illustrated in Figure 3.3, its robustness is considerably higher than the specified level (i.e., $1-\epsilon$) under all PDF cases. Moreover, taking a careful look at Figure 3.3 reveals that when $1-\epsilon = 90\%$, the robustness of Model 2 is significantly lower than when $1-\epsilon = 95\%$. Whereas, the robustness of Model 3 is very high for both $\epsilon = 0.1$ and $\epsilon = 0.05$, which implies that this model is less sensitive to the risk parameter ϵ.

Table 3.1 Performance comparison of Models 1-3 from the viewpoints of solution robustness, investment cost, and computation time for the 24-node test system.

MDEP Models		**Model 1**	**Model 2**		**Model 3**	
$1-\epsilon$ (%)		N/A	90	95	90	95
Robustness (%)	Avg.	29.86	44.95	80.05	99.06	99.89
	Min.	10.54	21.08	62.22	98.33	99.75
	Max.	49.18	69.48	92.23	99.62	99.97
Investment (10^6 US$)		6.699	7.002	7.161	7.218	7.365
Time (min)		15	18.5	19	23	24.5

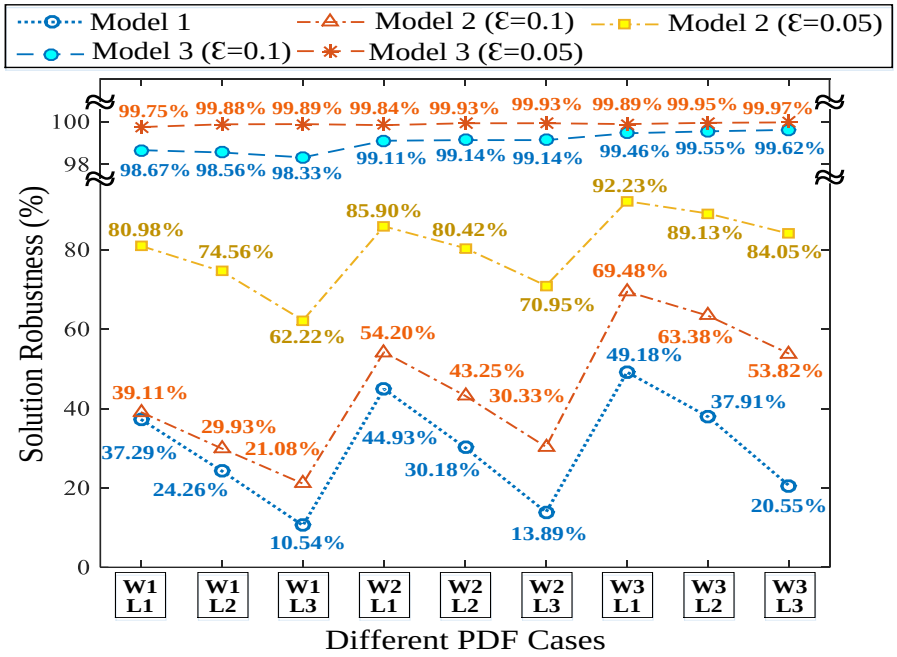

Figure 3.3 Solution robustness of Models 1-3 for the 24-node test system.

It should be noted that, as expected, the higher robustness of Model 3 is obtained at the cost of a small increase in computation time and investment. Nevertheless, it is worth to bear such a reasonable cost to achieve the reported substantial improvement in the robustness of the solution. To sum up, it can be stated that Model 3 has made an appropriate trade-off among the solution robustness, investment cost, and computational burden as compared to the other two models.

3.5.2 Sensitivity Analysis of Robustness of the Proposed DRCC-MILP Model

As described in Section 3.4, to overcome the nonlinearities of the DR reformulation of CCs, a combination of two linearization methods has been utilized: 1) polyhedral approximation, and 2) piecewise approximation. In this subsection, we analyze the impacts of the accuracy of these linearization methods on the robustness of the proposed DRCC-MILP model.

The accuracy of the polyhedral approximation depends on a parameter denoted by $\mathcal{L}$, so that the approximation error decreases as $\mathcal{L}$ is increased. In Section 2.4, it was shown that choosing an appropriate value for $\mathcal{L}$ causes the polyhedral approximation to be highly accurate. For instance, based on (2.62), setting $\mathcal{L}$ to 8 results in an approximation error of ϱ=1.88×10^{-5}, which is equivalent to the accuracy of almost 100%. Based on this fact, it can be stated that when $\mathcal{L}$ is greater than or equal to 8, the high accuracy of the polyhedral approximation is ensured. Thus, in order to linearize the DR reformulation of CCs, we have chosen $\mathcal{L}$=8 to make sure about the high accuracy of the polyhedral approximation.

On the other hand, the accuracy of the piecewise approximation is dependent on a parameter denoted by Λ, which determines the number of segments used for linearization. It is obvious that by increasing Λ, the approximation error will be decreased. However, it is not straightforward to quantify the effect of Λ on the accuracy of the piecewise approximation. As a result, we have conducted a sensitivity analysis to study the impacts of Λ on the robustness of the DRCC-MILP model. . In this regard, Λ is changed from 5 to 20 in steps of 1, and the corresponding changes in the robustness of the DRCC-MILP model are examined. The obtained results are illustrated in Figure 3.4. Note that the sensitivity analyses are performed for all the PDF cases defined in Section 3.5.1 while considering $\mathcal{L}$ = 8 and ϵ = 0.1. As can be seen, by increasing Λ in the range of 5 to 13, the robustness of the DRCC-MILP model is significantly improved. The reason is that in this range, an increase in Λ leads to a big improvement in the accuracy of the piecewise approximation,

which causes the accuracy of the linearized DR reformulation of CCs to be considerably improved. However, increasing Λ in the range beyond 14 does not make a tangible improvement in the robustness of the DRCC-MILP model. This is because when Λ reaches the value of 14, the piecewise approximation achieves its highest accuracy level (almost 100%) and hence the solution robustness remains constant beyond Λ=14.

Based on the above discussion, it can be stated that choosing suitable values for $\mathcal{L}$ and Λ causes the linearized DR reformulation of CCs to be highly accurate, so that the approximation errors have a negligible impact on the robustness of the DRCC-MILP model.

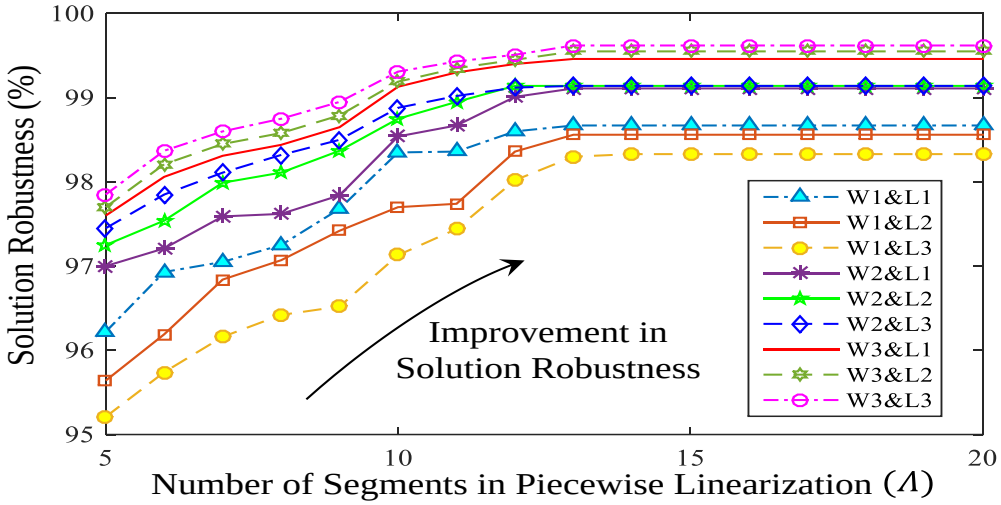

Figure 3.4 Impacts of the accuracy of the piecewise approximation on the robustness of the DRCC-MILP model for the 24-node test system.

3.5.3 Investigating the Impacts of the Proposed DRCCP Approach on DG Deployment Plans

One of the main purposes of our proposed planning methodology is to determine the optimal location, size, and type of DGs. This aspect is studied using the 138-node test system as it is large enough to provide a wide range of options for DG installation. In this regard, to investigate the impacts of the proposed DRCCP approach on the DG deployment plans, we have compared the deterministic MILP model developed in Chapter 2 with the DRCC-MILP model proposed in this chapter from the viewpoints of the location, size, and type of the installed DGs, as shown in Table 3.2. Note that in this table, "C" and "R" stand for "conventional" and "renewable", respectively. As can be seen, four DG locations (i.e., 10, 28, 85, and 108) are the same for both

models. However, the sizes and types of DGs are different for the deterministic and DRCC models. When utilizing the deterministic model, the uncertainties of renewable generations are entirely ignored. This causes the deterministic model to deploy more renewable DGs (7 MW) than conventional ones (4 MW) because renewable DGs do not have any generation costs. However, when the DRCC model is used, the uncertainties of renewable DGs are incorporated into the optimization process. As a result, the DRCC model deploys less renewable DGs (3 MW) to obtain more robust expansion plans. This fact implies that the robustness of the expansion plans has an inverse relationship with the penetration of renewable DGs. Therefore, making a proper trade-off between these two conflicting factors is of great importance.

Table 3.2 Comparison of the deterministic MILP model and the DRCC-MILP model from the viewpoint of DG deployment for the 138-node test system.

MDEP Models	Specifications of the installed DGs							
Deterministic MILP	Location	10	28	72	85	100	108	133
	Size (MW)	1	2	2	1	1	2	2
	Type	C	R	R	C	R	R	C
DRCC-MILP	Location	10	28	85	97	103	106	108
	Size (MW)	2	1	1	1	1	2	1
	Type	C	R	C	R	C	C	R

It is worthwhile to mention that for the risk parameter of $\epsilon = 0.05$ and the linearization parameters of $\mathcal{L} = 8$ and $\Lambda = 14$, the DRCC-MILP model consumes a computation time of 119 min to obtain the optimal solution of the MDEP problem. This reasonable computation time demonstrates the scalability of the proposed DRCC-MILP model.

3.6 Summary

In this chapter, a novel DRCCP approach has been proposed to deal with the major sources of uncertainty in the MDEP problem of ADNs. In this regard, the uncertainties have been modelled by defining a number of CCs which ensure that the constraints subject to uncertainty will be satisfied with a certain probability level. A DR reformulation has also been proposed for the CCs, which makes the optimal solution of the MDEP problem robust against the PDFs of the uncertain

parameters. Furthermore, a combination of the polyhedral and piecewise approximations has been utilized to overcome the nonlinearities of the DR reformulation proposed for the CCs, resulting in a DRCC-MILP model that can be efficiently solved using off-the-shelf mathematical programming solvers.

The 24-node and 138-node distribution systems have been employed to demonstrate the effectiveness of the proposed DRCC-MILP model. After testing the uncertain renewable generations and loads with several different PDFs, the simulation results demonstrate the significantly higher robustness level of the proposed DRCC-MILP model as compared to the deterministic and Gaussian chance-constrained MILP models. The simulation results also show that the proposed DRCC-MILP model is capable of making an appropriate trade-off among the solution robustness, investment cost, and computational burden.

4. A Fast Benders Decomposition-Based Solution Procedure for the Developed Planning Methodology

4.1 Introduction

In this chapter, a fast solution procedure based on an accelerated version of the Benders decomposition (BD) algorithm is proposed to solve the MDEP problem. To this end, by making use of the BD algorithm, the MDEP problem is partitioned into a master problem and two subproblems and the optimal solution is found through an iterative process. The straightforward implementation of the BD algorithm results in a very slow convergence rate, requiring a large number of iterations. To address this issue, the BD algorithm is accelerated by devising two innovative strategies that not only significantly decrease the number of iterations required to achieve the convergence, but also considerably shorten the time consumed by each iteration. In this way, the performance of the BD algorithm is greatly enhanced and a very fast solution procedure is obtained. It should be noted that for clarity and ease of understanding, the proposed fast solution procedure is here applied to the deterministic MILP model developed in Chapter 2.

4.2 Application of the BD Algorithm to the MDEP Problem

In this section, based on the BD algorithm [88], [89], the deterministic MILP model developed in Chapter 2 is decomposed into a master problem, an optimal operation subproblem, and a feasibility check subproblem. After that, the iterative process of finding the optimal solution is also described.

4.2.1 Master Problem

This problem only includes the binary decision variables of the MDEP problem and determines the investment and utilization decisions:

Minimize $c^{Inv.} + \Psi$ (4.1)

s.t. (2.2), (2.24)-(2.44)

$$\Psi \geq c^{Oper.(m)} + \sum_{t\in\Omega^T}\sum_{(ij)\in\Omega^F}\sum_{a\in\Omega^a} \vartheta_{ij,a,t}^{fF(m)} \left(\overline{I_a}\right)^2 \left(y_{ij,a,t} - \hat{y}_{ij,a,t}^{(m)}\right)$$

$$- \sum_{t\in\Omega^T}\sum_{(ij)\in\Omega^F}\left(\vartheta_{ij,t}^{\Delta V1(m)} + \vartheta_{ij,t}^{\Delta V2(m)}\right)\overline{\Delta V}\left[\sum_{a\in\Omega^a}\left(y_{ij,a,t} - \hat{y}_{ij,a,t}^{(m)}\right)\right]$$

$$+ \sum_{t\in\Omega^T}\sum_{i\in\Omega^{SR}} \vartheta_{i,t}^{SR(m)} \left[\sum_{v=1}^{t}\sum_{b\in\Omega^b} \overline{S_b}\left(x_{i,b,v}^{SR} - \hat{x}_{i,b,v}^{SR(m)}\right)\right]$$

$$+ \sum_{t\in\Omega^T}\sum_{i\in\Omega^{SC}} \vartheta_{i,t}^{SC(m)} \left[\sum_{v=1}^{t}\sum_{b\in\Omega^b} \overline{S_b}\left(x_{i,b,v}^{SC} - \hat{x}_{i,b,v}^{SC(m)}\right)\right]$$

$$+ \sum_{t\in\Omega^T}\sum_{i\in(\Omega^{NG}\cap\Omega_t^{NL})}\sum_{g\in\Omega^{gc}} \vartheta_{i,g,t}^{PGC(m)} \overline{P_g^{GC}}\left(x_{i,g,t}^{GC} - \hat{x}_{i,g,t}^{GC(m)}\right)$$

$$+ \sum_{t\in\Omega^T}\sum_{i\in(\Omega^{NG}\cap\Omega_t^{NL})}\sum_{g\in\Omega^{gc}} \left(\vartheta_{i,g,t}^{QGC1(m)} + \vartheta_{i,g,t}^{QGC2(m)}\right) \overline{Q_g^{GC}}\left(x_{i,g,t}^{GC} - \hat{x}_{i,g,t}^{GC(m)}\right)$$

$$+ \sum_{t\in\Omega^T}\sum_{i\in(\Omega^{NG}\cap\Omega_t^{NL})}\sum_{g\in\Omega^{gr}} \vartheta_{i,g,t}^{QGR(m)} \tan\left(\cos^{-1}(\rho^{GR})\right)\overline{\overline{P_g^{GR}}}\left(x_{i,g,t}^{GR} - \hat{x}_{i,g,t}^{GR(m)}\right)$$

$$+ \sum_{t\in\Omega^T}\sum_{i\in(\Omega^{NG}\cap\Omega_t^{NL})}\sum_{g\in\Omega^{gr}} \vartheta_{i,g,t}^{PGR(m)} \overline{\overline{P_g^{GR}}}\left(x_{i,g,t}^{GR} - \hat{x}_{i,g,t}^{GR(m)}\right) \qquad \forall m = 1, \dots, M^{Feas.} \qquad (4.2)$$

$$\mathcal{K}^{PQ(n)} + \sum_{t\in\Omega^T}\sum_{(ij)\in\Omega^F}\sum_{a\in\Omega^a} \omega_{ij,a,t}^{fF(n)} \left(\overline{I_a}\right)^2 \left(y_{ij,a,t} - \hat{y}_{ij,a,t}^{(n)}\right)$$

$$- \sum_{t\in\Omega^T}\sum_{(ij)\in\Omega^F}\left(\omega_{ij,t}^{\Delta V1(n)} + \omega_{ij,t}^{\Delta V2(n)}\right)\overline{\Delta V}\left[\sum_{a\in\Omega^a}\left(y_{ij,a,t} - \hat{y}_{ij,a,t}^{(n)}\right)\right]$$

$$+ \sum_{t\in\Omega^T}\sum_{i\in\Omega^{SR}} \omega_{i,t}^{SR(n)} \left[\sum_{v=1}^{t}\sum_{b\in\Omega^b} \overline{S_b}\left(x_{i,b,v}^{SR} - \hat{x}_{i,b,v}^{SR(n)}\right)\right]$$

$$+ \sum_{t\in\Omega^T}\sum_{i\in\Omega^{SC}} \omega_{i,t}^{SC(n)} \left[\sum_{v=1}^{t}\sum_{b\in\Omega^b} \overline{S_b}\left(x_{i,b,v}^{SC} - \hat{x}_{i,b,v}^{SC(n)}\right)\right]$$

$$+ \sum_{t\in\Omega^T}\sum_{i\in(\Omega^{NG}\cap\Omega_t^{NL})}\sum_{g\in\Omega^{gc}} \omega_{i,g,t}^{PGC(n)} \overline{P_g^{GC}}\left(x_{i,g,t}^{GC} - \hat{x}_{i,g,t}^{GC(n)}\right)$$

$$+ \sum_{t\in\Omega^T}\sum_{i\in(\Omega^{NG}\cap\Omega_t^{NL})}\sum_{g\in\Omega^{gc}} \left(\omega_{i,g,t}^{QGC1(n)} + \omega_{i,g,t}^{QGC2(n)}\right) \overline{Q_g^{GC}}\left(x_{i,g,t}^{GC} - \hat{x}_{i,g,t}^{GC(n)}\right)$$

$$+\sum_{t\in\Omega^T}\sum_{i\in(\Omega^{NG}\cap\Omega_t^{NL})}\sum_{g\in\Omega^{gr}}\omega_{i,g,t}^{QGR(n)}\ \tan\left(\cos^{-1}(\rho^{GR})\right)\overline{\overline{P_g^{GR}}}\left(x_{i,g,t}^{GR}-\hat{x}_{i,g,t}^{GR(n)}\right)$$

$$+\sum_{t\in\Omega^T}\sum_{i\in(\Omega^{NG}\cap\Omega_t^{NL})}\sum_{g\in\Omega^{gr}}\omega_{i,g,t}^{PGR(n)}\ \overline{\overline{P_g^{GR}}}\left(x_{i,g,t}^{GR}-\hat{x}_{i,g,t}^{GR(n)}\right)\leq 0\quad \forall n=1,\dots,N^{Infeas.} \tag{4.3}$$

where Ψ is a continuous variable required for generating optimality cuts; $c^{Oper.}$ is the objective value of the optimal operation subproblem; $\vartheta_{ij,a,t}^{fF}$, $\vartheta_{ij,t}^{\Delta V1}$, $\vartheta_{ij,t}^{\Delta V2}$, $\vartheta_{i,t}^{SR}$, $\vartheta_{i,t}^{SC}$, $\vartheta_{i,g,t}^{PGC}$, $\vartheta_{i,g,t}^{QGC1}$, $\vartheta_{i,g,t}^{QGC2}$, $\vartheta_{i,g,t}^{QGR}$, and $\vartheta_{i,g,t}^{PGR}$ are the dual variables of the optimal operation subproblem; m is the index of iterations in which the solution provided by the master problem is feasible; $M^{Feas.}$ denotes the number of iterations in which the solution provided by the master problem is feasible; $\mathcal{K}^{PQ}$ is the objective value of the feasibility check subproblem; $\omega_{ij,a,t}^{fF}$, $\omega_{ij,t}^{\Delta V1}$, $\omega_{ij,t}^{\Delta V2}$, $\omega_{i,t}^{SR}$, $\omega_{i,t}^{SC}$, $\omega_{i,g,t}^{PGC}$, $\omega_{i,g,t}^{QGC1}$, $\omega_{i,g,t}^{QGC2}$, $\omega_{i,g,t}^{QGR}$, and $\omega_{i,g,t}^{PGR}$ are the dual variables of the feasibility check subproblem; n is the index of iterations in which the solution provided by the master problem is infeasible; and $N^{Infeas.}$ denotes the number of iterations in which the solution provided by the master problem is infeasible.

The hat signs indicate the values of the binary decision variables obtained by solving the master problem in the previous iterations. Constraints (4.2) and (4.3) respectively represent the optimality and feasibility cuts added to the master problem in different iterations. As can be seen, these cuts are generated based on the information received from the optimal operation and feasibility check subproblems.

4.2.2 Optimal Operation Subproblem

This problem only includes the continuous variables of the MDEP problem and determines the optimal power flow for the system configuration found by the master problem:

Minimize $c^{Oper.}$ (4.4)

s.t. (2.3)-(2.6), Linearized (2.7), Linearized (2.8), (2.9)-(2.12), Linearized (2.13), Linearized (2.14), (2.15)

$$f_{ij,a,t}^{F}\leq\left(\overline{I_a}\right)^2\hat{y}_{ij,a,t}\qquad :\vartheta_{ij,a,t}^{fF}\qquad \forall(ij)\in\Omega^F,a\in\Omega^a,\forall t\in\Omega^T \tag{4.5}$$

$$\Delta V_{ij,t}\leq\overline{\Delta V}\left(1-\sum_{a\in\Omega^a}\hat{y}_{ij,a,t}\right)\qquad :\vartheta_{ij,t}^{\Delta V1}\qquad \forall(ij)\in\Omega^F,\forall t\in\Omega^T \tag{4.6}$$

$$-\Delta V_{ij,t} \le \overline{\Delta V}\left(1-\sum_{a\in\Omega^a}\hat{y}_{ij,a,t}\right) \quad : \vartheta_{ij,t}^{\Delta V2} \quad \forall (ij)\in\Omega^F, \forall t\in\Omega^T \tag{4.7}$$

$$S_{i,t}^S \le \overline{S_i^0} + \sum_{v=1}^{t}\sum_{b\in\Omega^b}\overline{S_b}\,\hat{x}_{i,b,v}^{SR} \quad : \vartheta_{i,t}^{SR} \quad \forall i\in\Omega^{SR}, \forall t\in\Omega^T \tag{4.8}$$

$$S_{i,t}^S \le \sum_{v=1}^{t}\sum_{b\in\Omega^b}\overline{S_b}\,\hat{x}_{i,b,v}^{SC} \quad : \vartheta_{i,t}^{SC} \quad \forall i\in\Omega^{SC}, \forall t\in\Omega^T \tag{4.9}$$

$$P_{i,g,t}^{GC} \le \sum_{v=1}^{t}\overline{P_g^{GC}}\hat{x}_{i,g,v}^{GC} \quad : \vartheta_{i,g,t}^{PGC} \quad \forall i\in(\Omega^{NG}\cap\Omega_t^{NL}), g\in\Omega^{gc}, \forall t\in\Omega^T \tag{4.10}$$

$$Q_{i,g,t}^{GC} \le \sum_{v=1}^{t}\overline{Q_g^{GC}}\,\hat{x}_{i,g,v}^{GC} \quad : \vartheta_{i,g,t}^{QGC1} \quad \forall i\in(\Omega^{NG}\cap\Omega_t^{NL}), g\in\Omega^{gc}, \forall t\in\Omega^T \tag{4.11}$$

$$-Q_{i,g,t}^{GC} \le \sum_{v=1}^{t}\overline{Q_g^{GC}}\,\hat{x}_{i,g,v}^{GC} \quad : \vartheta_{i,g,t}^{QGC2} \quad \forall i\in(\Omega^{NG}\cap\Omega_t^{NL}), g\in\Omega^{gc}, \forall t\in\Omega^T \tag{4.12}$$

$$P_{i,g,t}^{GR} = \sum_{v=1}^{t}\overline{\overline{P_g^{GR}}}\hat{x}_{i,g,v}^{GR} \quad : \vartheta_{i,g,t}^{PGR} \quad \forall i\in(\Omega^{NG}\cap\Omega_t^{NL}), g\in\Omega^{gr}, \forall t\in\Omega^T \tag{4.13}$$

$$Q_{i,g,t}^{GR} = \sum_{v=1}^{t}\tan\left(\cos^{-1}(\rho^{GR})\right)\overline{\overline{P_g^{GR}}}\hat{x}_{i,g,v}^{GR} \quad : \vartheta_{i,g,t}^{QGR} \quad \forall i\in(\Omega^{NG}\cap\Omega_t^{NL}), g\in\Omega^{gr}, \forall t\in\Omega^T \tag{4.14}$$

It should be mentioned that $\hat{y}_{ij,a,t}$, $\hat{x}_{i,b,v}^{SR}$, $\hat{x}_{i,b,v}^{SC}$, $\hat{x}_{i,g,t}^{GC}$, and $\hat{x}_{i,g,t}^{GR}$ have been previously determined by the master problem. Therefore, when solving the optimal operation subproblem, they should be considered as constant values.

4.2.3 Feasibility Check Subproblem

This problem is used to check the feasibility of the solution provided by the master problem in each iteration:

$$\text{Minimize } \mathcal{K}^{PQ} = \sum_{t\in\Omega^T}\sum_{i\in\Omega^N}\mathcal{K}_{i,t}^{P} + \sum_{t\in\Omega^T}\sum_{i\in\Omega^N}\mathcal{K}_{i,t}^{Q} \tag{4.15}$$

s.t. (2.6), Linearized (2.7), Linearized (2.8), (2.9)-(2.12), Linearized (2.13), Linearized (2.14), (2.15)

$$\sum_{(ki)\in\Omega^F}\sum_{a\in\Omega^a}\left[P_{ki,a,t}^{F} - R_a l_{ki} f_{ki,a,t}^{F}\right] - \sum_{(ij)\in\Omega^F}\sum_{a\in\Omega^a}P_{ij,a,t}^{F} + P_{i,t}^{S} + \sum_{g\in\Omega^{gc}}P_{i,g,t}^{GC}$$

$$+\sum_{g\in\Omega^{gr}}P_{i,g,t}^{GR} - \overline{\overline{P_{i,t}^{D}}} + \mathcal{K}_{i,t}^{P} = 0 \qquad \forall i\in\Omega^N, \forall t\in\Omega^T \tag{4.16}$$

$$\sum_{(ki)\in\Omega^F}\sum_{a\in\Omega^a}\left[Q_{ki,a,t}^{F} - X_a l_{ki} f_{ki,a,t}^{F}\right] - \sum_{(ij)\in\Omega^F}\sum_{a\in\Omega^a}Q_{ij,a,t}^{F} + Q_{i,t}^{S} + \sum_{g\in\Omega^{gc}}Q_{i,g,t}^{GC}$$

$$+\sum_{g\in\Omega^{gr}}Q_{i,g,t}^{GR} - \overline{\overline{Q_{i,t}^{D}}} + \mathcal{K}_{i,t}^{Q} = 0 \qquad \forall i\in\Omega^N, \forall t\in\Omega^T \tag{4.17}$$

$$f_{ij,a,t}^{F} \le \left(\overline{I_a}\right)^2 \hat{y}_{ij,a,t} \quad : \omega_{ij,a,t}^{ff} \quad \forall (ij) \in \Omega^F, a \in \Omega^a, \forall t \in \Omega^T \tag{4.18}$$

$$\Delta V_{ij,t} \le \overline{\Delta V}\left(1 - \sum_{a \in \Omega^a} \hat{y}_{ij,a,t}\right) \quad : \omega_{ij,t}^{\Delta V1} \quad \forall (ij) \in \Omega^F, \forall t \in \Omega^T \tag{4.19}$$

$$-\Delta V_{ij,t} \le \overline{\Delta V}\left(1 - \sum_{a \in \Omega^a} \hat{y}_{ij,a,t}\right) \quad : \omega_{ij,t}^{\Delta V2} \quad \forall (ij) \in \Omega^F, \forall t \in \Omega^T \tag{4.20}$$

$$S_{i,t}^{S} \le \overline{S_i^0} + \sum_{v=1}^{t} \sum_{b \in \Omega^b} \overline{S_b}\, \hat{x}_{i,b,v}^{SR} \quad : \omega_{i,t}^{SR} \quad \forall i \in \Omega^{SR}, \forall t \in \Omega^T \tag{4.21}$$

$$S_{i,t}^{S} \le \sum_{v=1}^{t} \sum_{b \in \Omega^b} \overline{S_b}\, \hat{x}_{i,b,v}^{SC} \quad : \omega_{i,t}^{SC} \quad \forall i \in \Omega^{SC}, \forall t \in \Omega^T \tag{4.22}$$

$$P_{i,g,t}^{GC} \le \sum_{v=1}^{t} \overline{P_g^{GC}} \hat{x}_{i,g,v}^{GC} \quad : \omega_{i,g,t}^{PGC} \quad \forall i \in (\Omega^{NG} \cap \Omega_t^{NL}), g \in \Omega^{gc}, \forall t \in \Omega^T \tag{4.23}$$

$$Q_{i,g,t}^{GC} \le \sum_{v=1}^{t} \overline{Q_g^{GC}}\, \hat{x}_{i,g,v}^{GC} \quad : \omega_{i,g,t}^{QGC1} \quad \forall i \in (\Omega^{NG} \cap \Omega_t^{NL}), g \in \Omega^{gc}, \forall t \in \Omega^T \tag{4.24}$$

$$-Q_{i,g,t}^{GC} \le \sum_{v=1}^{t} \overline{Q_g^{GC}}\, \hat{x}_{i,g,v}^{GC} \quad : \omega_{i,g,t}^{QGC2} \quad \forall i \in (\Omega^{NG} \cap \Omega_t^{NL}), g \in \Omega^{gc}, \forall t \in \Omega^T \tag{4.25}$$

$$P_{i,g,t}^{GR} = \sum_{v=1}^{t} \overline{\overline{P_g^{GR}}} \hat{x}_{i,g,v}^{GR} \quad : \omega_{i,g,t}^{PGR} \quad \forall i \in (\Omega^{NG} \cap \Omega_t^{NL}), g \in \Omega^{gr}, \forall t \in \Omega^T \tag{4.26}$$

$$Q_{i,g,t}^{GR} = \sum_{v=1}^{t} \tan\left(\cos^{-1}(\rho^{GR})\right) \overline{\overline{P_g^{GR}}} \hat{x}_{i,g,v}^{GR} \quad : \omega_{i,g,t}^{QGR} \quad \forall i \in (\Omega^{NG} \cap \Omega_t^{NL}), g \in \Omega^{gr}, \forall t \in \Omega^T \tag{4.27}$$

Note that $\mathcal{K}_{i,t}^{P}$ and $\mathcal{K}_{i,t}^{Q}$ are positive unconstrained slack variables defined to determine whether the solution provided by the master problem is feasible or not. In this regard, when the objective value of the feasibility check subproblem (i.e., $\mathcal{K}^{PQ}$) is equal to zero, the master problem solution is feasible. The reason is that the objective function of the feasibility check subproblem (which is equal to the sum of the slack variables) in fact measures the amount by which the constraints of the optimal operation subproblem are violated. Therefore, if the value of this objective function can be reduced to zero, it means that all the constraints in the optimal operation subproblem can be satisfied, implying that the solution provided by the master problem is feasible.

4.2.4 Iterative Process of Finding the Optimal Solution

The iterative procedure for finding the optimal solution of the MDEP problem using the BD algorithm is as follows:

- **Step 1:** Solve the master problem and obtain $\hat{y}_{ij,a,t}$, $\hat{x}_{i,b,v}^{SR}$, $\hat{x}_{i,b,v}^{SC}$, $\hat{x}_{i,g,t}^{GC}$, $\hat{x}_{i,g,t}^{GR}$, and Ψ.

- **Step 2:** Substitute $\hat{y}_{ij,a,t}$, $\hat{x}^{SR}_{i,b,v}$, $\hat{x}^{SC}_{i,b,v}$, $\hat{x}^{GC}_{i,g,t}$, and $\hat{x}^{GR}_{i,g,t}$ into the feasibility check subproblem and solve it to obtain $\mathcal{K}^{PQ}$. If this objective value is equal to zero, go to Step 3. Otherwise, obtain the dual variables $\omega^{ff}_{ij,a,t}$, $\omega^{\Delta V1}_{ij,t}$, $\omega^{\Delta V2}_{ij,t}$, $\omega^{SR}_{i,t}$, $\omega^{SC}_{i,t}$, $\omega^{PGC}_{i,g,t}$, $\omega^{QGC1}_{i,g,t}$, $\omega^{QGC2}_{i,g,t}$, $\omega^{PGR}_{i,g,t}$, and $\omega^{QGR}_{i,g,t}$, and form a feasibility cut. Append the feasibility cut to the master problem and go to Step 1.
- **Step 3:** Substitute $\hat{y}_{ij,a,t}$, $\hat{x}^{SR}_{i,b,v}$, $\hat{x}^{SC}_{i,b,v}$, $\hat{x}^{GC}_{i,g,t}$, and $\hat{x}^{GR}_{i,g,t}$ into the optimal operation subproblem and solve it to obtain $c^{Oper.}$.
- **Step 4:** Form the lower bound $LB = c^{Inv.} + \Psi$ and the upper bound $UB = c^{Inv.} + c^{Oper.}$.
- **Step 5:** If $UB - LB \leq \zeta \times LB$, the current solution is the final optimal one. Otherwise, obtain the dual variables $\vartheta^{ff}_{ij,a,t}$, $\vartheta^{\Delta V1}_{ij,t}$, $\vartheta^{\Delta V2}_{ij,t}$, $\vartheta^{SR}_{i,t}$, $\vartheta^{SC}_{i,t}$, $\vartheta^{PGC}_{i,g,t}$, $\vartheta^{QGC1}_{i,g,t}$, $\vartheta^{QGC2}_{i,g,t}$, $\vartheta^{QGR}_{i,g,t}$, and $\vartheta^{PGR}_{i,g,t}$, and form an optimality cut. Append the optimality cut to the master problem and go to Step 1.

Note that ζ is a small constant value (e.g., 0.001) used to define the convergence criterion of the BD algorithm.

4.3 Acceleration of the BD Algorithm for Solving the MDEP Problem

Using the classical BD algorithm, the MDEP problem is now partitioned into a master problem (which only includes binary variables) and two subproblems (which merely comprise continuous variables). Accordingly, the optimal solution of the MDEP problem can be found through an iterative process in which multiple feasibility and optimality cuts are generated and added to the master problem. However, the huge number of iterations and cuts required by the classical BD algorithm to achieve the convergence causes it to be very slow and time-consuming. Therefore, if the number of generated cuts and consequently iterations can be somehow reduced, the solution speed will be significantly increased. To this end, we have proposed two efficient acceleration strategies: 1) modification of the master problem, and 2) generation of auxiliary optimality cuts.

4.3.1 Modified Master Problem

The first acceleration strategy is to modify the master problem with the help of some auxiliary constraints that prevent it from producing a vast majority of solutions which are either infeasible or non-optimal. In this way, the quality of the master problem solutions is improved and consequently the BD algorithm will be able to converge to the optimal solution by generating a

relatively small number of feasibility and optimality cuts. The modified master problem is as follows:

Minimize $c^{Inv.} + \Psi$ (4.28)

s.t. (2.2), (2.24)-(2.44), (4.2), (4.3)

$$\sum_{(ki)\in\Omega^F}\sum_{a\in\Omega^a}\left(I^F_{ki,a,t}\right) - \sum_{(ij)\in\Omega^F}\sum_{a\in\Omega^a}\left(I^F_{ij,a,t}\right) + I^S_{i,t} + \sum_{g\in\Omega^{gc}}\left(I^{GC}_{i,g,t}\right) + \sum_{g\in\Omega^{gr}}\left(I^{GR}_{i,g,t}\right) = \overline{\overline{I^D_{i,t}}} \quad \forall i \in \Omega^N, \forall t \in \Omega^T \tag{4.29}$$

$$V_{i,t} - V_{j,t} = \sum_{a\in\Omega^a}\left(Z_a l_{ij} I^F_{ij,a,t}\right) + \Delta V_{ij,t} \quad \forall (ij) \in \Omega^F, \forall t \in \Omega^T \tag{4.30}$$

$$\underline{V} \le V_{i,t} \le \overline{V} \quad \forall i \in \Omega^N, \forall t \in \Omega^T \tag{4.31}$$

$$I^F_{ij,a,t} \le \overline{I_a}\, y_{ij,a,t} \quad \forall (ij) \in \Omega^F, a \in \Omega^a, \forall t \in \Omega^T \tag{4.32}$$

$$\left|\Delta V_{ij,t}\right| \le \overline{\Delta V}\left(1 - \sum_{a\in\Omega^a} y_{ij,a,t}\right) \quad \forall (ij) \in \Omega^F, \forall t \in \Omega^T \tag{4.33}$$

$$I^S_{i,t} \le \overline{I^{S0}_i} + \sum_{v=1}^{t}\sum_{b\in\Omega^b} \overline{I_b}\, x^{SR}_{i,b,v} \quad \forall i \in \Omega^{SR}, \forall t \in \Omega^T \tag{4.34}$$

$$I^S_{i,t} \le \sum_{v=1}^{t}\sum_{b\in\Omega^b} \overline{I_b}\, x^{SC}_{i,b,v} \quad \forall i \in \Omega^{SC}, \forall t \in \Omega^T \tag{4.35}$$

$$I^{GC}_{i,g,t} \le \overline{I^{GC}_g} x^{GC}_{i,g,t} \quad \forall i \in (\Omega^{NG} \cap \Omega^{NL}_t), g \in \Omega^{gc}, \forall t \in \Omega^T \tag{4.36}$$

$$I^{GR}_{i,g,t} = \overline{\overline{I^{GR}_g}} x^{GR}_{i,g,t} \quad \forall i \in (\Omega^{NG} \cap \Omega^{NL}_t), g \in \Omega^{gr}, \forall t \in \Omega^T \tag{4.37}$$

The auxiliary constraints added to the master problem include a simplified version of the power flow equations as well as the voltage and current limits. These additional constraints have a negligible impact on increasing the solution time of the master problem, while they can significantly decrease the number of required cuts and iterations. Therefore, the overall consequence of using them is the rapid acceleration of the BD algorithm.

The other important point is that when there are no optimality and feasibility cuts, the modified master problem is in fact an approximated version of the MDEP problem. As a result, in the first iteration (where no cuts are added yet), the modified master problem provides a solution that is quite close to the optimal solution of the MDEP problem. This feature provides an opportunity to further accelerate the BD algorithm, as discussed below.

4.3.2 Auxiliary Optimality Cuts

A deep understanding of the special characteristics of the decomposed MDEP problem can help find more ways to accelerate its solution process. One of these specific characteristics is the near-optimality of the solution found by the modified master problem in the first iteration. This unique feature can be utilized to significantly reduce the number of optimality cuts and iterations required for reaching the convergence. With this background, the second acceleration strategy is explained in the following.

Consider a hypothetical optimization problem with a small maser problem that only has one integer variable $\boldsymbol{y}$ and four potential optimality cuts as shown in Figure 4.1. This figure shows the step-by-step process of constraining the variable Ψ by adding the optimality cuts to the master problem. Suppose that in the first iteration, the master problem finds the solution $\boldsymbol{y_1}$ which is very close to the optimal solution of the original problem $\boldsymbol{y_{opt}}$. By passing $\boldsymbol{y_1}$ to the subproblem and solving its dual, the first optimality cut $\boldsymbol{C_1}$ which determines the lower bound of the variable Ψ is found. Note that the solid circle shown on $\boldsymbol{C_1}$ is in fact the objective value of the dual subproblem at point $\boldsymbol{y_1}$, which is also equal to the objective value of the primal subproblem based on the strong duality theorem. After adding $\boldsymbol{C_1}$ to the master problem and solving it in the second iteration, the new solution $\boldsymbol{y_2}$ is obtained. Obviously, since the master problem is minimizing the variable Ψ, $\boldsymbol{y_2}$ should lie to the left of $\boldsymbol{y_1}$. The solution $\boldsymbol{y_2}$ is again passed to the subproblem and the second optimality cut $\boldsymbol{C_2}$ is also found. The hollow circle shown on $\boldsymbol{C_1}$ indicates the value that the master problem has allocated to the variable Ψ. In fact, the master problem, given its current constraints on the variable Ψ, thinks that choosing the solution $\boldsymbol{y_2}$ will cause the subproblem to have the objective value represented by the hollow circle on $\boldsymbol{C_1}$. However, the subproblem actually gets the objective value shown by the solid circle on $\boldsymbol{C_2}$. The reason is that at point $\boldsymbol{y_2}$, the constraint $\boldsymbol{C_2}$ (which the master problem did not know about in the second iteration) is active and, hence, the objective value of the subproblem lies on this constraint. In the third iteration, $\boldsymbol{C_2}$ is also passed back to the master problem as another optimality cut and the new solution $\boldsymbol{y_3}$ is achieved. Then, the process continues in a similar way until all the potential optimality cuts are added to the master problem and consequently the hollow circle (i.e., the value allocated to the variable Ψ) coincides with the solid circle (i.e., the objective value of the subproblem) in the fifth iteration, which means that the BD algorithm has converged to the optimal solution.

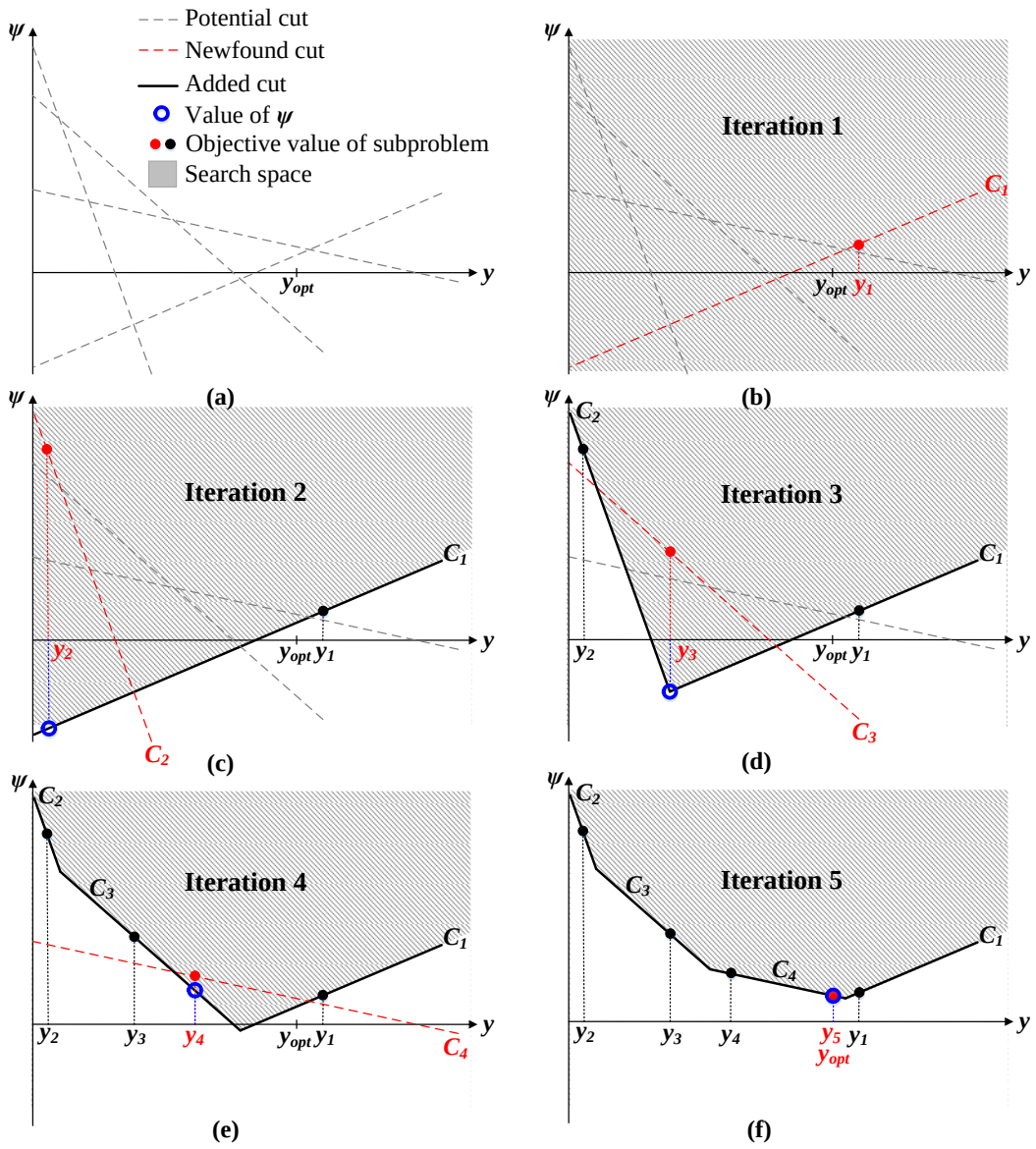

Figure 4.1 Step-by-step process of constraining the variable Ψ by adding the optimality cuts to the master problem.

The above discussion showed the fact that although the solution $\boldsymbol{y_1}$ obtained in the first iteration was quite close to the optimal solution $\boldsymbol{y_{opt}}$, the added optimality cuts caused the master problem to generate solutions that were relatively far from the optimal one in the next iterations. Accordingly, it was necessary to find all the potential optimality cuts to reach the optimal solution. That is, the BD algorithm required the maximum number of iterations to achieve the convergence. However, knowing the near-optimality of the master problem solution in the first iteration, it is possible to accelerate the BD algorithm by generating more clever cuts. To this end, in addition to the optimality cut generated in each iteration, an auxiliary optimality cut can also be produced to

keep the near-optimality of the master problem solutions in the next iterations. To clarify this matter, consider the above-discussed hypothetical optimization problem again. In the second iteration, besides the optimality cut C_1, an auxiliary optimality cut named C_1^{Aux} can also be generated and added to the master problem, as shown in Figure 4.2. This auxiliary optimality cut in fact restricts the variable y in such a way that the solution y_2 lies in the positive part of the optimality cut C_1. The reasons behind choosing such an auxiliary optimality cut are that, firstly, y_1 is located in the positive part of C_1 and, secondly, y_{opt} is very close to y_1. These two reasons together imply that y_{opt} is also located in the positive part of C_1. Therefore, by keeping the master problem solution y_2 in the positive part of C_1, we can make sure that it is not far from the optimal solution. After passing y_2 to the subproblem, the second optimality cut C_2 is also found. In the third iteration, by adding C_2 and C_2^{Aux} (which is generated in a similar way as C_1^{Aux}) to the master problem and solving it, the optimal solution is obtained as the hollow circle has coincided with the solid circle.

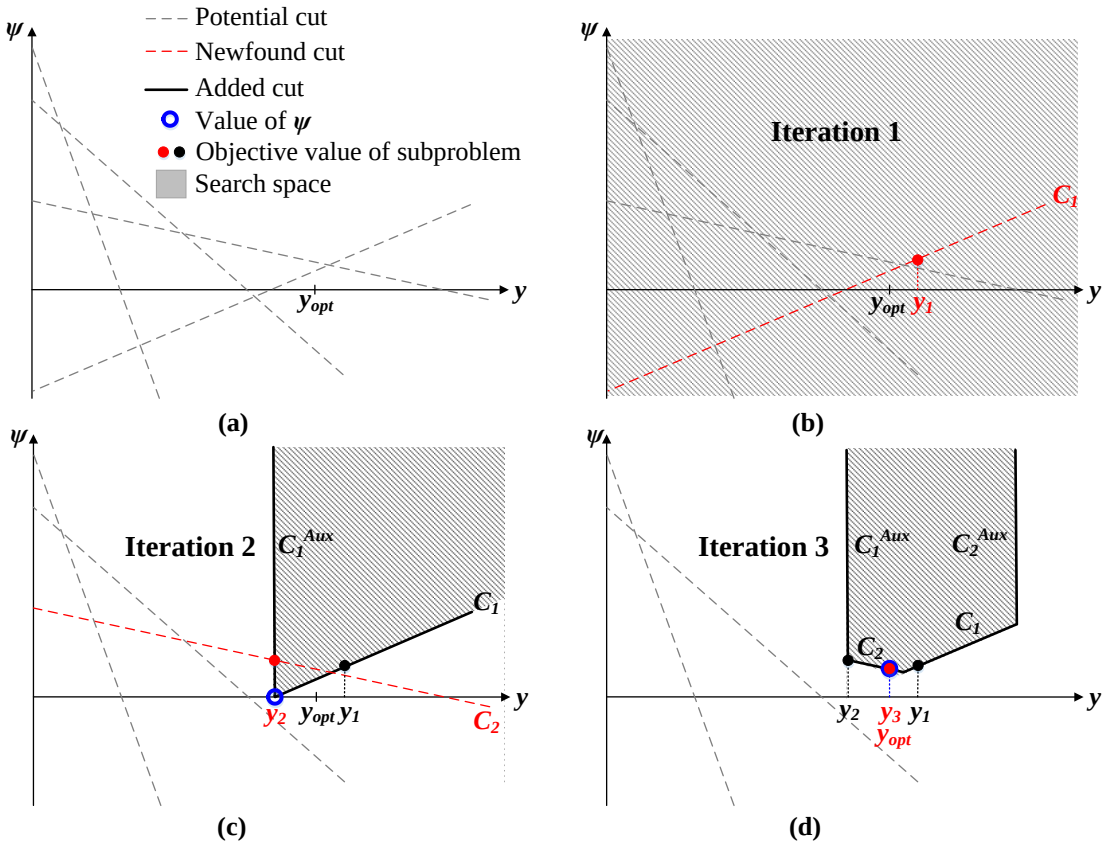

Figure 4.2 Step-by-step process of constraining the variable Ψ by adding both the optimality cuts and the auxiliary optimality cuts to the master problem.

Note that the optimal solution is here achieved by finding only two of the four potential optimality cuts, which means that the algorithm has saved two iterations as compared to the case in which the auxiliary optimality cuts are not used. Therefore, the first benefit of the auxiliary optimality cuts is to make savings in the number of iterations. Moreover, it is obvious that by adding the auxiliary optimality cuts to the master problem, its search space is significantly reduced and, hence, it can be solved in a considerably shorter time. That is, the second benefit of the auxiliary optimality cuts is to decrease the solution time of the master problem, which in turn reduces the overall time consumed by the algorithm to achieve the convergence.

The above discussion can be also generalized to the decomposed MDEP problem due to the following reasons:

- The modifications made in the master problem cause its solution in the first iteration to be quite close to the optimal solution of the original problem.
- The solution of the master problem always lies in the positive part of its corresponding optimality cut. This is due to the fact that, as can be seen in (4.2), substituting a master problem solution into the right-hand side of its corresponding optimality cut yields the objective value of the optimal operation subproblem which is always a positive value.

Therefore, when solving the decomposed MDEP problem, in addition to the optimality cut (4.2), the auxiliary optimality cut (4.38) can also be generated and added to the modified master problem. This auxiliary cut ensures that in each iteration, the modified master problem determines the optimal values of binary variables in such a way that the right-hand sides of all the optimality cuts discovered in the previous iterations remain positive. This will considerably accelerate the solution process by the same logic as described for the above hypothetical optimization problem.

$$c^{Oper.(m)} + \sum_{t\in\Omega^T}\sum_{(ij)\in\Omega^F}\sum_{a\in\Omega^a}\vartheta_{ij,a,t}^{fF(m)}\left(\overline{I_a}\right)^2\left(y_{ij,a,t}-\hat{y}_{ij,a,t}^{(m)}\right)$$

$$-\sum_{t\in\Omega^T}\sum_{(ij)\in\Omega^F}\left(\vartheta_{ij,t}^{\Delta V1(m)}+\vartheta_{ij,t}^{\Delta V2(m)}\right)\overline{\Delta V}\left[\sum_{a\in\Omega^a}\left(y_{ij,a,t}-\hat{y}_{ij,a,t}^{(m)}\right)\right]$$

$$+\sum_{t\in\Omega^T}\sum_{i\in\Omega^{SR}}\vartheta_{i,t}^{SR(m)}\left[\sum_{v=1}^{t}\sum_{b\in\Omega^b}\overline{S_b}\left(x_{i,b,v}^{SR}-\hat{x}_{i,b,v}^{SR(m)}\right)\right]$$

$$+\sum_{t\in\Omega^T}\sum_{i\in\Omega^{SC}}\vartheta_{i,t}^{SC(m)}\left[\sum_{v=1}^{t}\sum_{b\in\Omega^b}\overline{S_b}\left(x_{i,b,v}^{SC}-\hat{x}_{i,b,v}^{SC(m)}\right)\right]$$

$$+\sum_{t\in\Omega^T}\sum_{i\in(\Omega^{NG}\cap\Omega_t^{NL})}\sum_{g\in\Omega^{gc}}\vartheta_{i,g,t}^{PGC(m)}\overline{P_g^{GC}}\left(x_{i,g,t}^{GC}-\hat{x}_{i,g,t}^{GC(m)}\right)$$

$$+\sum_{t\in\Omega^T}\sum_{i\in(\Omega^{NG}\cap\Omega_t^{NL})}\sum_{g\in\Omega^{gc}}\left(\vartheta_{i,g,t}^{QGC1(m)}+\vartheta_{i,g,t}^{QGC2(m)}\right)\overline{Q_g^{GC}}\left(x_{i,g,t}^{GC}-\hat{x}_{i,g,t}^{GC(m)}\right)$$

$$+\sum_{t\in\Omega^T}\sum_{i\in(\Omega^{NG}\cap\Omega_t^{NL})}\sum_{g\in\Omega^{gr}}\vartheta_{i,g,t}^{QGR(m)}\ \tan\left(\cos^{-1}(\rho^{GR})\right)\overline{\overline{P_g^{GR}}}\left(x_{i,g,t}^{GR}-\hat{x}_{i,g,t}^{GR(m)}\right)$$

$$+\sum_{t\in\Omega^T}\sum_{i\in(\Omega^{NG}\cap\Omega_t^{NL})}\sum_{g\in\Omega^{gr}}\vartheta_{i,g,t}^{PGR(m)}\overline{\overline{P_g^{GR}}}\left(x_{i,g,t}^{GR}-\hat{x}_{i,g,t}^{GR(m)}\right)\geq 0\quad\forall m=1,\dots,M^{Feas.}\qquad(4.38)$$

4.4 Simulation Results and Discussion

In this section, the most important results obtained from the application of the proposed solution procedure to the MDEP problem are presented and discussed. All the simulations have been implemented on a PC with a 3.40 GHz Intel Core i7-4770 processor and 16 GB of RAM using MATLAB R2015a [84] and CPLEX 12.6.1 [85]. The 24-node and 138-node distribution systems are again utilized to carry out the simulations. The data related to the candidate conductor types, alternatives for construction/reinforcement of substations, alternatives for installation of renewable/conventional DGs, power demands, lengths of feeder sections, and other parameters of the problem are exactly the same as those presented in Chapter 2.

4.4.1 A Discussion on the Solution Optimality and Computation Time of the Accelerated BD Algorithm

The performance of the proposed solution procedure in solving the MDEP problem is here assessed from the optimality and computation time perspectives. To this end, the original MDEP problem is directly solved using the standard off-the-shelf mathematical programming solvers and the obtained results are compared with those achieved by solving the decomposed MDEP problem using the accelerated BD algorithm. Note that the simulations are conducted considering the convergence criterion of ζ=0.001.

Figure 4.3 depicts the expansion plans found by the proposed solution procedure and the direct solution method. As can be seen, the system topologies, substation constructions/reinforcements, feeder section replacements/constructions, and renewable/conventional DG installations obtained by the proposed solution procedure are exactly the same as those achieved by the direct solution

method. The only difference is that using the accelerated BD algorithm causes the feeder section 18-14 to be constructed with conductor type 2 (as shown in red color), while this feeder section is constructed with conductor type 1 when the direct solution method is utilized. This slight difference demonstrates the ability of the proposed accelerated BD algorithm to find the optimal solution of the MDEP problem.

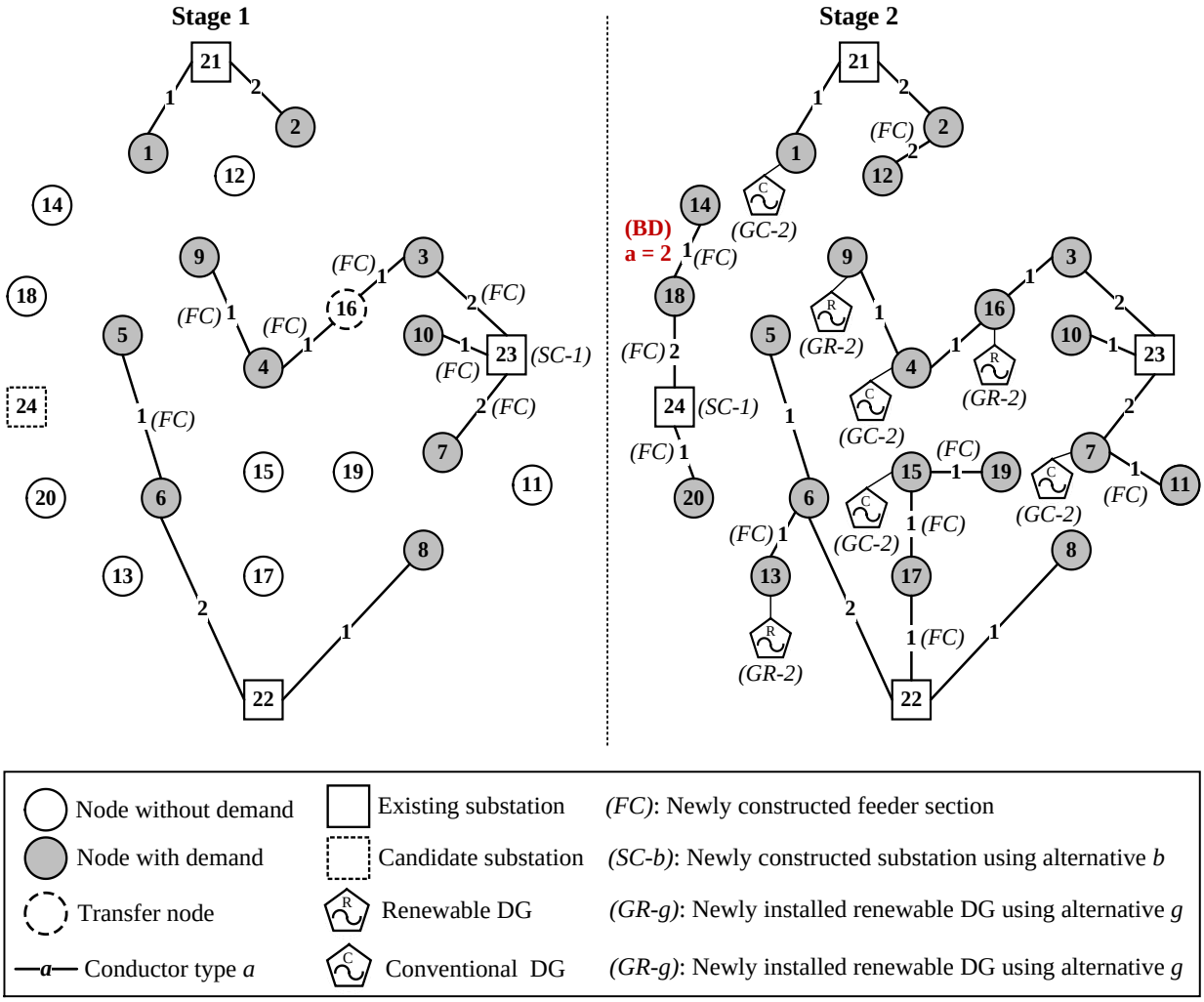

Figure 4.3 Comparison of the expansion plans obtained by the proposed solution procedure and the direct solution method for the 24-node test system.

Table 4.1 compares the investment, operation, and total costs obtained by the accelerated BD algorithm and the direct solution method at different planning stages. These cost information help to more accurately investigate the optimality of the expansion plans found by the proposed solution procedure. It can be observed that at stage 1, the accelerated BD algorithm and the direct solution method have resulted in the same investment and operation costs. At stage 2, however, there is a

slight difference between the investment and operation costs obtained by the accelerated BD algorithm and those achieved by the direct solution method. The total cost resulted from the accelerated BD algorithm is just 0.024% higher than that yielded by the direct solution method. This fact provides another evidence for the ability of the proposed solution procedure to find the optimal solution of the MDEP problem.

Table 4.1 Comparison of the investment, operation, and total costs obtained by the proposed solution procedure and the direct solution method for the 24-node test system (US$).

Solution method	Costs	Stages	
		1	2
Direct solution method (Original MDEP)	Investment	1,050,600	5,649,091
	Operation	10,245,971	21,646,837
	Total	38,592,499	
Accelerated BD algorithm (Decomposed MDEP)	Investment	1,050,600	5,659,091
	Operation	10,245,971	21,646,011
	Total	38,601,673	

The direct solution method and the accelerated BD algorithm required 15 min and 12 sec to solve the MDEP problem, respectively. That is, the accelerated BD algorithm has solved the MDEP problem 75 times faster than the direct solution method. This significant reduction of the computation time proves another outstanding merit of the proposed solution procedure.

4.4.2 Performance Evaluation of the Acceleration Strategies Proposed for the BD Algorithm

In Section 4.3, two acceleration strategies (i.e., modification of the master problem and generation of the auxiliary optimality cuts) were proposed to make the solution process of the decomposed MDEP problem more efficient and less time-consuming. In the following, these acceleration strategies are step by step applied to the BD algorithm and their impacts on different aspects of the solution process are analyzed.

Table 4.2 compares the performances of three different versions of the BD algorithm in solving the MDEP problem:

- **Version 1:** The classical BD algorithm.
- **Version 2:** The accelerated BD algorithm including only the modified master problem.
- **Version 3:** The accelerated BD algorithm including both the modified master problem and the auxiliary optimality cuts.

In Table 4.2, UB and LB stand for the upper and lower bounds, respectively. As can be observed, the classical BD algorithm is not able to converge to the optimal solution, so that even after 861 iterations taking 62 min, no feasible solution is found by the master problem. Whereas, the proposed acceleration strategies have caused the BD algorithm to achieve the convergence very fast. Moreover, the computation time and number of iterations required by Version 3 are significantly lower than those required by Version 2, which demonstrates the highly effective role of the auxiliary optimality cuts in the rapid acceleration of the solution process.

Table 4.2 Performance comparison of the classical BD algorithm and the proposed accelerated BD algorithm in solving the MDEP problem for the 24-node test system.

BD algorithm	Converged	Time	No. of iterations	Relative gap between UB and LB
Version 1	No	62 min	861	No feasible solution was found
Version 2	Yes	7 min	285	0.06%
Version 3	Yes	12 sec	77	0.03%

In order to clearly illustrate how the auxiliary optimality cuts can accelerate the solution process of the MDEP problem, the key features of some selected iterations of Versions 2 and 3 of the BD algorithm are tabulated in Tables 4.3 and 4.4. By comparing these two tables, it can be observed that the benefits of the auxiliary optimality cuts are twofold. The first benefit is to dramatically reduce the search space of the master problem, which causes its solution time to be significantly shortened. As can be seen in Table 4.3, when the auxiliary optimality cuts are not considered, the time consumed for solving the master problem in each iteration is between 1 to 2 sec. Whereas, the results presented in Table 4.4 show that by including the auxiliary optimality cuts in the master problem, its solution time is reduced to less than 0.25 sec from the second iteration onwards. The second benefit is to keep the near-optimality of the master problem solutions in all the iterations. Table 4.3 shows that when the auxiliary optimality cuts are not considered, in spite of the near-

optimality of the master problem solution in the first iteration, the relative gap between the upper and lower bounds experiences a large increase after the first iteration. That is, in the iterations following the first iteration, the master problem solution gets away from the optimal solution. However, as can be observed in Table 4.4, by adding the auxiliary optimality cuts to the master problem, the relative gap between the upper and lower bounds is always very small. This implies that the master problem solution is kept near-optimal and, hence, a small number of iterations are required to obtain the convergence.

It is necessary to mention that in the first iteration, the relative gap between the upper and lower bounds (i.e., $[(UB - LB)/LB] \times 100$) cannot be defined. The reason is that in the first iteration, in order to prevent the master problem from being unbounded, the variable Ψ is set to zero. This causes the lower bound to only include the investment costs (i.e., $LB = c^{Inv.} + \Psi = c^{Inv.} + 0$), while the upper bound includes both the investment and operation costs ($UB = c^{Inv.} + c^{Oper.}$). Therefore, the relative gap between the upper and lower bounds for the first iteration has not been reported in Tables 4.3 and 4.4.

Table 4.3 Key features of some selected iterations of Version 2 of the BD algorithm for the 24-node test system.

Iteration	Master problem solution time (sec)	Relative gap between UB and LB
1	1.27	−
2	1.06	-178.67%
3	1.15	-110.93%
4	1.80	-116.32%
5	1.79	-117.26%
…	…	…
281	1.44	1.39%
282	1.53	3.43%
283	1.62	2.2%
284	1.93	7.43%
285	1.84	0.06%

Table 4.4 Key features of some selected iterations of Version 3 of the BD algorithm for the 24-node test system.

Iteration	Master problem solution time (sec)	Relative gap between UB and LB
1	1.27	–
2	0.13	6.01%
3	0.09	5.55%
4	0.14	6.49%
5	0.19	6.11%
…	…	…
74	0.18	0.83%
75	0.21	1.38%
76	0.14	1.08%
77	0.17	0.03%

Figure 4.4 depicts the convergence trends of Versions 2 and 3 of the BD algorithm by comparing the value of the variable Ψ with the objective value of the optimal operation subproblem $c^{Oper.}$ for the second iteration onwards. As can be seen, when the auxiliary optimality cuts are not considered, the master problem solution gets away from the optimal one and the variable Ψ attains very large negative values at the beginning of the solution process (i.e., iterations 2 to 34). This causes the relative gap between the upper and lower bounds to significantly increase. Consequently, a relatively large number of iterations are required to decrease this big gap and achieve the convergence. However, by considering the auxiliary optimality cuts, the master problem solution is kept near-optimal and the variable Ψ always attains positive values that are quite close to $c^{Oper.}$. In this way, the relative gap between the upper and lower bounds remains small during the whole solution process and, hence, the BD algorithm quickly converges to the optimal solution.

It is worth noting that the difference between the upper and lower bounds is exactly the same as the difference between $c^{Oper.}$ and Ψ, as shown in (4.39). This is the reason why the convergence

trends of the proposed accelerated BD algorithm are investigated by comparing the values of $c^{Oper.}$ and Ψ in different iterations.

$$UB - LB = (c^{Inv.} + c^{Oper.}) - (c^{Inv.} + \Psi) = c^{Oper.} - \Psi \tag{4.39}$$

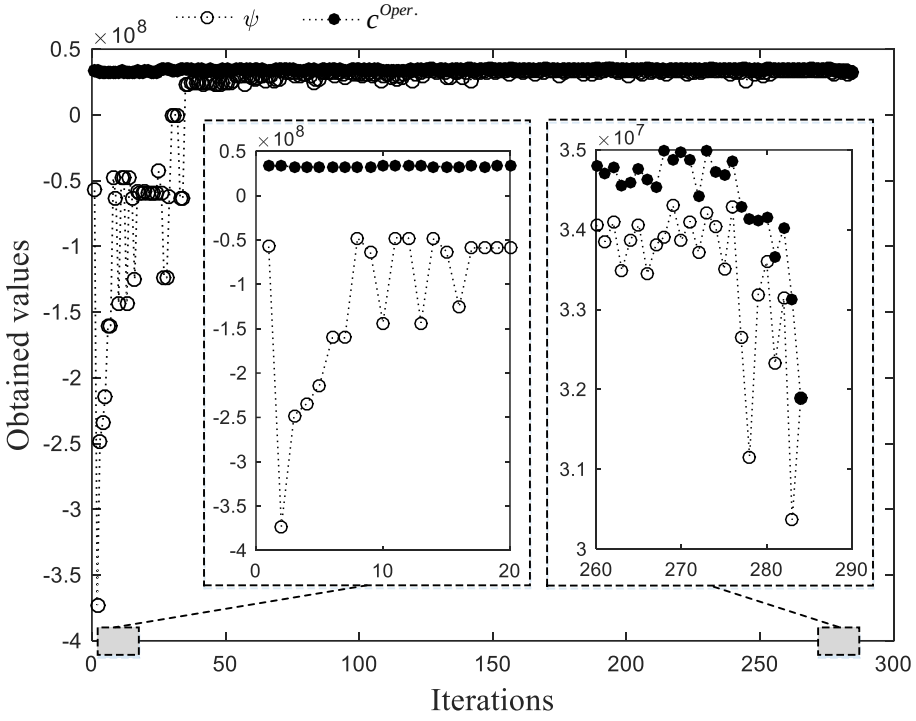

(a)

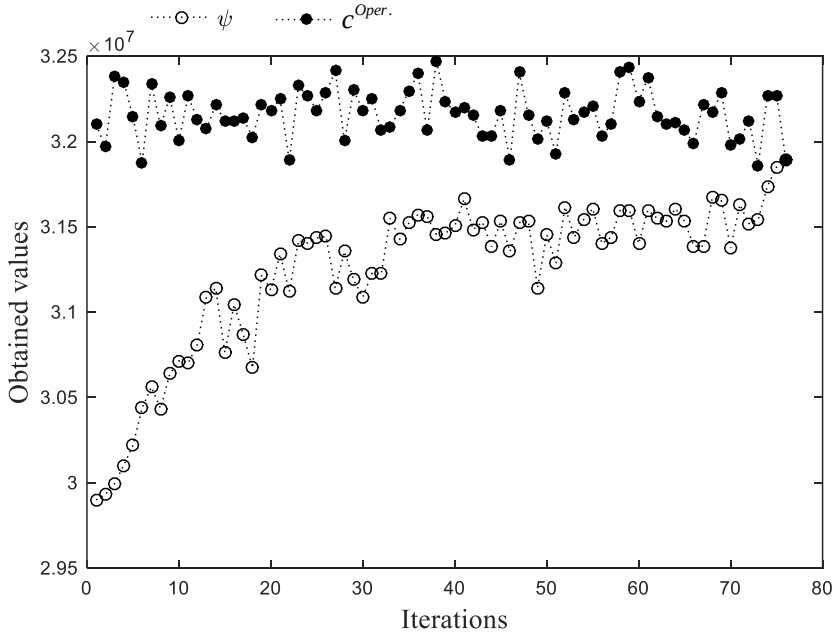

(b)

Figure 4.4 Convergence trends of the proposed accelerated BD algorithm for the 24-node test system: (a) Version 2, (b) Version 3.

4.4.3 An Extended Case Study

The 138-node distribution system is here employed to demonstrate the scalability of the solution procedure proposed for the MDEP problem. The data required to carry out the simulations are exactly the same as those presented in Chapter 2.

The simulation results show that the accelerated BD algorithm requires 95 iterations taking 76 sec to solve the MDEP problem of the 138-node test system, while the direct solution method consumes a computation time of 83 min to find the optimal solution. That is, the accelerated BD algorithm has solved the MDEP problem 65 times faster than the direct solution method. This fact demonstrates another outstanding merit of the proposed solution procedure, i.e., its ability to quickly solve large-scale MDEP problems that are time-consuming to be directly solved using the standard off-the-shelf mathematical programming solvers.

4.5 Summary

In this chapter, a fast BD-based solution procedure has been proposed for the MDEP problem. This solution procedure has been obtained by applying two novel acceleration strategies (namely modification of the master problem and generation of the auxiliary optimality cuts) to the classical BD algorithm. These acceleration strategies, when used together, not only decrease the number of iterations required by the BD algorithm to reach the convergence, but also shorten the time consumed by each iteration. In this way, an accelerated version of the BD algorithm has been achieved, which is capable of solving the MDEP problem in a computationally efficient manner.

The proposed solution procedure has been successfully validated using the 24-node and 138-node distribution systems. The simulation results show that the accelerated BD algorithm is able to find the optimal solution of the MDEP problem tens of times faster than the standard off-the-shelf mathematical programming solvers. The results also show that the straightforward application of the classical BD algorithm to the MDEP problem leads to a failure to achieve the convergence. Whereas, the accelerated BD algorithm is able to quickly converge to the optimal solution, which indicates the highly effective role of the proposed acceleration strategies in speeding up the solution process. Moreover, the scalability of the proposed solution procedure is demonstrated by solving a large-scale MDEP problem.

In fact, the proposed fast solution procedure has paved the way for Steps 4 and 5 of the project. The reason is that the incorporation of ESSs and DRLs into the MDEP problem requires us to consider the load and renewable generation profiles that reflect the chronological relationship between demand and generation. This necessitates simultaneous consideration of a wide range of operating conditions of ADNs. It is possible to deal with such a large number of operating conditions only if the developed planning methodology is fast enough.

5. A Robust Sequential-Time Simulation-Based Decomposed Model for Integrated Planning of Distribution Network, Distributed Generation, Energy Storage, and Demand Response

5.1 Introduction

Significant techno-economic and environmental benefits of DERs (i.e., DGs, ESSs, and DRLs) have brought them into the core of the future development of distribution systems [90], [91]. According to a recent report published by Navigant Research, the global capacity of DERs is forecasted to grow from 132.4 GW in 2017 to 528.4 GW in 2026 [92]. This tremendous growth of DERs will present serious challenges to distribution system planners from the viewpoints of simulation and analysis. One of the major challenges is that successful network integration of DERs requires a distribution system planning model with the capability of incorporating the short-term operation analysis into the long-term planning studies [48]. This is, on the one hand, due to the fact that ESSs store "energy" which is the time integral of power [78]. This fact makes it necessary to add the time dimension to the planning problem by simulating distribution system operation over a certain time period (e.g., one day). On the other hand, DRLs have the ability to make significant changes to daily demand profiles by shifting the load demand from one hour to another during the day [47]. This is another factor that necessitates analyzing the short-term operation of distribution system along with its long-term planning studies. To this end, there needs to be a planning model capable of carrying out sequential-time power flow simulation (STPFS) over a series of time slots (e.g., 24 hours) [78], [79]. As opposed to the static power flow simulation (SPFS) which only considers one single operating state, the STPFS provides the opportunity to account for a series of operating states [78]. In this way, the STPFS enables the distribution system

planners to perform chronological simulations required for analyzing the short-term operational impacts of ESSs and DRLs when deciding about the long-term expansion plans.

Based on the above discussion, the Electric Power Research Institute (EPRI) has identified the STPFS capability as the most important requirement for future distribution system planning tools [79]. However, the challenge is that the STPFS calls for simultaneous analysis of a relatively large number of operating states, which causes the planning problem to become very computationally demanding or even intractable, especially when dealing with large-scale distribution systems. This challenge can be met only if the planning model is computationally fast enough.

In the existing literature, two main approaches have been used to achieve the computational speed required for conducting STPFS. A group of researchers have increased the speed of their proposed planning models by using simplified distribution network models [11], [38-40], [44], [48], [93]. For instance, the authors of [48] propose an expansion planning model for ADNs incorporating ESSs, which performs a simple power flow analysis based on a linear relationship between nodal voltage magnitudes and current flows. The adopted network model completely ignores the energy losses and reactive power, while they are key factors in any study on distribution systems. In [11], [39], an MILP model is developed for joint of distribution network and DER planning, which uses an approximate network model based on DC power flow equations. Similarly, the distribution expansion planning models presented in [38], [44] also utilize a DC power flow model to reduce the computational complexity. Employing these simplified network models can obviously lead to inaccurate and undependable expansion plans for distribution systems. The planning models proposed in [40], [93] have a clear advantage over those presented in [11], [38], [39], [44], [48] as they use linearized versions of AC power flow equations. Nevertheless, they also make some error-prone assumptions to overcome the nonlinearities of AC power flow equations. Another group of researchers have utilized heuristic solution methods such as genetic algorithm (GA) [3], [47], [94], immune genetic algorithm (IGA) [32], particle swarm optimization (PSO) [9], [26], [31], tabu search (TS) [26], [33], simulated annealing (SA) [33], and artificial bee colony (ABC) [29] to solve their proposed planning models with the required speed. For instance, the authors of [47] present an integrated planning model that considers renewable DGs and DRLs as expansion alternatives to reduce the carbon footprint of distribution systems, where an interior-point-method-embedded discrete GA (IPM-DGA) is employed to find the

optimal solution. In [3], a scenario-based model is developed to investigated the impacts of large-scale electric vehicle (EV) penetration on the expansion planning of distribution networks, while a GA with the elitist strategy is used to solve the model. A long-term planning model to determine the optimal location, capacity, and power rating of ESSs in a distribution network integrated with wind-based DGs is presented in [9], which is solved using a hybrid solution method based on the TS and PSO algorithms. The authors of [26] develop an MINLP model for the expansion planning of ADNs, which takes the reactive power generation capability of different renewable DG technologies into consideration. This MINLP model is solved by a hybrid solution method based on the PSO algorithm and the ordinal optimization (OO) approach. In [33], the optimal planning of DGs and ESSs is considered as an option to mitigate the impacts of EVs on distribution systems, where the TS and SA algorithms are utilized to solve the short-term operation and long-term planning problems, respectively. The main drawback of the above-mentioned heuristic solution methods is that they not only cannot guarantee obtaining the global optimal solution, but also do not provide a measure of the quality of the obtained solution (i.e., distance to the global optimum). In summary, it can be stated that the planning models existing in the literature have attained the required computational speed by sacrificing either the accuracy of the network model or the optimality of the solution.

This chapter develops an MDEP model for integrated expansion of distribution network assets (i.e., feeders and substations) and DERs (i.e., DGs, ESSs, and DRLs), which is capable of performing sequential-time simulation (STS) without suffering from the above-described drawbacks. The developed STS-based MDEP model not only incorporates a highly accurate linearized distribution network model reflecting AC power flow equations, but is also able to quickly find the global optimal solution with a low computational effort. In this regard, by making use of the fast solution procedure proposed in Chapter 4, the MDEP model is partitioned into a master problem and two subproblems, and the optimal solution is found through an iterative process. The master problem determines the long-term expansion plans, while the subproblems conduct the short-term STS-based operation analysis considering the linearized AC power flow equations proposed in Chapter 2.

With regard to energy storage modelling, we have explored different ESS technologies that are appropriate for employment in ADNs. After careful comparison of different ESS technologies,

advanced adiabatic compressed air energy storage (AA-CAES) is chosen as the energy storage option for ADNs due to its lower costs and significantly longer lifetime compared to other technologies [80]. In this regard, a detailed AA-CAES model is proposed and incorporated into the developed STS-based MDEP model. Moreover, with regard to demand response modelling, we have considered an hourly real-time pricing (RTP) scheme which is the most effective time-based pricing structure to encourage consumers to use electricity in a more efficient manner [95]. In order to model the reaction of DRLs to electricity price changes, we have employed a demand function based on self-price and cross-price elasticities of demand. The proposed DRL model is successfully included in the developed STS-based MDEP model.

It should be noted that a new robust optimization-based approach is also proposed in this chapter to model the uncertainties of renewable generations, loads, and electricity prices [96], [97]. The reason for proposing this new uncertainty modelling approach is that the DRCCP approach proposed in Chapter 2 cannot be used when the BD algorithm is applied to the MDEP problem. In the BD algorithm, the subproblems should not include any binary variables, while the piecewise-based linearization method employed by the DRCCP approach will introduce binary variables to the subproblems. As a result, we have proposed a new robust optimization-based uncertainty modelling approach which has the significant advantages of the DRCCP approach, but it does not introduce any binary variables to the subproblems. This approach allows controlling the degree of conservatism of the solution and also provides the decision maker with a probabilistic bound on the robustness level of the obtained solution. These features make the proposed approach stand out among other robust optimization approaches existing in the literature.

5.2 Deterministic Sequential-Time Simulation-Based Decomposed Model Developed for the MDEP Problem

In this section, the uncertainties of renewable generations, loads, and electricity prices are ignored and a deterministic decomposed model with the ability to carry out STS is developed for the MDEP problem. This model consists of a master problem, an optimal operation subproblem, and a feasibility check subproblem, which are iteratively solved based on the accelerated BD algorithm proposed in Chapter 4. The master problem determines the long-term plans for construction/replacement of feeder sections, construction/reinforcement of substations,

installation of renewable/conventional DGs, installation of ESSs, and installation of smart meters. Whereas, the subproblems analyze the short-term STS-based operation of distribution system considering the expansion plans found by the master problem.

5.2.1 Master Problem

The master problem only includes the binary decision variables of the MDEP problem and determines the investment and utilization decisions. The objective function of this problem is to minimize the present value of the investment costs over the planning period:

$$\text{Minimize } \; c^{Inv.} + \Psi \tag{5.1}$$

$$\begin{aligned} c^{Inv.} = \sum_{t\in\Omega^T} \frac{1}{(1+r)^{(t-1)D}} \Bigg[& \sum_{(ij)\in\Omega^{FR}} \sum_{a\in\left(\Omega^a - a_{ij}^{FR}\right)} c_a^{FR} l_{ij} x_{ij,a,t}^{FR} + \sum_{(ij)\in\Omega^{FC}} \sum_{a\in\Omega^a} c_a^{FC} l_{ij} x_{ij,a,t}^{FC} \\ & + \sum_{i\in\Omega^{SR}} \sum_{b\in\Omega^b} c_b^{SR} x_{i,b,t}^{SR} + \sum_{i\in\Omega^{SC}} \sum_{b\in\Omega^b} c_b^{SC} x_{i,b,t}^{SC} + \sum_{i\in\left(\Omega^{NG}\cap\Omega_t^{NL}\right)} \sum_{g\in\Omega^{gr}} c_g^{GR} x_{i,g,t}^{GR} \\ & + \sum_{i\in\left(\Omega^{NG}\cap\Omega_t^{NL}\right)} \sum_{g\in\Omega^{gc}} c_g^{GC} x_{i,g,t}^{GC} + \sum_{i\in\left(\Omega^{NES}\cap\Omega_t^{NL}\right)} \sum_{s\in\Omega^{es}} c_s^{ES} x_{i,s,t}^{ES} \\ & + \sum_{i\in\left(\Omega^{NSM}\cap\Omega_t^{NL}\right)} \sum_{p\in\Omega^{sm}} \kappa_p^{SM} N_{i,t}^{C} c^{SM} x_{i,p,t}^{SM} \Bigg] \end{aligned} \tag{5.2}$$

In the above objective function, $c^{Inv.}$ represents the present value of the investment costs required for replacement of existing feeder sections, construction of new feeder sections, reinforcement of existing substations, construction of new substations, installation of renewable/conventional DGs, installation of ESSs, and installation of smart meters. Note that the planning horizon is divided into a number of stages with known duration, and the binary variables denoted by "x" are used to model the investment decisions made in each planning stage. In (5.1), Ψ is a continuous variable required for generating optimality cuts.

The constraints of the master problem can be categorized into three main groups: 1) constraints on binary investment and utilization variables, 2) radiality constraints, and 3) optimality and feasibility cuts. In the following, these three groups are described in detail.

5.2.1.1 Constraints on Binary Investment and Utilization Variables

Constraints (5.3)-(5.6) ensure that a maximum of one construction or reinforcement is performed for each feeder section or substation during the planning horizon. Constraint (5.7) limits the

number DG installations at each candidate node to one. Constraint (5.8) is used to avoid more than one ESS installation at each candidate node. Constraint (5.9) guarantees that each candidate node is equipped with smart meters at most once. Constraints (5.10)-(5.12) determine the maximum number of renewable DGs, conventional DGs, and ESSs that can be installed in the system. Constraint (5.13) specifies the maximum number of nodes that can be equipped with smart meters. Constraints (5.14)-(5.18) ensure that different types of feeder sections (i.e., existing replaceable, existing irreplaceable, and candidate for construction) can be operated only if their corresponding investments have already been made. The binary variables denoted by "y" represent the operating conditions of feeder sections. In this regard, $y_{ij,a,t} = 1$ indicates that feeder section ij with conductor type a is utilized at planning stage t. By contrast, $y_{ij,a,t} = 0$ means that feeder section ij with conductor type a is not operated at planning stage t. Constraint (5.19) is used to avoid simultaneous charging and discharging of ESSs. This constraint also makes sure that an ESS can be operated only if its corresponding investment has already been made.

$$\sum_{t\in\Omega^T}\sum_{a\in\Omega^a} x_{ij,a,t}^{FC} \le 1 \qquad \forall (ij)\in\Omega^{FC} \tag{5.3}$$

$$\sum_{t\in\Omega^T}\sum_{a\in\left(\Omega^a - a_{ij}^{FR}\right)} x_{ij,a,t}^{FR} \le 1 \qquad \forall (ij)\in\Omega^{FR} \tag{5.4}$$

$$\sum_{t\in\Omega^T}\sum_{b\in\Omega^b} x_{i,b,t}^{SC} \le 1 \qquad \forall i\in\Omega^{SC} \tag{5.5}$$

$$\sum_{t\in\Omega^T}\sum_{b\in\Omega^b} x_{i,b,t}^{SR} \le 1 \qquad \forall i\in\Omega^{SR} \tag{5.6}$$

$$\sum_{t\in\Omega^T}\sum_{g\in\Omega^{gc}} x_{i,g,t}^{GC} + \sum_{t\in\Omega^T}\sum_{g\in\Omega^{gr}} x_{i,g,t}^{GR} \le 1 \qquad \forall i\in\Omega^{NG} \tag{5.7}$$

$$\sum_{t\in\Omega^T}\sum_{s\in\Omega^{es}} x_{i,s,t}^{ES} \le 1 \qquad \forall i\in\Omega^{NES} \tag{5.8}$$

$$\sum_{t\in\Omega^T}\sum_{p\in\Omega^{sm}} x_{i,p,t}^{SM} \le 1 \qquad \forall i\in\Omega^{NSM} \tag{5.9}$$

$$\sum_{t\in\Omega^T}\sum_{i\in\left(\Omega^{NG}\cap\Omega_t^{NL}\right)}\sum_{g\in\Omega^{gr}} x_{i,g,t}^{GR} \le \overline{N^{GR}} \tag{5.10}$$

$$\sum_{t\in\Omega^T}\sum_{i\in\left(\Omega^{NG}\cap\Omega_t^{NL}\right)}\sum_{g\in\Omega^{gc}} x_{i,g,t}^{GC} \le \overline{N^{GC}} \tag{5.11}$$

$$\sum_{t\in\Omega^T}\sum_{i\in\left(\Omega^{NES}\cap\Omega_t^{NL}\right)}\sum_{s\in\Omega^{es}} x_{i,s,t}^{ES} \le \overline{N^{ES}} \tag{5.12}$$

$$\sum_{t\in\Omega^T}\sum_{i\in\left(\Omega^{NSM}\cap\Omega_t^{NL}\right)}\sum_{p\in\Omega^{sm}} x_{i,p,t}^{SM} \le \overline{N^{SM}} \tag{5.13}$$

$$y_{ij,a,t} \le \sum_{v=1}^{t} x_{ij,a,v}^{FR} \qquad \forall (ij) \in \Omega^{FR}, \forall a \in \left(\Omega^{a} - a_{ij}^{FR}\right), \forall t \in \Omega^{T} \qquad (5.14)$$

$$y_{ij,a,t} \le 1 - \sum_{v=1}^{t} \sum_{\omega \in \left(\Omega^{a} - a_{ij}^{FR}\right)} x_{ij,\omega,v}^{FR} \qquad \forall (ij) \in \Omega^{FR}, \forall a = a_{ij}^{FR}, \forall t \in \Omega^{T} \qquad (5.15)$$

$$y_{ij,a,t} = 0 \qquad \forall (ij) \in \Omega^{FI}, \forall a \in \left(\Omega^{a} - a_{ij}^{FI}\right), \forall t \in \Omega^{T} \qquad (5.16)$$

$$y_{ij,a,t} \le 1 \qquad \forall (ij) \in \Omega^{FI}, \forall a = a_{ij}^{FI}, \forall t \in \Omega^{T} \qquad (5.17)$$

$$y_{ij,a,t} \le \sum_{v=1}^{t} x_{ij,a,v}^{FC} \qquad \forall (ij) \in \Omega^{FC}, \forall a \in \Omega^{a}, \forall t \in \Omega^{T} \qquad (5.18)$$

$$\alpha_{i,s,h,t}^{Ch} + \alpha_{i,s,h,t}^{Dch} \le \sum_{v=1}^{t} x_{i,s,v}^{ES} \qquad \forall i \in (\Omega^{NES} \cap \Omega_{t}^{NL}), \forall s \in \Omega^{es}, \forall h \in \Omega^{H}, \forall t \in \Omega^{T} \qquad (5.19)$$

5.2.1.2 Radiality Constraints

Constraints (5.20)-(5.28) guarantee the radiality of the distribution network [36], [82]. If DGs were not considered as expansion alternatives, constraints (5.20)-(5.23) would be enough to ensure the radiality of the network. However, when DGs are brought into play, constraints (5.24)-(5.28) should also be considered in order to prevent the existence of areas exclusively supplied by DGs. These constraints assign fictitious current flow demands to the candidate nodes for DG installation and, in this way, keep them connected to the substations to preclude formation of isolated areas [36]. It should be noted that the distribution system is assumed to include a number of so-called "transfer nodes" at some of the planning stages [82]. These nodes are not connected to the loads or substations, but they can be used to connect different load nodes to each other and, in this way, may help to find better planning solutions. The binary variables denoted by "z" represent the operating conditions of the transfer nodes. In this regard, $z_{i,t} = 1$ indicates that transfer node i is operated at planning stage t. Whereas, $z_{i,t} = 0$ means that transfer node i is not utilized at planning stage t.

$$\sum_{(ij) \in \Omega^{F}} \sum_{a \in \Omega^{a}} y_{ij,a,t} = |\Omega^{N}| - |\Omega^{NS}| - \sum_{i \in \Omega_{t}^{NT}} \left(1 - z_{i,t}\right) \quad \forall t \in \Omega^{T} \qquad (5.20)$$

$$\sum_{(ki) \in \Omega^{F}} \sum_{a \in \Omega^{a}} y_{ki,a,t} + \sum_{(ij) \in \Omega^{F}} \sum_{a \in \Omega^{a}} y_{ij,a,t} \ge 2 z_{i,t} \qquad \forall i \in \Omega_{t}^{NT}, \forall t \in \Omega^{T} \qquad (5.21)$$

$$\sum_{a \in \Omega^{a}} y_{ki,a,t} \le z_{i,t} \qquad \forall (ki) \in \Omega^{F}, \forall i \in \Omega_{t}^{NT}, \forall t \in \Omega^{T} \qquad (5.22)$$

$$\sum_{a \in \Omega^{a}} y_{ij,a,t} \le z_{i,t} \qquad \forall (ij) \in \Omega^{F}, \forall i \in \Omega_{t}^{NT}, \forall t \in \Omega^{T} \qquad (5.23)$$

$$\sum_{(ki)\in\Omega^F} \tilde{\theta}^F_{ki,t} - \sum_{(ij)\in\Omega^F} \tilde{\theta}^F_{ij,t} + \tilde{\theta}^S_{i,t} = \tilde{\theta}^D_{i,t} \quad \forall i \in \Omega^N, \forall t \in \Omega^T \tag{5.24}$$

$$\tilde{\theta}^F_{ij,t} \le |\Omega^{NG}| \sum_{a\in\Omega^a} y_{ij,a,t} \quad \forall (ij) \in \Omega^F, \forall t \in \Omega^T \tag{5.25}$$

$$\tilde{\theta}^S_{i,t} \le |\Omega^{NG}| \quad \forall i \in \Omega^{SR}, \forall t \in \Omega^T \tag{5.26}$$

$$\tilde{\theta}^S_{i,t} \le |\Omega^{NG}| \left(\sum_{\upsilon=1}^{t} \sum_{b\in\Omega^b} x^{SC}_{i,b,\upsilon}\right) \quad \forall i \in \Omega^{SC}, \forall t \in \Omega^T \tag{5.27}$$

$$\tilde{\theta}^D_{i,t} = \begin{cases} 1 & \forall i \in (\Omega^{NG} \cap \Omega^{NL}_t), \forall t \in \Omega^T \\ 0 & \forall i \notin (\Omega^{NG} \cap \Omega^{NL}_t), \forall t \in \Omega^T \end{cases} \tag{5.28}$$

5.2.1.3 Optimality and Feasibility Cuts

As described in Section 4.2.4, the BD algorithm finds the optimal solution of the MDEP problem through an iterative process in which multiple optimality and feasibility cuts are generated and added to the master problem. Constraints (5.29) and (5.30) respectively represent the optimality and feasibility cuts added to the master problem in different iterations of the BD algorithm. These cuts are generated based on the information received from the optimal operation and feasibility check subproblems.

$$\Psi \ge c^{Oper.(m)} + \sum_{t\in\Omega^T} \sum_{h\in\Omega^H} \sum_{(ij)\in\Omega^F} \sum_{a\in\Omega^a} \vartheta^{fF(m)}_{ij,a,h,t} \left(\overline{I_a}\right)^2 \left(y_{ij,a,t} - \hat{y}^{(m)}_{ij,a,t}\right)$$

$$- \sum_{t\in\Omega^T} \sum_{h\in\Omega^H} \sum_{(ij)\in\Omega^F} \left(\vartheta^{\Delta V1(m)}_{ij,h,t} + \vartheta^{\Delta V2(m)}_{ij,h,t}\right) \overline{\Delta V} \left[\sum_{a\in\Omega^a} \left(y_{ij,a,t} - \hat{y}^{(m)}_{ij,a,t}\right)\right]$$

$$+ \sum_{t\in\Omega^T} \sum_{h\in\Omega^H} \sum_{i\in\Omega^{SR}} \vartheta^{SR(m)}_{i,h,t} \left[\sum_{\upsilon=1}^{t} \sum_{b\in\Omega^b} \overline{S_b} \left(x^{SR}_{i,b,\upsilon} - \hat{x}^{SR(m)}_{i,b,\upsilon}\right)\right]$$

$$+ \sum_{t\in\Omega^T} \sum_{h\in\Omega^H} \sum_{i\in\Omega^{SC}} \vartheta^{SC(m)}_{i,h,t} \left[\sum_{\upsilon=1}^{t} \sum_{b\in\Omega^b} \overline{S_b} \left(x^{SC}_{i,b,\upsilon} - \hat{x}^{SC(m)}_{i,b,\upsilon}\right)\right]$$

$$+ \sum_{t\in\Omega^T} \sum_{h\in\Omega^H} \sum_{i\in(\Omega^{NG}\cap\Omega^{NL}_t)} \sum_{g\in\Omega^{gc}} \vartheta^{PGC(m)}_{i,g,h,t} \left[\sum_{\upsilon=1}^{t} \overline{P^{GC}_g} \left(x^{GC}_{i,g,t} - \hat{x}^{GC(m)}_{i,g,t}\right)\right]$$

$$+ \sum_{t\in\Omega^T} \sum_{h\in\Omega^H} \sum_{i\in(\Omega^{NG}\cap\Omega^{NL}_t)} \sum_{g\in\Omega^{gc}} \left(\vartheta^{QGC1(m)}_{i,g,h,t} + \vartheta^{QGC2(m)}_{i,g,h,t}\right) \left[\sum_{\upsilon=1}^{t} \overline{Q^{GC}_g} \left(x^{GC}_{i,g,t} - \hat{x}^{GC(m)}_{i,g,t}\right)\right]$$

$$+ \sum_{t\in\Omega^T} \sum_{h\in\Omega^H} \sum_{i\in(\Omega^{NG}\cap\Omega^{NL}_t)} \sum_{g\in\Omega^{gr}} \vartheta^{QGR(m)}_{i,g,h,t} \left[\sum_{\upsilon=1}^{t} \tan\left(\cos^{-1}(\rho^{GR})\right) \overline{\overline{P^{GR}_{g,h}}} \left(x^{GR}_{i,g,t} - \hat{x}^{GR(m)}_{i,g,t}\right)\right]$$

$$+ \sum_{t\in\Omega^T} \sum_{h\in\Omega^H} \sum_{i\in(\Omega^{NG}\cap\Omega^{NL}_t)} \sum_{g\in\Omega^{gr}} \vartheta^{PGR(m)}_{i,g,h,t} \left[\sum_{\upsilon=1}^{t} \overline{\overline{P^{GR}_{g,h}}} \left(x^{GR}_{i,g,t} - \hat{x}^{GR(m)}_{i,g,t}\right)\right]$$

$$+\sum_{t\in\Omega^T}\sum_{h\in\Omega^H}\sum_{i\in\left(\Omega^{NES}\cap\Omega_t^{NL}\right)}\sum_{s\in\Omega^{es}}\vartheta_{i,s,h,t}^{PCh(m)}\,\overline{P_s^{Ch}}\left(\alpha_{i,s,h,t}^{Ch}-\hat{\alpha}_{i,s,h,t}^{Ch(m)}\right)$$

$$+\sum_{t\in\Omega^T}\sum_{h\in\Omega^H}\sum_{i\in\left(\Omega^{NES}\cap\Omega_t^{NL}\right)}\sum_{s\in\Omega^{es}}\vartheta_{i,s,h,t}^{PDch(m)}\,\overline{P_s^{Dch}}\left(\alpha_{i,s,h,t}^{Dch}-\hat{\alpha}_{i,s,h,t}^{Dch(m)}\right)$$

$$+\sum_{t\in\Omega^T}\sum_{h\in\Omega^H}\sum_{i\in\Omega^N}\left(\vartheta_{i,h,t}^{DSM(m)}-\vartheta_{i,h,t}^{PD,Unresp(m)}\right)\overline{\overline{P_{i,h,t}^{D}}}\left[\sum_{\upsilon=1}^{t}\sum_{p\in\Omega^{sm}}\kappa_p^{SM}\left(x_{i,p,\upsilon}^{SM}-\hat{x}_{i,p,\upsilon}^{SM(m)}\right)\right]$$

$$\forall m=1,\dots,M^{Feas.} \qquad (5.29)$$

$$\mathcal{K}^{PQ(n)}+\sum_{t\in\Omega^T}\sum_{h\in\Omega^H}\sum_{(ij)\in\Omega^F}\sum_{a\in\Omega^a}\omega_{ij,a,h,t}^{fF(n)}\left(\overline{I_a}\right)^2\left(y_{ij,a,t}-\hat{y}_{ij,a,t}^{(n)}\right)$$

$$-\sum_{t\in\Omega^T}\sum_{h\in\Omega^H}\sum_{(ij)\in\Omega^F}\left(\omega_{ij,h,t}^{\Delta V1(n)}+\omega_{ij,h,t}^{\Delta V2(n)}\right)\overline{\Delta V}\left[\sum_{a\in\Omega^a}\left(y_{ij,a,t}-\hat{y}_{ij,a,t}^{(n)}\right)\right]$$

$$+\sum_{t\in\Omega^T}\sum_{h\in\Omega^H}\sum_{i\in\Omega^{SR}}\omega_{i,h,t}^{SR(n)}\left[\sum_{\upsilon=1}^{t}\sum_{b\in\Omega^b}\overline{S_b}\left(x_{i,b,\upsilon}^{SR}-\hat{x}_{i,b,\upsilon}^{SR(n)}\right)\right]$$

$$+\sum_{t\in\Omega^T}\sum_{h\in\Omega^H}\sum_{i\in\Omega^{SC}}\omega_{i,h,t}^{SC(n)}\left[\sum_{\upsilon=1}^{t}\sum_{b\in\Omega^b}\overline{S_b}\left(x_{i,b,\upsilon}^{SC}-\hat{x}_{i,b,\upsilon}^{SC(n)}\right)\right]$$

$$+\sum_{t\in\Omega^T}\sum_{h\in\Omega^H}\sum_{i\in\left(\Omega^{NG}\cap\Omega_t^{NL}\right)}\sum_{g\in\Omega^{gc}}\omega_{i,g,h,t}^{PGC(n)}\left[\sum_{\upsilon=1}^{t}\overline{P_g^{GC}}\left(x_{i,g,\upsilon}^{GC}-\hat{x}_{i,g,\upsilon}^{GC(n)}\right)\right]$$

$$+\sum_{t\in\Omega^T}\sum_{h\in\Omega^H}\sum_{i\in\left(\Omega^{NG}\cap\Omega_t^{NL}\right)}\sum_{g\in\Omega^{gc}}\left(\omega_{i,g,h,t}^{QGC1(n)}+\omega_{i,g,h,t}^{QGC2(n)}\right)\left[\sum_{\upsilon=1}^{t}\overline{Q_g^{GC}}\left(x_{i,g,\upsilon}^{GC}-\hat{x}_{i,g,\upsilon}^{GC(n)}\right)\right]$$

$$+\sum_{t\in\Omega^T}\sum_{h\in\Omega^H}\sum_{i\in\left(\Omega^{NG}\cap\Omega_t^{NL}\right)}\sum_{g\in\Omega^{gr}}\omega_{i,g,h,t}^{QGR(n)}\left[\sum_{\upsilon=1}^{t}\tan\left(\cos^{-1}(\rho^{GR})\right)\overline{\overline{P_{g,h}^{GR}}}\left(x_{i,g,\upsilon}^{GR}-\hat{x}_{i,g,\upsilon}^{GR(n)}\right)\right]$$

$$+\sum_{t\in\Omega^T}\sum_{h\in\Omega^H}\sum_{i\in\left(\Omega^{NG}\cap\Omega_t^{NL}\right)}\sum_{g\in\Omega^{gr}}\omega_{i,g,h,t}^{PGR(n)}\left[\sum_{\upsilon=1}^{t}\overline{\overline{P_{g,h}^{GR}}}\left(x_{i,g,\upsilon}^{GR}-\hat{x}_{i,g,\upsilon}^{GR(n)}\right)\right]$$

$$+\sum_{t\in\Omega^T}\sum_{h\in\Omega^H}\sum_{i\in\left(\Omega^{NES}\cap\Omega_t^{NL}\right)}\sum_{s\in\Omega^{es}}\omega_{i,s,h,t}^{PCh(n)}\,\overline{P_s^{Ch}}\left(\alpha_{i,s,h,t}^{Ch}-\hat{\alpha}_{i,s,h,t}^{Ch(n)}\right)$$

$$+\sum_{t\in\Omega^T}\sum_{h\in\Omega^H}\sum_{i\in\left(\Omega^{NES}\cap\Omega_t^{NL}\right)}\sum_{s\in\Omega^{es}}\omega_{i,s,h,t}^{PDch(n)}\,\overline{P_s^{Dch}}\left(\alpha_{i,s,h,t}^{Dch}-\hat{\alpha}_{i,s,h,t}^{Dch(n)}\right)$$

$$+\sum_{t\in\Omega^T}\sum_{h\in\Omega^H}\sum_{i\in\Omega^N}\left(\omega_{i,h,t}^{DSM(n)}-\omega_{i,h,t}^{PD,Unresp(n)}\right)\overline{\overline{P_{i,h,t}^{D}}}\left[\sum_{\upsilon=1}^{t}\sum_{p\in\Omega^{sm}}\kappa_p^{SM}\left(x_{i,p,\upsilon}^{SM}-\hat{x}_{i,p,\upsilon}^{SM(n)}\right)\right]\leq 0$$

$$\forall n=1,\dots,N^{Infeas.} \qquad (5.30)$$

where Ψ is a continuous variable included in the objective function of the master problem; $c^{Oper.}$ is the objective value of the optimal operation subproblem; $\vartheta_{ij,a,h,t}^{fF}$, $\vartheta_{ij,h,t}^{\Delta V1}$, $\vartheta_{ij,h,t}^{\Delta V2}$, $\vartheta_{i,h,t}^{SR}$, $\vartheta_{i,h,t}^{SC}$, $\vartheta_{i,g,h,t}^{PGC}$, $\vartheta_{i,g,h,t}^{QGC1}$, $\vartheta_{i,g,h,t}^{QGC2}$, $\vartheta_{i,g,h,t}^{QGR}$, $\vartheta_{i,g,h,t}^{PGR}$, $\vartheta_{i,s,h,t}^{PCh}$, $\vartheta_{i,s,h,t}^{PDch}$, $\vartheta_{i,h,t}^{DSM}$, and $\vartheta_{i,h,t}^{PD,Unresp}$ are the dual variables of

the optimal operation subproblem; m is the index of iterations in which the solution provided by the master problem is feasible; $M^{Feas.}$ denotes the number of iterations in which the solution provided by the master problem is feasible; $\mathcal{K}^{PQ}$ is the objective value of the feasibility check subproblem; $\omega_{ij,a,h,t}^{fF}$, $\omega_{ij,h,t}^{\Delta V1}$, $\omega_{ij,h,t}^{\Delta V2}$, $\omega_{i,h,t}^{SR}$, $\omega_{i,h,t}^{SC}$, $\omega_{i,g,h,t}^{PGC}$, $\omega_{i,g,h,t}^{QGC1}$, $\omega_{i,g,h,t}^{QGC2}$, $\omega_{i,g,h,t}^{QGR}$, $\omega_{i,g,h,t}^{PGR}$, $\omega_{i,s,h,t}^{PCh}$, $\omega_{i,s,h,t}^{PDch}$, $\omega_{i,h,t}^{DSM}$, and $\omega_{i,h,t}^{PD,Unresp}$ are the dual variables of the feasibility check subproblem; n is the index of iterations in which the solution provided by the master problem is infeasible; and $N^{Infeas.}$ denotes the number of iterations in which the solution provided by the master problem is infeasible. Note that the hat signs indicate the values of the binary decision variables obtained by solving the master problem in the previous iterations.

5.2.2 Optimal Operation Subproblem

The optimal operation subproblem only includes the continuous variables of the MDEP problem and performs STPFS for the system configuration found by the master problem. The objective function of this problem is to minimize the present value of the operation costs over the planning period:

$$\text{Minimize } c^{Oper.} \tag{5.31}$$

$$c^{Oper.} = \sum_{t\in\Omega^T} \frac{1}{(1+r)^{(t-1)D}} \frac{(1+r)^D-1}{r(1+r)^D} \tau^{DinY} \Big[\sum_{h\in\Omega^H} \sum_{i\in\Omega^S} c_h^E P_{i,h,t}^S + \sum_{h\in\Omega^H} \sum_{i\in\Omega^S} c_h^E \phi^S f_{i,h,t}^S$$

$$+ \sum_{h\in\Omega^H} \sum_{i\in(\Omega^{NG}\cap\Omega_t^{NL})} \sum_{g\in\Omega^{gc}} c_g^{EGC} P_{i,g,h,t}^{GC} \Big] \tag{5.32}$$

In the above objective function, $c^{Oper.}$ represents the present value of the system operation costs including cost of electrical energy received from the upstream power grid, operation costs of substations, and generation costs of conventional DGs. It should be mentioned that $c^{Oper.}$ also includes the costs of energy losses in feeder sections because the active power received from the upstream grid (i.e., $P_{i,t}^S$) includes the power losses in feeder sections.

The constraints of the optimal operation subproblem can be categorized into three main groups: 1) distribution network model, 2) distributed generation model, 3) energy storage model, and 4) demand response model. In the following, these four groups are described in detail.

5.2.2.1 Distribution Network Model

Constraints (5.33)-(5.43) represent the AC power flow model in a radial distribution network based on the *DistFlow branch equations* (see Appendix A). In this regard, constraints (5.33) and (5.34) guarantee the active and reactive power balances in system nodes, respectively. Constraints (5.35)-(5.37) relate the active, reactive, and apparent power flows and the current flow of each feeder section to the voltages of its sending and receiving ends and, in this way, apply the Kirchhoff's voltage law (KVL) to feeder sections. Constraints (5.38)-(5.41) are used based on the fact that each feeder section uses only one of the candidate conductor types at each planning stage. Constraints (5.42) and (5.43) relate the active, reactive, and apparent power flows provided by each substation to its current flow and voltage magnitude. Constraint (5.44) specifies the acceptable range of the nodal voltage magnitudes. Constraint (5.45) represents the limits on the current flows of feeder sections based on the conductor types used for constructing them. Constraints (5.46) and (5.47) set appropriate bounds on the auxiliary variable $\Delta V_{ij,h,t}$ used in constraint (5.35). Constraints (5.48) and (5.49) cause the apparent power provided by each substation to be less than its installed capacity. Note that $\hat{y}_{ij,a,t}$, $\hat{x}^{SR}_{i,b,v}$, and $\hat{x}^{SC}_{i,b,v}$ have already been determined by the master problem.

$$\sum_{(ki)\in\Omega^F}\sum_{a\in\Omega^a}\left[P^F_{ki,a,h,t}-R_a l_{ki} f^F_{ki,a,h,t}\right]-\sum_{(ij)\in\Omega^F}\sum_{a\in\Omega^a}P^F_{ij,a,h,t}+P^S_{i,h,t}+\sum_{g\in\Omega^{gc}}P^{GC}_{i,g,h,t}$$
$$+\sum_{g\in\Omega^{gr}}P^{GR}_{i,g,h,t}+\sum_{s\in\Omega^{es}}\left[P^{Dch}_{i,s,h,t}-P^{Ch}_{i,s,h,t}\right]=P^D_{i,h,t}\quad \forall i\in\Omega^N,\forall h\in\Omega^H,\forall t\in\Omega^T \tag{5.33}$$

$$\sum_{(ki)\in\Omega^F}\sum_{a\in\Omega^a}\left[Q^F_{ki,a,h,t}-X_a l_{ki} f^F_{ki,a,h,t}\right]-\sum_{(ij)\in\Omega^F}\sum_{a\in\Omega^a}Q^F_{ij,a,h,t}+Q^S_{i,h,t}+\sum_{g\in\Omega^{gc}}Q^{GC}_{i,g,h,t}$$
$$+\sum_{g\in\Omega^{gr}}Q^{GR}_{i,g,h,t}=Q^D_{i,h,t}\qquad \forall i\in\Omega^N,\forall h\in\Omega^H,\forall t\in\Omega^T \tag{5.34}$$

$$u_{i,h,t}-u_{j,h,t}=\sum_{a\in\Omega^a}\left[2\left(R_a l_{ij}P^F_{ij,a,h,t}+X_a l_{ij}Q^F_{ij,a,h,t}\right)-\left(Z_a l_{ij}\right)^2 f^F_{ij,a,h,t}\right]+\Delta V_{ij,h,t}$$
$$\forall (ij)\in\Omega^F,\forall h\in\Omega^H,\forall t\in\Omega^T \tag{5.35}$$

$$u_{i,h,t}\hat{f}^F_{ij,h,t}=\left(\hat{S}^F_{ij,h,t}\right)^2\qquad \forall (ij)\in\Omega^F,\forall h\in\Omega^H,\forall t\in\Omega^T \tag{5.36}$$

$$\left(\hat{S}^F_{ij,h,t}\right)^2=\left(\hat{P}^F_{ij,h,t}\right)^2+\left(\hat{Q}^F_{ij,h,t}\right)^2\qquad \forall (ij)\in\Omega^F,\forall h\in\Omega^H,\forall t\in\Omega^T \tag{5.37}$$

$$\hat{f}^F_{ij,h,t}=\sum_{a\in\Omega^a}f^F_{ij,a,h,t}\qquad \forall (ij)\in\Omega^F,\forall h\in\Omega^H,\forall t\in\Omega^T \tag{5.38}$$

$$\hat{P}^F_{ij,h,t} = \sum_{a\in\Omega^a} P^F_{ij,a,h,t} \qquad \forall(ij)\in\Omega^F, \forall h\in\Omega^H, \forall t\in\Omega^T \qquad (5.39)$$

$$\hat{Q}^F_{ij,h,t} = \sum_{a\in\Omega^a} Q^F_{ij,a,h,t} \qquad \forall(ij)\in\Omega^F, \forall h\in\Omega^H, \forall t\in\Omega^T \qquad (5.40)$$

$$\hat{S}^F_{ij,h,t} = \sum_{a\in\Omega^a} S^F_{ij,a,h,t} \qquad \forall(ij)\in\Omega^F, \forall h\in\Omega^H, \forall t\in\Omega^T \qquad (5.41)$$

$$u_{i,h,t} f^S_{i,h,t} = \left(S^S_{i,h,t}\right)^2 \qquad \forall i\in\Omega^S, \forall h\in\Omega^H, \forall t\in\Omega^T \qquad (5.42)$$

$$\left(S^S_{i,h,t}\right)^2 = \left(P^S_{i,h,t}\right)^2 + \left(Q^S_{i,h,t}\right)^2 \qquad \forall i\in\Omega^S, \forall h\in\Omega^H, \forall t\in\Omega^T \qquad (5.43)$$

$$\left(\underline{V}\right)^2 \le u_{i,h,t} \le \left(\overline{V}\right)^2 \qquad \forall i\in\Omega^N, \forall h\in\Omega^H, \forall t\in\Omega^T \qquad (5.44)$$

$$f^F_{ij,a,h,t} \le \left(\overline{I_a}\right)^2 \hat{y}_{ij,a,t} \qquad :\vartheta^{fF}_{ij,a,h,t} \qquad \forall(ij)\in\Omega^F, \forall a\in\Omega^a, \forall h\in\Omega^H, \forall t\in\Omega^T \qquad (5.45)$$

$$\Delta V_{ij,h,t} \le \overline{\Delta V}\left(1 - \sum_{a\in\Omega^a} \hat{y}_{ij,a,t}\right) \qquad :\vartheta^{\Delta V1}_{ij,h,t} \qquad \forall(ij)\in\Omega^F, \forall h\in\Omega^H, \forall t\in\Omega^T \qquad (5.46)$$

$$-\Delta V_{ij,h,t} \le \overline{\Delta V}\left(1 - \sum_{a\in\Omega^a} \hat{y}_{ij,a,t}\right) \qquad :\vartheta^{\Delta V2}_{ij,h,t} \qquad \forall(ij)\in\Omega^F, \forall h\in\Omega^H, \forall t\in\Omega^T \qquad (5.47)$$

$$S^S_{i,h,t} \le \overline{S^0_i} + \sum_{v=1}^{t} \sum_{b\in\Omega^b} \overline{S_b}\, \hat{x}^{SR}_{i,b,v} \qquad :\vartheta^{SR}_{i,h,t} \qquad \forall i\in\Omega^{SR}, \forall h\in\Omega^H, \forall t\in\Omega^T \qquad (5.48)$$

$$S^S_{i,h,t} \le \sum_{v=1}^{t} \sum_{b\in\Omega^b} \overline{S_b}\, \hat{x}^{SC}_{i,b,v} \qquad :\vartheta^{SC}_{i,h,t} \qquad \forall i\in\Omega^{SC}, \forall h\in\Omega^H, \forall t\in\Omega^T \qquad (5.49)$$

It is clear that constraints (5.36), (5.37), (5.42), and (5.43) are non-convex and nonlinear. This causes the optimal operation subproblem to become a nonlinear programming problem (NLP) which is very difficult to solve. To address this issue, first the exact relaxation technique proposed in Section 2.3 is used to convexify these constraints. After that, the polyhedral-based linearization method proposed in Section 2.4 is employed to linearize the convexified constraints. In this way, the optimal operation subproblem is converted to a linear programming (LP) problem which can be solved to global optimality with a very high computational speed using standard mathematical programming solvers.

5.2.2.2 Distributed Generation Model

Constraints (5.50)-(5.52) limit the active and reactive powers generated by conventional DGs. Constraint (5.53) and (5.54) set the active and reactive power generations of renewable DGs equal to their expected values. It should be mentioned that renewable DGs are assumed to be operated

at a constant power factor (ρ^{GR}) as they often lack the ability to provide controlled reactive power. Constraints (5.50)-(5.54) also ensure that a DG can be operated only if its corresponding investment has already been made.

$$P_{i,g,h,t}^{GC} \leq \sum_{\upsilon=1}^{t} \overline{P_g^{GC}} \hat{x}_{i,g,\upsilon}^{GC} \quad : \vartheta_{i,g,h,t}^{PGC} \quad \forall i \in (\Omega^{NG} \cap \Omega_t^{NL}), g \in \Omega^{gc}, \forall h \in \Omega^H, \forall t \in \Omega^T \qquad (5.50)$$

$$Q_{i,g,h,t}^{GC} \leq \sum_{\upsilon=1}^{t} \overline{Q_g^{GC}}\, \hat{x}_{i,g,\upsilon}^{GC} \quad : \vartheta_{i,g,h,t}^{QGC1} \quad \forall i \in (\Omega^{NG} \cap \Omega_t^{NL}), g \in \Omega^{gc}, \forall h \in \Omega^H, \forall t \in \Omega^T \qquad (5.51)$$

$$-Q_{i,g,h,t}^{GC} \leq \sum_{\upsilon=1}^{t} \overline{Q_g^{GC}}\, \hat{x}_{i,g,\upsilon}^{GC} \quad : \vartheta_{i,g,h,t}^{QGC2} \quad \forall i \in (\Omega^{NG} \cap \Omega_t^{NL}), g \in \Omega^{gc}, \forall h \in \Omega^H, \forall t \in \Omega^T \qquad (5.52)$$

$$P_{i,g,h,t}^{GR} = \sum_{\upsilon=1}^{t} \overline{\overline{P_{g,h}^{GR}}} \hat{x}_{i,g,\upsilon}^{GR} \quad : \vartheta_{i,g,h,t}^{PGR} \quad \forall i \in (\Omega^{NG} \cap \Omega_t^{NL}), g \in \Omega^{gr}, \forall h \in \Omega^H, \forall t \in \Omega^T \qquad (5.53)$$

$$Q_{i,g,h,t}^{GR} = \sum_{\upsilon=1}^{t} \tan\left(\cos^{-1}(\rho^{GR})\right) \overline{\overline{P_{g,h}^{GR}}} \hat{x}_{i,g,\upsilon}^{GR} : \vartheta_{i,g,h,t}^{QGR}$$
$$\forall i \in (\Omega^{NG} \cap \Omega_t^{NL}), g \in \Omega^{gr}, \forall h \in \Omega^H, \forall t \in \Omega^T \qquad (5.54)$$

Note that $\hat{x}_{i,g,\upsilon}^{GC}$ and $\hat{x}_{i,g,\upsilon}^{GR}$ have already been determined by the master problem. As a result, they should be considered as constant values.

5.2.2.3 Energy Storage Model

Energy storage can be provided by a variety of technologies including flywheel energy storage (FWES), superconducting magnetic energy storage (SMES), supercapacitor energy storage (SCES), pumped hydroelectric storage (PHS), aboveground/underground compressed air energy storage (CAES), and battery energy storage system (BESS) [80], [98-102]. However, most of these technologies are not suitable for integration into distribution systems. Short-term energy storage technologies such as FWES, SMES, and SCES have short discharge times and small storage capacities. Hence, they cannot be used for energy management purposes such as load shifting, peak shaving, and load leveling, which are the most important applications of ESSs in distribution systems [98]. Moreover, long-term energy storage technologies such as PHS and underground CAES require special geographical conditions (i.e., underground caverns or height difference between water reservoirs) which are not usually available in distribution systems [98]. By contrast, BESS and aboveground CAES are quite appropriate for employment in distribution systems. In the existing literature, the vast majority of researchers working on ADNs have only focused on BESS and totally ignored the great potential of aboveground CAES [9], [103-106]. This is while

different studies have shown that aboveground CAES has lower costs and longer lifetime compared to BESS [80], [100]. Figure 5.1 shows the levelized cost of electricity (LCOE) related to aboveground CAES and various BESS technologies in distribution system support services considering different scenarios of electricity price and interest rate. It can be observed that aboveground CAES results in the lowest LCOE for different electricity price and interest rate scenarios. This fact demonstrates the higher cost-effectiveness of aboveground CAES than various BESS technologies.

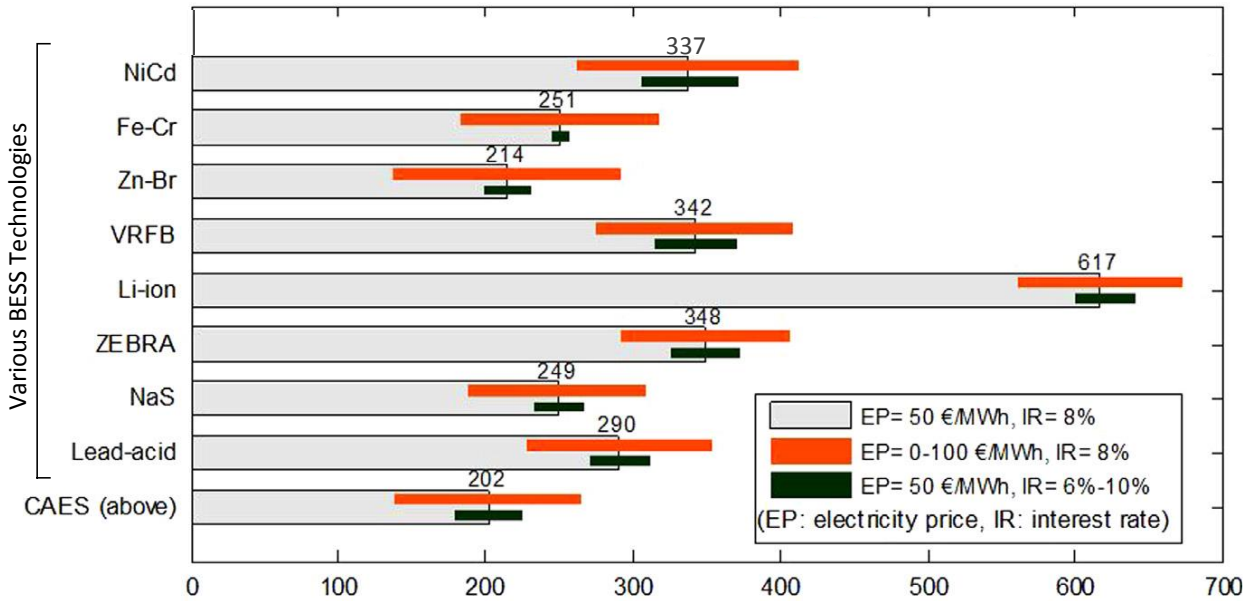

Figure 5.1 LCOE related to aboveground CAES and various BESS technologies in distribution system support services for different electricity price and interest rate scenarios [80].

Table 5.1 compares the lifetimes of aboveground CAES and BESS technologies. As can be seen, aboveground CAES has a considerably longer lifetime than different types of BESS.

Table 5.1 Comparison of the lifetimes of aboveground CAES and BESS technologies [80].

ESS Technologies	CAES (above)	NiCd	Fe-Cr	Zn-Br	VRFB	Li-ion	NaS	Lead-acid
Lifetime (year)	20-40	10-20	10-15	5-10	5-10	5-15	10-15	5-15

Based on the above-mentioned facts, aboveground CAES can be a viable alternative to BESS in distribution networks. Therefore, we have chosen aboveground CAES as the energy storage option for integration into ADNs.

In a typical aboveground CAES, the ambient air is first compressed to a high pressure using a series of compressors driven by electric power. This pressurized air is then injected into an air storage tank located above ground. Finally, the stored compressed air is released and expanded through a series of turbines to generate electric power. The important point is that the air reaches very high temperatures during the compression process, which can cause serious operational problems for CAES. The heat produced during the compression process must be removed from the air before it enters the air storage tank. In conventional CAES technology, this heat is removed and dumped into the atmosphere, which gives rise to the need for consumption of fossil fuels (typically natural gas) to reheat the air during the expansion process [107]. Consumption of fossil fuels in conventional CAES technology results in reduced efficiency and greenhouse gas (GHG) emissions. Recent advancements in CAES technology have led to the introduction of advanced adiabatic CAES (AA-CAES), which offers high efficiency and eliminates GHG emissions [108-111]. In AA-CAES, the heat released from the compression process is stored in a thermal energy storage unit for later use during the expansion process. In this way, AA-CAES eliminates the need for consumption of fossil fuels and overcomes the drawbacks of conventional CAES technology. In the following, we focus on AA-CAES and propose a detailed model for it.

Figure 5.2 illustrates the schematic diagram of the proposed AA-CAES model. As can be seen, the proposed model consists of a compression train, an expansion train, an air storage tank (AST), and a thermal energy storage (TES) system. The compression train is composed of a low pressure compressor (LPC), a high pressure compressor (HPC), an inter-cooler (IC), and an after-cooler (AC). During the compression process, an electric motor drives the LPC and HPC to compress the air to a high pressure. The heat produced during the compression process is removed from the air using the IC and AC. This heat is stored in the TES system which includes a hot oil tank (HOT), a cold oil tank (COT), and a number of pumps that circulate the heat transfer oil. The cooled-down pressurized air is then injected into the AST. The expansion train is composed of a high pressure turbine (HPT), a low pressure turbine (LPT), a pre-heater (PH), an inter-heater (IH), and a recuperator (RC). During the expansion process, the compressed air stored in the AST is released and expanded through the HPT and LPT to drive a generator. The heat stored in the TES system is transferred to the air using the PH and IH to raise its temperature before entering the turbines. An RC is also utilized to recover the heat from the exhaust air of the LPT.

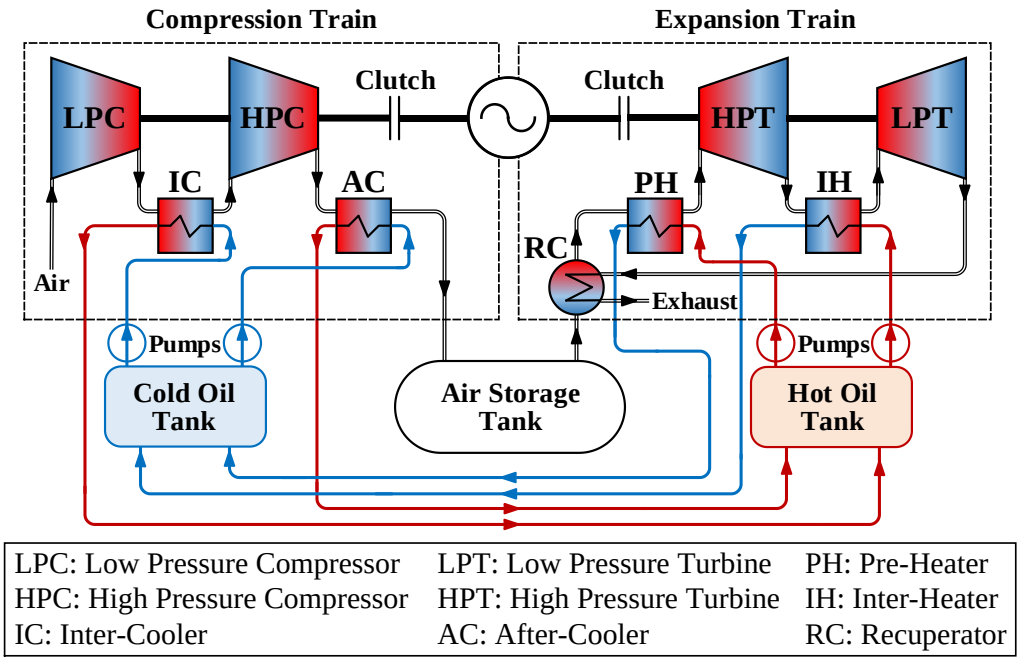

LPC: Low Pressure Compressor	LPT: Low Pressure Turbine	PH: Pre-Heater
HPC: High Pressure Compressor	HPT: High Pressure Turbine	IH: Inter-Heater
IC: Inter-Cooler	AC: After-Cooler	RC: Recuperator

Figure 5.2 Schematic diagram of AA-CAES.

In the following, a linear mathematical formulation is presented for the proposed AA-CAES model. It should be noted that the presented mathematical formulation is partly based on the thermodynamic models developed in [110] and [111].

- *Compression Train*

Constraint (5.55) determines the upper limit of the charging power of AA-CAES. Note that $\hat{\alpha}_{i,s,h,t}^{Ch}$ has already been determined by the master problem. Constraint (5.56) defines the relationship between the charging power of AA-CAES and the mechanical powers consumed by the LPC and HPC. Constraints (5.57) and (5.58) relate the mechanical powers consumed by the LPC and HPC to the air mass flow rate in the compression train. Constraints (5.59) and (5.60) calculate the outlet air temperatures of the LPC and HPC in terms of their inlet air temperatures. Constraints (5.61) and (5.62) ensure the energy balance in the IC and AC, respectively. In fact, constraints (5.57)-(5.62) represent the thermodynamic model of the compression train.

$$P_{i,s,h,t}^{Ch} \leq \overline{P_s^{Ch}} \hat{\alpha}_{i,s,h,t}^{Ch} \quad : \vartheta_{i,s,h,t}^{PCh} \quad \forall i \in (\Omega^{NES} \cap \Omega_t^{NL}), \forall s \in \Omega^{es}, \forall h \in \Omega^{H}, \forall t \in \Omega^{T} \quad (5.55)$$

$$P_{i,s,h,t}^{Ch} = \frac{1}{\eta^M}\left(W_{i,s,h,t}^{LPC} + W_{i,s,h,t}^{HPC}\right) \quad \forall i \in (\Omega^{NES} \cap \Omega_t^{NL}), \forall s \in \Omega^{es}, \forall h \in \Omega^{H}, \forall t \in \Omega^{T} \quad (5.56)$$

$$W_{i,s,h,t}^{LPC} = \frac{1}{\eta^{LPC}} \dot{m}_{i,s,h,t}^{Air,CT} c^{Air} \left(T^{LPC,out} - T^{LPC,in}\right)$$
$$\forall i \in (\Omega^{NES} \cap \Omega_t^{NL}), \forall s \in \Omega^{es}, \forall h \in \Omega^{H}, \forall t \in \Omega^{T} \quad (5.57)$$

$$W_{i,s,h,t}^{HPC} = \frac{1}{\eta^{HPC}} \dot{m}_{i,s,h,t}^{Air,CT} c^{Air} \left(T^{HPC,out} - T^{HPC,in}\right)$$
$$\forall i \in (\Omega^{NES} \cap \Omega_t^{NL}), \forall s \in \Omega^{es}, \forall h \in \Omega^{H}, \forall t \in \Omega^{T} \quad (5.58)$$

$$T^{LPC,out} = T^{LPC,in}\left[1 + \frac{1}{\eta^{LPC}}\left(\left(\pi^{LPC}\right)^{\frac{\gamma^{Air}-1}{\gamma^{Air}}} - 1\right)\right] \quad (5.59)$$

$$T^{HPC,out} = T^{HPC,in}\left[1 + \frac{1}{\eta^{HPC}}\left(\left(\pi^{HPC}\right)^{\frac{\gamma^{Air}-1}{\gamma^{Air}}} - 1\right)\right] \quad (5.60)$$

$$\dot{m}_{i,s,h,t}^{Air,CT} c^{Air}\left(T^{LPC,out} - T^{HPC,in}\right) = \dot{m}_{i,s,h,t}^{Oil,IC} c^{Oil}(T^{HOT} - T^{COT})$$
$$\forall i \in (\Omega^{NES} \cap \Omega_t^{NL}), \forall s \in \Omega^{es}, \forall h \epsilon \Omega^{H}, \forall t \epsilon \Omega^{T} \quad (5.61)$$

$$\dot{m}_{i,s,h,t}^{Air,CT} c^{Air}(T^{HPC,out} - T^{AST}) = \dot{m}_{i,s,h,t}^{Oil,AC} c^{Oil}(T^{HOT} - T^{COT})$$
$$\forall i \in (\Omega^{NES} \cap \Omega_t^{NL}), \forall s \in \Omega^{es}, \forall h \epsilon \Omega^{H}, \forall t \epsilon \Omega^{T} \quad (5.62)$$

where $P_{i,s,h,t}^{Ch}$ is the charging power of AA-CAES; $\overline{P_s^{Ch}}$ denotes the upper limit of charging power of AA-CAES; η^{M} is the efficiency of the electric motor; $W_{i,s,h,t}^{LPC}$ and $W_{i,s,h,t}^{HPC}$ are the mechanical powers consumed by the LPC and HPC, respectively; η^{LPC} and η^{HPC} denote the isentropic efficiencies of the LPC and HPC, respectively; $\dot{m}_{i,s,h,t}^{Air,CT}$ is the air mass flow rate in the compression train; c^{Air} is the specific heat of air at constant pressure; $T^{LPC,in}$ and $T^{LPC,out}$ are the inlet and outlet air temperatures of the LPC, respectively; $T^{HPC,in}$ and $T^{HPC,out}$ are the inlet and outlet air temperatures of the HPC, respectively; π^{LPC} and π^{HPC} denote the pressure ratios of the LPC and HPC, respectively; γ^{Air} is the ratio of specific heats of air; $\dot{m}_{i,s,h,t}^{Oil,IC}$ and $\dot{m}_{i,s,h,t}^{Oil,AC}$ are the oil mass flow rates in the IC and AC, respectively; c^{Oil} is the specific heat of the heat transfer oil; T^{HOT} and T^{COT} are the oil temperatures in the HOT and COT, respectively; and T^{AST} denotes the air temperature in the AST.

- *Expansion Train*

Constraint (5.63) specifies the upper limit of the discharging power of AA-CAES. Note that $\hat{\alpha}_{i,s,h,t}^{Dch}$ has already been determined by the master problem. Constraint (5.64) defines the

relationship between the discharging power of AA-CAES and the mechanical powers generated by the HPT and LPT. Constraints (5.65) and (5.66) relate the mechanical powers generated by the HPT and LPT to the air mass flow rate in the expansion train. Constraints (5.67) and (5.68) calculate the outlet air temperatures of the HPT and LPT in terms of their inlet air temperatures. Constraint (5.69) models the RC used to recover the heat from the exhaust air of the LPT. Constraints (5.70) and (5.71) ensure the energy balance in the PH and IH, respectively. In fact, constraints (5.65)-(5.71) represent the thermodynamic model of the expansion train.

$$P_{i,s,h,t}^{Dch} \le \overline{P_s^{Dch}} \hat{\alpha}_{i,s,h,t}^{Dch} \qquad : \vartheta_{i,s,h,t}^{PDch} \quad \forall i \in (\Omega^{NES} \cap \Omega_t^{NL}), \forall s \in \Omega^{es}, \forall h \in \Omega^H, \forall t \in \Omega^T \quad (5.63)$$

$$P_{i,s,h,t}^{Dch} = \eta^G \left(W_{i,s,h,t}^{HPT} + W_{i,s,h,t}^{LPT}\right) \qquad \forall i \in (\Omega^{NES} \cap \Omega_t^{NL}), \forall s \in \Omega^{es}, \forall h \in \Omega^H, \forall t \in \Omega^T \quad (5.64)$$

$$W_{i,s,h,t}^{HPT} = \eta^{HPT} \dot{m}_{i,s,h,t}^{Air,ET} c^{Air} \left(T^{HPT,in} - T^{HPT,out}\right) \qquad \forall i \in (\Omega^{NES} \cap \Omega_t^{NL}), \forall s \in \Omega^{es}, \forall h \in \Omega^H, \forall t \in \Omega^T \quad (5.65)$$

$$W_{i,s,h,t}^{LPT} = \eta^{LPT} \dot{m}_{i,s,h,t}^{Air,ET} c^{Air} \left(T^{LPT,in} - T^{LPT,out}\right) \qquad \forall i \in (\Omega^{NES} \cap \Omega_t^{NL}), \forall s \in \Omega^{es}, \forall h \in \Omega^H, \forall t \in \Omega^T \quad (5.66)$$

$$T^{HPT,out} = T^{HPT,in} \left[1 - \eta^{HPT} \left(1 - (\pi^{HPT})^{\frac{1-\gamma^{Air}}{\gamma^{Air}}}\right)\right] \quad (5.67)$$

$$T^{LPT,out} = T^{LPT,in} \left[1 - \eta^{LPT} \left(1 - (\pi^{LPT})^{\frac{1-\gamma^{Air}}{\gamma^{Air}}}\right)\right] \quad (5.68)$$

$$(T^{RC,out} - T^{AST}) = \varepsilon^{RC} (T^{LPT,out} - T^{AST}) \quad (5.69)$$

$$\dot{m}_{i,s,h,t}^{Air,ET} c^{Air} \left(T^{HPT,in} - T^{RC,out}\right) = \dot{m}_{i,s,h,t}^{Oil,PH} c^{Oil} (T^{HOT} - T^{COT}) \qquad \forall i \in (\Omega^{NES} \cap \Omega_t^{NL}), \forall s \in \Omega^{es}, \forall h \in \Omega^H, \forall t \in \Omega^T \quad (5.70)$$

$$\dot{m}_{i,s,h,t}^{Air,ET} c^{Air} \left(T^{LPT,in} - T^{HPT,out}\right) = \dot{m}_{i,s,h,t}^{Oil,IH} c^{Oil} (T^{HOT} - T^{COT}) \qquad \forall i \in (\Omega^{NES} \cap \Omega_t^{NL}), \forall s \in \Omega^{es}, \forall h \in \Omega^H, \forall t \in \Omega^T \quad (5.71)$$

where $P_{i,s,h,t}^{Dch}$ is the discharging power of AA-CAES; $\overline{P_s^{Dch}}$ denotes the upper limit of discharging power of AA-CAES; η^G is the efficiency of the generator; $W_{i,s,h,t}^{HPT}$ and $W_{i,s,h,t}^{LPT}$ are the mechanical powers generated by the HPT and LPT, respectively; η^{HPT} and η^{LPT} are the isentropic efficiencies

of the HPT and LPT, respectively; $\dot{m}_{i,s,h,t}^{Air,ET}$ denotes the air mass flow rate in the expansion train; $T^{HPT,in}$ and $T^{HPT,out}$ are the inlet and outlet air temperatures of the HPT, respectively; $T^{LPT,in}$ and $T^{LPT,out}$ are the inlet and outlet air temperatures of the LPT, respectively; π^{HPT} and π^{LPT} are the pressure ratios of the HPT and LPT, respectively; $T^{RC,out}$ is the outlet air temperature of the RC; ε^{RC} denotes the effectiveness of the RC; and $\dot{m}_{i,s,h,t}^{Oil,PH}$ and $\dot{m}_{i,s,h,t}^{Oil,IH}$ are the oil mass flow rates in the PH and IH, respectively.

- *Air Storage Tank*

Constraints (5.72)-(5.75) represent the state-of-charge (SOC) of AA-CAES in terms of the mass and pressure of the air stored in the AST. More specifically, constraint (5.72) uses the ideal gas law to model the behavior of air in the AST. Constraints (5.73) and (5.74) calculate the mass of the air stored in the AST. Constraint (5.75) determines the lower and upper limits of air pressure in the AST.

$$p_{i,s,h,t}^{AST} V_s^{AST} = m_{i,s,h,t}^{Air,AST} T^{AST} R^{Air} \qquad \forall i \in (\Omega^{NES} \cap \Omega_t^{NL}), \forall s \in \Omega^{es}, \forall h \in \Omega^H, \forall t \in \Omega^T \quad (5.72)$$

$$m_{i,s,h,t}^{Air,AST} = m_{i,s,h-1,t}^{Air,AST} + \dot{m}_{i,s,h,t}^{Air,AST} \tau^{SinH} \quad \forall i \in (\Omega^{NES} \cap \Omega_t^{NL}), \forall s \in \Omega^{es}, \forall h \in \Omega^H, \forall t \in \Omega^T \quad (5.73)$$

$$\dot{m}_{i,s,h,t}^{Air,AST} = \dot{m}_{i,s,h,t}^{Air,CT} - \dot{m}_{i,s,h,t}^{Air,ET} \qquad \forall i \in (\Omega^{NES} \cap \Omega_t^{NL}), \forall s \in \Omega^{es}, \forall h \in \Omega^H, \forall t \in \Omega^T \quad (5.74)$$

$$\underline{p^{AST}} \leq p_{i,s,h,t}^{AST} \leq \overline{p^{AST}} \qquad \forall i \in (\Omega^{NES} \cap \Omega_t^{NL}), \forall s \in \Omega^{es}, \forall h \in \Omega^H, \forall t \in \Omega^T \quad (5.75)$$

where $p_{i,s,h,t}^{AST}$ is the air pressure in the AST; V_s^{AST} denotes the volume of the AST; $m_{i,s,h,t}^{Air,AST}$ is the mass of the air stored in the AST; R^{Air} is the specific gas constant for air; $\dot{m}_{i,s,h,t}^{Air,AST}$ is the net air mass flow entering the AST; $\underline{p^{AST}}$ and $\overline{p^{AST}}$ are the lower and upper limits of air pressure in the AST; and τ^{SinH} denotes the number of seconds in one hour.

- *Thermal Energy Storage*

Constraints (5.76)-(5.77) represent the amount of heat stored in the TES. In this regard, constraints (5.76) and (5.77) calculate the mass of the heat transfer oil stored in the HOT. Constraint (5.78) determines the lower and upper limits of the mass of the heat transfer oil stored in the HOT.

$$m_{i,s,h,t}^{Oil,HOT} = m_{i,s,h-1,t}^{Oil,HOT} + \dot{m}_{h}^{Oil,HOT}\tau^{SinH} \quad \forall i \in (\Omega^{NES} \cap \Omega_t^{NL}), \forall s \in \Omega^{es}, \forall h \in \Omega^{H}, \forall t \in \Omega^{T} \quad (5.76)$$

$$\dot{m}_{i,s,h,t}^{Oil,HOT} = \dot{m}_{i,s,h,t}^{Oil,IC} + \dot{m}_{i,s,h,t}^{Oil,AC} - \dot{m}_{i,s,h,t}^{Oil,PH} - \dot{m}_{i,s,h,t}^{Oil,IH} \quad \forall i \in (\Omega^{NES} \cap \Omega_t^{NL}), \forall s \in \Omega^{es}, \forall h \in \Omega^{H}, \forall t \in \Omega^{T} \quad (5.77)$$

$$0 \leq m_{i,s,h,t}^{Oil,HOT} \leq \rho^{Oil} V_s^{HOT} \quad \forall i \in (\Omega^{NES} \cap \Omega_t^{NL}), \forall s \in \Omega^{es}, \forall h \in \Omega^{H}, \forall t \in \Omega^{T} \quad (5.78)$$

where $m_{i,s,h,t}^{Oil,HOT}$ is the mass of the heat transfer oil stored in the HOT; $\dot{m}_{h}^{Oil,HOT}$ is the net oil mass flow entering the HOT; ρ^{Oil} is the density of the heat transfer oil; and V_s^{HOT} denotes the volume of the HOT.

5.2.2.4 Demand Response Model

Demand response refers to changes in the electricity usage by consumers in response to changes in the electricity price over time [112]. In general, time-based pricing of electricity can have different structures such as time-of-use (TOU) pricing, critical peak pricing (CPP), and real-time pricing (RTP). Different studies have shown that among different time-based pricing structures, RTP is the most effective scheme to encourage consumers to use electricity in a more efficient manner [95], [113], [114]. Therefore, we have considered an hourly RTP scheme here and proposed an RTP-based DRL model, as presented in (5.79)-(5.83). In the proposed DRL model, as can be seen in constraint (5.79), the power demand of each load node is assumed to be composed of two parts: 1) unresponsive, and 2) responsive. The unresponsive part of the power demand is not equipped with smart meters and hence cannot be subject to time-dependent pricing. However, the responsive part of the power demand can be affected by changes in the electricity price as it is equipped with smart meters. Constraints (5.80) and (5.81) define the unresponsive and responsive parts of the power demand, respectively. Note that $\hat{x}_{i,p,v}^{SM}$ has already been determined by the master problem. Constraint (5.82) models the reaction of the responsive part of the power demand to the electricity price changes using a demand function based on self-price and cross-price elasticities [95]. Self-price elasticity represents the change in the demand at a certain hour in response to the change in the electricity price at the same hour of the day, while cross-price elasticity characterizes the change in the demand at a certain hour in response to the change in the electricity price at other hours of the day [95]. In fact, self-price and cross-price elasticities are measures of consumer reactions to the electricity price changes. For example, a self-price elasticity of $\varepsilon^{Self} = -0.4$

indicates that an increase of 1% in the electricity price at hour h of the day leads to a decrease of 0.4% in the demand at hour h of the day. As another example, a cross-price elasticity of ε^{Cross} =0.01 means that an increase of 1% in the electricity price at hour γ of the day results in an increase of 0.01% in the demand at hour h of the day. It should be noted that while self-price elasticity is negative, cross-price elasticity is positive [115]. Constraint (5.83) calculates the reactive power demands of load nodes in terms of their active power demands.

$$P^{D}_{i,h,t} = P^{D,Unresp}_{i,h,t} + P^{D,Resp}_{i,h,t} \qquad \forall i \in \Omega^N, \forall h \in \Omega^H, \forall t \in \Omega^T \quad (5.79)$$

$$P^{D,Unresp}_{i,h,t} = \left(1 - \sum_{\upsilon=1}^{t} \sum_{p \in \Omega^{sm}} \kappa^{SM}_{p} \hat{x}^{SM}_{i,p,\upsilon}\right) \overline{\overline{P^{D}_{i,h,t}}} \quad : \vartheta^{PD,Unresp}_{i,h,t} \quad \forall i \in \Omega^N, \forall h \in \Omega^H, \forall t \in \Omega^T \quad (5.80)$$

$$P^{D,SM}_{i,h,t} = \left(\sum_{\upsilon=1}^{t} \sum_{p \in \Omega^{sm}} \kappa^{SM}_{p} \hat{x}^{SM}_{i,p,\upsilon}\right) \overline{\overline{P^{D}_{i,h,t}}} \quad : \vartheta^{DSM}_{i,h,t} \quad \forall i \in \Omega^N, \forall h \in \Omega^H, \forall t \in \Omega^T \quad (5.81)$$

$$P^{D,Resp}_{i,h,t} = P^{D,SM}_{i,h,t} \left[1 + \varepsilon^{Self} \frac{c^{E}_{h} - \overline{\overline{c^{E}}}}{\overline{\overline{c^{E}}}} + \sum_{\gamma \in (\Omega^H - h)} \varepsilon^{Cross} \frac{c^{E}_{\gamma} - \overline{\overline{c^{E}}}}{\overline{\overline{c^{E}}}}\right] \quad \forall i \in \Omega^N, \forall h \in \Omega^H, \forall t \in \Omega^T \quad (5.82)$$

$$Q^{D}_{i,h,t} = \tan\left(\cos^{-1}(\rho^{D})\right) P^{D}_{i,h,t} \qquad \forall i \in \Omega^N, \forall h \in \Omega^H, \forall t \in \Omega^T \quad (5.83)$$

where $P^{D}_{i,h,t}$ and $Q^{D}_{i,h,t}$ are the active and reactive power demands of load nodes, respectively; $P^{D,Unresp}_{i,h,t}$ and $P^{D,Resp}_{i,h,t}$ denote the unresponsive and responsive parts of the active power demands of load nodes, respectively; κ^{SM}_{p} is the penetration level of smart meters; $\overline{\overline{P^{D}_{i,h,t}}}$ represents the expected active power demands of load nodes; ε^{Self} and ε^{Cross} are the self-price and cross-price elasticities, respectively; c^{E}_{h} is the hourly real-time electricity price; $\overline{\overline{c^{E}}}$ denotes the fixed electricity price; and ρ^{D} is the load power factor.

5.2.3 Feasibility Check Subproblem

The feasibility check subproblem only includes the continuous variables of the MDEP problem and is employed to check the feasibility of the solution found by the master problem in each iteration of the BD algorithm. The objective function and constraints of this problem are as follows:

$$\text{Minimize } \mathcal{K}^{PQ} = \sum_{t \in \Omega^T} \sum_{h \in \Omega^H} \sum_{i \in \Omega^N} \mathcal{K}^{P}_{i,h,t} + \sum_{t \in \Omega^T} \sum_{h \in \Omega^H} \sum_{i \in \Omega^N} \mathcal{K}^{Q}_{i,h,t} \quad (5.84)$$

s.t. (5.35), Linearized (5.36), Linearized (5.37), (5.38)-(5.41), Linearized (5.42), Linearized (5.43), (5.44), (5.57)-(5.79), (5.82), (5.83)

$$\sum_{(ki)\in\Omega^F}\sum_{a\in\Omega^a}\left[P^F_{ki,a,h,t}-R_a l_{ki} f^F_{ki,a,h,t}\right]-\sum_{(ij)\in\Omega^F}\sum_{a\in\Omega^a}P^F_{ij,a,h,t}+P^S_{i,t}+\sum_{g\in\Omega^{gc}}P^{GC}_{i,g,h,t}$$

$$+\sum_{g\in\Omega^{gr}}P^{GR}_{i,g,h,t}+\sum_{s\in\Omega^{es}}\left[P^{Dch}_{i,s,h,t}-P^{Ch}_{i,s,h,t}\right]+\mathcal{K}^P_{i,h,t}=P^D_{i,h,t}\ \forall i\in\Omega^N,\forall h\in\Omega^H,\forall t\in\Omega^T \quad (5.85)$$

$$\sum_{(ki)\in\Omega^F}\sum_{a\in\Omega^a}\left[Q^F_{ki,a,h,t}-X_a l_{ki} f^F_{ki,a,h,t}\right]-\sum_{(ij)\in\Omega^F}\sum_{a\in\Omega^a}Q^F_{ij,a,h,t}+Q^S_{i,h,t}+\sum_{g\in\Omega^{gc}}Q^{GC}_{i,g,h,t}$$

$$+\sum_{g\in\Omega^{gr}}Q^{GR}_{i,g,h,t}+\mathcal{K}^Q_{i,h,t}=Q^D_{i,h,t} \qquad \forall i\in\Omega^N,\forall h\in\Omega^H,\forall t\in\Omega^T \quad (5.86)$$

$$f^F_{ij,a,h,t}\le\left(\overline{I_a}\right)^2\hat{y}_{ij,a,t} \qquad :\omega^{fF}_{ij,a,h,t} \quad \forall(ij)\in\Omega^F,\forall a\in\Omega^a,\forall h\in\Omega^H,\forall t\in\Omega^T \quad (5.87)$$

$$\Delta V_{ij,h,t}\le\overline{\Delta V}\left(1-\sum_{a\in\Omega^a}\hat{y}_{ij,a,t}\right) \qquad :\omega^{\Delta V1}_{ij,h,t} \qquad \forall(ij)\in\Omega^F,\forall h\in\Omega^H,\forall t\in\Omega^T \quad (5.88)$$

$$-\Delta V_{ij,h,t}\le\overline{\Delta V}\left(1-\sum_{a\in\Omega^a}\hat{y}_{ij,a,t}\right) \qquad :\omega^{\Delta V2}_{ij,h,t} \qquad \forall(ij)\in\Omega^F,\forall h\in\Omega^H,\forall t\in\Omega^T \quad (5.89)$$

$$S^S_{i,h,t}\le\overline{S^0_i}+\sum_{v=1}^{t}\sum_{b\in\Omega^b}\overline{S_b}\,\hat{x}^{SR}_{i,b,v} \qquad :\omega^{SR}_{i,h,t} \qquad \forall i\in\Omega^{SR},\forall h\in\Omega^H,\forall t\in\Omega^T \quad (5.90)$$

$$S^S_{i,h,t}\le\sum_{v=1}^{t}\sum_{b\in\Omega^b}\overline{S_b}\,\hat{x}^{SC}_{i,b,v} \qquad :\omega^{SC}_{i,h,t} \qquad \forall i\in\Omega^{SC},\forall h\in\Omega^H,\forall t\in\Omega^T \quad (5.91)$$

$$P^{GC}_{i,g,h,t}\le\sum_{v=1}^{t}\overline{P^{GC}_g}\hat{x}^{GC}_{i,g,v} \qquad :\omega^{PGC}_{i,g,h,t} \quad \forall i\in(\Omega^{NG}\cap\Omega^{NL}_t),g\in\Omega^{gc},\forall h\in\Omega^H,\forall t\in\Omega^T \quad (5.92)$$

$$Q^{GC}_{i,g,h,t}\le\sum_{v=1}^{t}\overline{Q^{GC}_g}\,\hat{x}^{GC}_{i,g,v} \qquad :\omega^{QGC1}_{i,g,h,t} \quad \forall i\in(\Omega^{NG}\cap\Omega^{NL}_t),g\in\Omega^{gc},\forall h\in\Omega^H,\forall t\in\Omega^T \quad (5.93)$$

$$-Q^{GC}_{i,g,h,t}\le\sum_{v=1}^{t}\overline{Q^{GC}_g}\,\hat{x}^{GC}_{i,g,v} \qquad :\omega^{QGC2}_{i,g,h,t} \quad \forall i\in(\Omega^{NG}\cap\Omega^{NL}_t),g\in\Omega^{gc},\forall h\in\Omega^H,\forall t\in\Omega^T \quad (5.94)$$

$$P^{GR}_{i,g,h,t}=\sum_{v=1}^{t}\overline{\overline{P^{GR}_{g,h}}}\hat{x}^{GR}_{i,g,v} \qquad :\omega^{PGR}_{i,g,h,t} \quad \forall i\in(\Omega^{NG}\cap\Omega^{NL}_t),g\in\Omega^{gr},\forall h\in\Omega^H,\forall t\in\Omega^T \quad (5.95)$$

$$Q^{GR}_{i,g,h,t}=\sum_{v=1}^{t}\tan\left(\cos^{-1}(\rho^{GR})\right)\overline{\overline{P^{GR}_{g,h}}}\hat{x}^{GR}_{i,g,v} :\omega^{QGR}_{i,g,h,t}$$

$$\forall i\in(\Omega^{NG}\cap\Omega^{NL}_t),g\in\Omega^{gr},\forall h\in\Omega^H,\forall t\in\Omega^T \quad (5.96)$$

$$P^{Ch}_{i,s,h,t}\le\overline{P^{Ch}_s}\hat{\alpha}^{Ch}_{i,s,h,t} \qquad :\omega^{PCh}_{i,s,h,t} \quad \forall i\in(\Omega^{NES}\cap\Omega^{NL}_t),\forall s\in\Omega^{es},\forall h\in\Omega^H,\forall t\in\Omega^T \quad (5.97)$$

$$P^{Dch}_{i,s,h,t}\le\overline{P^{Dch}_s}\hat{\alpha}^{Dch}_{i,s,h,t} \qquad :\omega^{PDch}_{i,s,h,t} \quad \forall i\in(\Omega^{NES}\cap\Omega^{NL}_t),\forall s\in\Omega^{es},\forall h\in\Omega^H,\forall t\in\Omega^T \quad (5.98)$$

$$P^{D,Unresp}_{i,h,t}=\left(1-\sum_{v=1}^{t}\sum_{p\in\Omega^{sm}}\kappa^{SM}_p\hat{x}^{SM}_{i,p,v}\right)\overline{\overline{P^D_{i,h,t}}} \quad :\omega^{PD,Unresp}_{i,h,t} \quad \forall i\in\Omega^N,\forall h\in\Omega^H,\forall t\in\Omega^T \quad (5.99)$$

$$P^{D,SM}_{i,h,t}=\left(\sum_{v=1}^{t}\sum_{p\in\Omega^{sm}}\kappa^{SM}_p\hat{x}^{SM}_{i,p,v}\right)\overline{\overline{P^D_{i,h,t}}} \qquad :\omega^{DSM}_{i,h,t} \qquad \forall i\in\Omega^N,\forall h\in\Omega^H,\forall t\in\Omega^T \quad (5.100)$$

where $\mathcal{K}^{P}_{i,h,t}$ and $\mathcal{K}^{Q}_{i,h,t}$ are positive unconstrained slack variables defined to determine whether the solution provided by the master problem is feasible or not. As can be seen in constraints (5.85) and (5.86), these slack variables are included in the active and reactive power balance constraints to identify the lack of enough generation for supplying the demand. That is, $\mathcal{K}^{P}_{i,h,t}$ and $\mathcal{K}^{Q}_{i,h,t}$ measure the amount by which the active and reactive power balance constraints are violated. It is obvious that if the objective value of the feasibility check subproblem $\mathcal{K}^{PQ}$ (which is equal to the sum of the slack variables) can be reduced to zero, the load demands can be completely fulfilled without violating any of the operational constraints. Therefore, $\mathcal{K}^{PQ} = 0$ indicates that the solution found by the master problem is feasible. Note that, except for the power balance constraints, all the constraints of the feasibility check subproblem are exactly the same as those of the optimal operation subproblem.

5.2.4 BD Algorithm Acceleration Strategies

As discussed in the previous chapter, the straightforward implementation of the classical BD algorithm results in a very slow convergence rate, requiring a large number of iterations. To address this issue, two acceleration strategies were proposed in Section 4.3: 1) modification of the master problem, and 2) generation of auxiliary optimality cuts. In the following, the modified master problem and the auxiliary optimality cuts are described.

5.2.4.1 Modified Master Problem

The modified master problem is obtained by adding a number of auxiliary constraints to the master problem as follows:

$$\text{Minimize } \ c^{Inv.} + \Psi \tag{5.101}$$

s.t. (5.2)-(5.30)

$$\sum_{(ki)\in\Omega^F}\sum_{a\in\Omega^a} I^{F}_{ki,a,h,t} - \sum_{(ij)\in\Omega^F}\sum_{a\in\Omega^a} I^{F}_{ij,a,h,t} + I^{S}_{i,h,t} + \sum_{g\in\Omega^{gc}} I^{GC}_{i,g,h,t} + \sum_{g\in\Omega^{gr}} I^{GR}_{i,g,h,t}$$

$$+\sum_{s\in\Omega^{es}}\left[I^{Dch}_{i,s,h,t} - I^{Ch}_{i,s,h,t}\right] = I^{D}_{i,h,t} \qquad \forall i\in\Omega^N, \forall h\in\Omega^H, \forall t\in\Omega^T \tag{5.102}$$

$$V_{i,h,t} - V_{j,h,t} = \sum_{a\in\Omega^a}\left(Z_a l_{ij} I^{F}_{ij,a,h,t}\right) + \Delta V_{ij,h,t} \qquad \forall (ij)\in\Omega^F, \forall h\in\Omega^H, \forall t\in\Omega^T \tag{5.103}$$

$$\underline{V} \le V_{i,h,t} \le \overline{V} \qquad \forall i\in\Omega^N, \forall h\in\Omega^H, \forall t\in\Omega^T \tag{5.104}$$

$$I^{F}_{ij,a,h,t} \le \overline{I_a}\, y_{ij,a,t} \qquad \forall (ij) \in \Omega^{F}, \forall a \in \Omega^{a}, \forall h \in \Omega^{H}, \forall t \in \Omega^{T} \qquad (5.105)$$

$$\left|\Delta V_{ij,h,t}\right| \le \overline{\Delta V}\left(1 - \sum_{a \in \Omega^{a}} y_{ij,a,t}\right) \qquad \forall (ij) \in \Omega^{F}, \forall h \in \Omega^{H}, \forall t \in \Omega^{T} \qquad (5.106)$$

$$I^{S}_{i,h,t} \le \overline{I^{S0}_{i}} + \sum_{\upsilon=1}^{t} \sum_{b \in \Omega^{b}} \overline{I_b}\, x^{SR}_{i,b,\upsilon} \qquad \forall i \in \Omega^{SR}, \forall h \in \Omega^{H}, \forall t \in \Omega^{T} \qquad (5.107)$$

$$I^{S}_{i,h,t} \le \sum_{\upsilon=1}^{t} \sum_{b \in \Omega^{b}} \overline{I_b}\, x^{SC}_{i,b,\upsilon} \qquad \forall i \in \Omega^{SC}, \forall h \in \Omega^{H}, \forall t \in \Omega^{T} \qquad (5.108)$$

$$I^{GC}_{i,g,h,t} \le \sum_{\upsilon=1}^{t} \overline{I^{GC}_{g}} x^{GC}_{i,g,\upsilon} \qquad \forall i \in (\Omega^{NG} \cap \Omega^{NL}_{t}), g \in \Omega^{gc}, \forall h \in \epsilon\Omega^{H}, \forall t \in \Omega^{T} \qquad (5.109)$$

$$I^{GR}_{i,g,h,t} = \sum_{\upsilon=1}^{t} \overline{\overline{I^{GR}_{g,h}}} x^{GR}_{i,g,\upsilon} \qquad \forall i \in (\Omega^{NG} \cap \Omega^{NL}_{t}), g \in \Omega^{gr}, \forall h \in \Omega^{H}, \forall t \in \Omega^{T} \qquad (5.110)$$

$$I^{Ch}_{i,s,h,t} \le \overline{I^{Ch}_{s}} \alpha^{Ch}_{i,s,h,t} \qquad \forall i \in (\Omega^{NES} \cap \Omega^{NL}_{t}), \forall s \in \Omega^{es}, \forall h \in \Omega^{H}, \forall t \in \Omega^{T} \qquad (5.111)$$

$$I^{Dch}_{i,s,h,t} \le \overline{I^{Dch}_{s}} \alpha^{Dch}_{i,s,h,t} \qquad \forall i \in (\Omega^{NES} \cap \Omega^{NL}_{t}), \forall s \in \Omega^{es}, \forall h \in \Omega^{H}, \forall t \in \Omega^{T} \qquad (5.112)$$

$$\sum_{h \in \Omega^{H}} I^{Ch}_{i,s,h,t} \le \overline{I^{Ch}_{s}}\, \overline{T^{Ch}_{s}} \qquad \forall i \in (\Omega^{NES} \cap \Omega^{NL}_{t}), \forall s \in \Omega^{es}, \forall t \in \Omega^{T} \qquad (5.113)$$

$$\sum_{h \in \Omega^{H}} I^{Dch}_{i,s,h,t} \le \overline{I^{Dch}_{s}}\, \overline{T^{Dch}_{s}} \qquad \forall i \in (\Omega^{NES} \cap \Omega^{NL}_{t}), \forall s \in \Omega^{es}, \forall t \in \Omega^{T} \qquad (5.114)$$

$$I^{D}_{i,h,t} = I^{D,Unresp}_{i,h,t} + I^{D,Resp}_{i,h,t} \qquad \forall i \in \Omega^{N}, \forall h \in \Omega^{H}, \forall t \in \Omega^{T} \qquad (5.115)$$

$$I^{D,Unresp}_{i,h,t} = \left(1 - \sum_{\upsilon=1}^{t} \sum_{p \in \Omega^{sm}} \kappa^{SM}_{p} x^{SM}_{i,p,\upsilon}\right) \overline{\overline{I^{D}_{i,h,t}}} \qquad \forall i \in \Omega^{N}, \forall h \in \Omega^{H}, \forall t \in \Omega^{T} \qquad (5.116)$$

$$I^{D,SM}_{i,h,t} = \left(\sum_{\upsilon=1}^{t} \sum_{p \in \Omega^{sm}} \kappa^{SM}_{p} x^{SM}_{i,p,\upsilon}\right) \overline{\overline{I^{D}_{i,h,t}}} \qquad \forall i \in \Omega^{N}, \forall h \in \Omega^{H}, \forall t \in \Omega^{T} \qquad (5.117)$$

$$I^{D,Resp}_{i,h,t} = I^{D,SM}_{i,h,t} \left[1 + \varepsilon^{Self} \frac{c^{E}_{h} - \overline{\overline{c^{E}}}}{\overline{\overline{c^{E}}}} + \sum_{\gamma \in (\Omega^{H} - h)} \varepsilon^{Cross} \frac{c^{E}_{\gamma} - \overline{\overline{c^{E}}}}{\overline{\overline{c^{E}}}}\right] \forall i \in \Omega^{N}, \forall h \in \Omega^{H}, \forall t \in \Omega^{T} \qquad (5.118)$$

In fact, the above auxiliary constraints include an approximate distribution network model (i.e., constraints (5.102)-(5.108)) and a simplified version of the DER models (i.e., constraints (5.109)-(5.118)) in the master problem. These auxiliary constraints improve the quality of solutions found by the master problem and significantly reduce the number of optimality and feasibility cuts required to achieve the convergence. Constraints (5.102) ensures the current flow balance in each system node. Constraint (5.103) applies an approximate form of the Kirchhoff's voltage law (KVL) to each feeder section. Constraint (5.104) determines the allowable range of the nodal voltage magnitudes. Constraint (5.105) represents the limits on the current flows of feeder sections

based on the conductor types used for constructing them. Constraint (5.106) sets appropriate bounds on the auxiliary variable $\Delta V_{ij,h,t}$ used in constraint (5.103). Constraints (5.107) and (108) limit the current flows provided by substations based on their installed capacities. Constraint (5.109) limits the current flows provided by conventional DGs. Constraint (5.110) sets the current flows provided by renewable DGs equal to their expected values. Constraint (5.111) and (5.112) determine the upper limits of the charging and discharging currents of ESSs. Constraint (5.113) defines the maximum amount of energy that can be stored in each ESS. Constraint (5.114) limits the amount of energy that can be discharged form an ESS. Constraints (5.15) splits the current flow demand of each load node into an unresponsive part and a responsive part. Constraints (5.116) and (5.117) define the unresponsive and responsive parts of the current flow demands of load nodes, respectively. Constraint (5.118) models the reaction of the responsive part of the current flow demands to the electricity price changes using a demand function based on self-price and cross-price elasticities (see Section 5.2.2.4).

5.2.4.2 Auxiliary Optimality Cuts

To further accelerate the convergence rate of the BD algorithm, in addition to the optimality cut (5.29), the auxiliary optimality cut (5.119) should also be generated and added to the master problem. This will considerably speed up the solution process of the MDEP problem, as thoroughly discussed in Section 4.3.2.

$$
\begin{aligned}
&c^{Oper.(m)} + \sum_{t\in\Omega^T}\sum_{h\in\Omega^H}\sum_{(ij)\in\Omega^F}\sum_{a\in\Omega^a}\vartheta_{ij,a,h,t}^{fF(m)}\left(\overline{I_a}\right)^2\left(y_{ij,a,t}-\hat{y}_{ij,a,t}^{(m)}\right)\\
&-\sum_{t\in\Omega^T}\sum_{h\in\Omega^H}\sum_{(ij)\in\Omega^F}\left(\vartheta_{ij,h,t}^{\Delta V1(m)}+\vartheta_{ij,h,t}^{\Delta V2(m)}\right)\overline{\Delta V}\left[\sum_{a\in\Omega^a}\left(y_{ij,a,t}-\hat{y}_{ij,a,t}^{(m)}\right)\right]\\
&+\sum_{t\in\Omega^T}\sum_{h\in\Omega^H}\sum_{i\in\Omega^{SR}}\vartheta_{i,h,t}^{SR(m)}\left[\sum_{\upsilon=1}^{t}\sum_{b\in\Omega^b}\overline{S_b}\left(x_{i,b,\upsilon}^{SR}-\hat{x}_{i,b,\upsilon}^{SR(m)}\right)\right]\\
&+\sum_{t\in\Omega^T}\sum_{h\in\Omega^H}\sum_{i\in\Omega^{SC}}\vartheta_{i,h,t}^{SC(m)}\left[\sum_{\upsilon=1}^{t}\sum_{b\in\Omega^b}\overline{S_b}\left(x_{i,b,\upsilon}^{SC}-\hat{x}_{i,b,\upsilon}^{SC(m)}\right)\right]\\
&+\sum_{t\in\Omega^T}\sum_{h\in\Omega^H}\sum_{i\in\left(\Omega^{NG}\cap\Omega_t^{NL}\right)}\sum_{g\in\Omega^{gc}}\vartheta_{i,g,h,t}^{PGC(m)}\left[\sum_{\upsilon=1}^{t}\overline{P_g^{GC}}\left(x_{i,g,\upsilon}^{GC}-\hat{x}_{i,g,\upsilon}^{GC(m)}\right)\right]\\
&+\sum_{t\in\Omega^T}\sum_{h\in\Omega^H}\sum_{i\in\left(\Omega^{NG}\cap\Omega_t^{NL}\right)}\sum_{g\in\Omega^{gc}}\left(\vartheta_{i,g,h,t}^{QGC1(m)}+\vartheta_{i,g,h,t}^{QGC2(m)}\right)\left[\sum_{\upsilon=1}^{t}\overline{Q_g^{GC}}\left(x_{i,g,\upsilon}^{GC}-\hat{x}_{i,g,\upsilon}^{GC(m)}\right)\right]\\
&+\sum_{t\in\Omega^T}\sum_{h\in\Omega^H}\sum_{i\in\left(\Omega^{NG}\cap\Omega_t^{NL}\right)}\sum_{g\in\Omega^{gr}}\vartheta_{i,g,h,t}^{QGR(m)}\left[\sum_{\upsilon=1}^{t}\tan\left(\cos^{-1}(\rho^{GR})\right)\overline{\overline{P_{g,h}^{GR}}}\left(x_{i,g,\upsilon}^{GR}-\hat{x}_{i,g,\upsilon}^{GR(m)}\right)\right]
\end{aligned}
$$

$$+\sum_{t\in\Omega^T}\sum_{h\in\Omega^H}\sum_{i\in\left(\Omega^{NG}\cap\Omega_t^{NL}\right)}\sum_{g\in\Omega^{gr}}\vartheta_{i,g,h,t}^{PGR(m)}\left[\sum_{\upsilon=1}^{t}\overline{\overline{P_{g,h}^{GR}}}\left(x_{i,g,\upsilon}^{GR}-\hat{x}_{i,g,\upsilon}^{GR(m)}\right)\right]$$

$$+\sum_{t\in\Omega^T}\sum_{h\in\Omega^H}\sum_{i\in\left(\Omega^{NES}\cap\Omega_t^{NL}\right)}\sum_{s\in\Omega^{es}}\vartheta_{i,s,h,t}^{PCh(m)}\,\overline{P_s^{Ch}}\left(\alpha_{i,s,h,t}^{Ch}-\hat{\alpha}_{i,s,h,t}^{Ch(m)}\right)$$

$$+\sum_{t\in\Omega^T}\sum_{h\in\Omega^H}\sum_{i\in\left(\Omega^{NES}\cap\Omega_t^{NL}\right)}\sum_{s\in\Omega^{es}}\vartheta_{i,s,h,t}^{PDch(m)}\,\overline{P_s^{Dch}}\left(\alpha_{i,s,h,t}^{Dch}-\hat{\alpha}_{i,s,h,t}^{Dch(m)}\right)$$

$$+\sum_{t\in\Omega^T}\sum_{h\in\Omega^H}\sum_{i\in\Omega^N}\left(\vartheta_{i,h,t}^{DSM(m)}-\vartheta_{i,h,t}^{PD,Unresp(m)}\right)\overline{\overline{P_{i,h,t}^{D}}}\left[\sum_{\upsilon=1}^{t}\sum_{p\in\Omega^{sm}}\kappa_p^{SM}\left(x_{i,p,\upsilon}^{SM}-\hat{x}_{i,p,\upsilon}^{SM(m)}\right)\right]\geq 0$$

$$\forall m=1,\dots,M^{Feas.} \qquad (5.119)$$

5.3 Proposed Robust Optimization-Based Uncertainty Modelling Approach

In this section, a new robust optimization-based approach is proposed to model the uncertainties of renewable generations, loads, and electricity prices [96], [97]. As previously discussed, the necessity of proposing this new uncertainty modelling approach arises from the fact that when the MDEP problem is decomposed into a master problem and two subproblems using the BD algorithm, the DRCCP approach proposed in Chapter 2 cannot be employed. The reason is that the DRCCP approach requires binary variables to overcome the nonlinearities, while the subproblems should not include any binary variables in the BD algorithm. Therefore, a new robust optimization-based uncertainty modelling approach is proposed here, which not only retains the significant advantages of the DRCCP approach, but also does not introduce any binary variables to the subproblems. This new approach offers the following advantages:

1) It is computationally tractable.
2) It only needs the mean and the lower and upper bounds of the uncertain parameters, rather than detailed knowledge about their PDFs.
3) It immunizes the solution of the MDEP problem against all realizations of the uncertain parameters within the uncertainty sets specified by the decision maker.
4) It allows to control the degree of conservatism of the solution in a straightforward manner.
5) Most importantly, it provides the decision maker with a probabilistic bound on the robustness level of the obtained solution, which makes it stand out among other robust optimization approaches existing in the literature.

In the following, the proposed uncertainty modelling approach is described in detail.

Taking a careful look at the STS-based decomposed MDEP model developed in Section 5.2 reveals that the uncertainties of renewable generations, loads, and electricity prices only affect the subproblems. In the optimal operation subproblem, the uncertainties have a direct impact on the objective function (5.32), the active power balance constraint (5.33), the reactive power balance constraint (5.34), and the demand function (5.82). To incorporate the uncertainties into the optimal operation subproblem, first the random variables $\widetilde{\chi_h^{GR}}$, $\widetilde{\chi_h^{D}}$, and $\widetilde{\chi_h^{CE}}$ are defined to characterize the stochasticity of renewable generations, loads, and electricity prices. Then, with the help of these random variables, (5.32)-(5.34) and (5.82) are changed to (5.120)-(5.123), respectively:

$$c^{Oper.} = \sum_{t\in\Omega^T} \frac{1}{(1+r)^{(t-1)D}} \frac{(1+r)^D-1}{r(1+r)^D} \tau^{DinY} \left[\sum_{h\in\Omega^H}\sum_{i\in\Omega^S} c_h^E \widetilde{\chi_h^{CE}} P_{i,h,t}^S + \sum_{h\in\Omega^H}\sum_{i\in\Omega^s} c_h^E \widetilde{\chi_h^{CE}} \phi^S f_{i,h,t}^S \right.$$

$$\left. + \sum_{h\in\Omega^H}\sum_{i\in(\Omega^{NG}\cap\Omega_t^{NL})}\sum_{g\in\Omega^{gc}} c_g^{EGC} P_{i,g,h,t}^{GC}\right] \quad (5.120)$$

$$\sum_{(ki)\in\Omega^F}\sum_{a\in\Omega^a}\left[P_{ki,a,h,t}^F - R_a l_{ki} f_{ki,a,h,t}^F\right] - \sum_{(ij)\in\Omega^F}\sum_{a\in\Omega^a} P_{ij,a,h,t}^F + P_{i,t}^S + \sum_{g\in\Omega^{gc}} P_{i,g,h,t}^{GC}$$

$$+\left(\sum_{g\in\Omega^{gr}} P_{i,g,h,t}^{GR}\right)\widetilde{\chi_h^{GR}} + \sum_{s\in\Omega^{es}}\left[P_{i,s,h,t}^{Dch} - P_{i,s,h,t}^{Ch}\right] \geq P_{i,h,t}^D \widetilde{\chi_h^D} \;\forall i\in\Omega^N, \forall h\in\Omega^H, \forall t\in\Omega^T \quad (5.121)$$

$$\sum_{(ki)\in\Omega^F}\sum_{a\in\Omega^a}\left[Q_{ki,a,h,t}^F - X_a l_{ki} f_{ki,a,h,t}^F\right] - \sum_{(ij)\in\Omega^F}\sum_{a\in\Omega^a} Q_{ij,a,h,t}^F + Q_{i,h,t}^S + \sum_{g\in\Omega^{gc}} Q_{i,g,h,t}^{GC}$$

$$+\left(\sum_{g\in\Omega^{gr}} Q_{i,g,h,t}^{GR}\right)\widetilde{\chi_h^{GR}} \geq Q_{i,h,t}^D \widetilde{\chi_h^D} \qquad \forall i\in\Omega^N, \forall h\in\Omega^H, \forall t\in\Omega^T \quad (5.122)$$

$$P_{i,h,t}^{D,Resp} \geq P_{i,h,t}^{D,SM}\left[1 + \varepsilon^{Self}\frac{c_h^E\widetilde{\chi_h^{CE}} - \overline{\overline{c^E}}}{\overline{\overline{c^E}}} + \sum_{\gamma\in(\Omega^H-h)}\varepsilon^{Cross}\frac{c_\gamma^E\widetilde{\chi_\gamma^{CE}} - \overline{\overline{c^E}}}{\overline{\overline{c^E}}}\right]$$

$$\forall i\in\Omega^N, \forall h\in\Omega^H, \forall t\in\Omega^T \quad (5.123)$$

On the other hand, in the feasibility check subproblem, the uncertainties directly affect the demand function (5.82), the active power balance constraint (5.85), and the reactive power balance constraint (5.86). Note that the objective function of this subproblem is not subject to uncertainty. Similarly, with the help of the random variables $\widetilde{\chi_h^{GR}}$, $\widetilde{\chi_h^{D}}$, and $\widetilde{\chi_h^{CE}}$, the uncertainties can be incorporated into the feasibility check subproblem by changing (5.82), (5.85), and (5.86) to (5.124)-(5.126), respectively:

$$P_{i,h,t}^{D,Resp} \geq P_{i,h,t}^{D,SM}\left[1+\varepsilon^{Self}\frac{c_h^E\widetilde{\chi_h^{CE}}-\overline{\overline{c^E}}}{\overline{\overline{c^E}}}+\sum_{\gamma\in(\Omega^H-h)}\varepsilon^{Cross}\frac{c_\gamma^E\widetilde{\chi_\gamma^{CE}}-\overline{\overline{c^E}}}{\overline{\overline{c^E}}}\right]$$

$$\forall i\in\Omega^N,\forall h\in\Omega^H,\forall t\in\Omega^T \quad (5.124)$$

$$\sum_{(ki)\in\Omega^F}\sum_{a\in\Omega^a}\left[P_{ki,a,h,t}^F-R_a l_{ki} f_{ki,a,h,t}^F\right]-\sum_{(ij)\in\Omega^F}\sum_{a\in\Omega^a}P_{ij,a,h,t}^F+P_{i,t}^S+\sum_{g\in\Omega^{gc}}P_{i,g,h,t}^{GC}$$

$$+\left(\sum_{g\in\Omega^{gr}}P_{i,g,h,t}^{GR}\right)\widetilde{\chi_h^{GR}}+\sum_{s\in\Omega^{es}}\left[P_{i,s,h,t}^{Dch}-P_{i,s,h,t}^{Ch}\right]+\mathcal{K}_{i,h,t}^P\geq P_{i,h,t}^D\widetilde{\chi_h^D}$$

$$\forall i\in\Omega^N,\forall h\in\Omega^H,\forall t\in\Omega^T \quad (5.125)$$

$$\sum_{(ki)\in\Omega^F}\sum_{a\in\Omega^a}\left[Q_{ki,a,h,t}^F-X_a l_{ki} f_{ki,a,h,t}^F\right]-\sum_{(ij)\in\Omega^F}\sum_{a\in\Omega^a}Q_{ij,a,h,t}^F+Q_{i,h,t}^S+\sum_{g\in\Omega^{gc}}Q_{i,g,h,t}^{GC}$$

$$+\left(\sum_{g\in\Omega^{gr}}Q_{i,g,h,t}^{GR}\right)\widetilde{\chi_h^{GR}}+\mathcal{K}_{i,h,t}^Q\geq Q_{i,h,t}^D\widetilde{\chi_h^D} \qquad \forall i\in\Omega^N,\forall h\in\Omega^H,\forall t\in\Omega^T \quad (5.126)$$

By making the above changes to the optimal operation and feasibility check subproblems, the uncertainties of renewable generations, loads, and electricity prices are included in the developed STS-based decomposed MDEP model. Now, the proposed robust optimization-based uncertainty modelling approach can be explained.

In order to simplify the notation, each of the optimal operation and feasibility check subproblems can be expressed in the following general form:

$$\text{Min} \quad \sum_{n=1}^{\mathcal{N}}\widetilde{c_n}x_n \quad (5.127)$$

$$\text{s.t.} \quad \sum_{n=1}^{\mathcal{N}}\widetilde{a_{m,n}}x_n\leq b_m \qquad \forall m=1,\dots,\mathcal{M} \quad (5.128)$$

$$\sum_{n=1}^{\mathcal{N}}d_{p,n}x_n\leq e_p \qquad \forall p=1,\dots,\mathcal{P} \quad (5.129)$$

$$\sum_{n=1}^{\mathcal{N}}f_{q,n}x_n=g_q \qquad \forall q=1,\dots,\mathcal{Q} \quad (5.130)$$

$$\underline{x_n}\leq x_n\leq\overline{x_n} \qquad \forall n=1,\dots,\mathcal{N} \quad (5.131)$$

where x_n denotes the decision variables of the optimization problem; $\mathcal{N}/n$ is the number/index of the decision variables; $\widetilde{c_n}$ denotes the coefficients of the decision variables in the objective function; $\mathcal{M}/m$ is the number/index of the constraints subject to uncertainty; $\widetilde{a_{m,n}}$ denotes the coefficients of the decision variables in the constraints subject to uncertainty; b_m denotes the constant values located at the right-hand sides of the constraints subject to uncertainty; $\mathcal{P}/p$ is the number/index of the inequality constraints which are not subject to uncertainty; $d_{p,n}$ denotes the

coefficients of the decision variables in the inequality constraints which are not subject to uncertainty; e_p denotes the constant values located at the right-hand sides of the inequality constraints which are not subject to uncertainty; $\mathcal{Q}/q$ is the number/index of the equality constraints which are not subject to uncertainty; $f_{q,n}$ denotes the coefficients of the decision variables in the equality constraints which are not subject to uncertainty; g_q denotes the constant values located at the right-hand sides of the equality constraints which are not subject to uncertainty; and $\underline{x_n}$ and $\overline{x_n}$ are the lower and upper bounds of the decision variables, respectively.

Let us assume that the coefficients $\widetilde{a_{m,n}}$ and $\widetilde{c_n}$ can take values in the following uncertainty sets:

$$\widetilde{a_{m,n}} \in \left[\overline{\overline{a_{m,n}}} - \widehat{a_{m,n}}\,, \overline{\overline{a_{m,n}}} + \widehat{a_{m,n}}\right] \tag{5.132}$$

$$\widetilde{c_n} \in \left[\,\overline{\overline{c_n}}\,, \overline{\overline{c_n}} + \widehat{c_n}\,\right] \tag{5.133}$$

where $\overline{\overline{a_{m,n}}}$ is the expected value of $\widetilde{a_{m,n}}$; $\widehat{a_{m,n}}$ denotes the maximum deviation of $\widetilde{a_{m,n}}$ from its expected value; $\overline{\overline{c_n}}$ is the expected value of $\widetilde{c_n}$; and $\widehat{c_n}$ is the maximum deviation of $\widetilde{c_n}$ from its expected value. Note that in the case when any of the coefficients $\widetilde{a_{m,n}}$ and $\widetilde{c_n}$ are certain, their corresponding deviation values $\widehat{a_{m,n}}$ and $\widehat{c_n}$ are equal to zero (i.e., $\widehat{a_{m,n}} = 0$ and $\widehat{c_n} = 0$).

For every constraint m that is subject to uncertainty, we define a parameter Γ_m as follows:

$$0 \le \Gamma_m \le |\mathcal{J}_m| \quad , \quad \mathcal{J}_m = \left\{n | \widehat{a_{m,n}} > 0\right\} \quad \forall m = 1, \dots, \mathcal{M} \tag{5.134}$$

where $\mathcal{J}_m$ is the set of all coefficients $\widetilde{a_{m,n}}$ which are uncertain (i.e., coefficients with $\widehat{a_{m,n}} > 0$). Note that Γ_m is not necessarily integer and can take real values in the interval $[0, |\mathcal{J}_m|]$.

We also define a parameter Γ_0 for the objective function as follows:

$$0 \le \Gamma_0 \le |\mathcal{J}_0| \quad , \quad \mathcal{J}_0 = \{n | \widehat{c_n} > 0\} \tag{5.135}$$

where $\mathcal{J}_0$ is the set of all coefficients $\widetilde{c_n}$ which are uncertain (i.e., coefficients with $\widehat{c_n} > 0$). Note that Γ_0 can also take real values in the interval $[0, |\mathcal{J}_0|]$.

The parameters Γ_m and Γ_0 are defined to adjust the degree of conservatism of the solution. In the proposed robust optimization-based approach, these parameters will be used to allow only a subset of all uncertain $\widetilde{a_{m,n}}$ and $\widetilde{c_n}$ coefficients to deviate from their expected values. In other words, it is unlikely that all uncertain $\widetilde{a_{m,n}}$ and $\widetilde{c_n}$ coefficients deviate from their expected values as much

as $\widehat{a_{m,n}}$ and $\widehat{c_n}$. Hence, the parameters Γ_m and Γ_0 are defined to specify the number of uncertain $\widetilde{a_{m,n}}$ and $\widetilde{c_n}$ coefficients that are allowed to deviate from their expected values. In this regard, when Γ_m is set to a value in the interval $[0, |\mathcal{J}_m|]$, the optimal solution will be found under the condition that $\lfloor \Gamma_m \rfloor$ of uncertain $\widetilde{a_{m,n}}$ coefficients deviate from their expected values as much as $\widehat{a_{m,n}}$ and one uncertain $\widetilde{a_{m,n}}$ coefficient deviates from its expected value as much as $(\Gamma_m - \lfloor \Gamma_m \rfloor)\widehat{a_{m,n}}$. Similarly, when Γ_0 is set to a value in the interval $[0, |\mathcal{J}_0|]$, the optimal solution will be found under the condition that $\lfloor \Gamma_0 \rfloor$ of uncertain $\widetilde{c_n}$ coefficients deviate from their expected values as much as $\widehat{c_n}$ and one uncertain $\widetilde{c_n}$ coefficient deviates from its expected value as much as $(\Gamma_0 - \lfloor \Gamma_0 \rfloor)\widehat{c_n}$. It is obvious that increasing the values of Γ_m and Γ_0 will allow a larger number of uncertain $\widetilde{a_{m,n}}$ and $\widetilde{c_n}$ coefficients to deviate from their expected values, which results in obtaining a more conservative solution. This is how the degree of conservatism of the solution will be controlled by the parameters Γ_m and Γ_0.

Based on the above discussion, the robust counterpart of the optimization problem (5.127)-(5.131) is proposed as follows [96], [97]:

$$\text{Min} \sum_{n=1}^{\mathcal{N}} \overline{\widehat{c_n}} x_n + \max_{\{\mathcal{D}_0 \cup \{\delta_0\} | \mathcal{D}_0 \subseteq \mathcal{J}_0,\ |\mathcal{D}_0| \le \lfloor \Gamma_0 \rfloor,\ \delta_0 \in \mathcal{J}_0 \setminus \mathcal{D}_0\}} \left\{ \sum_{n \in \mathcal{D}_0} \widehat{c_n} |x_n| + (\Gamma_0 - \lfloor \Gamma_0 \rfloor) \widehat{c_{\delta_0}} |x_{\delta_0}| \right\} \quad (5.136)$$

s.t. (5.129)-(5.131)

$$\sum_{n=1}^{\mathcal{N}} \overline{\widehat{a_{m,n}}} x_n + \max_{\{\mathcal{D}_m \cup \{\delta_m\} | \mathcal{D}_m \subseteq \mathcal{J}_m,\ |\mathcal{D}_m| \le \lfloor \Gamma_m \rfloor, \delta_m \in \mathcal{J}_m \setminus \mathcal{D}_m\}} \left\{ \sum_{n \in \mathcal{D}_m} \widehat{a_{m,n}} |x_n| \right.$$

$$\left. + (\Gamma_m - \lfloor \Gamma_m \rfloor) \widehat{a_{m,\delta_m}} |x_{\delta_m}| \right\} \le b_m \qquad \forall m = 1, \dots, \mathcal{M} \quad (5.137)$$

As can be seen in the second terms of (5.136) and (5.137), the above robust optimization problem finds the optimal solution considering the level of conservatism defined by the parameters Γ_m and Γ_0. For instance, in the case when $\Gamma_m = |\mathcal{J}_m|$ and $\Gamma_0 = |\mathcal{J}_0|$, all the uncertain $\widetilde{a_{m,n}}$ and $\widetilde{c_n}$ coefficients will be allowed to have the maximum deviations $\widehat{a_{m,n}}$ and $\widehat{c_n}$ from their expected values. This case will result in the most conservative solution possible. By contrast, in the case when $\Gamma_m = 0$ and $\Gamma_0 = 0$, none of the uncertain $\widetilde{a_{m,n}}$ and $\widetilde{c_n}$ coefficients will be allowed to deviate from their expected values. This case will lead to a deterministic solution which completely ignores all the uncertainties. Thus, by setting Γ_m and Γ_0 to appropriate values in the intervals $[0, |\mathcal{J}_m|]$ and $[0, |\mathcal{J}_0|]$, the decision maker will be able to flexibly adjust the level of conservatism of the solution.

It should be noted that the absolute value operators (i.e., $|-|$) in (5.136) and (5.137) cause the above robust optimization problem to become a nonlinear programming (NLP) problem which is very difficult to solve. The authors of [96], [97] demonstrate that this NLP problem can be equivalently reformulated as the following linear programming (LP) problem:

$$\text{Min } \sum_{n=1}^{\mathcal{N}} \overline{\overline{c_n}} x_n + \alpha_0 \Gamma_0 + \sum_{n \in \mathcal{J}_0} \beta_{0,n} \tag{5.138}$$

s.t. (5.129)-(5.131)

$$\sum_{n=1}^{\mathcal{N}} \overline{\overline{a_{m,n}}} x_n + \alpha_m \Gamma_m + \sum_{n \in \mathcal{J}_m} \beta_{m,n} \leq b_m \quad \forall m = 1, \dots, \mathcal{M} \tag{5.139}$$

$$\alpha_0 + \beta_{0,n} \geq \widehat{c_n} w_n \qquad \forall n \in \mathcal{J}_0 \tag{5.140}$$

$$\alpha_m + \beta_{m,n} \geq \widehat{a_{m,n}} w_n \qquad \forall m = 1, \dots, \mathcal{M}, \forall n \in \mathcal{J}_m \tag{5.141}$$

$$-w_n \leq x_n \leq w_n \qquad \forall n \in (\mathcal{J}_0 \cup \mathcal{J}_m) \tag{5.142}$$

$$\alpha_0 \geq 0 \tag{5.143}$$

$$\beta_{0,n} \geq 0 \qquad \forall n \in \mathcal{J}_0 \tag{5.144}$$

$$\alpha_m \geq 0 \qquad \forall m = 1, \dots, \mathcal{M} \tag{5.145}$$

$$\beta_{m,n} \geq 0 \qquad \forall m = 1, \dots, \mathcal{M}, \forall n \in \mathcal{J}_m \tag{5.146}$$

$$w_n \geq 0 \qquad \forall n \in (\mathcal{J}_0 \cup \mathcal{J}_m) \tag{5.147}$$

where α_0, $\beta_{0,n}$, α_m, $\beta_{m,n}$, and w_n are auxiliary variables.

The above LP problem is the final robust counterpart of the optimization problem (5.127)-(5.131). In [96], [97], it is proved that for the optimal solution of the above robust LP problem, the probability that the constraints subject to uncertainty (i.e., $\sum_{n=1}^{\mathcal{N}} \widetilde{a_{m,n}} x_n \leq b_m$) are violated can be obtained as follows:

$$\mathbb{P}\left\{\sum_{n=1}^{\mathcal{N}} \widetilde{a_{m,n}} x_n^* > b_m\right\} \leq \mathcal{B}(|\mathcal{J}_m|, \Gamma_m) \tag{5.148}$$

$$\mathcal{B}(|\mathcal{J}_m|,\Gamma_m) \leq \left(1-\frac{\Gamma_m+|\mathcal{J}_m|}{2}+\left\lfloor\frac{\Gamma_m+|\mathcal{J}_m|}{2}\right\rfloor\right)\mathcal{F}\left(|\mathcal{J}_m|,\left\lfloor\frac{\Gamma_m+|\mathcal{J}_m|}{2}\right\rfloor\right)+\sum_{\ell=\left\lfloor\frac{\Gamma_m+|\mathcal{J}_m|}{2}\right\rfloor+1}^{|\mathcal{J}_m|}\mathcal{F}(|\mathcal{J}_m|,\ell) \quad (5.149)$$

$$\mathcal{F}(|\mathcal{J}_m|,\ell)=\begin{cases}\frac{1}{2^{|\mathcal{J}_m|}} & \forall \ell \in \{0,|\mathcal{J}_m|\} \\ \frac{1}{\sqrt{2\pi}}\sqrt{\frac{|\mathcal{J}_m|}{(|\mathcal{J}_m|-\ell)\ell}}\exp\left(|\mathcal{J}_m|\log\left(\frac{|\mathcal{J}_m|}{2(|\mathcal{J}_m|-\ell)}\right)+\ell\log\left(\frac{|\mathcal{J}_m|-\ell}{\ell}\right)\right) & \forall \ell \notin \{0,|\mathcal{J}_m|\}\end{cases} \quad (5.150)$$

where x_n^* denotes the optimal solution of the robust LP problem; $\mathcal{B}$ is a bound on the probability of violation of constraints subject to uncertainty; and $\mathcal{F}$ is a function required to calculate $\mathcal{B}$.

In fact, equations (5.148)-(5.150) provide a probabilistic bound on the robustness level of the solution obtained by the robust LP problem. These equations enable the decision maker to have an accurate estimation of the solution robustness for different values of the parameter Γ_m. In this way, the proposed robust optimization-based uncertainty modelling approach provides the decision maker with the opportunity to not only adjust the degree of conservatism of the solution, but also calculate the robustness level of the obtained solution.

By applying the above-described uncertainty modelling approach to the optimal operation and feasibility check subproblems, the deterministic model developed in Section 5.2 will be converted to a robust one.

5.4 Simulation Results and Discussion

In this section, the most important results obtained from the implementation of the proposed STS-based decomposed MDEP model are presented and discussed. This model has been implemented on a PC with a 3.40 GHz Intel Core i7-4770 processor and 16 GB of RAM using MATLAB R2015a [84] and CPLEX 12.6.1 [85]. The 24-node system is again utilized to carry out the simulations. The data related to the candidate conductor types, alternatives for construction/reinforcement of substations, alternatives for installation of renewable/conventional DGs, expected nodal peak power demands, and lengths of feeder sections are exactly the same as those presented in Chapter 2. The data related to the alternatives for installation of ESSs are presented in Table 5.2. Furthermore, the set of candidate nodes for ESS installation is defined as $\Omega^{NES}=\{1,2,3,4,5,7,9,13,14,15,16,17,18,19\}$. It should be mentioned that the candidate nodes considered for ESS installation are the same as those considered for DG installation (i.e., $\Omega^{NES}=\Omega^{NG}$). Another important point is that as an illustrative example, renewable DGs are here assumed

to be wind turbines. However, the proposed planning methodology is fully applicable to other renewables DG technologies such as photovoltaic panels.

Table 5.2 Data related to alternatives for installation of ESSs.

Ω^{es}	$\overline{P_s^{Ch}}$ (MW)	$\overline{P_s^{Dch}}$ (MW)	$\overline{T_s^{Ch}}$ (h)	$\overline{T_s^{Dch}}$ (h)	c_s^{ES} ($)
1	1	1	6	4.2	550000
2	1.5	1.5	6	4.2	825000

Table 5.3 shows the data related to the alternatives for installation of smart meters. Moreover, the set of candidate nodes for smart meter installation is defined as $\Omega^{NSM} = \{2,6,7,8,10,11,12,14, 16,17,20\}$. Table 5.4 presents the data related to the parameters of AA-CAES. Other required data are given in Table 5.5.

Table 5.3 Data related to alternatives for installation of smart meters.

Ω^{sm}	κ_p^{SM} (%)	c^{SM} ($)
1	40	400
2	60	400

Table 5.4 Parameters of AA-CAES.

Parameter	Value	Parameter	Value	Parameter	Value
γ^{Air}	1.4	T^{AST}	293.15 (K)	c^{Air}	1.005 (kJ/kg.K)
ε^{RC}	0.8	T^{COT}	293.15 (K)	c^{Oil}	2.2 (kJ/kg.K)
η^{G}	0.97	T^{HOT}	573.15 (K)	ρ^{Oil}	750 (kg/m^3)
η^{M}	0.95	$T^{HPC,in}$	313.15 (K)	V^{AST}	900 m^3 $\forall s = 1$
η^{LPC}, η^{HPC}	0.87	$T^{HPC,out}$	605.22 (K)	V^{AST}	1400 m^3 $\forall s = 2$
η^{HPT}, η^{LPT}	0.9	$T^{LPC,in}$	293.15 (K)	V^{HOT}	40 m^3 $\forall s = 1$
π^{LPC}	8	$T^{LPC,out}$	566.57 (K)	V^{HOT}	60 m^3 $\forall s = 2$
π^{HPC}	8	$T^{HPT,in}$	675.15 (K)	$\overline{p^{AST}}$	72 (bar)
π^{HPT}	8	$T^{HPT,out}$	402.96 (K)	$\underline{p^{AST}}$	42 (bar)
π^{LPT}	8	$T^{LPT,in}$	675.15 (K)	R^{Air}	287.05×10^{-5} (bar.m^3/kg.K)
$T^{RC,out}$	381(K)	$T^{LPT,out}$	402.96 (K)		

Table 5.5 Other required data.

Parameter	Value	Parameter	Value	Parameter	Value
a_{ij}^{FR}	1	ε^{Cross}	0.01	$\underline{V}$	0.95×20=19 (kV)
a_{ij}^{FI}	2	ε^{Self}	−0.4	$\overline{V}$	1.05×20=21 (kV)
$\overline{N^{GC}}$	4	τ^{DinY}	365	$\overline{\Delta V}$	$(\overline{V})^2-(\underline{V})^2=80$
$\overline{N^{GR}}$	4	τ^{SinH}	3600	$\overline{S_i^0}$	7.5 (MVA)
$\overline{N^{ES}}$	3	ρ^{GR},ρ^{D}	0.9	$\overline{\overline{c^E}}$	85 ($/MWh)
$\overline{N^{SM}}$	5	r	0.1	D	5 (year)
$N_{i,t}^{C}$	$\max\{\overline{\overline{P_{i,h,t}^{D}}}\ \forall h\in\Omega^{H}\}$/(10kW)			ϕ^{S}	0.15

As discussed in Section 5.3, the proposed robust optimization-based uncertainty modelling approach requires the mean and the lower and upper bounds of the uncertain parameters to define the uncertainty sets. In this regard, we have used the historical data provided in [116] to calculate the mean and the lower and upper bounds of the load, wind generation, and electricity price at different hours of the day. Figure 5.3 shows the box plots and the expected values of the acquired historical data of load, wind generation, and electricity price.

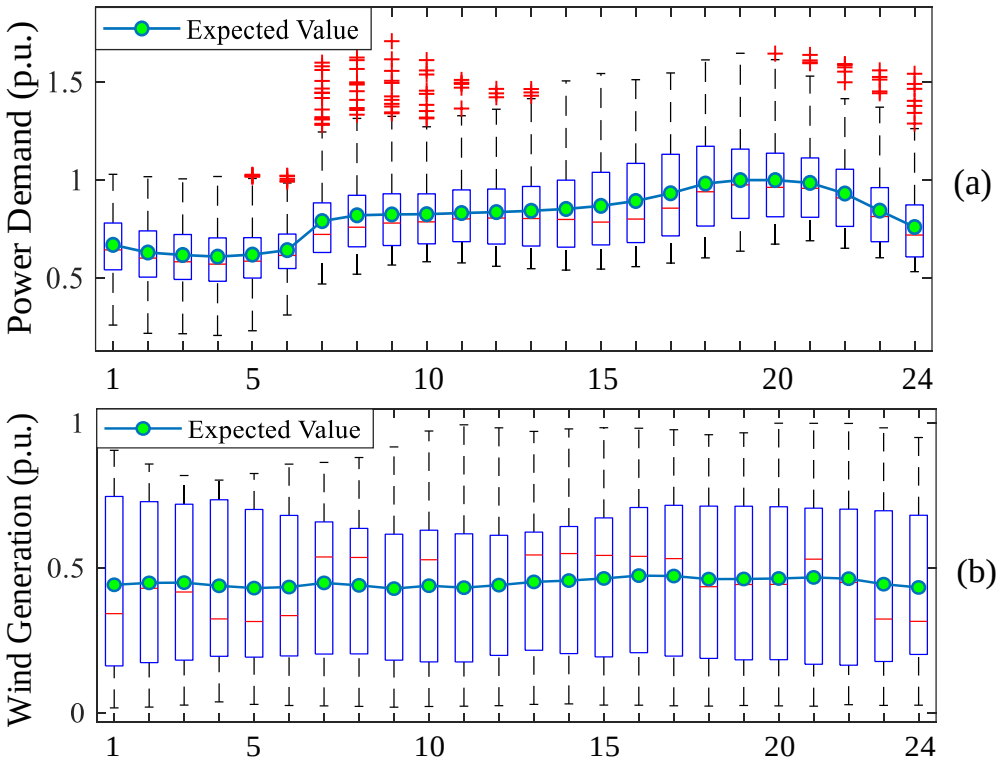

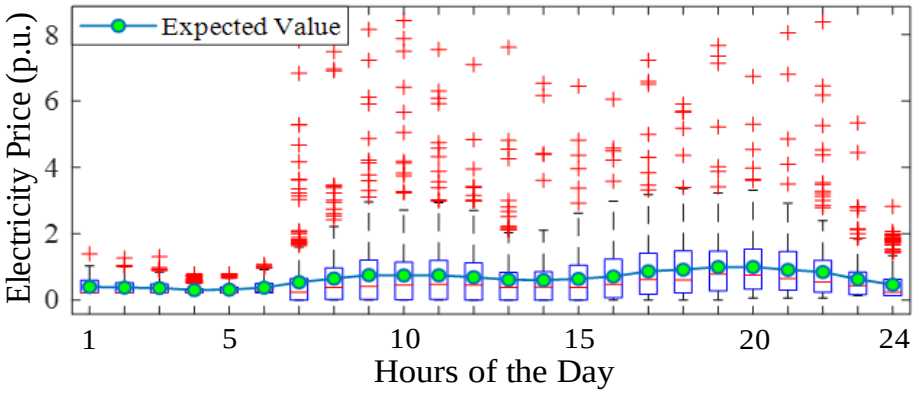

(c)

Figure 5.3 Box plots and expected values of the historical data: (a) load; (b) wind generation; (c) electricity price.

Table 5.6 shows the test cases defined to conduct the simulations: Case 1) deterministic expansion planning of the network assets (feeders and substations); Case 2) deterministic expansion planning of the network assets and renewable/conventional DGs; Case 3) deterministic expansion planning of the network assets, renewable/conventional DGs, and ESSs; Case 4) deterministic expansion planning of the network assets, renewable/conventional DGs, ESSs, and DRLs; Case 5) robust expansion planning of the network assets, renewable/conventional DGs, ESSs, and DRLs.

Table 5.6 Defined test cases.

Test Cases	Feeders	Substations	DGs		ESSs	DRLs	Uncertainty Modelling
			Conv.	Ren.			
Case 1	✓	✓	×	×	×	×	×
Case 2	✓	✓	✓	✓	×	×	×
Case 3	✓	✓	✓	✓	✓	×	×
Case 4	✓	✓	✓	✓	✓	✓	×
Case 5	✓	✓	✓	✓	✓	✓	✓

5.4.1 Techno-Economic Analysis of DER Benefits

In this subsection, a comparative analysis is performed to weigh the benefits of network integration of DERs. In this regard, the numerical results obtained for Cases 1-4 are compared to evaluate the DER benefits from two different perspectives: economic and technical. Note that the uncertainties of loads, wind generations, and electricity prices are ignored here.

5.4.1.1 Economic Benefits of DERs

Table 5.7 compares the investment, operation, and total costs obtained for Cases 1-4. It can be observed that the incorporation of DERs into the MDEP problem leads to an increase in the investment costs and a decrease in the operation costs. However, the decrease in the operation costs is considerably higher than the increase in the investment costs. As a result, DERs make significant reductions in the total costs. For instance, the incorporation of renewable/conventional DGs into the MDEP problem decreases the total costs from $117.27 million in Case 1 to $82.08 million in Case 2, which shows a 30% reduction. By incorporation of both DGs and ESSs into the MDEP problem, the total costs decrease to $80.50 million in Case 3, which shows a 31.35% reduction compared with Case 1. Furthermore, the incorporation of DRLs along with DGs and ESSs into the MDEP problem decreases the total costs to $78.69 million in Case 4, which demonstrates a 32.90% reduction compared with Case 1.

Table 5.7 Comparison of investment, operation, and total costs for Cases 1-4.

Test Cases	Costs (10^6 $)		
	Investment	Operation	Total
Case 1	2.67	114.60	117.27
Case 2	8.07	74.01	82.08
Case 3	9.79	70.71	80.50
Case 4	9.87	68.82	78.69

Table 5.8 presents the costs and benefits associated with different types of DERs. These information help to better quantify the net economic benefits gained by integrating each DER type into the distribution system. Note that DG costs/benefits are calculated by comparing Cases 1 and 2, ESS costs/benefits are calculated by comparing Cases 2 and 3, and DRL costs/benefits are calculated by comparing Cases 3 and 4. As can be seen, the costs of different types of DERs are considerably lower than their benefits. The net benefits offered by DGs, ESSs, and DRLs are $35.19 million, $1.58 million, and $1.81 million, respectively. It can be observed that DGs yield the highest net benefit among different DER types. This is obviously due to the ability of DGs to generate electric power, which provides the opportunity to substantially decrease the operation costs by reducing the electrical energy received from the upstream power grid.

Table 5.8 Costs and benefits associated with different types of DERs.

Test Case Comparisons	DER Types	Costs (10^6 \$)	Benefits (10^6 \$)	Net Benefits (10^6 \$)
Case 1 & Case 2	DG	5.40	40.59	**35.19**
Case 2 & Case 3	ESS	1.72	3.30	**1.58**
Case 3 & Case 4	DRL	0.08	1.89	**1.81**

For illustration purposes, the expansion plans obtained for the 24-node distribution system for Case 4 are depicted in Figure 5.4. It is worthwhile to mention that for this case, the accelerated BD algorithm consumes 47 min to solve the STS-based MDEP model, while the direct solution method requires a computation time of more than 17 hours to find the optimal solution of the STS-based MDEP model. This fact demonstrates the necessity of having a fast solution method in order to incorporate the STS capability into the planning problem.

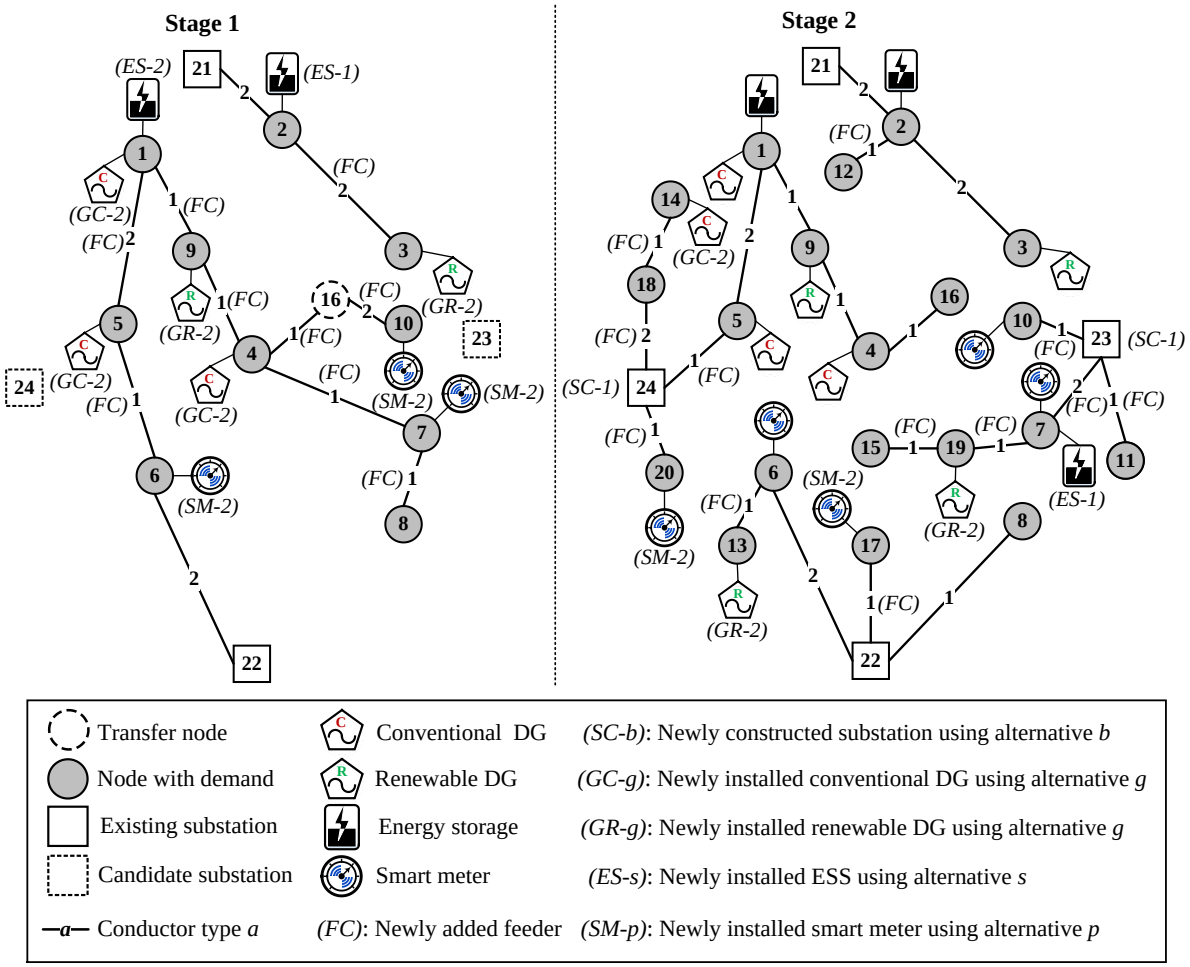

Figure 5.4 Expansion plans obtained for the 24-node distribution system for Case 4.

5.4.1.2 Technical Benefits of DERs

The technical benefits of DERs are evaluated based on their impacts on four important operational aspects of the distribution system: 1) power demand profile, 2) nodal voltage magnitudes, 3) power losses, and 4) loading of feeder sections.

Figure 5.5 illustrates the total power demand profiles of the system for Cases 1-4. It can be observed that the peak power demand of the system in Case 2 is significantly lower than that in Case 1, which is obviously due to the incorporation of DGs into the MDEP problem in Case 2. Moreover, as can be seen, the incorporation of ESSs and DRLs into the MDEP problem in Cases 3 and 4 not only further reduces the peak power demand of the system, but also makes the power demand profile smoother by shifting the demand from peak hours to off-peak hours. The peak power demand of the system in Case 1 is 42.17 MW, while the network integration of DERs reduces it to 30.55 MW, 27.65 MW, and 26.32 MW in Cases 2-4, respectively. Furthermore, the peak-to-average ratios of the power demand profiles of the system for Cases 1-4 are 1.22, 1.33, 1.18, and 1.13, respectively. These values further clarify the role of ESSs and DRLs in making the power demand profile smoother.

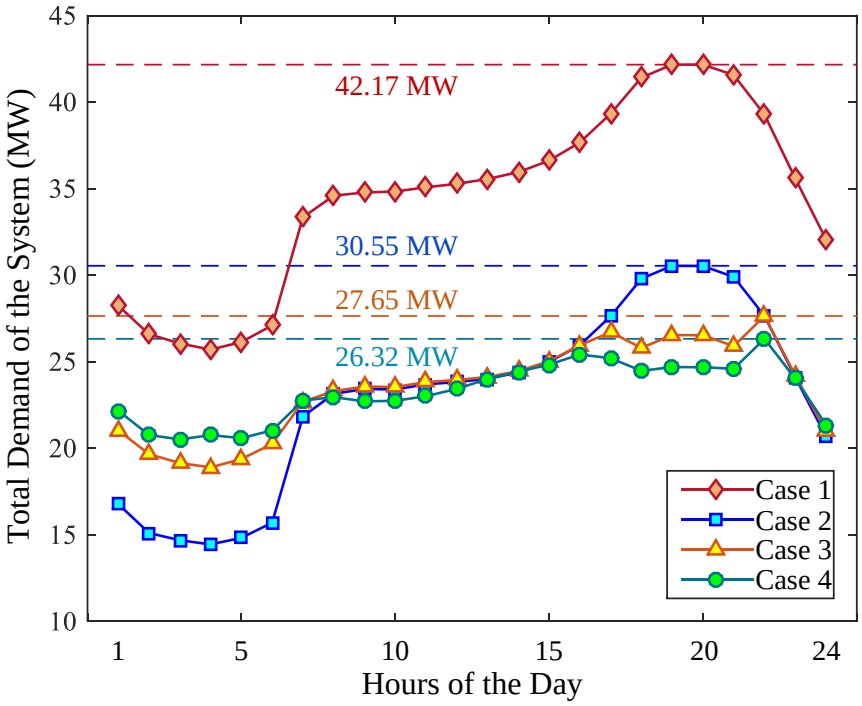

Figure 5.5 Power demand profiles of the system for Cases 1-4.

Figure 5.6 depicts the minimum nodal voltage magnitudes as well as the power losses of the system during peak hours for Cases 1-4. As can be observed, the network integration of DERs not only improves the nodal voltage magnitudes of the system, but also reduces the power losses in feeder sections. For instance, DERs increase the minimum nodal voltage magnitude of the system from 1.0265 p.u. in Case 1 to 1.0394 p.u. in Case 4. Moreover, by incorporation of DERs into the MDEP problem, the average of the system power losses during peak hours is decreased from 340 kW in Case 1 to 128 kW in Case 4.

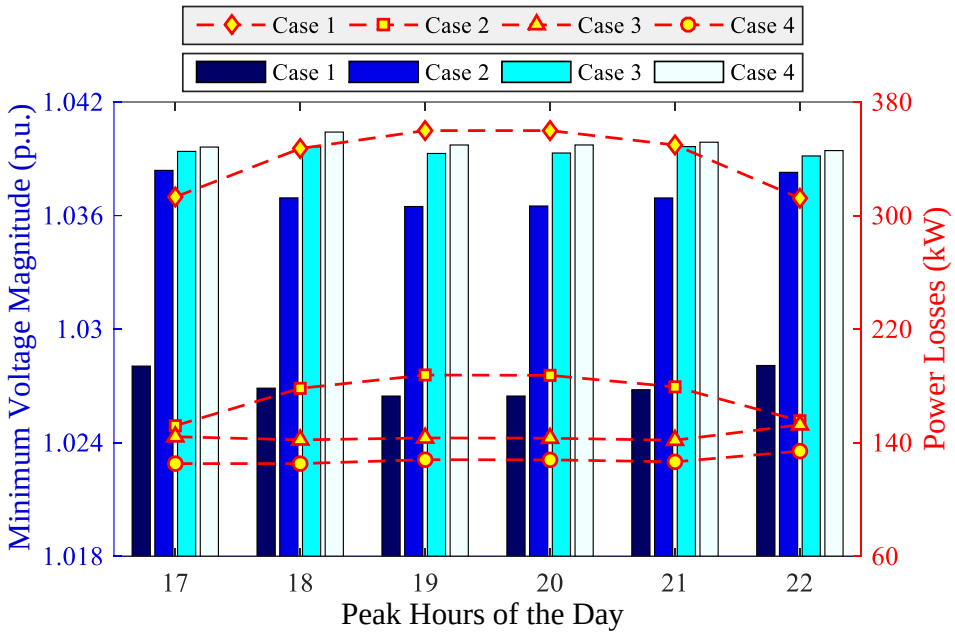

Figure 5.6 Minimum nodal voltage magnitudes and power losses of the system during peak hours for Cases 1-4.

Table 5.9 compares the percentage loading of feeder sections for Cases 1-4. It can be seen that as more and more DERs are integrated into the distribution system, the loading of feeder sections is gradually decreased. For instance, the network integration of DERs causes the average loading of feeder sections to decrease from 46.01% in Case 1 to 32.89% in Case 4. Table 5.9 also shows that DERs reduce the number of highly loaded feeder sections. For instance, there are six feeder sections with loading of greater than 70% in Case 1, while Case 4 has only one feeder section with loading of greater than 70%. Similarly, Case 1 has two feeder sections with loading of greater than 90%, whereas there is no feeder section with loading of greater than 90% in Case 4. Based on the above discussion, reduced loading of distribution network assets is another substantial technical benefit of DERs.

Table 5.9 Comparison of the percentage loading of feeder sections for Cases 1-4.

Test Cases	Avg. Loading of Feeder Sections	No. of Feeder Sections with Loading of		
		≥ 70%	≥ 80%	≥ 90%
Case 1	46.01%	6	3	2
Case 2	34.64%	2	1	1
Case 3	33.15%	2	1	0
Case 4	32.89%	1	1	0

5.4.2 Robustness Evaluation of the Proposed Planning Model

In this subsection, the robustness of the proposed STS-based decomposed MDEP model against the uncertainties of loads, wind generations, and electricity prices is assessed. To this end, first the solutions of Case 4 (deterministic) and Case 5 (robust) are obtained for comparison purposes. Then, the hourly historical data shown in figure 5.3 are used to produce a large number of samples of load, wind generation, and electricity price. Finally, the solution robustness of each of the Cases 4 and 5 is assessed using the produced samples.

Figure 5.7 compares the performances of Cases 4 and 5 from the viewpoint of solution robustness. Note that the solution robustness of Case 5 is evaluated considering ten different values for $\mathcal{B}$ which denotes the probabilistic bound on violation of constraints subject to uncertainty (see equations (5.148)-(5.150)). In this regard, $\mathcal{B}$ is changed from 1% to 10% in steps of 1%, and the corresponding changes in the solution robustness of Case 5 are examined. It can be observed that Case 4 has the lowest level of robustness, so that its solution robustness goes down to 55% during peak hours of the day. This poor performance is obviously due to the fact that in Case 4, the expansion plans are obtained without having any information about the uncertainties. By contrast, Case 5 results in considerably higher robustness levels for different values of $\mathcal{B}$, so that its solution robustness reaches 100% during off-peak hours of the day. Taking a careful look at Figure 5.7 also reveals that the solution robustness of Case 5 is always above the specified requirement (i.e., $1 - \mathcal{B}$), even during the peak hours of the day. It is worthwhile to note that by decreasing the value of $\mathcal{B}$, the degree of conservatism of Case 5 is increased and consequently the solution robustness is also increased.

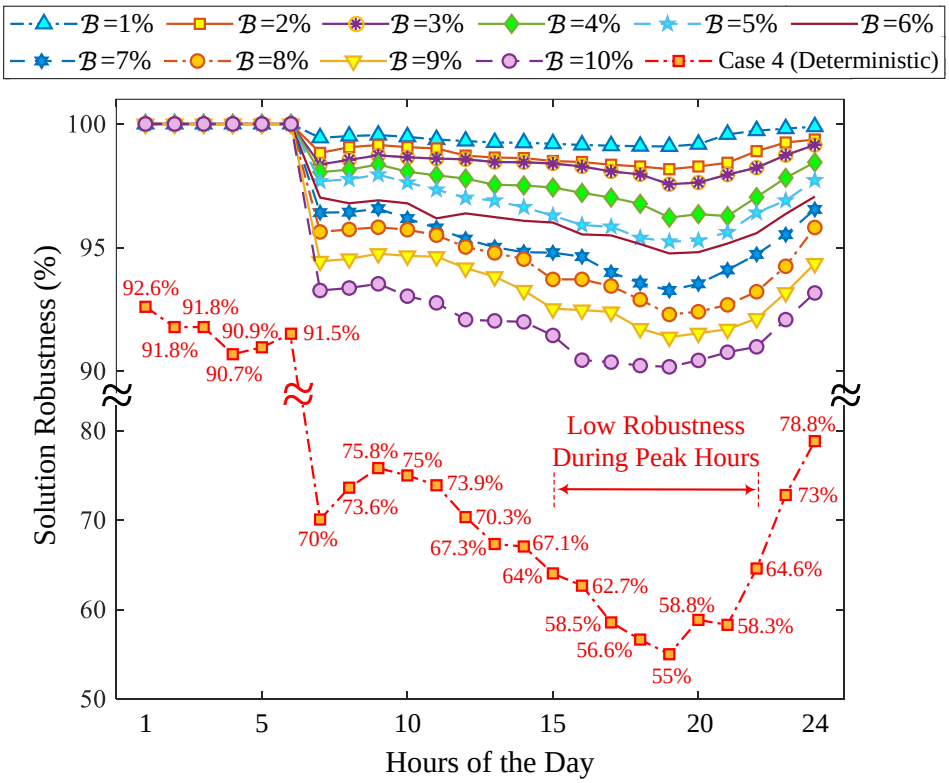

Figure 5.7 Robustness comparison of Case 4 (deterministic) and Case 5 (robust) at different hours of the day.

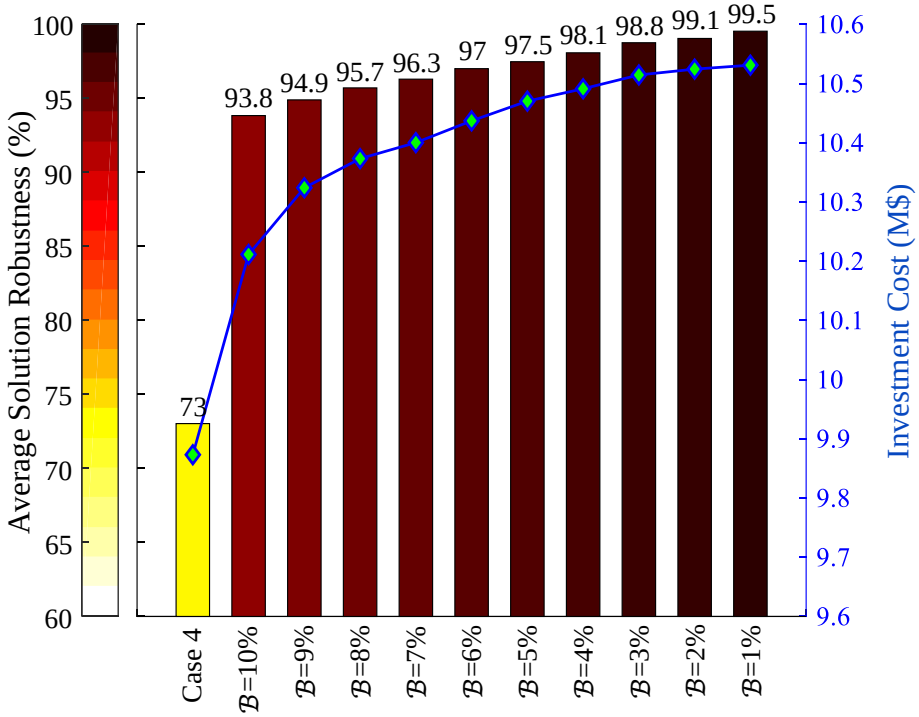

Figure 5.8 Investment costs and average solution robustness of Case 4 (deterministic) and Case 5 (robust).

Figure 5.8 compares Cases 4 and 5 from the viewpoints of investment cost and average solution robustness (i.e., average of the robustness levels at different hours of the day). As can be observed, the average solution robustness of Case 5 for different values of $\mathcal{B}$ is significantly higher than that of Case 4. As expected, the higher robustness of Case 5 is achieved at the cost of an increase in the investment costs. However, it is worth to bear such a reasonable cost to obtain the reported substantial improvement in the average solution robustness. Therefore, it can be stated that the proposed robust STS-based decomposed MDEP model makes an appropriate trade-off between the solution robustness and the investment cost.

5.4.3 An Extended Case Study

The 138-node distribution system is here used to demonstrate the scalability of the proposed robust STS-based decomposed MDEP model. The data related to the candidate conductor types, alternatives for construction/reinforcement of substations, alternatives for installation of renewable/conventional DGs, expected nodal peak power demands, and lengths of feeder sections are exactly the same as those presented in Chapter 2. The data related to the alternatives for installation of ESSs and smart meters are the same as those presented in Tables 5.2 and 5.3. The set of candidate nodes for ESS installation is defined as $\Omega^{NES} = \{4,10,19,25,28,31,42,52,56,64,$ $68,72,78,85,94,97,100,103,106,108,111,116,120,122,126,133\}$. It should be noted that the candidate nodes considered for ESS installation are the same as those considered for DG installation (i.e., $\Omega^{NES} = \Omega^{NG}$). Moreover, the set of candidate nodes for smart meter installation is defined as $\Omega^{NSM} = \{1,3,7,12,15,22,27,30,38,49,54,60,66,75,83,91,102,109,114,125,132\}$. The parameters of AA-CAES and other required data are the same as those presented in Tables 5.4 and 5.5 (except that $\overline{S_i^0}$=12 MVA , $\underline{V}$=0.95×13.8=13.11 kV , $\overline{V}$=1.05×13.8=14.49 kV , $\overline{\Delta V}$=38.08). The historical data of load, wind generation, and electricity price are the same as those depicted in Figure 5.3.

The simulation results show that for Case 5, the accelerated BD algorithm requires 159 min to solve the proposed robust STS-based MDEP model. Whereas, due to the large scale of the 138-node distribution system, the direct solution method cannot find the optimal solution of the proposed robust STS-based MDEP model, even after an extremely long computation time (e.g., several days). This fact once again demonstrates the necessity of having a fast solution method in order to incorporate the

STS capability into the planning problem, especially when dealing with large-scale distribution systems.

5.5 Summary

In this chapter, a robust STS-based decomposed MDEP model has been developed for ADNs incorporating various types of DERs (i.e., DGs, ESSs, and DRLs). This model has the ability to perform STPFS which is identified as the most important requirement for future distribution system planning tools. To achieve the computational speed required for performing STPFS, the fast solution procedure proposed in Chapter 4 has been employed. In this regard, the MDEP model has been decomposed into a master problem which determines the long-term expansion plans and two subproblems which conduct the short-term STS-based operation analysis. With regard to ESS modelling, after careful comparison of different technologies, AA-CAES has been chosen as the energy storage option for ADNs and a detailed model has been proposed for it. With regard to DRL modelling, an RTP scheme has been considered and a demand function based on self-price and cross-price elasticities has been employed to model the reaction of DRLs to electricity price changes. Furthermore, in order to model the uncertainties of renewable generations, loads, and electricity prices, a new robust optimization-based approach has been proposed, which provides the decision maker with the opportunity to not only adjust the degree of conservatism of the solution, but also calculate the robustness level of the obtained solution.

The developed robust STS-based decomposed MDEP model has been successfully validated using the 24-node and 138-node distribution systems. The simulation results show that the network integration of DERs provides significant techno-economic benefits. From the economic point of view, the incorporation of DERs into the MDEP problem leads to significant reductions in the costs. From the technical point of view, DERs have a positive effect on four important operational aspects of the distribution system: first, they reduce the peak power demand of the system and also make the power demand profile smoother; second, they improve the nodal voltage magnitudes of the system; third, they reduce the power losses in feeder sections; fourth, they decrease the loading of feeder sections. The simulation results also demonstrate the high solution robustness of the developed robust STS-based decomposed MDEP model, so that the robustness of this model is always above the level specified by the decision maker. The results also show that in order to

incorporate the STS capability into the planning problem of large-scale distribution systems, it is essential to have a fast solution method, otherwise it will be extremely time-consuming or even impossible to find the optimal solution of the problem.

6. Conclusions and Suggestions for Future Work

6.1 Conclusions

This project has developed a comprehensive planning methodology for ADNs, which is able to jointly expand both the network assets (feeders and substations) and DERs (DGs, ESSs, and DRLs), while giving full consideration to accurate distribution network modelling and efficient uncertainty modelling. To this end, five major steps have been defined for the project and a thorough description of the works done in each step has been presented.

Regarding the first step of the project, a novel polyhedral-based MILP model has been proposed for the MDEP problem, which has two outstanding merits: first, it incorporates a highly accurate linearized network model reflecting AC power flow equations and energy losses; second, its linear formulation ensures the computational tractability and solution optimality. The simulation results showed that the developed MILP model can provide better solutions than the most accurate MILP model available in the literature. This superiority is due to the great performance of the polyhedral-based linearization method proposed for eliminating the nonlinearities of the MDEP problem, so that the accuracy of this method can go up to almost 100% by choosing an appropriate value for the linearization parameter. The obtained results also demonstrated the scalability of the developed MILP model.

Regarding the second step of the project, a novel DRCCP approach has been proposed to deal with the uncertainties associated with renewable generations and loads. In this regard, the uncertainties have been modelled by defining a number of CCs which ensure that the constraints subject to uncertainty will be satisfied with a certain probability level. A DR reformulation has also been proposed for the CCs, which makes the optimal solution of the MDEP problem robust against the PDFs of the uncertain parameters. Moreover, highly accurate linearization methods have been utilized to overcome the nonlinearities of the DR reformulation proposed for the CCs.

In this way, a DRCC-MILP model has been obtained, which can be efficiently solved using off-the-shelf mathematical programming solvers. The simulation results showed that the proposed DRCC-MILP model is capable of making an appropriate trade-off among the solution robustness, investment cost, and computational burden.

Regarding the third step of the project, a fast solution procedure based on an accelerated version of the BD algorithm has been proposed to solve the MDEP problem. This solution procedure has been obtained by applying two novel acceleration strategies (i.e., modification of the master problem and generation of the auxiliary optimality cuts) to the classical BD algorithm. The simulation results showed that the accelerated BD algorithm is able to find the optimal solution of the MDEP problem tens of times faster than the standard off-the-shelf mathematical programming solvers. The obtained results also demonstrated the highly effective role of the proposed acceleration strategies in speeding up the solution process, so that they not only decrease the total number of iterations required by the BD algorithm to reach the convergence, but also shorten the time consumed by each iteration.

Regarding the fourth and fifth steps of the project, a robust STS-based decomposed model has been developed for the MDEP problem, which takes ESSs and DRLs along with DGs into account. This model is capable of performing STPFS to analyze the short-term operational impacts of ESSs and DRLs when deciding about the long-term expansion plans. In this regard, the accelerated BD algorithm proposed in the third step of the project has been employed to achieve the computational speed required for performing STPFS. With respect to energy storage and demand response modelling, AA-CAES has been chosen as the ESS option and an RTP scheme has been considered for DRLs. Moreover, a robust optimization-based approach has been proposed for modelling the uncertainties of renewable generations, loads, and electricity prices, which allows controlling the degree of conservatism of the solution and also provides the decision maker with a probabilistic bound on the robustness level of the obtained solution. The simulation results showed that DERs provide significant techno-economic benefits as they not only make substantial reductions in the costs, but also positively affect the important operational aspects of the distribution system. The simulation results also showed the high robustness level of the robust STS-based decomposed model developed for the MDEP problem.

By completing the above-described steps, a comprehensive planning methodology has been developed for ADNs incorporating various types of DERs.

6.2 Suggestions for Future Work

The following studies are recommended for future extension of the research work carried out in this thesis:

- The planning methodology developed in this thesis can be extended to consider the reliability issues of the distribution system (e.g., component failures). To this end, it is necessary to incorporate the distribution system reliability assessment into the optimization process, which is an extremely difficult task. The difficulty of incorporating the distribution system reliability assessment into the optimization process stems from the fact that the network topology must be known in order to perform the contingency analysis and calculate the reliability indices, but the network topology itself is an outcome of the optimization process and hence is not known before solving the optimization problem. To address this issue, the conventional simulation-based reliability assessment approaches must be equivalently formulated as explicit algebraic expressions. That is, the topology-dependent reliability indices must be explicitly formulated in terms of the topology-related decision variables of the optimization problem. To the best of our knowledge, such explicit algebraic expressions for reliability assessment are not currently available in the literature. Therefore, it is recommended to develop the explicit algebraic expressions required for incorporating the reliability considerations into the developed planning methodology.
- The planning methodology developed in this thesis can be extended to take EVs (which are special DERs capable of acting as both DRLs and ESSs) into consideration. On the one hand, the high penetration of EVs can place a huge charging power demand on the distribution system. This huge demand, if not carefully considered at the planning stage, can adversely affect the normal operation of the distribution system. On the other hand, EVs can serve as active elements and feed the electrical energy stored in their batteries back into the grid. This capability, which is called vehicle-to-grid (V2G), enables EVs to act as ESSs. The possibility to operate EVs as some dispersed ESS units can introduce potential benefits to the distribution system planners. Based on the above discussion, it is recommended to model EVs and

incorporate them into the developed planning methodology considering their demand responsiveness and V2G capability.

- The high penetration of DERs can significantly change the pattern of bulk power transfer, which in turn affects the expansion planning studies of the transmission system. Based on this fact, it is recommended to develop a new planning methodology which concurrently considers both transmission and distribution systems. This can lead to an integrated planning tool for transmission and distribution systems with high penetration of DERs.

List of Publications

Journal Papers

1. **A. Zare**, C. Y. Chung, J. Zhan, and S. O. Faried, "A distributionally robust chance-constrained MILP model for multistage distribution system planning with uncertain renewables and loads," *IEEE Trans. Power Syst.*, vol. 33, pp. 5248-5262, 2018.

Conference Papers

1. **A. Zare**, C. Y. Chung, N. Safari, S. O. Faried, and S. M. Mazhari, "A bi-level polyhedral-based MILP model for expansion planning of active distribution networks incorporating distributed generation," *2018 IEEE Power and Energy Society General Meeting,* Portland, August 2018.

2. **A. Zare**, C. Y. Chung, B. Khorramdel, and N. Safari, S. O. Faried, "A Novel Unscented Transformation-Based Framework for Distribution Network Expansion Planning Considering Smart EV Parking Lots," *31st Canadian Conference on Electrical and Computer Engineering*, Quebec City, May 2018.

Miscellaneous Journal and Conference Papers

1. J. Zhan, C. Y. Chung, and **A. Zare**, "A fast solution method for stochastic transmission expansion planning," *IEEE Trans. Power Syst.,* vol. 32, no. 6, 2017.

2. B. Khorramdel, **A. Zare**, C. Y. Chung, and P. N. Gavriliadis, "A generic convex model for a chance-constrained look-ahead economic dispatch problem incorporating an accurate wind power distribution model," submitted to *IEEE Trans. Power Syst.*

3. B. Khorramdel, H. Khorramdel, **A. Zare**, N. Safari, H. Sangrody, and C. Y. Chung, "A nonparametric probability distribution model for short-term wind power prediction error," *31st Canadian Conference on Electrical and Computer Engineering*, Quebec City, May 2018.

4. N. Safari, O. A. Ansari, **A. Zare**, and C. Y. Chung, "A novel decomposition-based localized short-term tidal current speed and direction prediction model," *2017 IEEE Power and Energy Society General Meeting*, Chicago, July 2017.

5. N. Safari, B. Khorramdel, **A. Zare**, and C. Y. Chung, "An advanced multistage multi-step tidal current speed and direction prediction model," 2017 *IEEE Electrical Power and Energy Conference* (*EPEC*), Saskatoon, October 2017.

Appendix A

Proof of Exactness of DistFlow Branch Equations

In order to understand how *DistFlow branch equations* are derived, consider the illustrative example depicted in Figure A, which shows the flow of power in a radial distribution network [45], [117], [118]. Based on this illustrative example, the active and reactive power balance equations in a node of the network can be written as follows:

$$P_{ki}^{F} - R_{ki}(I_{ki}^{F})^{2} - P_{ij}^{F} + P_{i}^{S} + P_{i}^{GC} + P_{i}^{GR} = \overline{\overline{P_{i}^{D}}} \qquad \forall i \in \Omega^{N} \tag{A.1}$$

$$Q_{ki}^{F} - X_{ki}(I_{ki}^{F})^{2} - Q_{ij}^{F} + Q_{i}^{S} + Q_{i}^{GC} + Q_{i}^{GR} = \overline{\overline{Q_{i}^{D}}} \qquad \forall i \in \Omega^{N} \tag{A.2}$$

These two equations are in fact representing the Kirchhoff's current law (KCL) as they give rise to nodal power balance. On the other hand, regarding the Kirchhoff's voltage law (KVL), the voltage drop across a feeder section can be expressed as:

$$\overrightarrow{V_{i}} - \overrightarrow{V_{j}} = \overrightarrow{I_{ij}^{F}}\left(R_{ij} + jX_{ij}\right) \qquad \forall (ij) \in \Omega^{F} \tag{A.3}$$

$$\overrightarrow{I_{ij}^{F}} = \left[\left(P_{ij}^{F} + jQ_{ij}^{F}\right)/\overrightarrow{V_{i}}\right]^{*} \qquad \forall (ij) \in \Omega^{F} \tag{A.4}$$

where the rightwards arrows denote complex variables; the asterisk denotes complex conjugate; and j is the imaginary unit (i.e., $j = \sqrt{-1}$).

Substituting (A.4) into (A.3) results in the following equation:

$$\left(\overrightarrow{V_{i}} - \overrightarrow{V_{j}}\right)\overrightarrow{V_{i}}^{*} = \left(P_{ij}^{F} - jQ_{ij}^{F}\right)\left(R_{ij} + jX_{ij}\right) \qquad \forall (ij) \in \Omega^{F} \tag{A.5}$$

Bearing in mind that $\overrightarrow{V_{i}} = V_{i}\angle\theta_{i}$ and $\overrightarrow{V_{j}} = V_{j}\angle\theta_{j}$, equation (A.5) can be rewritten as:

$$(V_{i})^{2} - V_{i}V_{j}\left(\cos\theta_{ij} - j\,\sin\theta_{ij}\right) = \left(P_{ij}^{F} - jQ_{ij}^{F}\right)\left(R_{ij} + jX_{ij}\right) \qquad \forall (ij) \epsilon \Omega^{F} \tag{A.6}$$

where θ_i and θ_j denote the voltage phase angles of sending and receiving ends of the feeder section, respectively; and $\theta_{ij} = \theta_i - \theta_j$ is the voltage phase angle difference across the feeder section.

By separating the real and imaginary parts of (A.6), the following equations will be obtained:

$$V_i V_j \cos\theta_{ij} = (V_i)^2 - \left(R_{ij}P_{ij}^F + X_{ij}Q_{ij}^F\right) \qquad \forall (ij) \in \Omega^F \tag{A.7}$$

$$V_i V_j \sin\theta_{ij} = \left(X_{ij}P_{ij}^F - R_{ij}Q_{ij}^F\right) \qquad \forall (ij) \in \Omega^F \tag{A.8}$$

Summing the squares of (A.7) and (A.8) leads to:

$$(V_i)^4 - (V_i)^2\left(V_j\right)^2 = 2(V_i)^2\left(R_{ij}P_{ij}^F + X_{ij}Q_{ij}^F\right) - \left[\left(R_{ij}\right)^2 + \left(X_{ij}\right)^2\right]\left[\left(P_{ij}^F\right)^2 + \left(Q_{ij}^F\right)^2\right] \quad \forall (ij) \in \Omega^F \tag{A.9}$$

Dividing both sides of (A.9) by $(V_i)^2$ gives the following final equations:

$$(V_i)^2 - \left(V_j\right)^2 = 2\left(R_{ij}P_{ij}^F + X_{ij}Q_{ij}^F\right) - \left(Z_{ij}\right)^2\left(I_{ij}^F\right)^2 \quad \forall (ij) \in \Omega^F \tag{A.10}$$

$$\left(I_{ij}^F\right)^2 = \left(S_{ij}^F\right)^2/(V_i)^2 \qquad \forall (ij) \in \Omega^F \tag{A.11}$$

$$\left(S_{ij}^F\right)^2 = \left(P_{ij}^F\right)^2 + \left(Q_{ij}^F\right)^2 \qquad \forall (ij) \in \Omega^F \tag{A.12}$$

Considering that $f_{ij}^F = \left(I_{ij}^F\right)^2$ and $u_i = (V_i)^2$, equations (A.1), (A.2), and (A.10)-(A.12) are equivalent to constraints (2.4)-(2.8), respectively.

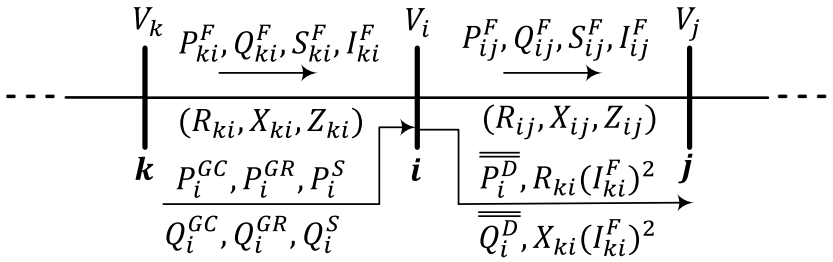

Figure A.1 Illustration of a radial distribution network.

Appendix B

Data Related to the 138-Node Test System

Table B.1 Nodal power demands at different planning stages (kVA).

Nodes	Stages		Nodes	Stages	
	1	2		1	2
1	284.9	375.55	69	98.27833	129.5487
2	56.56472	74.56258	70	257.9862	340.0727
3	50.37446	66.4027	71	27.57662	36.351
4	103.022	135.8017	72	6.008053	7.919706
5	368.5496	485.8154	73	85.99321	113.3547
6	176.2413	232.318	74	480.634	633.563
7	282.5523	372.4553	75	203.5	268.25
8	73.75343	97.22043	76	119.6907	157.7741
9	147.4983	194.4295	77	170.2769	224.4559
10	165.932	218.7285	78	114.7465	151.2567
11	138.2871	182.2876	79	358.9665	473.1831
12	295.0182	388.8877	80	168.747	222.4392
13	344.8884	454.6256	81	334.3513	440.7358
14	359.564	473.9707	82	104.3166	137.5082
15	254.9924	336.1264	83	291.3405	384.0398
16	235.1019	309.9071	84	296.003	390.1857
17	471.9	622.05	85	466.4	614.8
18	173.8	229.1	86	107.3824	141.5496
19	82.5	108.75	87	1358.792	1791.135
20	36.88823	48.62539	88	547.6056	721.8438
21	282.805	372.7884	89	460.2191	606.6525
22	73.77891	97.25402	90	73.7	97.15
23	282.805	372.7884	91	95.11212	125.3751
24	147.5544	194.5035	92	104.3166	137.5082
25	295.9	390.05	93	286	377
26	69.76851	91.96758	94	88.41308	116.5445
27	446.5078	588.5785	95	277.2429	365.4566
28	237.6	313.2	96	169.44	223.3528
29	152.6235	201.1855	97	73.7	97.15
30	69.76851	91.96758	98	91.33795	120.4

31	414.7	546.65	99	399.3	526.35
32	104.655	137.9543	100	61.31719	80.82721
33	188.1	247.95	101	71.53461	94.29562
34	485.7756	640.3406	102	143	188.5
35	410.3	540.85	103	246.4	324.8
36	221.8041	292.3781	104	19.08532	25.4471
37	296.5158	390.8618	105	1718.087	2290.783
38	92.21836	121.5606	106	356.9817	475.9756
39	157.3	207.35	107	91.04335	121.3911
40	1.497971	1.974598	108	55.7429	75.25292
41	7.496052	9.88116	109	73	98.55
42	188.1	247.95	110	219.8776	296.8348
43	140.8378	185.6498	111	0	85.92696
44	74.45057	98.13939	112	0	64.41182
45	205.8435	271.3392	113	0	197.6
46	547.8671	722.1884	114	0	221.7802
47	314.1719	414.1356	115	0	146.25
48	281.6756	371.2996	116	0	339.6218
49	224.4	295.8	117	0	443.75
50	130.4904	172.0101	118	0	93.14168
51	317.9	419.05	119	0	41.80178
52	86.98906	114.6674	120	0	79.61486
53	308.8089	407.0662	121	0	327.6
54	82.64017	108.9348	122	0	121.1235
55	26.09724	34.4009	123	0	63.822
56	486.2	640.9	124	0	157.6554
57	24.52488	32.32825	125	0	100.2937
58	179.8699	237.1012	126	0	178.1274
59	263.6699	347.5649	127	0	26.1646
60	110.3763	145.4961	128	0	91.5734
61	467.5	616.25	129	0	266.3954
62	270.8395	357.0157	130	0	41.62426
63	401.5	529.25	131	0	291.3636
64	348.0761	458.8276	132	0	352.5436
65	98.27833	129.5487	133	0	371.5778
66	98.27833	129.5487	134	0	277.4892
67	122.8492	161.9376	135	0	317
68	208.8444	275.2949			

Table B.2 Lengths of feeder sections (km).

Sections		l_{ij}	Sections		l_{ij}	Sections		l_{ij}
i	j		i	j		i	j	
1	2	0.4106	43	44	0.00472	86	202	0.83536
1	201	0.83536	43	52	0.17463	87	88	0.11799
2	3	0.28789	44	45	0.9209	87	89	0.02359
3	4	0.08019	45	108	0.53541	89	90	0.42476
4	5	0.58895	46	47	0.16046	90	91	0.87545
5	6	0.1537	46	129	0.97444	91	92	0.48117
6	7	0.44974	47	48	0.33037	92	93	0.64249
6	8	0.96991	48	49	0.15574	93	94	0.1537
8	9	0.16708	49	50	0.28789	94	106	0.02831
8	10	0.56753	50	101	0.64249	94	110	1.633
10	11	0.08019	51	101	0.87807	95	96	0.64249
10	12	0.33196	52	53	1.40097	95	202	0.39173
10	13	0.83536	53	54	0.40089	96	97	0.02831
11	121	1.1516	53	57	0.11327	97	98	1.0525
13	14	0.00472	54	55	0.06607	97	99	0.17214
13	15	0.56162	55	56	0.15102	99	100	1.1044
15	16	0.27374	56	107	1.2207	100	128	0.11327
15	120	0.3328	57	58	0.07551	101	102	0.55651
15	121	0.35001	58	59	0.05191	102	103	1.05191
16	120	0.62108	59	104	1.213	103	203	0.29733
17	18	0.21238	60	61	0.27374	104	105	0.59966
17	201	0.07949	60	202	0.00472	105	122	0.24542
18	19	0.33509	61	62	0.28912	106	107	0.29733
19	20	0.41434	62	63	0.47116	107	122	0.34924
20	21	0.80312	63	64	0.56753	107	125	1.10855
20	22	0.4578	64	65	0.37479	108	109	0.23125
22	23	0.34266	65	131	0.53541	108	122	0.40588
22	24	0.06135	65	133	0.81176	108	203	2.4168
24	25	0.11327	66	67	0.23558	109	110	0.53462
25	26	0.04719	66	202	0.56169	111	112	0.56136
26	27	0.16306	67	68	0.34924	112	113	0.41434
27	28	0.03341	68	69	0.01887	113	114	0.916562
28	29	0.21416	69	70	1.67962	114	123	1.702315
28	31	0.44974	70	71	0.96279	115	116	0.276255
29	30	0.08019	71	72	0.83064	115	129	0.90413
30	113	0.61037	72	73	0.82592	116	117	1.254929
31	32	0.10708	72	119	0.36812	117	118	0.862264
31	123	0.07459	74	75	0.42948	118	130	0.555482
32	33	0.47116	74	202	0.25014	119	120	0.641857

33	34	1.12849	75	76	0.63178	121	132	0.964302
35	36	0.30741	76	77	0.14631	123	124	0.581637
35	201	0.19351	76	78	0.79241	124	125	0.357121
36	37	0.10692	78	79	1.1565	126	127	1.358272
36	38	0.37424	78	80	0.16991	126	203	1.1469
38	39	0.25958	80	81	1.3992	127	128	0.359297
39	40	0.41762	80	82	0.02831	130	203	1.751
39	46	0.29983	82	83	1.8359	132	133	0.307052
40	41	0.08015	83	84	0.56634	133	134	0.452773
41	42	0.83536	84	85	0.52388	134	135	0.560965
42	43	0.29733	85	111	0.3115			
42	51	3.1323	86	87	0.33981			

Appendix C

Copyright Permission Letters from Co-Authors

To Whom It May Concern:

I, Chi Yung Chung, hereby grant permission to Mr. Alireza Zare to include the following papers in his thesis titled "Multistage Expansion Planning of Active Distribution Systems: Towards Network Integration of Distributed Energy Resources".

1. A. Zare, **C. Y. Chung**, J. Zhan, and S. O. Faried, "A distributionally robust chance-constrained MILP model for multistage distribution system planning with uncertain renewables and loads," *IEEE Trans. Power Syst.*, vol. 33, pp. 5248-5262, 2018.

2. A. Zare, **C. Y. Chung**, B. Khorramdel, and S. O. Faried, "A robust sequential-time simulation-based decomposed model for distribution network and DER planning—part I: deterministic formulation," to be submitted to *IEEE Trans. Power Syst.*

3. A. Zare, B. Khorramdel, **C. Y. Chung**, and S. O. Faried, "A robust sequential-time simulation-based decomposed model for distribution network and DER planning—part II: uncertainty modelling and numerical analysis," to be submitted to *IEEE Trans. Power Syst.*

I am aware that all University of Saskatchewan theses are also posted in the digital USask eCommons thesis repository, making the thesis openly available on the internet.

Date:

Signature:

To Whom It May Concern:

I, Junpeng Zhan, hereby grant permission to Mr. Alireza Zare to include the following paper in his thesis titled "Multistage Expansion Planning of Active Distribution Systems: Towards Network Integration of Distributed Energy Resources".

1. A. Zare, C. Y. Chung, **J. Zhan**, and S. O. Faried, "A distributionally robust chance-constrained MILP model for multistage distribution system planning with uncertain renewables and loads," *IEEE Trans. Power Syst.*, vol. 33, pp. 5248-5262, 2018.

I am aware that all University of Saskatchewan theses are also posted in the digital USask eCommons thesis repository, making the thesis openly available on the internet.

Date:

Signature:

To Whom It May Concern:

I, Sherif Omar Faried, hereby grant permission to Mr. Alireza Zare to include the following papers in his thesis titled "Multistage Expansion Planning of Active Distribution Systems: Towards Network Integration of Distributed Energy Resources".

1. A. Zare, C. Y. Chung, J. Zhan, and **S. O. Faried**, "A distributionally robust chance-constrained MILP model for multistage distribution system planning with uncertain renewables and loads," *IEEE Trans. Power Syst.*, vol. 33, pp. 5248-5262, 2018.

2. A. Zare, C. Y. Chung, B. Khorramdel, and **S. O. Faried**, "A robust sequential-time simulation-based decomposed model for distribution network and DER planning—part I: deterministic formulation," to be submitted to *IEEE Trans. Power Syst.*

3. A. Zare, B. Khorramdel, C. Y. Chung, and **S. O. Faried**, "A robust sequential-time simulation-based decomposed model for distribution network and DER planning—part II: uncertainty modelling and numerical analysis," to be submitted to *IEEE Trans. Power Syst.*

I am aware that all University of Saskatchewan theses are also posted in the digital USask eCommons thesis repository, making the thesis openly available on the internet.

Date:

Signature:

To Whom It May Concern:

I, Benyamin Khorramdel, hereby grant permission to Mr. Alireza Zare to include the following papers in his thesis titled "Multistage Expansion Planning of Active Distribution Systems: Towards Network Integration of Distributed Energy Resources".

1. A. Zare, C. Y. Chung, **B. Khorramdel**, and S. O. Faried, "A robust sequential-time simulation-based decomposed model for distribution network and DER planning—part I: deterministic formulation," to be submitted to *IEEE Trans. Power Syst.*

2. A. Zare, **B. Khorramdel**, C. Y. Chung, and S. O. Faried, "A robust sequential-time simulation-based decomposed model for distribution network and DER planning—part II: uncertainty modelling and numerical analysis," to be submitted to *IEEE Trans. Power Syst.*

I am aware that all University of Saskatchewan theses are also posted in the digital USask eCommons thesis repository, making the thesis openly available on the internet.

Date:

Signature:

Bibliography

[1] S. Heidari, M. Fotuhi-Firuzabad, and S. Kazemi, "Power distribution network expansion planning considering distribution automation," *IEEE Trans. Power Syst.,* vol. 30, pp. 1261-1269, 2015.

[2] S. Heidari, M. Fotuhi-Firuzabad, and M. Lehtonen, "Planning to equip the power distribution networks with automation system," *IEEE Trans. Power Syst.,* 2017 (Early Access).

[3] W. Yao, C. Y. Chung, F. Wen, M. Qin, and Y. Xue, "Scenario-based comprehensive expansion planning for distribution systems considering integration of plug-in electric vehicles," *IEEE Trans. Power Syst.,* vol. 31, pp. 317-328, 2016.

[4] S. Ganguly, N. Sahoo, and D. Das, "Recent advances on power distribution system planning: a state-of-the-art survey," *Energy Systems,* vol. 4, pp. 165-193, 2013.

[5] P. S. Georgilakis and N. D. Hatziargyriou, "A review of power distribution planning in the modern power systems era: Models, methods and future research," *Electr. Power Syst. Res.,* vol. 121, pp. 89-100, 2015.

[6] A. Tabares, J. F. Franco, M. Lavorato, and M. J. Rider, "Multistage long-term expansion planning of electrical distribution systems considering multiple alternatives," *IEEE Trans. Power Syst.,* vol. 31, pp. 1900-1914, 2016.

[7] S. Haffner, L. F. A. Pereira, L. A. Pereira, and L. S. Barreto, "Multistage model for distribution expansion planning with distributed generation - part I: problem formulation," *IEEE Trans. Power Del.,* vol. 23, pp. 915-923, 2008.

[8] S. Haffner, L. F. A. Pereira, L. A. Pereira, and L. S. Barreto, "Multistage model for distribution expansion planning with distributed generation—part II: numerical results," *IEEE Trans. Power Del.,* vol. 23, pp. 924-929, 2008.

[9] M. Sedghi, A. Ahmadian, and M. Aliakbar-Golkar, "Optimal storage planning in active distribution network considering uncertainty of wind power distributed generation," *IEEE Trans. Power Syst.*, vol. 31, pp. 304-316, 2016.

[10] V. F. Martins and C. L. Borges, "Active distribution network integrated planning incorporating distributed generation and load response uncertainties," *IEEE Trans. Power Syst.*, vol. 26, pp. 2164-2172, 2011.

[11] M. Asensio, P. M. de Quevedo, G. Munoz-Delgado, and J. Contreras, "Joint distribution network and renewable energy expansion planning considering demand response and energy storage - part I: stochastic programming model," *IEEE Trans. Smart Grid*, 2016 (Early Access).

[12] M. Asensio, P. M. de Quevedo, G. Munoz-Delgado, and J. Contreras, "Joint distribution network and renewable energy expansion planning considering demand response and energy storage - part II: numerical results and considered metrics," *IEEE Trans. Smart Grid*, 2016 (Early Access).

[13] European Distribution System Operators' Association (EDSO) for Smart Grids [Online]. Available: https://www.edsoforsmartgrids.eu/home/why-smart-grids/

[14] M. Gitizadeh, A. A. Vahed, and J. Aghaei, "Multistage distribution system expansion planning considering distributed generation using hybrid evolutionary algorithms," *Applied Energy*, vol. 101, pp. 655-666, 2013.

[15] J. Aghaei, K. M. Muttaqi, A. Azizivahed, and M. Gitizadeh, "Distribution expansion planning considering reliability and security of energy using modified PSO (Particle Swarm Optimization) algorithm," *Energy*, vol. 65, pp. 398-411, 2014.

[16] K. M. Muttaqi, A. D. Le, J. Aghaei, E. Mahboubi-Moghaddam, M. Negnevitsky, and G. Ledwich, "Optimizing distributed generation parameters through economic feasibility assessment," *Applied Energy*, vol. 165, pp. 893-903, 2016.

[17] M. Nayeripour, E. Mahboubi-Moghaddam, J. Aghaei, and A. Azizi-Vahed, "Multi-objective placement and sizing of DGs in distribution networks ensuring transient stability using

hybrid evolutionary algorithm," *Renewable and Sustainable Energy Reviews,* vol. 25, pp. 759-767, 2013.

[18] E. Naderi, H. Seifi, and M. S. Sepasian, "A dynamic approach for distribution system planning considering distributed generation," *IEEE Trans. Power Del.,* vol. 27, pp. 1313-1322, 2012.

[19] E. G. Carrano, F. G. Guimarães, R. H. Takahashi, O. M. Neto, and F. Campelo, "Electric distribution network expansion under load-evolution uncertainty using an immune system inspired algorithm," *IEEE Trans. Power Syst.,* vol. 22, pp. 851-861, 2007.

[20] A. Bagheri, H. Monsef, and H. Lesani, "Integrated distribution network expansion planning incorporating distributed generation considering uncertainties, reliability, and operational conditions," *Int. J. Elect. Power Energy Syst.,* vol. 73, pp. 56-70, 2015.

[21] S. Ganguly and D. Samajpati, "Distributed generation allocation on radial distribution networks under uncertainties of load and generation using genetic algorithm," *IEEE Trans. Sustain. Energy,* vol. 6, pp. 688-697, 2015.

[22] S. Abapour, K. Zare, and B. Mohammadi-Ivatloo, "Dynamic planning of distributed generation units in active distribution network," *IET Gener. Transm. Distrib. ,* vol. 9, pp. 1455-1463, 2015.

[23] S. M. Mazhari, H. Monsef, and R. Romero, "A multi-objective distribution system expansion planning incorporating customer choices on reliability," *IEEE Trans. Power Syst.,* vol. 31, pp. 1330-1340, 2016.

[24] S. Sharma, S. Bhattacharjee, and A. Bhattacharya, "Grey wolf optimisation for optimal sizing of battery energy storage device to minimise operation cost of microgrid," *IET Gener. Transm. Distrib. ,* vol. 10, pp. 625-637, 2016.

[25] W. Yao, J. Zhao, F. Wen, Z. Dong, Y. Xue, Y. Xu, *et al.*, "A multi-objective collaborative planning strategy for integrated power distribution and electric vehicle charging systems," *IEEE Trans. Power Syst.,* vol. 29, pp. 1811-1821, 2014.

[26] K. Zou, A. P. Agalgaonkar, K. M. Muttaqi, and S. Perera, "Distribution system planning with incorporating DG reactive capability and system uncertainties," *IEEE Trans. Sustain. Energy,* vol. 3, pp. 112-123, 2012.

[27] S. Mohtashami, D. Pudjianto, and G. Strbac, "Strategic distribution network planning with smart grid technologies," *IEEE Trans. Smart Grid,* 2016.

[28] Y. Atwa, E. El-Saadany, M. Salama, and R. Seethapathy, "Optimal renewable resources mix for distribution system energy loss minimization," *IEEE Trans. Power Syst.,* vol. 25, pp. 360-370, 2010.

[29] A. M. El-Zonkoly, "Multistage expansion planning for distribution networks including unit commitment," *IET Gener. Transm. Distrib. ,* vol. 7, pp. 766-778, 2013.

[30] I. Ziari, G. Ledwich, A. Ghosh, and G. Platt, "Integrated distribution systems planning to improve reliability under load growth," *IEEE Trans. Power Del.,* vol. 27, pp. 757-765, 2012.

[31] Y. Gao, X. Hu, W. Yang, H. Liang, and P. Li, "Multi-objective bi-level coordinated planning of distributed generation and distribution network frame based on multi-scenario technique considering timing characteristics," *IEEE Trans. Sustain. Energy,* 2017.

[32] M. Moradijoz, M. P. Moghaddam, and M.-R. Haghifam, "A flexible distribution system expansion planning model: a dynamic bi-level approach," *IEEE Trans. Smart Grid,* 2017.

[33] A. Ahmadian, M. Sedghi, and M. Aliakbar-Golkar, "Fuzzy load modeling of plug-in electric vehicles for optimal storage and DG planning in active distribution network," *IEEE Trans. Veh. Technol.,* vol. 66, pp. 3622-3631, 2017.

[34] N. Mansor and V. Levi, "Integrated planning of distribution networks considering utility planning concepts," *IEEE Trans. Power Syst.,* 2017.

[35] S. Montoya-Bueno, J. I. Muoz, and J. Contreras, "A stochastic investment model for renewable generation in distribution systems," *IEEE Trans. Sustain. Energy,* vol. 6, pp. 1466-1474, 2015.

[36] G. Muñoz-Delgado, J. Contreras, and J. M. Arroyo, "Joint expansion planning of distributed generation and distribution networks," *IEEE Trans. Power Syst.,* vol. 30, pp. 2579-2590, 2015.

[37] G. Muñoz-Delgado, J. Contreras, and J. M. Arroyo, "Multistage generation and network expansion planning in distribution systems considering uncertainty and reliability," *IEEE Trans. Power Syst.,* vol. 31, pp. 3715-3728, 2016.

[38] S. F. Santos, D. Z. Fitiwi, A. W. Bizuayehu, M. Shafie-khah, M. Asensio, J. Contreras, *et al.*, "Novel multi-stage stochastic DG investment planning with recourse," *IEEE Trans. Sustain. Energy* vol. 8, pp. 164-178, 2017.

[39] M. Asensio, G. Munoz-Delgado, and J. Contreras, "A bi-level approach to distribution network and renewable energy expansion planning considering demand response," *IEEE Trans. Power Syst.,* 2017 (Early Access).

[40] S. F. Santos, D. Z. Fitiwi, M. Shafie-Khah, A. W. Bizuayehu, C. M. Cabrita, and J. P. Catalão, "New multistage and stochastic mathematical model for maximizing RES hosting capacity - part I: problem formulation," *IEEE Trans. Sustain. Energy,* vol. 8, pp. 304-319, 2017.

[41] S. F. Santos, D. Z. Fitiwi, M. Shafie-khah, A. W. Bizuayehu, C. M. Cabrita, and J. P. Catalão, "New multi-stage and stochastic mathematical model for maximizing RES hosting capacity - part II: numerical results," *IEEE Trans. Sustain. Energy,* vol. 8, pp. 320-330, 2017

[42] R. R. Gonçalves, J. F. Franco, and M. J. Rider, "Short-term expansion planning of radial electrical distribution systems using mixed-integer linear programming," *IET Gener. Transm. Distrib. ,* vol. 9, pp. 256-266, 2014.

[43] R. C. Lotero and J. Contreras, "Distribution system planning with reliability," *IEEE Trans. Power Del.,* vol. 26, pp. 2552-2562, 2011.

[44] S. F. Santos, D. Z. Fitiwi, A. W. Bizuayehu, M. Shafie-Khah, M. Asensio, J. Contreras, *et al.*, "Impacts of operational variability and uncertainty on distributed generation investment

planning: a comprehensive sensitivity analysis," *IEEE Trans. Sustain. Energy*, vol. 8, pp. 855-869, 2017.

[45] J. F. Franco, M. J. Rider, M. Lavorato, and R. Romero, "Optimal conductor size selection and reconductoring in radial distribution systems using a mixed-integer LP approach," *IEEE Trans. Power Syst.*, vol. 28, pp. 10-20, 2013.

[46] J. F. Franco, M. J. Rider, and R. Romero, "A mixed-integer quadratically-constrained programming model for the distribution system expansion planning," *Int. J. Elect. Power Energy Syst.*, vol. 62, pp. 265-272, 2014.

[47] B. Zeng, J. Zhang, X. Yang, J. Wang, J. Dong, and Y. Zhang, "Integrated planning for transition to low-carbon distribution system with renewable energy generation and demand response," *IEEE Trans. Power Syst.*, vol. 29, pp. 1153-1165, 2014.

[48] X. Shen, M. Shahidehpour, Y. Han, S. Zhu, and J. Zheng, "Expansion planning of active distribution networks with centralized and distributed energy storage systems," *IEEE Trans. Sustain. Energy*, vol. 8, pp. 126-134, 2017.

[49] J. Zhan, C. Y. Chung, and A. Zare, "A fast solution method for stochastic transmission expansion planning," *IEEE Trans. Power Syst.*, 2017 (Early Access).

[50] S. N. Ravadanegh, N. Jahanyari, A. Amini, and N. Taghizadeghan, "Smart distribution grid multistage expansion planning under load forecasting uncertainty," *IET Gener. Transm. Distrib.* , vol. 10, pp. 1136-1144, 2016.

[51] M. Moeini-Aghtaie, A. Abbaspour, and M. Fotuhi-Firuzabad, "Incorporating large-scale distant wind farms in probabilistic transmission expansion planning—Part I: Theory and algorithm," *IEEE Trans. Power Syst.*, vol. 27, pp. 1585-1593, 2012.

[52] A. Kavousi-Fard and T. Niknam, "Optimal distribution feeder reconfiguration for reliability improvement considering uncertainty," *IEEE Trans. Power Del.*, vol. 29, pp. 1344-1353, 2014.

[53] A. Kavousi-Fard and T. Niknam, "Considering uncertainty in the multi-objective stochastic capacitor allocation problem using a novel self adaptive modification approach," *Electr. Power Syst. Res.,* vol. 103, pp. 16-27, 2013.

[54] M. Dadkhah and B. Venkatesh, "Cumulant based stochastic reactive power planning method for distribution systems with wind generators," *IEEE Trans. Power Syst.,* vol. 27, pp. 2351-2359, 2012.

[55] A. Kavousi-Fard, T. Niknam, and M. Fotuhi-Firuzabad, "Stochastic reconfiguration and optimal coordination of V2G plug-in electric vehicles considering correlated wind power generation," *IEEE Trans. Sustain. Energy,* vol. 6, pp. 822-830, 2015.

[56] M. Aien, M. Fotuhi-Firuzabad, and F. Aminifar, "Probabilistic load flow in correlated uncertain environment using unscented transformation," *IEEE Trans. Power Syst.*, vol. 27, pp. 2233-2241, 2012.

[57] Z. Wang, B. Chen, J. Wang, J. Kim, and M. M. Begovic, "Robust optimization based optimal DG placement in microgrids," *IEEE Trans. Smart Grid,* vol. 5, pp. 2173-2182, 2014.

[58] P. Xiong, P. Jirutitijaroen, and C. Singh, "A distributionally robust optimization model for unit commitment considering uncertain wind power generation," *IEEE Trans. Power Syst.,* vol. 32, pp. 39-49, 2017 (Early Access).

[59] C. Zhao and R. Jiang, "Distributionally robust contingency-constrained unit commitment," *IEEE Trans. Power Syst.*, 2017 (Early Access).

[60] A. Khodaei, S. Bahramirad, and M. Shahidehpour, "Microgrid planning under uncertainty," *IEEE Trans. Power Syst.*, vol. 30, pp. 2417-2425, 2015.

[61] R. Jabr, "Robust transmission network expansion planning with uncertain renewable generation and loads," *IEEE Trans. Power Syst.*, vol. 28, pp. 4558-4567, 2013.

[62] S. Dehghan, N. Amjady, and A. J. Conejo, "Adaptive robust transmission expansion planning using linear decision rules," *IEEE Trans. Power Syst.,* 2017.

[63] W. Wei, S. Mei, L. Wu, J. Wang, and Y. Fang, "Robust operation of distribution networks coupled with urban transportation infrastructures," *IEEE Trans. Power Syst.*, vol. 32, pp. 2118-2130, 2017.

[64] Y. Guo and C. Zhao, "Islanding-aware robust energy management for microgrids," *IEEE Trans. Smart Grid*, 2016.

[65] H. Gao, J. Liu, and L. Wang, "Robust coordinated optimization of active and reactive power in active distribution systems," *IEEE Trans. Smart Grid*, 2017.

[66] W. Hu, P. Wang, and H. Gooi, "Towards optimal energy management of microgrids via robust two-stage optimization," *IEEE Trans. Smart Grid*, 2016.

[67] R. García-Bertrand and R. Mínguez, "Dynamic robust transmission expansion planning," *IEEE Trans. Power Syst.*, vol. 32, pp. 2618-2628, 2017.

[68] A. Ben-Tal and A. Nemirovski, "On polyhedral approximations of the second-order cone," *Mathematics of Operations Research*, vol. 26, pp. 193-205, 2001.

[69] A. Charnes and W. W. Cooper, "Chance-constrained programming," *Management science*, vol. 6, pp. 73-79, 1959.

[70] J. F. Franco, M. J. Rider, and R. Romero, "Robust multi-stage substation expansion planning considering stochastic demand," *IEEE Trans. Power Syst.*, vol. 31, pp. 2125-2134, 2016.

[71] D. Bienstock, M. Chertkov, and S. Harnett, "Chance-constrained optimal power flow: Risk-aware network control under uncertainty," *SIAM Review*, vol. 56, pp. 461-495, 2014.

[72] D. Bienstock, M. Chertkov, and S. Harnett, "Robust modeling of probabilistic uncertainty in smart grids: data ambiguous chance constrained optimum power flow," in *Decision and Control (CDC), 2013 IEEE 52nd Annual Conference on*, 2013, pp. 4335-4340.

[73] F. Qiu and J. Wang, "Distributionally robust congestion management with dynamic line ratings," *IEEE Trans. Power Syst.*, vol. 30, pp. 2198-2199, 2015.

[74] F. Qiu and J. Wang, "Chance-constrained transmission switching with guaranteed wind power utilization," *IEEE Trans. Power Syst.*, vol. 30, pp. 1270-1278, 2015.

[75] R. Jiang and Y. Guan, "Data-driven chance constrained stochastic program," *Mathematical Programming*, vol. 158, pp. 291-327, 2016.

[76] A. Shapiro, "On duality theory of conic linear problems," in *Semi-infinite programming*, ed: Springer, 2001, pp. 135-165.

[77] V. A. Yakubovich, "S-procedure in nonlinear control theory," *Vestnik Leningrad University*, vol. 1, pp. 62-77, 1971.

[78] R. C. Dugan, J. A. Taylor, and D. Montenegro, "Energy storage modeling for distribution planning," *IEEE Trans. Ind. Appl.*, vol. 53, pp. 954-962, 2017.

[79] R. F. Arritt and R. C. Dugan, "Value of sequential-time simulations in distribution planning," *IEEE Trans. Ind. Appl.*, vol. 50, pp. 4216-4220, 2014.

[80] B. Zakeri and S. Syri, "Electrical energy storage systems: a comparative life cycle cost analysis," *Renewable Sustain. Energy Rev.*, vol. 42, pp. 569-596, 2015.

[81] M. E. Baran and F. F. Wu, "Network reconfiguration in distribution systems for loss reduction and load balancing," *IEEE Trans. Power Del.*, vol. 4, pp. 1401-1407, 1989.

[82] M. Lavorato, J. F. Franco, M. J. Rider, and R. Romero, "Imposing radiality constraints in distribution system optimization problems," *IEEE Trans. Power Syst.*, vol. 27, pp. 172-180, 2012.

[83] M. Farivar and S. H. Low, "Branch flow model: relaxations and convexification-part I," *IEEE Trans. Power Syst.*, vol. 28, pp. 2554-2564, 2013.

[84] MathWorks Products, MATLAB, [Online]. Available: http://www.mathworks.com/products/matlab/

[85] IBM ILOG CPLEX Optimization Studio, [Online]. Available: http://www-03.ibm.com/software/products/en/ibmilogcpleoptistud

[86] Hourly Historical Data of Wind Generation, [Online]. Available: www.pjm.com/markets-and-operations/ops-analysis.aspx

[87] Hourly Historical Data of Load, [Online]. Available: www.pjm.com/markets-and-operations/ops-analysis/historical-load-data.aspx

[88] J. F. Benders, "Partitioning procedures for solving mixed-variables programming problems," *Numerische mathematik*, vol. 4, pp. 238-252, 1962.

[89] M. Shahidehpour and Y. Fu, "Benders decomposition in restructured power systems," *IEEE Techtorial*, 2005.

[90] J. R. Aguero and A. Khodaei, "Grid modernization, DER integration, and utility business models - trends and challenges," *IEEE Power Energy Mag.*, vol. 16, pp. 112-121, 2018.

[91] C. Eid, P. Codani, Y. Perez, J. Reneses, and R. Hakvoort, "Managing electric flexibility from distributed energy resources: a review of incentives for market design," *Renewable Sustain. Energy Rev.*, vol. 64, pp. 237-247, 2016.

[92] Global DER Deployment Forecast Database, Navigant Research, [Online]. Available: https://www.navigantresearch.com/research/global-der-deployment-forecast-database#

[93] M. G. Damavandi, J. R. Martí, and V. Krishnamurthy, "A methodology for optimal distributed storage planning in smart distribution grids," *IEEE Trans. Sustain. Energy*, vol. 9, pp. 729-740, 2018.

[94] N. C. Koutsoukis, P. S. Georgilakis, and N. D. Hatziargyriou, "Multistage coordinated planning of active distribution networks," *IEEE Trans. Power Syst.*, vol. 33, pp. 32-44, 2018.

[95] M. Doostizadeh and H. Ghasemi, "A day-ahead electricity pricing model based on smart metering and demand-side management," *Energy*, vol. 46, pp. 221-230, 2012.

[96] D. Bertsimas and M. Sim, "The price of robustness," *Operations Research*, vol. 52, pp. 35-53, 2004.

[97] D. Bertsimas and M. Sim, "Robust discrete optimization and network flows," *Mathematical Programming*, vol. 98, pp. 49-71, 2003.

[98] H. Saboori, R. Hemmati, S. M. S. Ghiasi, and S. Dehghan, "Energy storage planning in electric power distribution networks – a state-of-the-art review," *Renewable Sustain. Energy Rev.*, vol. 79, pp. 1108-1121, 2017.

[99] A. Abdon, X. Zhang, D. Parra, M. K. Patel, C. Bauer, and J. Worlitschek, "Techno-economic and environmental assessment of stationary electricity storage technologies for different time scales," *Energy*, vol. 139, pp. 1173-1187, 2017.

[100] X. Luo, J. Wang, M. Dooner, and J. Clarke, "Overview of current development in electrical energy storage technologies and the application potential in power system operation," *Applied Energy*, vol. 137, pp. 511-536, 2015.

[101] H. Safaei and D. W. Keith, "How much bulk energy storage is needed to decarbonize electricity?," *Energy & Environmental Science*, vol. 8, pp. 3409-3417, 2015.

[102] H. Zhao, Q. Wu, S. Hu, H. Xu, and C. N. Rasmussen, "Review of energy storage system for wind power integration support," *Applied Energy*, vol. 137, pp. 545-553, 2015.

[103] M. Nick, R. Cherkaoui, and M. Paolone, "Optimal planning of distributed energy storage systems in active distribution networks embedding grid reconfiguration," *IEEE Trans. Power Syst.*, vol. 33, pp. 1577-1590, 2018.

[104] H. Alharbi and K. Bhattacharya, "Stochastic optimal planning of battery energy storage systems for isolated microgrids," *IEEE Trans. Sustain. Energy*, vol. 9, pp. 211-227, 2018.

[105] H. Hejazi and H. Mohsenian-Rad, "Energy storage planning in active distribution grids: a chance-constrained optimization with non-parametric probability functions," *IEEE Trans. Smart Grid*, 2016.

[106] R. Li, W. Wang, and M. Xia, "Cooperative planning of active distribution system with renewable energy sources and energy storage systems," *IEEE Access*, vol. 6, pp. 5916-5926, 2018.

[107] X. Luo and J. Wang, "Overview of current development on compressed air energy storage," *School of Engineering, University of Warwick*, 2013.

[108] H. Mozayeni, M. Negnevitsky, X. Wang, F. Cao, and X. Peng, "Performance study of an advanced adiabatic compressed air energy storage system," *Energy Procedia*, vol. 110, pp. 71-76, 2017.

[109] G. Grazzini and A. Milazzo, "A thermodynamic analysis of multistage adiabatic CAES," *Proceedings of the IEEE*, vol. 100, pp. 461-472, 2012.

[110] J.-L. Liu and J.-H. Wang, "A comparative research of two adiabatic compressed air energy storage systems," *Energy Convers. Manag.*, vol. 108, pp. 566-578, 2016.

[111] P. Zhao, Y. Dai, and J. Wang, "Design and thermodynamic analysis of a hybrid energy storage system based on A-CAES (adiabatic compressed air energy storage) and FESS (flywheel energy storage system) for wind power application," *Energy*, vol. 70, pp. 674-684, 2014.

[112] P. Siano, "Demand response and smart grids—a survey," *Renewable Sustain. Energy Rev.*, vol. 30, pp. 461-478, 2014.

[113] P. Samadi, A.-H. Mohsenian-Rad, R. Schober, V. W. Wong, and J. Jatskevich, "Optimal real-time pricing algorithm based on utility maximization for smart grid," in *First IEEE International Conference on Smart Grid Communications (SmartGridComm)*, 2010, pp. 415-420.

[114] A. J. Conejo, J. M. Morales, and L. Baringo, "Real-time demand response model," *IEEE Trans. Smart Grid*, vol. 1, pp. 236-242, 2010.

[115] K. Dietrich, J. M. Latorre, L. Olmos, and A. Ramos, "Demand response and its sensitivity to participation rates and elasticities," in *Energy Market (EEM), 8th International Conference on the European*, 2011, pp. 717-716.

[116] Hourly Historical Data of Load, Wind Generation, and Electricity Price, [Online]. Available: http://www.ieso.ca/en/power-data/data-directory

[117] M. E. Baran and F. F. Wu, "Optimal capacitor placement on radial distribution systems," *IEEE Trans. Power Del.*, vol. 4, pp. 725-734, 1989.

[118] R. Cespedes, "New method for the analysis of distribution networks," *IEEE Trans. Power Del.*, vol. 5, pp. 391-396, 1990.